

Investigations in the Area of High bit rate Data Transmitting Systems for Remote Sensing Satellites

THESIS

Submitted in partial fulfillment of the requirements for the degree of

DOCTOR OF PHILOSOPHY

By

VENIGALLA SAMBASIVA RAO

Under the Supervision of

Dr. SURENDRA PAL




**BIRLA INSTITUTE OF TECHNOLOGY AND SCIENCE
PILANI (RAJASTHAN) INDIA**

2010

**BIRLA INSTITUTE OF TECHNOLOGY AND SCIENCE
PILANI (RAJASTHAN)**

CERTIFICATE

This is to certify that the thesis entitled "**Investigations in the Area of High bit rate Data Transmitting Systems for Remote Sensing Satellites**" submitted by Mr. Venigalla Sambasiva Rao, ID No. 2006PHXF412 for award of Ph.D. Degree of the Institute, embodies original work done by him under my supervision.


Dr. Surendra Pal
Distinguished Scientist
Associate Director
ISRO Satellite Centre
Bangalore

Date: March 09, 2010.

Acknowledgements

I wish to place on record my deep sense of gratitude to my mentor and research supervisor Dr. Surendra Pal, Distinguished Scientist; Associate Director, ISRO Satellite centre and Program Director, Satellite Navigation Program, ISRO for his inspiring guidance throughout my career. Without his encouragement and prodigious suggestions, my Ph.D work would not have got started and taken shape. I am indebted to him for constant inspiration and guidance in completing my Ph.D work.

I am extremely grateful to Dr. K. Radhakrishnan, Chairman, ISRO and Dr. G. Madhavan Nair, Former Chairman, ISRO, Dr. T.K. Alex, Director, ISRO Satellite Centre, Dr. K.N. Shankara, Dr. P.S. Goel, former Directors of ISRO Satellite Centre for permitting me to carry out my research work at ISRO Satellite Centre and for their kind guidance.

I am immensely thankful to Prof. L. K. Maheshwari, Vice-Chancellor, BITS, Pilani for providing me this opportunity to pursue the off-campus PhD of the Institute. I express my gratitude to Prof. Ravi Prakash, Dean, Research and Consultancy Division (RCD), BITS, Pilani for his constant official support, encouragement and making the organization of my research work through the past few years easy.

I thank Dr. Hemanth Jadav, Mr. Dinesh Kumar, Ms. Monica Sharma, Mr. Sharad Shrivastava, Mr. Gunjan Soni, Mr. Amit Kumar and Ms. Sunita Bansal, nucleus members of RCD, BITS, Pilani, without whose cooperation and guidance it would not have been possible for me to pursue such goal oriented research during each of the past few semesters.

I also express my gratitude to the office staff of RCD whose secretarial assistance helped me in submitting the various evaluation documents in time and give pre-submission seminar smoothly.

I thank the Doctoral Advisory Committee (DAC) members, Prof.V.K. Choubey and Prof. Anu Gupta, who spared their valuable time to go through my draft thesis and were audience to my pre-submission seminar in order to provide several valuable suggestions that immensely helped in improving the quality of my PhD thesis report.

I am greatly thankful to Dean, Student Welfare Division and Dean Academic Registration & Counseling of BITS and their staff for their helpful support throughout.

I am obliged to Mr. P.K.Reddy former Scientist/Engineer, ISAC/ISRO, who inspired me with constant guidance and helped me in understanding antenna concepts and in designing and realizing spherical phased array.

I would like to express my sincere thanks and place on record the help and continuous support extended by Scientists/Engineers of Communication systems Group, ISAC/ISRO, particularly Mr. V.V.Srinivasan, Mr. Parimal Kumar, Ms. N.Ramalakshmi, Mr. Yogesh Prasad, Dr. D.V.Ramana, Mr. B.Pichaiah, Mr. M.Kumar, Mr. Senthil Kumar, Mr. V.Mahadevan (Group Director), Dr. V.K.Lakshmeesha (Outstanding Scientist & Ex-Group Director) and Ms. Satyavathi. Thanks are also due to Dr. P.K.Jain, Mr. K. Kamaraju, Mr. Suresh R Naik, Mr. Hanumantha Rayappa of ISRO Head Quarters, Mr. M. Satyanarayana, General Manager, NRSC, Mr. Nagachenchaiah, Director, SCL and Dr. A. Bhaskaranarayana, Ex. Director, SCPO/ ISRO Head Quarters for their suggestions and help in carrying out my Ph.D work.

I wish to express my grateful thanks to Prof. Balasubramanian, former Group Head, BITS, Pilani for his kind guidance to take up my Ph.D at BITS.

I am extremely grateful to Dr. T.C. Sarma, for encouraging me at all moments to carry out the Ph.D work with valuable suggestions and guidance at every stage.

Finally I am thankful to my family for their support and cooperation while I am on my Ph.D work.

V. Sambasiva Rao

ABSTRACT

The quest for improving resolution of the imageries from remote sensing satellites to less than a meter is necessitating transmission of higher data rates starting from a few Megabits to Gigabits/second. As data rates are increasing, consideration of spectrum and channel bandwidth has become more stringent to conserve spectrum and to assure optimum data transmission capability. This led to migration to higher frequency bands and search for a wide variety of techniques viz., frequency re-use, use of spectrally efficient modulation and source coding. New techniques are continuously explored for transmitting the increasing data in the limited Radio Frequency (RF) spectrum to provide a secured data transmission from satellites to the designated ground stations.

Transmitting systems are designed based on the Link estimates which help in understanding about the RF transmission power requirements, sizing of ground and onboard antenna systems, configuring the ground and onboard systems for desired data quality. Often, spectrum distortions, loss of RF link, and increased bit errors are noticed in high bit rate data transmission links of many Indian Remote Sensing (IRS) satellites. This work involves basic investigation of the high bit rate data transmission links to identify the causes for these effects including link performance degradation. Various parameters that effect RF performance of the high bit rate data transmission link are identified and their affect is studied to design a high bit rate data transmission system, with optimum utilization of the premium satellite power, for ensuring reliable Space to Earth data link. Suitable satellite data transmission system configurations are suggested for high bit rate data transmission.

The iso-flux antennas along with high power Traveling Wave Tube Amplifiers (TWTA), are commonly used for high bit rate data transmission from satellites. These antennas have wide beam width of about $\pm 60^\circ$ to $\pm 65^\circ$ (for spacecrafts in 500 to 800 Kms orbit), and radiate signals over entire visible area on ground that may be undesirable and also an inefficient way of onboard power utilization. This wide area antenna coverage sometimes poses a problem in applications that demand data transmission for a selected area or a ground station. The present work includes the study of alternate transmitting systems and reports the development of a novel spherical active phased array system that ensures the data transmission to intended ground stations efficiently.

TABLE OF CONTENTS

Abstract	iii
List of Tables	viii
List of figures	ix
List of Abbreviations	xiv
Chapter 1: Introduction.	1
1.1 Literature survey / Historical review	4
1.1.1 Remote sensing satellites	4
1.1.2 Data transmission from satellites	5
1.2 Regulations on spectrum usage and Power Flux Density(PFD)	8
1.2.1 Spectrum management	8
1.2.2 Power Flux Density (PFD)	9
1.3 Satellite link analysis	9
1.4 Scope of the present work	10
1.5 Organization of the thesis	12
Chapter 2 : System engineering and design considerations for remote sensing satellite systems.	15
2.1 Remote sensing satellite payloads	15
2.2 Passive sensors	16
2.2.1 Optical IR sensors	16
2.2.2 Data rate estimation for optical sensors	21
2.2.3 Remote sensing satellites with optical sensors	22
2.2.4 Passive microwave radiometer	25
2.3 Active microwave sensors	27
2.4 Satellites with scientific payloads	28
2.5 Data handling (formatting & Transmitting)	29
2.6 Frequency band for data transmission	30

2.7	Choice of modulation	31
2.7.1	Comparison of digital modulations	32
2.8	Transmitting system onboard remote sensing satellites	37
2.8.1	Data transmitting system	37
2.8.2	Transmitting antennas	39
2.8.3	Iso-flux antennas	39
2.8.4	High gain antennas	41
2.8.5	Active phased array antennas	41
2.8.6	Planar phased array antenna	42
2.8.7	Spherical phased array	44
2.8.8	Alternative schemes for high bit rate data transmission	48
Chapter 3: IRS data transmission and reception systems.		49
3.1	Data transmitting system	49
3.1.1	Compatibility with other missions	49
3.1.2	IRS data transmitting system configurations	49
3.1.3	Transmitting antennas	52
3.2	Data Reception Station (DRS)	55
3.2.1	Calibration	55
3.2.2	Local loop test system	55
3.2.3	Bore site transmission system	55
3.3	Issues effecting link performance	57
3.4	Characterization of receive chain	58
Chapter 4: Space to earth data transmission link considerations.		59
4.1	Effective Isotropic Radiated Power (EIRP)	61
4.2	Slant range and look angle	61
4.3	Free space loss	63
4.4	Losses other than path loss	64
4.5	G/T (Figure of merit of the ground station)	67
4.6	Estimation of C/No	70

4.7	Probability of error	70
4.8	Implementation margin	71
4.8.1	Degradation due to data quality	72
4.8.2	Degradation due to QPSK modulator parameters	73
4.8.3	Degradation due to AM/PM conversion	74
4.8.4	Degradation due to bandwidth limiting	75
4.8.5	Degradation due to interference	76
Chapter 5: Performance analysis of data transmission links of IRS missions.		77
5.1	IRS – P4 (Oceansat-1)	79
5.1.1	Suggestions for avoiding signal loss problem	86
5.2	IRS P6 (Resourcesat-1)	86
5.2.1	Suggestions to take care of the visible problematic observations in the spectrum	93
5.3	IRS P5 (Cartosat-1)	94
5.3.1	Mitigation techniques	101
5.4	Effects of high bit rate data on QPSK spectrum	103
5.5	Frequency reuse	113
5.6	Observations and recommendations	113
Chapter 6: Onboard high gain antenna systems with directional beams		116
6.1	Mission requirements	116
6.2	High gain antennas	118
6.2.1	Mechanically steered high gain antennas	119
6.3	Electronically steerable antenna	122
6.3.1	Spherical phased array	122
6.3.2	Design and analysis	124
6.3.3	Simulation	127
6.3.4	Spherical active array configuration	134
6.3.5	Simulation results	135
6.3.6	Element failure analysis	137

6.4	Phased array antenna configuration for Cartosat-2	138
6.4.1	Realization	142
6.4.2	Driver amplifier	145
6.4.3	Phased array electronics assembly	148
6.4.4	Radiating elements	155
6.4.5	Assembly and integration	159
6.4.6	Redundancy and Quality Assurance (QA) aspects	160
6.4.7	Test philosophy	160
6.5	Summary	169
6.6	Dual beam generation - concept	170
Chapter 7	Summary, Outcome of the present work and Specific contributions	176
7.1	Summary and outcome of the work	176
7.2	Specific contributions	178
Chapter 8	Scope for further studies	180
Chapter 9	References	182
Chapter 10	Annexures	201
A.	Flow chart for single beam generation – Cartosat-2A	201
B.	Determination of G/T	203
C.	Specific attenuation model for rain- Rec. ITU-R P.838-3	208
D.	Frequency allocation by ITU for space communication	216
Chapter 11	List of publications and presentations	218
Chapter 12	Biography	223
12.1	of V. Sambasiva Rao	223
12.2	of Dr. Surendra Pal (Mentor/Supervisor)	224

List of Tables

<u>Table No</u>	<u>Nomenclature</u>
Table 1.1	Indian Remote sensing satellites & Characteristics
Table 1.2	The power flux density Limits from space stations
Table 2.1	Comparison of different digital modulation systems
Table 2.2	Bandwidth efficiency on a main lobe spectrum of M-ary systems
Table 2.3	Comparison of PSK modulation schemes
Table 3.1	Link estimation for Resourcesat & Oceansat missions
Table 4.1	Comparison of G/T (Noise) with and with out Rain attenuation
Table 5.1	Degradation estimation due to carrier leakage
Table 5.2	IM products vs Input Back Off of 40 watts X-band TWTA
Table 6.1	Link Estimate for data transmission from IRS satellite in 600 Kms orbit
Table 6.2	Specifications of dual gimbal antenna of Chandrayaan
Table 6.3	Directivity for hemispheres of different radius – simulation results
Table 6.4	Directivity versus cone angle - simulation results
Table 6.5	Element distribution on hemisphere
Table 6.6	Element location and unit amplifiers distribution data
Table 6.7	Operating levels of various amplifier stages
Table 6.8	Power dissipation and junction temperature details
Table 6.9	Test results of amplifier-phase shifter assembly
Table 6.10	Specifications of radiating elements
Table 6.11	Directivity versus cone angle - simulation results

List of Figures

<u>Figure No</u>	<u>Nomenclature</u>
Fig. 1.1	Growth of satellite based remote sensing in India
Fig. 2.1	Classification of remote sensing payloads
Fig. 2.2	Push broom concept of remote imaging
Fig. 2.3	Schematic of optical sensors indicating resolutions
Fig. 2.4	Step and Stare imaging concept
Fig. 2.5	Photograph of IRS 1C/ 1D satellite
Fig. 2.6	IRS P6 (Resourcesat-1) satellite visualized in orbit
Fig. 2.7	Resourcesat-2 (IRS P6) ground coverage/scanning schematic
Fig. 2.8	Cartosat -1 (IRS P5) satellite visualized in orbit
Fig. 2.9	Oceansat-1 satellite
Fig. 2.10	Schematic of Data handling system of Remote Sensing Satellites
Fig. 2.11	BER probability for various digital modulations
Fig. 2.12	Bit Error Probability versus E_b/N_0 , for M-ary systems
Fig. 2.13	Block schematic of basic data transmitter
Fig. 2.14	Schematic showing satellite looks angles
Fig. 2.15	Path loss vs Elevation
Fig. 2.16	Coordinate system of an array grid
Fig. 2.17	Effective area of a planar array antenna
Fig. 2.18	Effective (Projected) area of a spherical antenna
Fig. 2.19	Normalized performance versus scan angle from zenith
Fig. 3.1	Frequency plan for two carrier data transmission
Fig. 3.2	Configuration of Data transmitting system
Fig. 3.3	Iso-flux antenna and it's radiation pattern
Fig. 3.4	Radiation pattern (co and cross polarizations) of iso-flux antenna
Fig. 3.5	AGC plot of IRS-1D X-band signal
Fig. 3.6	Block Diagram of Data Reception System

Fig. 4.1(a)	Typical satellite link
Fig. 4.1(b)	Satellite communication link configuration
Fig. 4.2	Satellite earth/orbit geometry
Fig. 4.3(a)	Satellite Range with respect to ground station antenna elevation
Fig. 4.3(b)	Path loss with respect to ground station antenna elevation
Fig. 4.3(c)	Satellite antenna look angle with respect to ground station antenna elevation
Fig. 4.4	Attenuation due to rain fall
Fig. 4.5.	Back Ground Radio Noise Spectrum
Fig. 4.6	Theoretical $P_e=f(E_b/N_o)$ performance of coherent BPSK/QPSK modems
Fig. 4.7	Degradation with rise time
Fig. 4.8	Degradation with data asymmetry
Fig. 4.9	Phaser diagram of QPSK signal
Fig. 4.10	Degradation due to Phase imbalance in QPSK modulation
Fig. 4.11	Degradation due to amplitude imbalance in QPSK modulation
Fig. 4.12	AM/PM characteristics of TWTA
Fig. 4.13	Bandwidth limiting degradation of QPSK signals
Fig. 4.14	Degradation due to interference
Fig. 5.1	A view of Data Reception Station
Fig. 5.2(a)	Noise Temperature with ground station antenna elevation
Fig. 5.2(b)	G/T vs Ground station antenna elevation angle
Fig. 5.3(a)	Noise temperature over full azimuth rotation of the antenna recorded on 15 th October 2008.
Fig. 5.3(b)	Noise temperature over full azimuth rotation of the antenna recorded on 16 th October, 2008.
Fig. 5.4	Noise temperature vs frequency for different elevations
Fig. 5.5	G/T of receiving station as measured at Shadnagar
Fig. 5.6	Measured Radiation pattern of onboard (IRS P4) iso-flux antenna
Fig. 5.7	QPSK spectrum with 1010... type data
Fig. 5.8	QPSK spectrum with PRBS data

Fig. 5.9	QPSK spectrums with 1MHz and 100 KHZ resolution bandwidth on spectrum analyzer
Fig. 5.10	QPSK spectrum at different instances
Fig. 5.11	QPSK spectrums with different length PRBS datas
Fig. 5.12	QPSK spectrum with good and poor quality data input
Fig. 5.13	Block schematic of data transmission system of IRS P5
Fig. 5.14	RF spectrum of two unfiltered two QPSK modulated carriers at the output of TWTA
Fig. 5.15	Spectrum of two QPSK modulated carriers with common filter at the output of TWTA
Fig. 5.16	Degradation due to interference
Fig. 5.17	Spectrum at the output of TWTA with two QPSK modulated and filtered carriers.
Fig. 5.18	Spectrum with additional common filter at the output of TWTA
Fig. 5.19	Power spectra (normalized) of conventional QPSK signal before and after filtering and amplifying
Fig. 5.20	Power spectra (normalized) of OQPSK signals before and after filtering and amplifying
Fig. 5.21	Spectrum of two QPSK carriers, with IM products and without filter, radiated by Active Phased Array Antenna
Fig. 5.22	Practically observed QPSK spectrum
Fig. 5.23	Typical ideal QPSK spectrum (simulated)
Fig. 5.24	Data pulses of finite rise/fall time
Fig. 5.25	Simulated spectrums with different equal rise/fall times of data
Fig. 5.26	Simulated spectrums for different un equal rise and fall times of data
Fig. 5.27	Simulated QPSK spectrum with increasing DC content in the data
Fig. 5.28	Phaser diagram of QPSK signal
Fig. 5.29	AGC plot of Oceansat-II.
Fig. 6.1	Co-ordinate system for high gain antenna
Fig. 6.2	Dual gimbal controlled paraboloid antenna
Fig. 6.3	Dual gimbal mounted planar phased array antenna of Cartosat-2

Fig. 6.4	Coordinate system for spherical array
Fig. 6.5	Simulated radiation patterns for different size hemispheres
Fig. 6.6	Directivity vs a/λ for different cone angles
Fig. 6.7	Simulated radiation patterns for different cone angles
Fig. 6.8	Conventional Spherical Array Configuration
Fig. 6.9	Element distribution on 175 mm dia hemisphere.
Fig. 6.10	Radiation patterns at different elevation angles
Fig. 6.11	Degradation of EIRP over elevation at a typical azimuth angle of 90° for one element failure
Fig. 6.12	Single beam spherical array with 64 elements and 16 unit amplifiers
Fig. 6.13	Simulated EIRP vs. Elevation angle
Fig. 6.14	Block schematic diagram of phased array antenna of Cartosat-2
Fig. 6.15	Element location on the hemisphere dome
Fig. 6.16	Schematic of Driver amplifier
Fig. 6.17	Photograph of the realized X-band driver amplifier
Fig. 6.18	Frequency response of X-band 2 watts driver amplifier
Fig. 6.19	Assembly of Phased Array electronics
Fig. 6.20	Layout of 16-way microstrip power divider
Fig. 6.21	Return loss response microstrip power divider
Fig. 6.22	Schematic of MMIC amplifier-phase shifter module
Fig. 6.23	Block schematic of beam steering electronics.
Fig. 6.24	Beam steering electronics package
Fig. 6.25	Assembly of the radiator (Helical antenna)
Fig. 6.26	Return loss response of the helical antenna
Fig. 6.27	Radiation pattern of helical antenna
Fig. 6.28	Axial ratio of the helical antenna
Fig. 6.29	Final Assembly of spherical X-band, 64 element phased array
Fig. 6.30	Radiation measurement set up
Fig. 6.31	Spherical phased array with and without Quartz wool blanket under radiation test in anechoic chamber
Fig. 6.32	Radiation patterns of single beam at different directions.

Fig. 6.33	Phased Array on Vibration Table
Fig. 6.34	Phased array mounted in a special fixture with receiving probes mounted in different directions
Fig. 6.35	Phased array being loaded into thermovacuum chamber
Fig. 6.36	EIRP, azimuth and elevation over a pass
Fig. 6.37	EIRP with frequency over a typical visible orbit
Fig. 6.38	Recorded spectrum of the signal received from Cartosat-2A
Fig. 6.39	AGC plot indicating signal strength of Cartosat -2 over a typical pass
Fig. 6.40	Dual beams from satellite in LEO orbit
Fig. 6.41	Directivity versus hemisphere radius (in Lambda)
Fig. 6.42	Hemi sphere showing common elements of two beams
Fig. 6.43	Simulated contours of two beams
Fig. 6.44	Schematic block diagram of spherical active phased array antenna generating dual beams

Abbreviations used in the text.

ACU	Antenna Control Unit
AGC	Automatic Gain Control
AIT	Assembly, Integration and Testing
AM	Amplitude Modulation
AOCE	Attitude and Orbit Control Electronics
AOS	Acquisition of satellite
ASK	Amplitude Shift Keying
AUT	Antenna Under Test
AWIFS	Advanced Wide Image Field Sensor
A_z	Azimuth
BCD	Binary Coded Decimal
BER	Bit Error Rate
BPF	Band Pass Filter
BPSK	Bi Phase Shift Keying
BW	Band Width
C/I	Carrier to Interference ration
C/N	Carrier to Noise Ratio
C/ N_o	Carrier to Noise density
CCD	Charge Coupled Device
dB	Decibel
dB/k	Decibel per Kelvin deg temperature
dBc	Decibel with respect to carrier level
dBm	Decibel with respect to milliwatt
dBw	Decibel with respect to watt
DC	Direct Current
Demod	Demodulator
DPSK	Differential Phase Shift Keying
DRS	Data Reception Station
E_b/N_o	Energy per bit to Noise density ratio
EIRP	Effective Isotropic Radiated Power
E_L	Elevation
EMC	Electro Magnetic Control
EMI	Electro Magnetic Interference
ERS	European Remote Sensing
Fig.	Figure
FM	Frequency Modulation
FOV	Field of View
FPGA	Field Programmable Gate Array
FSK	Frequency Shift Keying

G/T		Figure of Merit (Gain to Temperature ratio)
GaAs FET		Gallium Arsenide Field Effect Transistor
GHz		Giga Hertz
gms		Grams
GMSK		Gaussian Minimal Shift Keying
HPA		High Power Amplifier
HPBW		Half Power Beam Width
I/O		Input/Output
IF		Intermediate Frequency
IM		Inter Modulation
INSAT		Indian National Satellite
IRS		Indian Remote Sensing Satellite
ISAC		ISRO Satellite Centre
ISRO		Indian Space Research Organisation
ITU		International Telecommunication Union
KBPS		Kilo Bits Per Second
Kgs		Kilo grams
Kms		Kilo meters
LHC		Left Hand Circular
LISS		Linear Imaging Self scanning Sensor
LNA		Low Noise Amplifier
LO		Local Oscillator
LOS		Loss of Sight
MBPS	:	Mega Bits Per Second
MHz	:	Mega Hertz
MIC	:	Microwave Integrated Circuit
MMIC	:	Microwave Monolithic Integrated Circuit
Mod	:	Modulator
MPSK	:	M-ary Phase Shift Keying
MSK	:	Minimal Shift Keying
MSMR	:	Microwave Scatterometer
mtrs	:	Meters
NRSC	:	National Remote Sensing Centre
NRZL	:	Non Return to Zero reference Level
NRZS	:	Non Return to Zero reference Space
OCM	:	Ocean Color Monitor
OQPSK	:	Offset QPSK
PAA	:	Phased Array Antenna
PAN	:	Panchromatic
PFD	:	Power Flux Density
PL	:	Path Loss

PM	:	Phase Modulation
PRBS	:	Pseudo Random Bit Sequence
PROM	:	Programmable Read Only Memory
PSK	:	Phase Shift Keying
QA	:	Quality Assurance
QASK	:	Quadrature Amplitude Shift Keying
QPSK	:	Quadrature Phase Shift Keying
RAM	:	Random Access Memory
RF	:	Radio frequency
RHC	:	Right Hand Circular
RISAT	:	Radar Imaging Satellite
RS	:	Reid Solemn
Rx.	:	Receiver
SMA	:	Sub Miniature Assembly
SNR	:	Signal to Noise Ratio
SQPSK	:	Staggered QPSK
SROSS	:	Stretched Rohini Satellite series
SSPA	:	Solid State Power Amplifier
SSR	:	Solid State Recorder
T&E	:	Test and Evaluation
TC	:	Telecommand
TCXO	:	Temperature Compensated Crystal Oscillator
TFG	:	Teflon Fibre Glass
TM	:	Telemetry
TPG	:	Test Pattern Generator
TTL	:	Transistor Transistor Logic
TWTA	:	Traveling Wave Tube Amplifier
Tx.	:	Transmitter
UQPSK	:	Unbalanced QPSK
VCO	:	Voltage Controlled Oscillator
vs	:	Versus
VSWR	:	Voltage Standing Wave Ratio
WARC	:	World administrative Radio Conference
WIFS	:	Wide image Field Sensor

Chapter 1

INTRODUCTION

India operates and manages the largest remote sensing satellites constellation in the world today. With a host of payloads, the Indian earth observation system has been providing operational services to various users in India & abroad. Indian Remote Sensing (IRS) series of satellites have been planned with a view to provide necessary continuity of operational services in an assured manner for the land and water resources management; the cartographic and large scale mapping applications; and the ocean and atmospheric research areas. IRS satellites provide data in a variety of spatial, spectral and temporal resolutions. The data transmission requirement from IRS satellites has gone up from a few Kilo bits per second (KBPS) of first remote sensing satellite Bhaskara-1 to 640 Mega bits per second (MBPS) with Radar Imaging Satellite (RISAT). The quest for improving resolution of the imageries to less than a meter is necessitating transmission of higher data rates of hundreds of MBPS (Fig.1.1).

The detailed features of the Indian Remote Sensing satellites are given in Table.1. The data rates are progressively increasing due to an enormous amount of progress being made in imaging by satellites to improve ground pixel size resolution and spectral bandwidth resolution. This calls for constantly upgrading data transmitting capacity substantially, develop new techniques for meeting the requirements and provide a secured data transmission from satellites to the designated ground stations. The complexity of data transmission systems is also increasing proportionately.

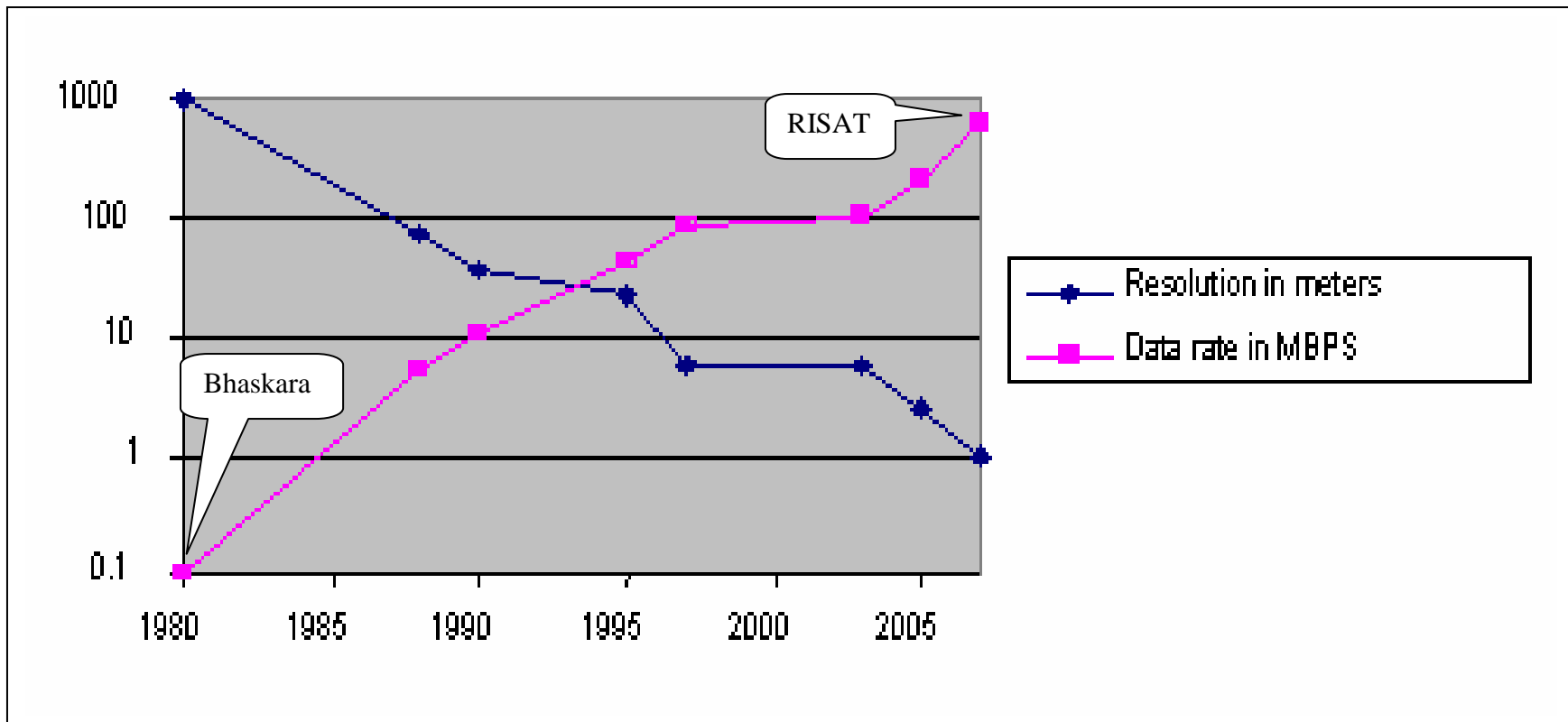


Fig. 1.1 Growth of satellite based remote sensing in India

Table 1.1 Indian Remote Sensing satellites & characteristics

Spacecraft	Type of payload	Orbit (kms)	Resolution(mtrs)	Swath (Kms)	Data rate (MBPS)	Freq. (MHz)	Modulation	Tx. EIRP-dBw
Bhaskara-I & II					0.001	VHF	FSK/PM	-10
IRS 1A & 1B	LISS-I	902	73	148	5.2	2217.6	BPSK	11
	LISS-II		36.5	145	20.8	8316	QPSK	18
IRS 1C & 1D	PAN LISS, WIFS	817	10	70	84.9	8150	QPSK	20
			23	141	42.45	8350	QPSK	20
IRS P2	LISS-IIA/B	817	37	128 (67+67)	20.8	8316	QPSK	15
IRS P3	WiFS MOS	817	188	810 192-200	5.2	2280	BPSK	10
Oceansat-1	OCM MSMR	720	360 -	1400	20.8	8316	QPSK	15
SROSS	MEOSS	520			10.4	2280	BPSK	10
TES	PAN	560	2.5		170	8150 8350	QPSK QPSK	+22
Resourcesat-1	LISS IV, LISS III AWIFS	817	5.8	70	105	8125	QPSK	20
			23.5	140	105	8300	QPSK	20
Cartosat-I	LISS LISS	630	<2.5		210	8125	QPSK	22
					8300	QPSK		
Cartosat-II, IIA, IIB	LISS	630	<1		105	8125	QPSK	19
IMS-1	LISS	620	36	151	8.0	2280	BPSK	10
Chandrayan-1	TMC & HySI		5		16.4	8414	QPSK	27
Oceansat-2	OCM Scatterometer	720	360 4-24 m/s	1400 H(IB) V(OB)	21.25 21.25	8300	QPSK	15
Resourcesat-1	LISS IV, LISS III AWIFS	817	5.8	70	105	8125	QPSK	20
			23.5	140	105	8300	QPSK	20
RISAT-1	SAR	600			640	8212.5	QPSK	26
Astrosat	X-ray, Astronomy	800	-	-	210	8125 8300	QPSK QPSK	22

1.1 Literature survey / Historical review

1.1.1 Remote sensing satellites:

Since the launch of first satellite Sputnik-I in 1957 by Soviet Union[1] followed by Explorer-I (Satellite 1958 Alpha) by United States[2], thousands of satellites have been sent into space on missions to collect data about the Earth.

Remote sensing began in the United States and France. The first satellite to be used for Earth observation purposes was Explorer VII [3], launched in October 1959. By the early 1980s, with the launch of Landsat-4, the era of space based remote sensing system started [4, 5]. NASA launched SeaSat, an ocean observation satellite with a synthetic aperture radar, or SAR [6] in 1978, the Soviet Union launched a similar series of satellites known as Okean. Later, during the late 1980s, the Soviet Union orbited several large radar satellites. In 1991 the Soviet Union launched Almaz-1, which although was part of this series [7], is the first one that the Soviet government openly acknowledged. SPOT (a French acronym for Preoperational Earth Observation System) satellite program of French Space Agency, (Centre National d'Etudes Spaciales CNES) has launched five satellites since 1986 [8]. Latest in the series, SPOT-5 which was launched on 4th May 2002, is an improved version as compared to the first four SPOT satellites and ensures service continuity. On 17 July 1991 the European Space Agency launched ERS-1 into a Sun-synchronous, polar orbit at an altitude of about 780 km, followed by ERS-2 in 1995 [9-11]. Japan has launched many remote sensing satellites and contributed most profoundly to global remote sensing [12, 13]. Japan is now operating 3 earth observation satellites, i. e. MOS-1 (Marine Observation Satellite-1, Momo-1 in Japanese), EGS (Experimental Geodetic Satellite, Ajisai in Japanese) and GMS (Geostationary Meteorological Satellite, Himawari in Japanese) [14, 15]. Japan's Earth Observation Satellites include GMS series, MOS-1/1b, JERS-1, ADEOS, TRMM and follow-on ADEOS (ADEOS-II, etc). GMS-4, MOS-1/1b are in service. China too joined in building remote sensing satellites [16-18]. Radarsat-1, an active microwave remote sensing system [19] was launched by the Canadian Space Agency in November 1995.

India has built over the years a strong earth observation programme comprising space borne, air borne and in-situe observation infrastructure. Indian Remote Sensing program received impetus with the launch of its first operational remote sensing spacecraft IRS-1A in 1988. Currently, it has the largest constellation of remote sensing satellites providing observations over land, ocean and atmosphere with assured continuity of services.

The earlier IRS series [20, 21] of satellites (IRS-1A, IRS-1B, IRS-1C, IRS-1D, Resourcesat-1, etc.) carried optical cameras viz., Linear Imaging Self Scanning (LISS)-I, II, III, IV, Wide Field Sensor (WiFS) & Panchromatic (PAN), designed predominantly to meet the needs of land-based applications. IRS-P4 (Oceansat-1) was the first Indian satellite envisaged to meet the data requirements of the oceanographic community [22]. Recently launched satellite Oceansat-II will be providing the continuity of Oceansat-I services with Ocean Color Monitor (OCM) payload. It also carries a scatterometer for measuring ocean surface winds and a ROSA payload for finding Radio Occultation.

In the science program front, India had placed a satellite Chandrayaan-1 [23-25] in moon orbit on 22 October 2008 and is planning to launch two more scientific satellites Meghatropiques [26] and Astrosat [27], a multi-wavelength astronomy satellite, in 2010. Many more satellites are planned to provide earth imageries with centimeters resolution (Cartosat – 3 series) and microwave remote sensing with RISAT-II and RISAT-I.

The data to be transmitted to ground by all the IRS satellites is growing with each mission.

1.1.2 Data transmission from satellites:

Technology for the transmission of data from satellites has changed drastically since the launch of Sputnik-1. While Sputnik-1 satellite transmitted continuously two radio signals at frequencies of 20.005 MHz and 40.002 MHz in the form of telegraph pulses of about 0.3 second's duration [1], current remote sensing satellites are transmitting hundreds of MBPS data with advanced transmission techniques.

Technology for high bit rate data transmission has advanced multifold to transmit very high bit rate data [28-31]. Performance analysis for channel impairments that affect the service quality of a high data rate satellite communication system are discussed by various authors [32, 33].

RF frequency and available channel bandwidth, data rate, modulation and Figure of Merit of ground stations play a major role in configuring data transmission system for a satellite. Exhaustive work on high bit rate data transmission has been done by various academic and research institutes and many authors published books [34-41]. Many authors reported their research work on modulation techniques [42-44], interference studies to assess bit error rate performance [45-48]. Up to now, telemetry systems for earth observation satellites have relied on Quadrature Phase Shift Keying (QPSK) modulation. A feasibility study of adaptive modulation techniques for small satellite communications [49] is discussed by Sasada, T., Shirakura, & Yajima, M. M. in 2004.

Low Earth Orbit (LEO) satellite based remote sensing systems, are often built as mono-satellites with limited on-board memory and with mono-ground station. To virtually increase this visibility time or alternatively improve the throughput during this time, several techniques have to be addressed. The Tracking and Data Relay Satellite System (TDRSS) provides a flexible communications system for low-earth-orbit spacecraft [50]. Central to the TDRSS ground terminal is the integrated receiver which provides data demodulation, decoding, and deinterleaving over the range of 100 bits/second to 12 MBPS, and all the tracking services in a single high-performance design. The requirements and design of the integrated receiver (IR), as well as an Unbalanced Quadri Phase Shift Keying (UQPSK) receiver/demodulator were developed for use in the TDRSS [51]. The need to increase data-rate capabilities of the TDRSS has prompted NASA researchers to investigate bandwidth-efficient modulation schemes [52, 53]. Based upon current technology the most promising scheme is Trellis-Coded Modulation (TCM) operating with Octal Phase Shift Keying (8 PSK). Alcatel has developed, in co-operation with CNES, a new telemetry system based on trellis-coded 8PSK modulation

[54], offering a 622 Mbps download capability in the X band (8025-8400 MHz). Pulse shaping is examined as a means to improve the performance of a differential Offset Quadrature Phase Shift Keying (OQPSK) system in a bandwidth-constrained environment [55]. ISRO adopted Binary Phase Shift Keying (BPSK) & Quadrature Phase Shift Keying (QPSK) modulation techniques for data transmission in all its IRS missions [56, 57].

For data transmission from remote sensing satellites, wide beam, iso-flux antennas are commonly used. The antenna radiation (gain) pattern of these antennas is shaped to compensate the path loss variation. Various transmitting antennas, viz., shaped beam antennas for having constant signal at receiving station are dealt in detail by various authors [58-62].

Secure and efficient way of data transmission is made possible through high gain narrow beam antennas. These antennas need to be steered. Mechanical steering of dual gimbal mounted parabolic reflector or sub-reflector [63] and phased array antennas are explored and used in some missions. Weerackody and Gonzalez [64] presented the performance of satellite communication with antenna pointing errors in IEEE conference on Military Communications held in 2006.

Phased array antenna concepts are explored by various authors so far [65-75]. Phased array technology is also extended for multi band [76-78] and multi beam [79] generation. Reconfiguration and steering of the beams is obtained by various techniques of beam forming in active phased arrays [80 to 93]. Miniaturization of phase shifters advent of MMICs and high speed switching devices have made it possible to realize onboard light weight phased arrays. Phased arrays used for satellite communication applications are presented by quite a few authors [94-108]. Degradation of planar phased arrays due to wide scan angle is studied by different authors [109-111]. Alternate antenna systems are explored to cover a wide angular region of space, typically wider than that can be realized with one planar array antenna. There are a few phased array options available for hemispherical coverage. The Electronic beam steering over hemispherical coverage can be realized with multiple planar arrays, cylindrical, conical, or spherical arrays. Spherical

phased arrays made of number of planar arrays are considered to overcome wide scan angle issues for different applications [112-120].

Microwave components viz., phase shifters, MMIC amplifier units, which are required for steering the beam in phased arrays are exhaustively covered in literature [121-29]. Testing and performance evaluation is carried out by various authors [130 to 134]. Calibration, pattern prediction was also carried out in detail [135-138].

Exhaustive studies have been conducted to understand inter modulation and interference effects in communication links [139-142]. Various simulation techniques were developed by different authors for realizing and analyzing the performance of phased arrays [143-156].

1.2 Regulations on spectrum usage and Power Flux Density(PFD)

1.2.1 Spectrum management:

Spectrum management is an important activity that facilitates the orderly use of the electromagnetic frequency spectrum not only for satellite communications but for other telecommunications applications as well. This is done under the auspices of the International Telecommunication Union (ITU), which is a specialized agency of the United Nations (UN). The ITU has developed rules and guidelines called radio regulations [157-159] at a series of international radio conferences. The Radio Regulations incorporate the decisions of the World Radio communication Conferences, including all Appendices, Resolutions, Recommendations and ITU-R Recommendations incorporated by reference. The frequency bands allocated for space to earth data transmission by ITU as article 5 of Radio Regulations along with ITU recommendation references are given below:

S-band	- 20 MHz (in 2200 to 2290 MHz band in coordination with other users)	--- ITU-R: SA-1154
X-band	- 375 MHz (8025 to 8400 MHz)	--- ITU-R: SA-1277
Ka band	- 1500 MHz (25,500 to 27,000 MHz)	--- ITU-R: SA-1278

Annexure D provides list of frequency bands allotted by ITU for satellite communication. Of course, these frequency bands are not limited, but can extend to other bands with proper coordination in specific areas.

Recent efforts for the exploitation of even higher frequency bands as a valuable alternative to conventional spectrum portions [160] will go a long way to address the need for increase in transmission bit rates.

1.2.2 Power Flux Density:

Besides spectrum restrictions, space to earth PFD regulations are also in force. ITU as per article 21-4 of Radio regulations puts a limit on the PFD for space to earth radio frequency transmissions for all conditions and for all methods of modulation. This shall not exceed the limit given in the Table 1.2 as per radio regulations.

Table 1.2 The power flux density Limits from space stations:

Frequency band	Service	Limit in dB(W/m ²) for angle of arrival (δ) above the horizontal plane			Reference bandwidth
		0°-5°	5°-25°	25°-90°	
2200-2300 MHz	Earth Exploration satellite (space to earth)	-154	-154+0.5(δ -5)	-144	4 KHz
8025-8500 MHz	-do-	-150	-150+0.5(δ -5)	-140	4 KHz
25.25-27.5 GHz	-do-	-115	-115+0.5(δ -5)	-105	1 MHz

1.3 Satellite link analysis

Quite a few authors discussed satellite link budget analysis [161-163]. Sidney Skje, a professional engineer has described how a Fishbone Diagram [164] can be used to identify problems with satellite link performance in April/May 2005 issue of The Orbiter. Many rain attenuation studies are reported based on the data collected from the temperate

regions [165-171]. Quite a good amount of research work has been carried out by many scientists/engineers on G/T measurements [172-175] which is the figure of merit of a ground station.

1.4 Scope of the present work

Although data transmission from space to earth is prevalent for almost three decades, satellite data transmission system has been neither systematically studied nor documented. Satellite transmission link design is satellite specific and unique in requirements. Trade off among size, weight, onboard power requirements, complexity of the system design and the cost is essential for configuring a satellite data transmission system which was hardly addressed by anyone.

Various factors limit the transmission of data from satellites and the design of the system becomes more complex with the increase in data rates. As data rates are increasing, conservation of spectrum and channel bandwidth has become more important to assure optimum data transmission capability. This led to the search for a wide variety of techniques viz., new allocation of higher frequencies, frequency re-use, use of spectrally efficient modulation techniques, and optimum transmission techniques. The study of the implications in implementing the new techniques and their effects on satellite data transmission link performance has become essential which forms the part of the present work.

IRS satellite data transmission systems are basically configured to have reliable RF link with the ground station situated at National Remote Sensing Centre (NRSC) at Shadnagar near Hyderabad. In order to accommodate the known performance deviations and also unknown effects of various parameters in the RF link chain, onboard power is suitably increased to provide comfortable system margins (> 6 to 8 dB) for receiving the data with acceptable Bit Error Rate (BER). Spectrum distortions, loss of RF link, and increased bit errors are noticed in the high bit rate data transmission links of many IRS satellites in various testing and operating phases.

It has become pertinent to investigate the high bit rate data transmission links to ensure optimum utilization of satellite power, which is always at premium for any satellite. Conventionally, shaped beam antennas are used for transmitting the data from the satellite. These antennas are designed to provide radiation pattern to ensure constant signal (iso-flux) at ground station during the satellite visible period. These iso-flux antennas radiate signals over entire visible area on ground that is rather an inefficient way of onboard power utilization. This also prohibits the applications that demand selective coverage on ground on account of data reception only on a selected region or location.

There is, hence, a need to investigate alternate transmission techniques to address these issues.

The scope of the present investigation involves:

- i. The study of high bit rate data transmission systems of remote sensing satellites, and identifying the parameters that affect the RF performance of the transmission link and suggesting suitable solutions to obtain a suitable configuration.
- ii. Analysis of the problems and anomalies reported with some of the IRS satellite missions as case studies and suggesting mitigation techniques.
- iii. Study of mechanically and electronically steerable high gain antennas that provides solution to the problems associated with iso-flux antennas, conventionally flown onboard IRS satellites. **The work covers the design, simulation, realization/fabrication, calibration and testing of the X-band active spherical phased array antenna system for IRS satellites.** The investigation also involves the development of new concepts for generating two beams from spherical phased array to transmit data from satellite to two designated ground stations simultaneously and realization of the antenna system practically.

1.5 Organization of the thesis:

Chapter 1: Introduction:

Back ground for the research work along with the literature survey carried out for better understanding of the concepts of data transmission techniques, regulations on spectrum usage, power flux density and link analysis are provided here. Subsequent chapters describe the relevant theory and present research work.

Chapter 2: System engineering and design considerations for remote sensing satellite systems:

Overview of the payloads of different types of remote sensing satellites is provided. Analysis of data rate estimation is dealt with. Selection of suitable modulation techniques to enable efficient transmission of high bit rate data, selection of frequency band of operation are also covered. A typical configuration of the onboard payload system emphasizing high bit rate data transmitter and data transmitting antennas are also addressed.

Chapter 3: Data transmission and reception systems of IRS missions

Onboard high bit rate data transmitting system configurations along with transmitting antennas adopted for IRS missions is explained. The configuration of a typical remote sensing satellite data reception station, receive system characterization and limitations of tracking systems are also briefly addressed.

Chapter 4: Space to earth data transmission link considerations

Here, the space to earth data transmission link considerations are presented. Parasitic elements affect QPSK spectrum as data rate increases and degrades the link performance. Detailed study on these phenomena has been carried out. Degradation to be accounted for link performance is brought out.

Chapter 5: Performance analysis of data transmission links of IRS missions.

Performance of data transmission links of IRS missions are studied and detailed. Performance deviations and anomalies observed in different IRS satellites are taken as **case studies**. Causes for deviations and performance degradation are discussed and appropriate mitigation techniques are recommended to overcome some of the effects.

Chapter 6: Onboard antenna systems with directional beams for remote sensing satellites:

Study of new type of directional transmitting antenna systems for secured data transmission only to the intended ground station has been carried out and presented. The antenna system considered is mechanically and electronically steerable antennas. The concept of spherical phased array adopted is explained with Matlab simulations to optimize the performance. Simulated results are presented. Design, fabrication, calibration and testing along with reliability advantages are explained. Test results are provided. The concept for generating dual beams from spherical phased array is also presented,

Chapter 7: The total outcome of the present study, investigation and development work is presented. The specific contributions made through the present work are presented.

Chapter 8: Scope for further studies is identified.

References: List of the references used during the study is provided.

Annexure A: Flow charts developed for the design of phased array antenna system for single beam generation is provided.

Annexure B: G/T measurement procedure is provided.

Annexure C: An ITU reference model for Rain attenuation is provided

List of publications and presentations made by the candidate are given subsequently.
Finally, brief biography of the candidate and supervisor are also included.

Chapter 2

System engineering and design considerations for remote sensing satellite systems

The present work is intended for investigations in the space to earth links of the remote sensing satellites for high bit rate data transmission & for completeness sake the concepts of system engineering and design considerations for remote sensing satellite systems along with basic concepts of data rate estimation are also presented. Various digital modulations are compared and selection of modulation for high bit rate data transmission is explained. A typical configuration for payload data transmitting system along with antenna systems & limitations of the conventionally used is-flux antenna are explained. Alternate suitable antennas are also discussed. Advantages and limitations of high gain antennas along with Phased array antenna concepts are addressed

2.1 Remote sensing satellite payloads:

Payloads for earth observation are mainly for remote sensing or weather monitoring. The instruments are usually passive detectors or radiometers capable of imaging in visual, Infra-Red (IR) and microwave band as in Landsat of US, SPOT of France, Quickbird of US, ISRO's IRS 1A/1B/1C/1D/P5/P6 etc., or active detectors like Scatterometers, LIDAR or Synthetic Aperture Radar (SAR) as in Canada's Radarsat & ISRO's RISAT.

Remote sensing in general involves measurement of spectral features of the energy radiated and/or reflected by earth's surface and atmosphere for subsequent analysis and earth resource management. Satellite based remote sensing has the unique advantage of repetitive and global coverage of earth terrain from an overhead perspective. The sensors used for remote sensing can be classified as shown in Fig. 2.1.

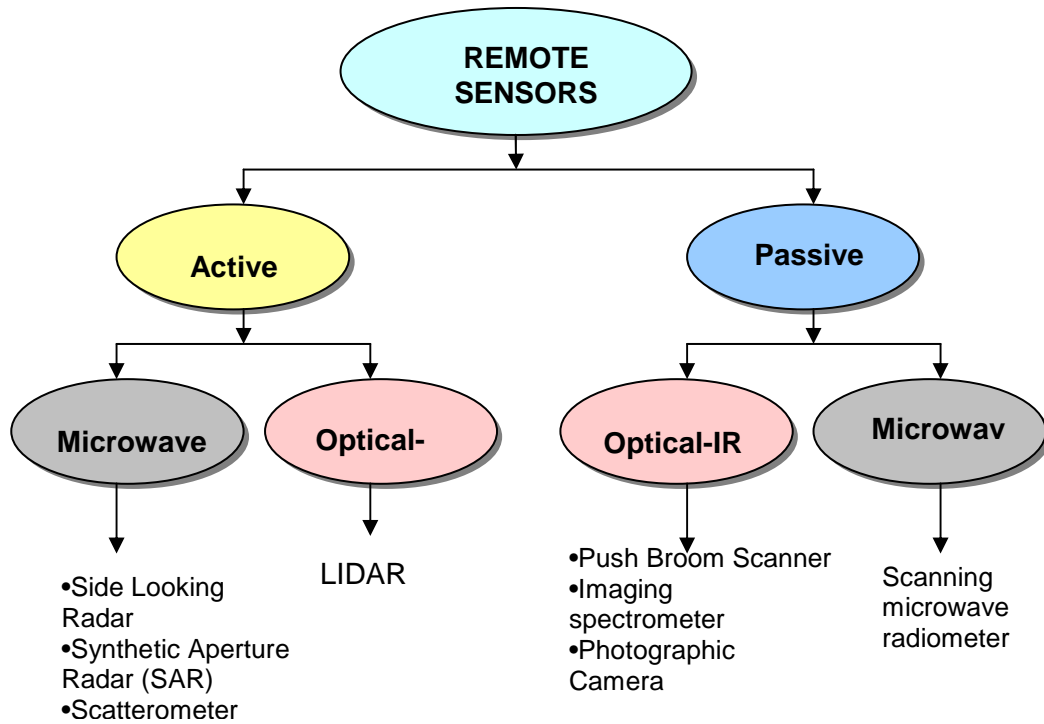


Fig. 2.1 Classification of remote sensing payloads.

The passive sensors detect radiation from the target (earth) that is naturally reflected or emitted by them. The active sensors on the other hand, are the ones that produce their own radiation to irradiate the target object, and then receive the back scattered radiation. Unlike passive sensors which depend on external illumination condition by sun, active sensors can operate on any time of the day. The sensors can be further divided in microwave and optical infrared category according to the wavelength of operation, because their technologies differ widely.

2.2 Passive sensors:

2.2.1 Optical IR sensors:

The satellite platforms which carry passive sensors [184] in Optical-Infra Red (OIR) are to be maintained in circular polar sun-synchronous orbits. For sun synchronous orbits, the orbital plane regresses at a rate exactly equal to the sun's apparent motion around the earth. Thus the angle between the sun-earth line and the orbital plane remains nearly fixed and the satellite crosses any given latitude under the same back ground solar illumination condition. This greatly facilitates the comparison of images of a given target area taken at successive satellite revisit.

A payload operating in OIR region, in general, consists of a collecting optics to focus the incoming radiation, a spectral dispersing system (for multi-spectral imagers), a detector, an associated processing electronics and an in-flight calibration system. Presently, most of the imaging payloads for optical remote sensing make use of Push Broom Scanning technique using linear array of Charge Coupled Devices (CCD) as imaging detectors. The linear array placed on the focal plane of the camera optics captures a strip of earth terrain instantaneously and successive lines of the image are produced as result of satellite's forward motion. Push broom concept of remote sensing with Linear Imaging Self-scanning Sensors (LISS) is shown in Fig. 2.2.

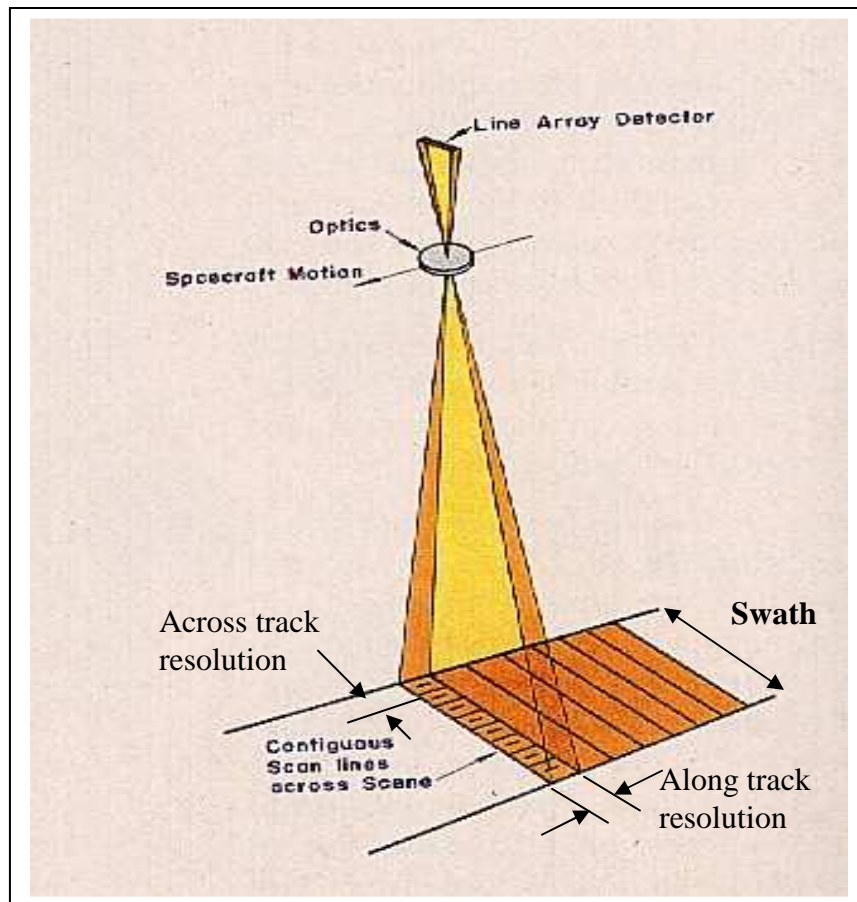


Fig. 2.2 Push broom concept of remote imaging

Each detector array provides data in a single spectral band visible and near IR region. Refractive type of collecting optics with spectral selection by appropriate filters is used

for each of the spectral bands of LISS imaging sensors in the satellite. In CCD operation, signal charge is accumulated in a potential well and transferred to a charge shift register. The register collects charges from all connected pixels and transfers the charges sequentially. The charge is transferred from one well to another like a packet, towards the output section with out being mixed with any other pixel charges.

- **Spatial resolution**

The ability of a sensor to image two closely spaced objects so that they can be distinguished in the image is quantified in terms of spatial resolution. For an array of detector elements (like linear array CCD), spatial resolution is related to the projection of an element (pixel) projected on ground. The angle (in radian) subtended on ground by a single detector is called Instantaneous Field of View (IFOV). Instantaneous Geometric Field of View (IGFOV) is the geometric projection of the IFOV on ground (Refer Fig. 2.3).

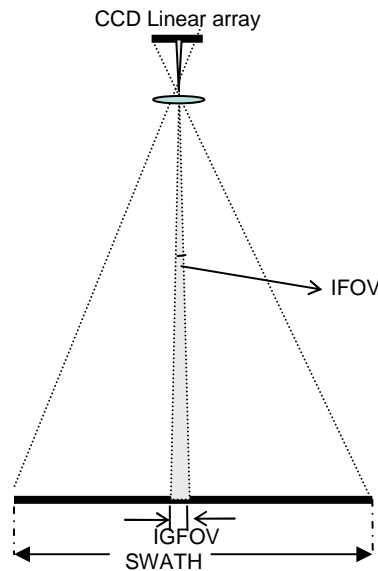


Fig. 2.3 Schematic of optical sensors indicating resolutions

IGFOV can be calculated by equation 1.

$$\text{IGFOV} = w \cdot h / f \quad \text{---- (1)}$$

Where w : is the dimension of the detector (length of a square pixel)

F : is the focal length of the optics

h : is the altitude of the spacecraft platform from ground.

High spatial resolution imagery inherently requires smaller IFOV. However, this results in considerable reduction in signal strength. Hence, the signal to noise (S/N) ratio will not be adequate, even for current state-of-the art CCD detectors unless the aperture size of the telescope is greatly increased. Currently, two techniques are used to get high resolution images with CCD, namely Time Delay and Integration (TDI) and Step and Stare (SNS) mode imaging. Both results in an effective increase of dwell time to achieve the desired S/N ratio.

- **Time Delay Integration**

For high resolution cameras with sub-meter resolution, swath needs to be large. Hence linear detectors with long arrays are required. Such cameras have small integration time leading to poor signal to noise ratio (SNR). Time delay integrating (TDI) detectors are developed to overcome this limitation. TDI technique enables integration of charges collected from the same objects through multiple lines positioned along track. These detectors have 2-dimensional arrays instead of a single linear array as in conventional push broom detectors. In TDI mode, shift resistors are used to shift charge in both vertical and horizontal directions. Here the linear arrays of the detector are spaced one integration time apart, so that succeeding rows of pixels view the same spot. The charges transferred sequentially in vertical direction are added with previous charges. TDI mode synchronizes this vertical transfer timing with object motion, so that signal charges integrated a number of times equal to number of vertical stages of the CCD pixels. The accumulation of charge (integration) for the same strip results in overall increase in SNR; because the signals add coherently while noise addition is incoherent. These summed signals are shifted out to readout amplifier through horizontal shift resistors. This technique is used in IKONOS satellite [177].

The final signals are converted to digital PCM stream data through precision Analog to Digital Converters (ADC). Number of streams of data are multiplexed and formatted to two high data rate streams and fed into I and Q channels of Quadri Phase Shift Keying (QPSK) modulator and transmitted to ground in X-band.

- **Step and stare imaging** [178]:

Under conventional push-broom imaging, the optical axis of the camera is aligned with the yaw axis and hence points towards the sub-satellite point along the radius vector joining satellite to the earth's center. However, for the same integration time of the CCD, the dwell time can be increased by reducing the spacecraft ground track velocity (Refer Fig. 2.4) . This kind of effective ground track velocity reduction can be done by tilting the optical axis such that its projection on ground always moves in a direction opposite with respect to sub-satellite velocity vector; hence this calls for appropriate orientation and angular rate control on the platform.

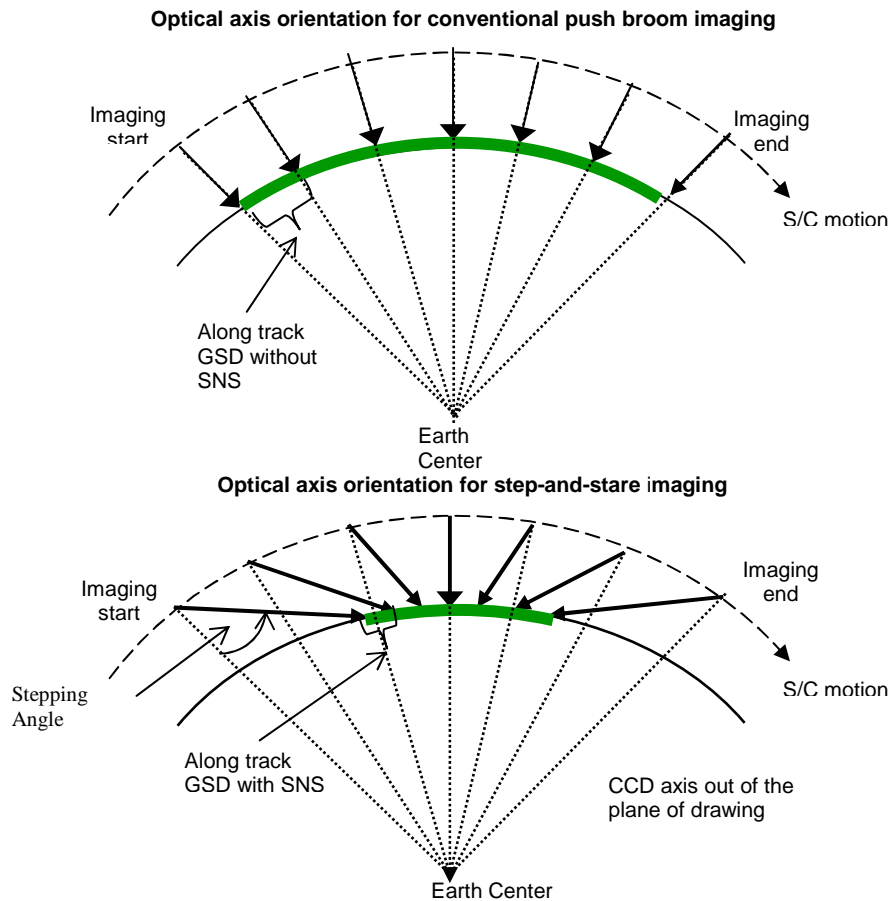


Fig. 2.4 Step and stare imaging concept

The strip is imaged for a duration which is more than that would have been done for conventional nadir imaging; hence the expression “staring” is used. An attitude bias is

imparted to make the optical axis “look ahead” of sub satellite point in order to obtain optimal coverage. This is called stepping effective ground velocity reduction by step and stare and used in a remote sensing satellite to improve resolution. Cartosat-2 [178] makes use of the same technique to achieve sub meter resolution imagery.

2.2.2 Data rate estimation for optical sensors:

The data rate depends on the resolution of the imagery, swath of the imagery and the type of payload used for imaging purpose, and the data handling system. A typical example for estimating data rate to be transmitted from satellite is explained below:

A remote sensing satellite in about 800 kms orbit carrying Linear Image Scanning Sensor (LISS) camera working on push broom concept (Fig.2.2) is taken as an example to estimate data rate to be transmitted from the spacecraft. The optical camera onboard satellite focuses **140 kms** width of image (called **swath**) on to a **CCD detector** having **6000 pixels**.

Number of pixels and swath decide across track resolution.

Across track resolution = Swath ÷ no. of pixels

i.e. : 140 kms/6000 ≈ **23 meters**.

Time per one scan decides the along track resolution. For the required resolution, scan time is calculated:

Along track resolution required : 36 meters. (for example)

Ground track velocity : 7.2 kms/sec (for 600 kms orbit)

The time required for one scan : along track resolution ÷ ground track velocity

i.e. : 36/7.2kms = **5 milliseconds**

The CCD output is converted to digital bits using Analog to Digital converter.

Quantization levels of ADC : 10 bit.

Total data in one scan : no. of pixels * quantization levels

i.e. : 6000*10 = **60,000 bits**.

This data has to be transmitted in one scan time of 5 milliseconds

The data rate to be transmitted : $60,000/5*10^{-3} = \mathbf{12\ MBPS}$.

For step and stare imaging same procedure is followed except that the ground track velocity is slower than push broom technique.

2.2.3 Remote sensing satellites with optical sensors:

- **IRS 1A/1B satellites:**

In the area of Satellite based remote sensing in the past, the first generation satellite IRS-1A and 1B [20] were designed, developed and launched successfully during 1988 and 1991 with multi-spectral cameras (LISS-1 and LISS-2) with spatial resolution of 72.5 m and 36 m. respectively. While the LISS-1 payload data (5.2 MBPS) is transmitted with BPSK modulation on S-band carrier, the LISS-2 payload data (20.8MBPS) is transmitted on X-band carrier with QPSK modulation [56,186,187].

- **IRS 1C/1D satellites**

Subsequently, the second generation remote sensing satellites IRS-1C [21] and 1D (Fig.2.5) with improved spatial resolutions of 70 meters in multi-spectral and 5.8 meters in Panchromatic bands and a wide field sensor with 188 meters resolution and 800 Km. swath, have been developed and successfully launched in 1995 and 1997 respectively.



Fig.2.5 Photograph of IRS 1C/ 1D satellite

These satellites have become the principal components in the National Natural Resource Management System(NNRMS) and the data was used in various

applications, viz., agriculture and soil, land form and land use studies, water resource, forestry, drought and flood monitoring, cartography, town planning and coastal zone monitoring.. LISS data of 42.5 MBPS and PAN data of 85 MBPS are transmitted on two X-band Carriers (8150 and 8300 MHz) with QPSK modulation [57, 185,188].

- **Resourcesat satellites**

Resourcesat-1 (also known as IRS-P6) is an advanced remote sensing satellite built by ISRO and launched in October 2003 into 817 kms orbit. The tenth satellite of ISRO in IRS series, IRS P6 (Fig.2.6) is intended to continue the remote sensing data services provided by IRS-1C and IRS-1D, both of which have far outlived their designed mission lives.



Fig. 2.6 IRS P6 (Resourcesat-1) satellite visualized in orbit

IRS P6 carries three cameras similar to those of IRS-1C and IRS-1D but with vastly improved spatial resolutions - a high resolution Linear Imaging Self Scanner (LISS-4) operating in three spectral bands in the Visible and Near Infrared Region (VNIR) with 5.8 metre spatial resolution and steerable up to 26 degrees across track to obtain stereoscopic imagery and achieve five day revisit capability; a medium resolution LISS-3 operating in three spectral bands in VNIR and one in Short Wave Infrared (SWIR) band with 23.5 metre spatial resolution; and an Advanced Wide Field Sensor

(AWiFS) operating in three spectral bands in VNIR and one band in SWIR with 56 metre spatial resolution. Fig.2.7 shows the imaging details of Resourcesat-1.

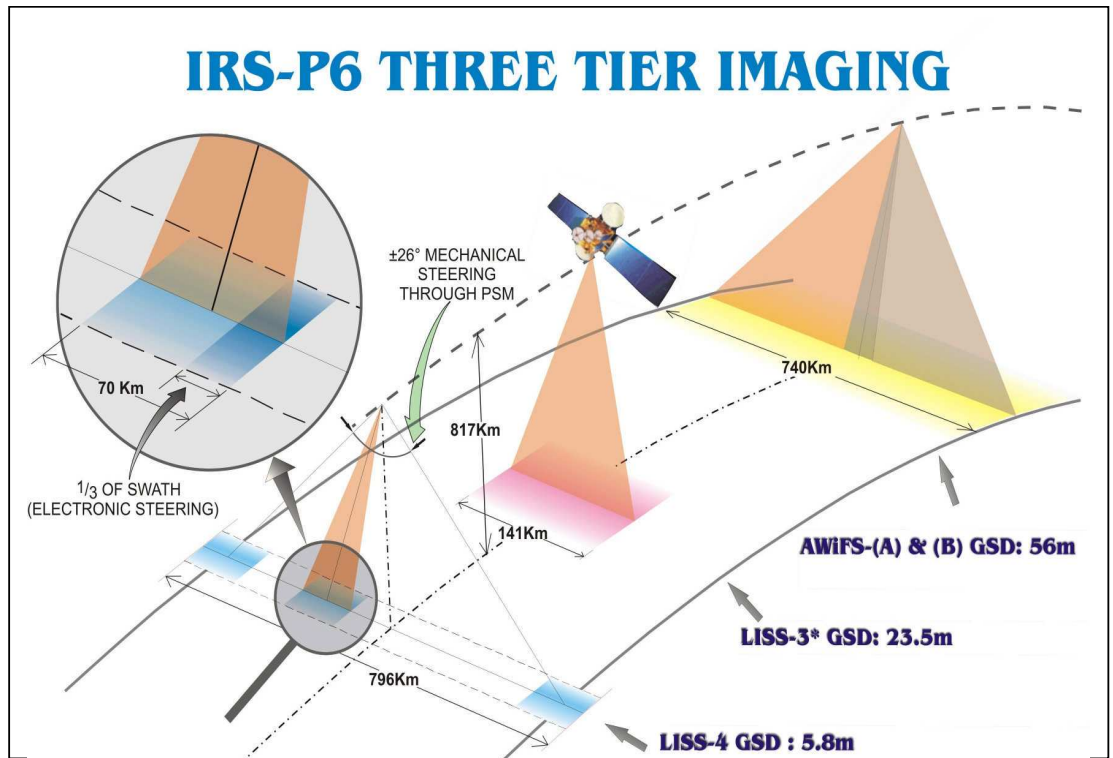


Fig. 2.7 Resourcesat-2 (IRS P6) ground coverage/scanning schematic

IRS P6 also carries a solid state recorder with a capacity of 120 Giga Bits to store the images taken by its cameras and read out later to the ground stations. Two X-band carriers (8125 and 8300 MHz) transmit 105 MBPS on each carrier with QPSK modulation.

- **Cartosat-1 satellite [189]:**

With the above scenario, India has a lead in the civilian remote sensing field in the world not only in terms of realization and launching of complex satellites with high, medium and coarse resolution cameras, but also in the application areas as well. In order to maintain this lead and also to provide continuity of data to global users, Cartosat-1 (Fig. 2.8) with two (fore and aft) PAN cameras, mainly intended for

cartographic applications, was launched in 2005.

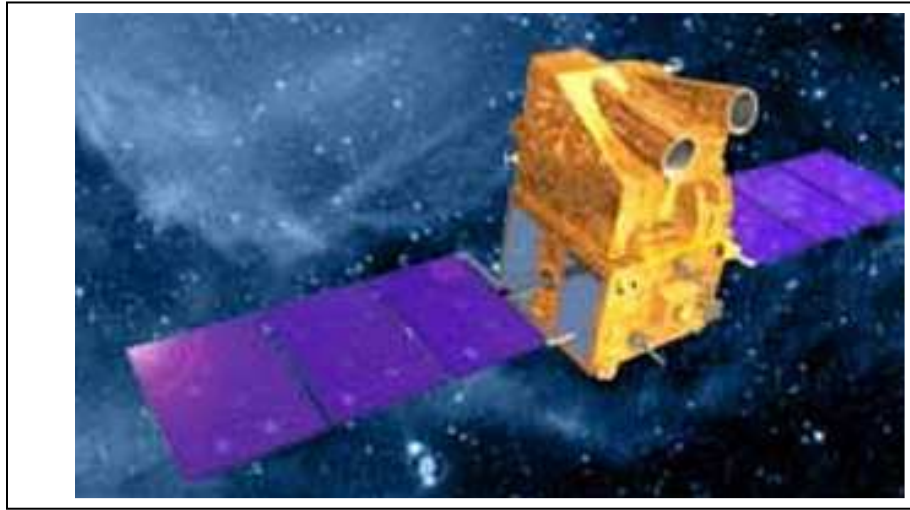


Fig. 2.8 Cartosat -1 (IRS P5) satellite visualized in orbit

Cartosat-1(IRS P6) carries two state-of-the-art Panchromatic (PAN) cameras that take black and white stereoscopic pictures of the earth in the visible region of the electromagnetic spectrum. The swath covered by these high resolution PAN cameras is 30 km and their spatial resolution is 2.5 meters. The images taken by Cartosat-1 cameras are compressed, encrypted, formatted and transmitted to the ground stations on two X-band carriers with QPSK modulation at 210 MBPS data rate. Cartosat-1 also carries a Solid State Recorder with a capacity of 120 Giga Bits to store the images taken by its cameras. The stored images are transmitted when the satellite comes within the visibility zone of a ground station.

2.2.4 Passive microwave radiometer:

Microwave radiometer [176] measures energy emitted at sub-millimetre-to-centimetre wavelengths (at frequencies of 1-1000 GHz). Generally, the term “radiometer” denotes an infrared radiation detector, yet it also comprises detectors operating on any electromagnetic wavelength, e.g. spectroradiometer [176 to 178]. The radiometer's radiation-detecting bolometer absorbs radiation falling upon it, raising its temperature, and then is measured with a temperature sensor.

Their primary application has been onboard spacecraft measuring atmospheric and terrestrial radiation and are almost solely used for meteorological or oceanographic remote-sensing. The scanning multichannel microwave radiometer [176] was a 5-frequency radiometer flown on the Seasat and Nimbus 7 satellites. Both were launched in 1978. The Nimbus 7 radiometer measured dual-polarized microwave radiances, at 6.63, 10.69, 18.0, 21.0, and 37.0 GHz, from the Earth's atmosphere and surface. Its primary legacy has been the creation of areal sea-ice climatologies for the Arctic and Antarctic.

- **Oceansat-1 (IRS P4):**

While the earlier IRS series of satellites carried cameras (LISS-I, II, III, WiFS & PAN) designed predominantly to meet the needs of land-based applications, IRS-P4 (named as Oceansat-1) is the first Indian satellite [22] envisaged to meet the data requirements of the oceanographic community. The 1036 kg satellite (Fig. 2.9) was placed in a polar sunsynchronous orbit of 720 km height in 1999.

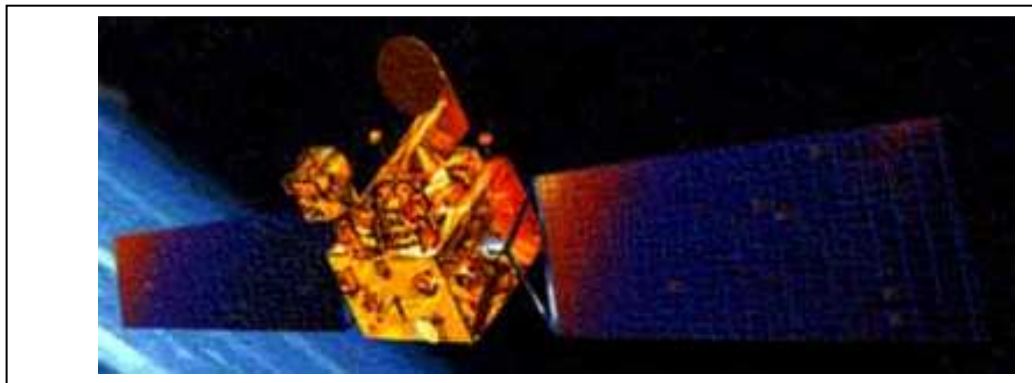


Fig. 2.9 Oceansat-1 satellite

The IRS-P4 spacecraft is a polar orbiting satellite in sun synchronous orbit with nominal altitude of 720 km. The payloads flown on-board IRS-P4 are:

Ocean Color Monitor (OCM), a solid state camera operating in eight narrow spectral bands, is used to collect data on chlorophyll concentration, detect and monitor

phytoplankton blooms and obtain data on atmospheric aerosols and suspended sediments in the water. The Multifrequency Scanning Microwave Radiometer (MSMR) is envisaged to provide information on physical oceanographic parameters such as sea surface temperature, wind speed and atmospheric water vapour. The combined data of these two payloads is transmitted at 20.8 MBPS with QPSK modulation on X-band carrier.

2.3 Active Microwave Sensors:

A scatterometer is a microwave radar sensor [179 to 181] used to measure the reflection or scattering effect produced while scanning the surface of the earth from an aircraft or a satellite. Scatterometer wind measurements are used for air-sea interaction, climate studies and are particularly useful for monitoring hurricanes. Scatterometer backscatter data are applied to the study of vegetation, soil moisture, polar ice, and global change. Scatterometer measurements have been used to measure winds over sand and snow dunes from space.

- **Radar Imaging Satellite (RISAT):**

RISAT the first IRS Synthetic Aperture Radar (SAR) system of ISRO will facilitate data collection in day/night and all weather conditions. The basic nature of data, which is a function of a microwave (C-band) returned signal, will significantly enhance the scope of satellite remote sensing and develop newer applications. With its capabilities to operate in day, night and all weather conditions, SAR is an important sensor [182], which either in stand-alone mode or as complementary to electro-optical sensors, will cater to diverse resources and environmental monitoring applications. SAR is an appropriate sensor to serve agricultural applications even under cloud cover. It also effectively serves for flood monitoring, oceanography and damage assessment in case of natural calamities. The system can provide imageries over 10 km swath in spot mode and 240 kms swath in scan mode with resolution at 1m to 50 m in single and/or dual polarization.

In the various modes of operation of the SAR, The data collected is recorded on to a solid state recorder with storage capability of 240 Giga Bits (GB). At the rate of transmission of 640 MBPS it takes 6.25 minutes to completely down link the data. The data at 640 MBPS rate is transmitted in X-band with QPSK modulation in two polarizations.

- **Oceansat-2:**

ISRO's 2nd satellite for ocean studies launched on 23rd September 2009, is envisaged to provide service continuity for the operational users of OCM (Ocean Color Monitor) data of Oceansat-1 (IRS P4) as well as to enhance the application potential in other areas. Oceansat-II is equipped with passive sensors viz., Ocean Color Monitor, an improved version of the one flown on Oceansat-1, and ROSA (Radio Occultation Sounder for Atmospheric Studies) payload, to characterize the lower atmosphere and the ionosphere & a scanning microwave (Ku band) scatterometer to monitor ocean surface wind speed and directions. The total data at the rate of 42.5 MBPS is transmitted with QPSK modulation on an X-band carrier.

2.4 Satellites with scientific payloads:

These are instruments mainly aimed for space exploration, i.e., study of the environment around the earth, the sun, the moon, other planets, comets, asteroids or even deep space. Such payloads comprise of instruments such as optical, UV and Gamma ray telescopes, interferometers, spectrometers etc for scientific observation; rovers, robotic instruments for manned or sample return missions

- **Astrosat:**

An Indian multiwavelength astronomy satellite [27]. The uniqueness of Astrosat lies in its wide spectral coverage extending over visible, ultraviolet, soft x-ray and hard x-ray regions. It will provide an opportunity for the Indian astronomers to carry out cutting edge research in the frontier areas of X-ray astronomy and ultraviolet astronomy and allow them to address some of the outstanding problems in the high energy astrophysics.

The data from all the payloads put together is 30 Gb per orbit. For the proposed orbit of Astrosat (800 Kms) and considering only one ground station for data reception at Bangalore, there is a maximum visibility gap of 4 orbits per day. During this time the data is to be stored and played back in the next visible orbit. That means 120 Gb of data is to be transmitted in a time period of approximately 10 minutes. At the rate of 210 MBPS (on two channels of 105 Mbps) it takes 9.52 minutes to play back the complete data. The data is planned to be transmitted on two X-band carriers 8125 and 8300 MHz with QPSK modulation.

- **Chandrayaan-1- mission to moon [24, 25]:**

Chandrayaan-1, the first Indian planetary exploration mission, launched on 22 October 2008, carried eleven payloads of various countries for studying the moon to further our understanding about its origin and evolution. The scientific payload data was stored in two solid state recorders and subsequently played back and down-linked at the rate of 16 MBPS in X-band through 20 MHz bandwidth with QPSK modulation. A gimbaled high gain steerable antenna system transmitted the payload data to the Indian Deep Space Network (IDSN) established near Bangalore.

2.5 Data handling (formatting & transmitting):

The realization of high precision cameras calls for the development of very high speed precision electronic systems, and requires gain bandwidth of low noise analog system in the range of a few GHz. Due to small IFOV, the signal amplitudes are also expected to be very low. The detectors also require ultra low noise, biases and high frequency read out clocks. The analog output from sensor is first quantized within payload electronics; the no. of quantization levels determines the radiometric resolution of the image (that is the number of grey levels that can be discerned). This base band data, which is of immense user interest, is suitably formatted, modulated and amplified before being down linked to the receiving ground station in real-time[56, 57]. Typical Data handling system of a Remote Sensing Satellite is shown in Fig. 2.10.

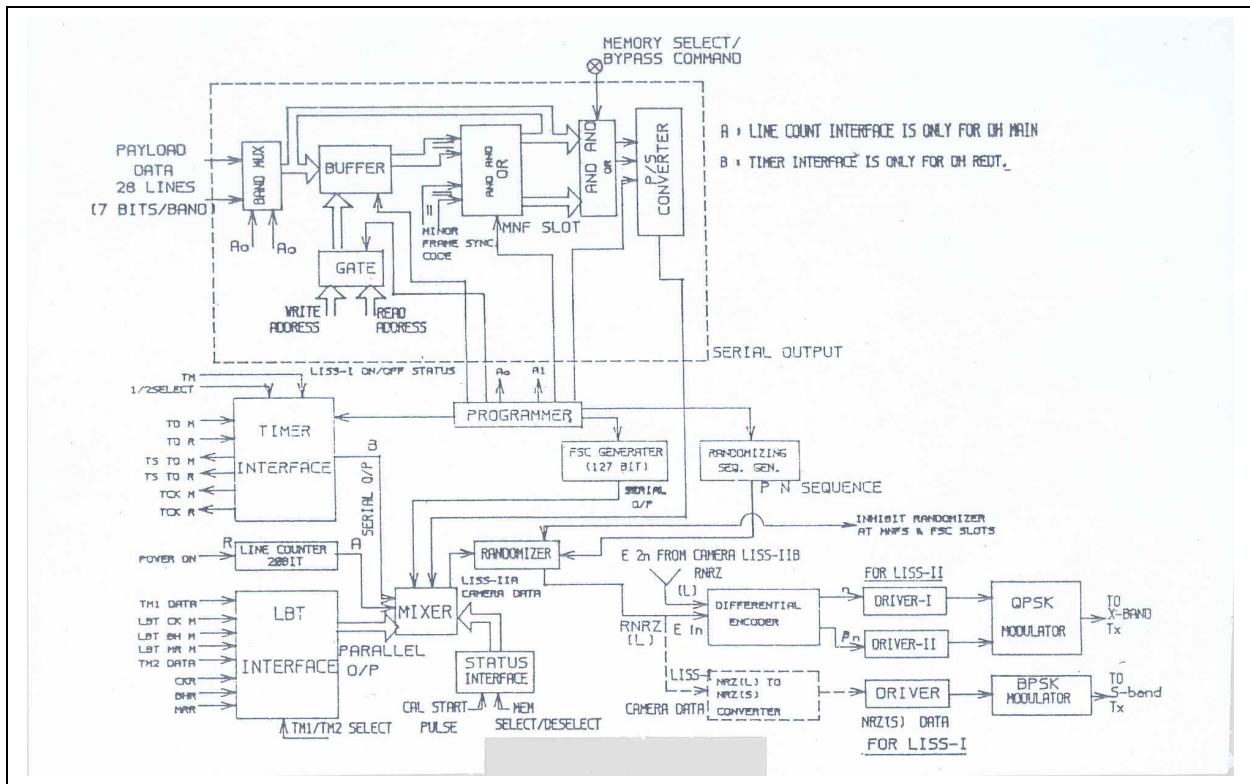


Fig. 2.10 Schematic of Data handling system of Remote Sensing Satellites

The data handling system consists of formatter, encoder for forward error correction, randomizer, differential encoder, modulator, microwave power amplifier and antenna system. Depending on the payload, encryption, source coding and appropriate data compression techniques are used and the transmitting data rate is made compatible for X-band data transmission system. A solid state recorder with 120 GB capacity to store about 9.5 min. of payload data and playback to the required ground station is also planned for the global operation of the payloads.

2.6 Frequency band for data transmission:

Conservation of electro magnetic spectra is quite essential as limited frequency band width is only allotted by International Telecommunication Union (ITU) for space to earth data transmission (refer Section 1.3.1). S-band is over crowded and more over, higher bit rate data can not be accommodated in the allowed 20 MHz bandwidth in S-band. X and Ka bands are suitable for high bit rate data transmission from space to earth. Though the allocated 1500 MHz band width in Ka band is quite attractive for higher bit rate data

transmission, at present, data transmission from remote sensing satellites is confined to X-band as Ka band signals get affected with significant rain attenuation. All possible techniques to utilize effectively the available 375 MHz spectrum in X-band are explored. However, the 375 MHz bandwidth in X-band is not sufficient to transmit the increasing data rate with high resolution remote sensing satellites being planned. Inadequate frequency bandwidth availability puts a limit on the data rate to be transmitted from satellite. Higher data rate may be increased by adopting various techniques like:

- i) Storing the data onboard and transmitting to ground station at lower data rate. However, this can not be done in true real time.
- ii) Migrating to Ka band. This calls for developing adoptive power and modulation and data rate techniques to over come rain attenuation/atmospheric losses.
- iii) Adopting higher order modulation techniques like 8PSK and 16 PSK. This calls for higher EIRP to take care of increased E_b/N_0 requirement.
- iv) Using high gain antennas to provide higher EIRP with low RF power. However, this calls for antenna beam steering techniques.

2.7 Choice of modulation:

Since space links are both power and bandwidth limited, one has to choose spectrally efficient and optimum power modulations. The primary objective of spectrally efficient modulation is to maximize the bandwidth efficiency, defined as the ratio of data rate to channel bandwidth (bits/s/Hz). Various modulation schemes can be compared for power efficiency on the basis of their bit error rate (BER) performance i.e., the average number of errors in transmitting a long bit stream, through an ideal channel. The ratio of signal energy per bit E_b and noise level N_0 to achieve a given BER, such as 1 error in 10^6 bits, is of interest.

For data transmission, digital modulation is used because of its greater noise immunity, robustness to channel impairments with higher spectral efficiency and provides greater security. More over, it has inherent advantage of requiring less bit energy for achieving

the required Bit Error Rate, occupies a minimum of bandwidth, easy to multiplex number of data streams and is simple and cost effective to implement.

2.7.1 Comparison of digital modulations:

The performance of a modulation scheme is measured in terms of its power efficiency and bandwidth efficiency [35, 36, 39, 40]. Some schemes are better in terms of the bit error rate performance, while others are better in terms of bandwidth efficiency. In bandwidth-limited systems, spectrally efficient modulation techniques shall be used to save bandwidth at the expense of power. In power-limited systems, power efficient modulation techniques along with error-correcting codes can be used to save power or to improve error performance at the expense of bandwidth. Some coding techniques like Trellis-Coded Modulation (TCM) and RS coding can improve the error performance of bandwidth-limited channels. The bandwidth efficiency η_B of a system is a function of data rate R and the available / occupied bandwidth. In general, trade-off is to be made while selecting a digital modulation scheme for satellite links as both power and bandwidth are at premium.

Amplitude Shift Keying (ASK), Frequency Shift Keying (FSK) and Phase Shift Keying (PSK) modulation schemes are the basic digital modulation techniques. ASK does not provide constant envelope for the modulated signal, thereby power amplifiers do not give maximum power output when operated in saturation while FSK and PSK provide constant envelope and are better suited for satellite links. The measure of system performance for digital data communication is the probability of error P_e . Fig. 2.11 shows Bit Error Rate P_e vs E_b/N_o for a variety of digital modulation and demodulation schemes [38].

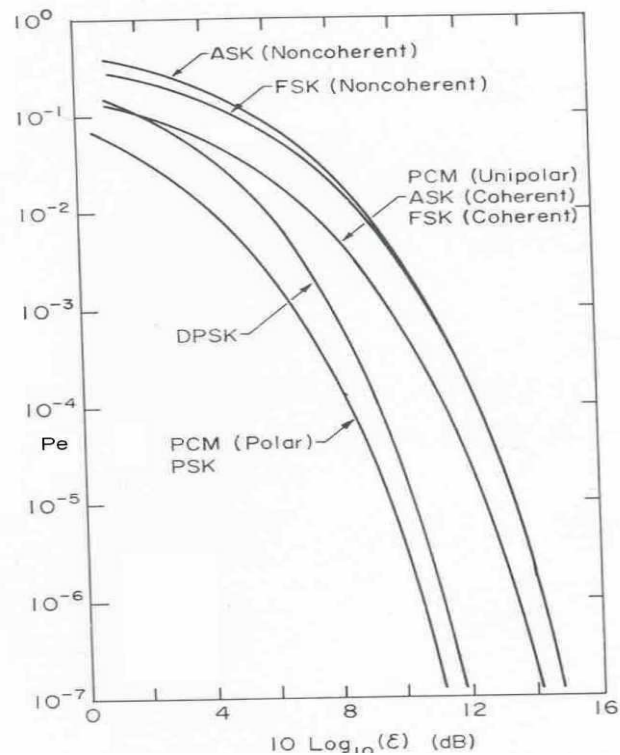


Fig. 2.11 BER probability for various digital modulations [38]

From the above picture, it is evident that PSK modulation is superior to both ASK and FSK in that they require less transmitted power for a given error probability.

Simplest form of PSK is binary PSK (BPSK), wherein the digital data modulates a sinusoidal carrier with one of two possible phase states (say 0 and π radians) representing either a binary 0 or a binary 1. Typical bandwidth occupied by the modulated BPSK signal is approximately 1.1 to 1.2 times the bit rate [x10]. A more efficient utilization of radio frequency band width can be achieved with 4 phase (Quaternary PSK-QPSK), 8 phase (8-PSK) and 16 phase (16-PSK) systems. Minimum Shift Keying (MSK) and Gaussian MSK (GMSK) schemes can also be used to meet some applications which call least interference to adjacent carriers. Different digital modulation schemes described above are compared for performance and are given in Table 2.1.

Table 2.1: Comparison of different digital modulation systems:

Modulation Scheme	Signaling Waveform	Bandwidth	Probability Of Error	Frequency Spectrum
ASK	$S_1(t) = A \cos \omega_0 t$ $S_0(t) = 0$	Double of base band signal	$P_e = \text{erfc} [\sqrt{E_b/N_0}]$ where E_b : Energy per bit $N_0/2$: Noise Spectral Density	Power spectral density is centered at center frequency
FSK	$S_1(t) = A \cos \omega_1 t$ $S_2(t) = A \cos \omega_2 t$ Where ω_1 and ω_2 are two different frequencies.	Depends on separation of both the frequencies	$P_e = \frac{1}{2} \text{erfc} [\sqrt{E_b/2N_0}]$ for coherent detection. $P_e = \frac{1}{2} \text{erfc} [-E_b/2N_0]$ For non coherent detection.	Two line spectrum occur for two different frequencies.
BPSK	$S_1(t) = A \cos \omega_0 t$ $S_2(t) = A \cos (\omega_0 t + \pi)$	BW=1.25 times the bit rate (practical). Theoretically BW = bit rate.	$P_e = \frac{1}{2} \text{erfc} \sqrt{[E_b/N_0]}$	Spectrum: $\text{Sin}2X/X^2$ without spectral line at carrier frequency
QPSK	$S_1(t) = a_i(t) \cos 2\pi f_c t$ $+ a_q(t) \sin 2\pi f_c t$	BW = 0.5 times bitrate (theoretical) BW = 0.6 times bit rate (practical)	For each $P_e = \frac{1}{2} \text{erfc} \sqrt{[E_b/N_0]}$	Spectrum: $\text{Sin}2X/X^2$ and no discrete spectral line at carrier frequency
MSK	$S_1(t) = a_i(t) \cos 2\pi f_c t$ $+ a_q(t) \sin 2\pi f_c t$ $\sin(\pi/2T)$	Bandwidth is 1.5 times more than that of QPSK	$P_e = \frac{1}{2} [\text{erfc}(\sqrt{\gamma_b}) - \frac{1}{4} \text{erfc}^2(\sqrt{\gamma_b})]$	Spectrum $\text{Sin}6X/X^6$

A QPSK modulated signal is constituted by operating two BPSK modulators in quadrature. Bandwidth of the QPSK signal is exactly half that of the BPSK signal for the same bit rate. Bandwidth required for 8-PSK is a factor of 3 less than that of BPSK, but additional power is required to maintain the same bit error rate as orthogonality characteristic of QPSK can not be maintained. MSK has some excellent special properties that make it an attractive alternative when other channel constraints require bandwidth efficiencies below 1bits/s/Hz. For example, the continuous phase nature of

MSK makes it highly desirable for high power transmitters driving highly reactive loads. Since inter symbol switching occurs when the instantaneous amplitude of $p(t)$ is zero, the finite rise and fall times and data asymmetry inevitably present in practical situations have a minimal effect on the MSK performance. In addition, MSK has simple demodulation and synchronization circuits.

- **Spectral efficiency:**

A general system design objective would be to use the two premium resources viz., transmitted power and channel bandwidth, as efficiently as possible. In many communication channels, one of the resources may be more precious than the other and hence most channels can be classified primarily as power-limited or band-limited. In power-limited channels, coding schemes would be generally used to save power at the expense of bandwidth, whereas in band-limited channels “spectrally efficient modulation” techniques would be used to save bandwidth.

Important objective of modulation schemes for satellite communication may be to achieve bandwidth efficiency at a prescribed average bit error rate with minimum expenditure of signal power. Some channels may have other restrictions and limitations, which may force other constraints on the modulation techniques. For example, communication systems using certain types of non-linear channels call for an additional feature, namely a constant envelope, which makes the modulation impervious to such impairments. If one considers the required BW to be that required to pass the main lobe of the signal spectrum (null to null), then the BW efficiency of various M-ary schemes be as indicated in Table 2.2.

Table 2.2 Bandwidth efficiency on a main lobe spectrum of M-ary systems.

M-ary scheme	BW Efficiency (bits/s/Hz)
PSK, QASK	$0.5\log_2 M$
FSK	$\frac{\log_2 M}{M + 1}$

- **Basic considerations for selection of modulation:**

In a digital communication system, particularly in satellite links, there is often a trade off between bandwidth efficiency and power efficiency. Adding error control coding to a message increase the bandwidth occupancy (lesser bandwidth efficiency), but at the same time reduces the required received power for a particular bit error rate, and hence trades bandwidth efficiency for power efficiency. On the other hand, higher-level modulation schemes (M-ary keying) decrease bandwidth occupancy but increase the required power, and hence trade power efficiency for bandwidth efficiency. The most important objectives of satellite communications include: power and bandwidth or spectrum efficiency combined with robust Bit Error Rate (BER) performance in a noisy and/or strong interference environment. High performance BER specification is generally expressed as a function of Energy per Bit (E_b) divided by Noise Density (N_0), that is, by the $BER=f(E_b/N_0)$ expression. Fig. 2.12 shows the bit error performance (BER vs E_b/N_0) for various digital PSK modulation schemes [40].

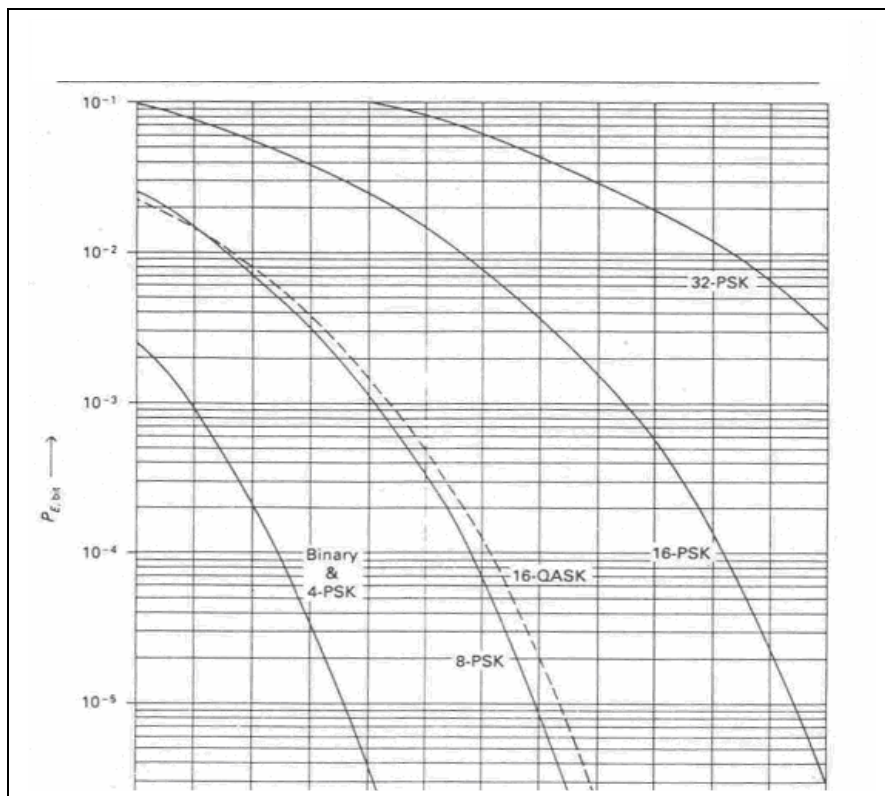


Fig. 2.12 Bit error probability versus E_b/N_0 , for M-ary systems

The RF spectral efficiency of the four state modulation systems, such as QPSK, is limited to 2 b/s/Hz, while the spectral efficiency of multi-state or multi-ary systems such as 8 PSK, 16 PSK and 64 state QAM are limited to 3 b/s/Hz , 4 b/s/Hz, and 6 b/s/Hz. An increased number of signaling states increases the complexity of a transceiver and increases the required C/N, that is it has a negative impact on the BER=f(Eb/No) performance, as increased C/N requirement and increased Eb/No requirement leads to more expensive and larger transceivers and/or reduced margins. Realization of systems with high spectral efficiency requires very complex implementations, steep filters and a significantly increased C/N requirement. Comparison of PSK modulation schemes is provided in Table 2.3.

Table 2.3 Comparison of PSK modulation schemes

	BPSK	QPSK	OQPSK	8 PSK	16 PSK
Eb/No for 1 in 10 ⁻⁶ BER	10.8 dB	10.8 dB	10.8 dB	13.0 dB	18.5 dB
Spectrum efficiency	0.5 B/Hz	1 B/Hz	1 B/Hz	1.5 B/Hz	2 B/Hz
RF band width (Main lobe width)	2 x BR	1 x BR	1 x BR	2/3 x BR	0.5 x BR

QPSK modulation technique, being optimum modulation scheme in terms of power and bandwidth efficiency, is generally adopted for high bit rate data transmission from remote sensing satellites [185,188].

2.8 Transmitting system onboard remote sensing satellite

2.8.1 Data transmitting system: Typical basic block schematic [186] of the data transmitting system of Remote sensing satellites is shown in Fig.2.13.

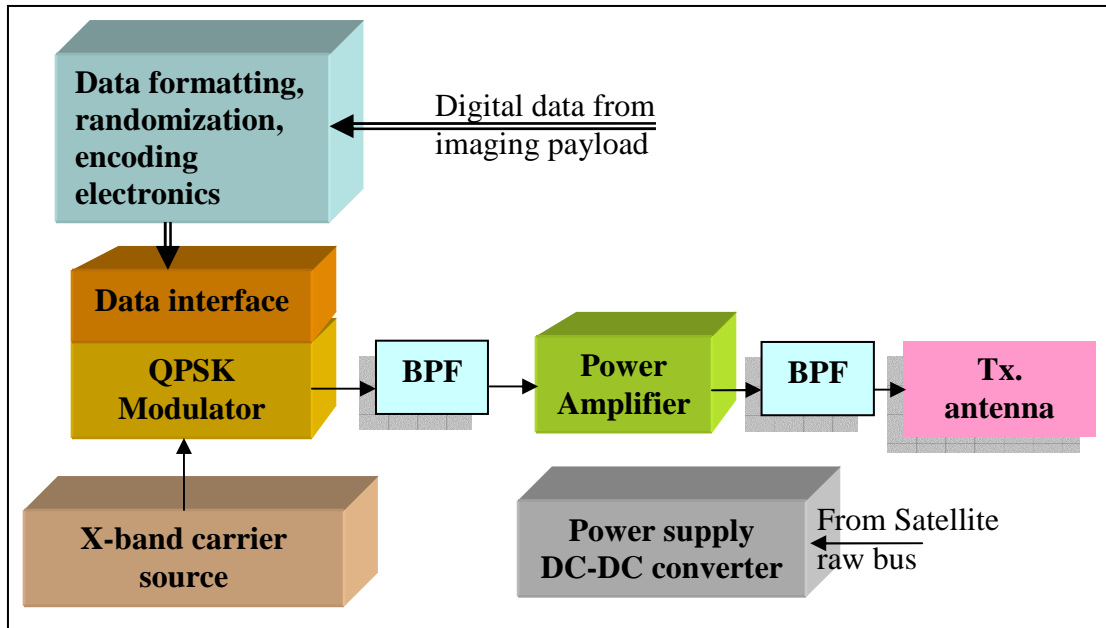


Fig.2.13. Block schematic of basic data transmitter.

Various techniques, like multiplying a low frequency signal of a stable Temperature Compensated Crystal Oscillator (TCXO) using frequency multipliers and amplifiers, or phase locking an X-band Voltage Controlled Oscillator (VCO) with a reference signal obtained from a low frequency TCXO, can be used for generating X-band carrier. The carrier is QPSK Modulated with high bit rate data which is formatted, randomized to aid clock recovery at data reception station, and differentially encoded to take care of the 90 deg. Phase ambiguity in demodulation. From the link analysis, the power to be transmitted is estimated. The QPSK modulated X-band carrier is amplified by a power amplifier sized to deliver the power estimated by link analysis. Generally, Solid State Power Amplifiers (SSPA) are ideally suitable, but limited to requirements less than about 20 watts. Above 20 watts, Traveling Wave Tube Amplifiers (TWTA) are preferred due to associated high power added efficiency. Spectrum is limited to the allotted bandwidth with band pass filters at appropriate stages.

For transmitting higher bit rate data on a single carrier, high RF power is required to be transmitted involving complex design and also limited by space qualified high RF power generating devices. Multi carrier techniques are preferred for increasing the transmitting capacity within the limitations of available onboard power and bandwidth.

2.8.2 Transmitting antennas:

Special antennas are to be designed for transmitting the X-band QPSK modulated signals with optimum utilization of the onboard power. In an orbit, during visibility period, the range thereby path loss depends on the ground station antenna elevation angle.

The range of a satellite in a circular orbit can be computed as given in section 2.5.2.

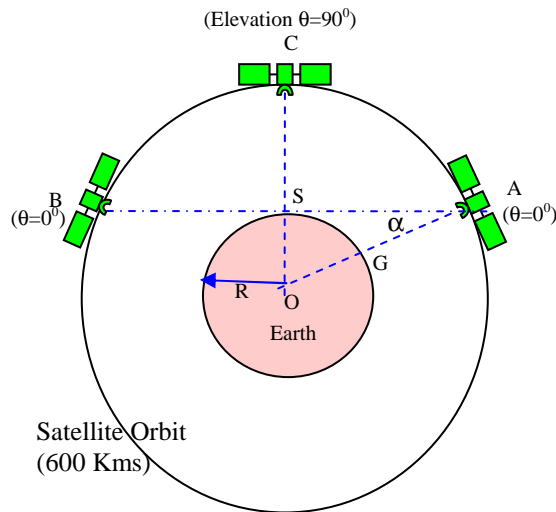


Fig. 2.14 Schematic showing satellite looks angles

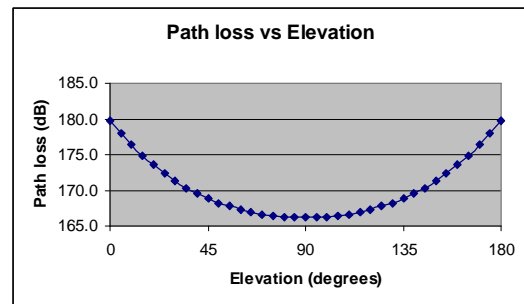


Fig. 2.15 Path loss vs Elevation

The range of the satellite in an orbit from an antenna at ground station S varies from 2831 kms (SA or SB in Fig.2.14) when satellite is at point A or B, corresponding to 0° and 180° ground antenna elevation, to 600kms when the satellite is over head i.e. at point C. Accordingly path loss is computed from the formula $[4. \pi. r / \lambda]^2$ at 8125 MHz carrier frequency which varies from 179.7 to 166.2 dB as shown in Fig. 2.15 and the signal received at ground station, when satellite transmits with constant gain antenna, accordingly increases by about 13.5 dB from 0° elevation to 90° elevation.

2.8.3 Iso-flux antenna:

Iso-flux antennas [58-62] are often used onboard remote sensing satellites for transmitting the high bit rate modulated signals. The antenna radiation pattern (gain) is

shaped to compensate the path loss variation shown in Fig.2.14 for optimum utilization of onboard power through out the visible period of the orbit. The gain at about $\pm 66^\circ$ look angle of onboard antenna, corresponding to 0° elevation of ground antenna, is increased while decreasing gain at 0° to have gain pattern identical to path loss pattern over elevation angle by shaping the primary reflecting surface. Practically, the gain at $\pm 66^\circ$ is measured to be +7 dBi and the gain pattern is near equivalent to the path loss pattern. The iso-flux antennas ensure near constant signal strength at the receiving station when the satellite is traveling through the visible portion of the orbit for optimum utilization of onboard power.

- **Limitations of iso-flux antennas:**

Iso-flux antennas are simple but have certain constraints:

- Isoflux antennas have near constant signal strength at the receiver while providing coverage to any ground station during visible orbit period. Since, the satellite transmits the data over the entire visible surface of the earth due to the wide beam width of the radiation pattern, unintended ground stations situated in a large area can receive the satellite signals and becomes undesirable in some applications.
- The wide beam low gain antenna requires very high power for transmitting high bit rate data. Due to low gain of only +7 dBi at maximum range, to maintain the Effective Isotropic Radiate Power (EIRP), typically about 40 watts RF power is required to be transmitted for proper reception of about 105 MBPS data.
- The RF power generated onboard is not effectively used as the antenna radiates over a wide area (about $\pm 65^\circ$ beam width).
- The cross polarization isolation is rather poor in the wide beam iso-flux antennas and transmission in dual polarization is supported with higher polarization isolation only.
- Of late, the remote sensing satellites are tilted during imaging to get images of earth over wide range. In addition, step and stare technique is also adopted to improve the resolution of the imagery. To comply these requirements, the satellite is made agile and tilted during imaging to increase its imaging range and resolution. For example, satellites like CARTOSAT-1 & 2 are designed for tilting

the platform by +/- 26 deg. This puts a requirement of radiating the signal over more than +/- 90° range. Iso-flux antennas cannot support this requirement with good gain.

This type of antennas put a limit on the data rate to be transmitted due to poor cross polarization isolation and high RF power requirement.

2.8.4 High Gain Antennas:

Radiating the signals through high gain, narrow beam antennas can provide a solution to many of the above issues. High gain antennas also reduce the requirement of high RF power there by significant reduction of DC power requirement onboard. Simple low power Solid State Power Amplifiers (SSPA) can be used. It is possible to achieve better cross polarization isolation with high gain antennas and are suitable for transmission in dual polarization thus enhancing data throughput.

High gain antenna, due to associated narrow beam width, needs to be steered for pointing the beam to the designated ground station which can be accomplished by either mechanical steering of high gain antenna or by electrical steering of the beam by controlling the phase of the signals fed to the radiating elements of an array antenna. A high gain antenna like a parabolic reflector antenna or a planar phased array antenna can be steered by a dual gimbal mechanism. This is simple with less weight and consumes less power. But, needs moving mechanism resulting in torque disturbances that moving antennas impart to the spacecraft. This disturbance due to mechanical jitter on the platform causes distortion in the high resolution imaging payloads effecting the imaging quality and definition of the image. In addition, mechanical and thermal issues also pose more problems on the design of satellite platform. An active phased array provides a better solution when mechanical disturbance due to rotating motors is not acceptable.

2.8.5 Active phased array antennas:

Electronic steering of the beam is the best approach for fine resolution imaging satellites. An active phased array can provide a better solution. A phased array is a group of

radiating antennas either microstrip patches or helices etc. By controlling the phase of individual radiating elements, the beam can be pointed to any desired angle. The major advantage of phased array antennas is their ability to dynamically reconfigure their radiation pattern, to achieve an optimum signal reception/transmission in a changing environment.

With the availability of miniaturized RF components (phase shifters) with high switching speeds and computer technology for phased array control, the beam of the antenna can be steered in a certain new direction which is very much differing from its current position without delay due to mechanical inertia. This reconfiguration is carried out by processing the signals originating from or going to distinct radiators that are placed in some spatial configuration. Often that configuration is planar.

2.8.6 Planar phased array antenna:

Conventional phased array antenna consists of an array of $n \times m$ elements mounted on a planar surface with a feed network consisting of controlled phase shifted amplifiers and provides high gain, narrow beam with nearly cosine scan behaviour to 60° of scan over the hemisphere.

The array factor (AF) for a $(M \times N)$ elements of planar array antenna can be written as [71]:

$$F(u, v) = \sum_{m=1}^{M/2} \sum_{n=1}^{N/2} A_{mn} \cos[(m - 0.5)kd_x u] \cos[(n - 0.5)kd_y v] \quad \text{--- (2)}$$

$$u = \sin \theta \cos \phi - \sin \theta_0 \cos \phi_0; \quad v = \sin \theta \sin \phi - \sin \theta_0 \sin \phi_0 \quad \text{--- (3)}$$

$$A_{mn} = S(m,n)\exp(j\varphi_{mn}) \quad \text{--- (4)}$$

Where θ_0 and ϕ_0 are the beam pointing angles and

$S(m, n)$ and φ_{mn} are the amplitude and phase values for the mn^{th} array element placed at the location (m, n) in the array grid [coordinate system is shown in Fig. 2.16].

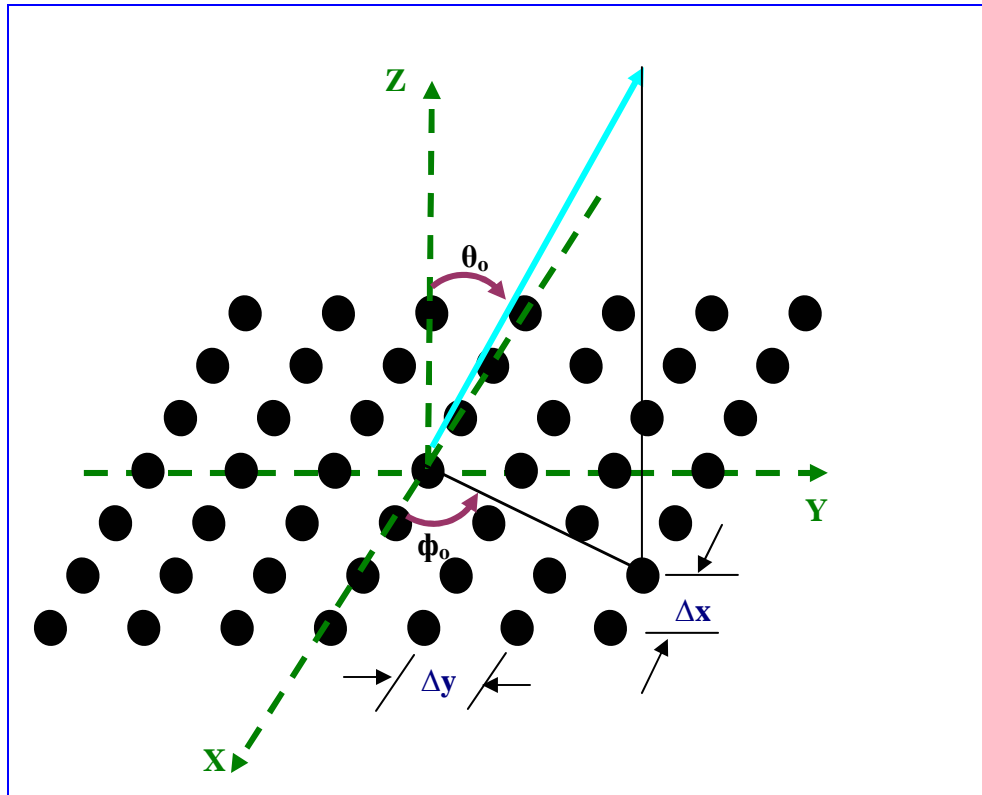


Fig. 2.16 Coordinate system of an array grid.

Planar phased array with phase control provides angular steering of the beam but, the radiation intensity is at its maximum only in the broadside of the array and reduces as cosine function with angular displacement from perpendicular axis. The beam can usually not be steered more than 60° - 70° from the normal of the array due to reduction in antenna gain. The variation is approximately given by $(\cos \theta_s)^\alpha$, where θ_s is the scan angle from the normal to the surface and α is a parameter, introduced to account for scan loss which is close to one. $\alpha = 1$ corresponds to the ideal case with no mismatch, where as a value greater than 1.0, up to 1.3, can be introduced to account for increasing mismatch loss as the beam is scanned away from the normal .

The reduction varies roughly as the projection of the antenna surface in the scan direction as shown in Fig. 2.17.

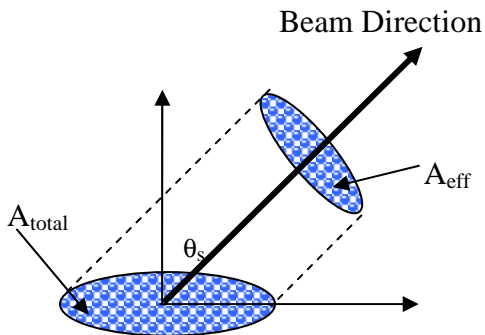


Fig. 2.17 Effective area of a planar array antenna.

This type of arrays suffices the normal requirements of transmitting data from near earth orbiting stabilized satellites. With the requirement of resolution for the imageries taken by the satellite becoming stringent day by day, need for agile satellites arises in which the scan requirement for the radiating beam could be more than $\pm 60^\circ$ to have proper data transmission link from satellite to earth. More over, the system gets complicated further when more than one beam is required to transmit the data to different ground stations. This makes electronic steering of the radiating beam from planar phased array unsuitable for space to earth communication.

2.8.7 Spherical phased array:

Spherical arrays represent another canonical case of interest. Objective may be the realization of hemispherical coverage, although other shapes can also be used to obtain this. A spherical array is derived with the concept of a large number of panels with fewer elements per panel with the elements located on a spherical surface. The projected aperture is the same for any beam direction. This ensures the minimum variation in directivity with scan angle of the hemisphere thus avoiding any over sizing factor such as $\sqrt{2}$ times as in the case of planar arrays.

A Geodesic sphere/dome phased array antenna that preserves all the advantages of spherical arrays while its fabrication is based on well developed, easily manufactured,

planar array technology is proposed and described in [2-6,10]. It is constructed with many near-equilateral triangular planar sub-arrays arranged in an icosahedra geodesic dome configuration. This faceted dome antenna provides communication function for satellite operations and radar function for air/space surveillance with full hemispherical coverage while exhibiting the following advantages over the conventional pyramid-like and conformal array structures:

A number of possible generic surfaces can be considered to realize hemispherical coverage, but; the attractive feature of spherical array is that all radiating elements see essentially the same environment, thus reducing the design effort. A near uniform element distribution is possible. Pattern characteristics remain unchanged as the active region is moved over the spherical surface. An active area was determined from the maximum element look angle. The effective area of a curved, conformal array is the projection of the active part of the array in the beam direction as shown in Fig. 2.18.

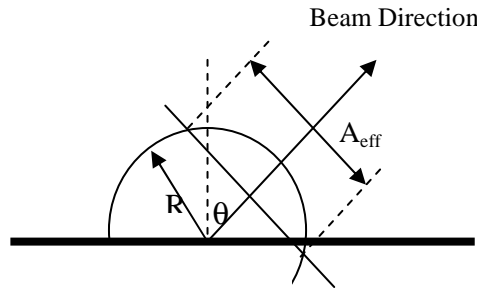


Fig.2.18 Effective (Projected) area of a spherical antenna.

The radiation pattern from a uniformly excited radiating elements on a hemispherical shell with radius R and phased for maximum radiation in the direction θ is simply a Sinc function [6]:

$$E(\theta) \propto 4\pi R^2 \frac{\sin(\alpha R)}{\alpha R} \quad \text{--- (5)}$$

$$\text{where } \alpha = \frac{4\pi}{\lambda} \sin\left(\frac{\theta}{2}\right)$$

If the active region is enlarged, the directivity increases, unless the element spacing becomes too large leading to increased losses in the grating lobes. To simplify the analysis, it is assumed that the elements had circular polarization with a cosine amplitude pattern. Uniform element excitation was assumed and mutual coupling was neglected. The element distribution was made as uniform as possible using icosahedron distribution approach where elements were evenly distributed on each triangle and then projected onto the surface of a circumscribed hemisphere.

The general configuration for a spherical array consists of a large number of radiating elements placed on a spherical surface. The basic theoretical and experimental aspects of spherical phased arrays are given in [113 to 117]. For a given beam direction only a sector of the array elements is excited while all other elements are turned off. The active sector is the area encompassed by a cone angle of $2\alpha_0$ degrees, with its axis coinciding with the antenna beam direction, and is the part of the sphere that is turned on to receive (or transmit) electromagnetic energy. Beam scanning is accomplished by activating different sectors of the spherical surface. All array elements in the active sector are phased to produce an equi-phase front normal to the desired beam axis. Each array element must have a radio frequency (RF) on/off switch and a phase shifter. The radiating elements in the active sector are assumed to have symmetry in the plane perpendicular to the axis of the antenna beam, and consequently a spherical array can be used to cover the hemisphere with practically identical beams. Thus, in contrast to other array configurations which suffer from beam degradation as the beam is steered over wide angular regions, spherical arrays can provide uniform patterns and gain over the entire sky. In addition, in [10] we have shown that the spherical array has much lower polarization losses and mismatch losses in comparison to multi-sided pyramid array structures. Furthermore, in contrast to conventional multi-face pyramid structures which suffer from gain degradation due to beam squint as the frequency changes, spherical arrays have no beam shift vs. frequency, resulting in much wider signal bandwidth [10].

With all advantages that spherical arrays offer, however, they have not been used in practice primarily because implementation of curved beam forming network, radiators,

fabrication, and assembly are much more difficult than for the architectures based on planar array geometry.

Beam steering was accomplished simply by shifting the active part in small steps across the hemispherical array and by adjusting the element phase simultaneously to produce a plane wave front and, hence, maximum directivity in the required beams direction. The extent of the active area in the curved case is one parameter that has to be selected in the design of the array antenna. Each element is pointing in the direction of the normal to the surface. The angle between the normal and the desired scan (beam) direction determines whether the element will be active or not. With an assumption of the maximum useful scan angle of 60° , the hemispherical surface provides an active area subtended by a conical angle of 120° .

The effective area is given by

$$A_{eff} = \frac{3}{4} \pi R^2 \quad \text{--- (6)}$$

and could be expected to be independent of scan direction with a spherical surface. However, since we are dealing with hemisphere, for scan angles larger than a certain value, in our case 30° from the zenith, the effective area decreases and is halved at 90° scan limit as can be seen from Fig.4.4. For scan angles θ_s between 30° and 90° from the zenith, the effective area variation is given by [71]

$$\begin{aligned} A_{eff} = & (\pi - \Psi) R^2 \sin^2 \theta_{max} + \\ & 0.5 R^2 \sin 2\theta_{max} \cot \theta_s \sin \Psi + \\ & R^2 \cos \theta_s (X - 0.5 \sin 2X) \end{aligned} \quad \text{--- (7)}$$

where

$$\begin{aligned} \cos \Psi &= \cos \theta_s \cot \theta_{max} \quad \text{and} \\ \sin X &= \sin \theta_{max} \sin \Psi, \\ \theta_{max} &\text{ is maximum local scan angle.} \end{aligned}$$

Dividing by the total area $2\pi R^2$, we get the performance index with respect to scan angle and is shown in Fig. 2.19 as solid line.

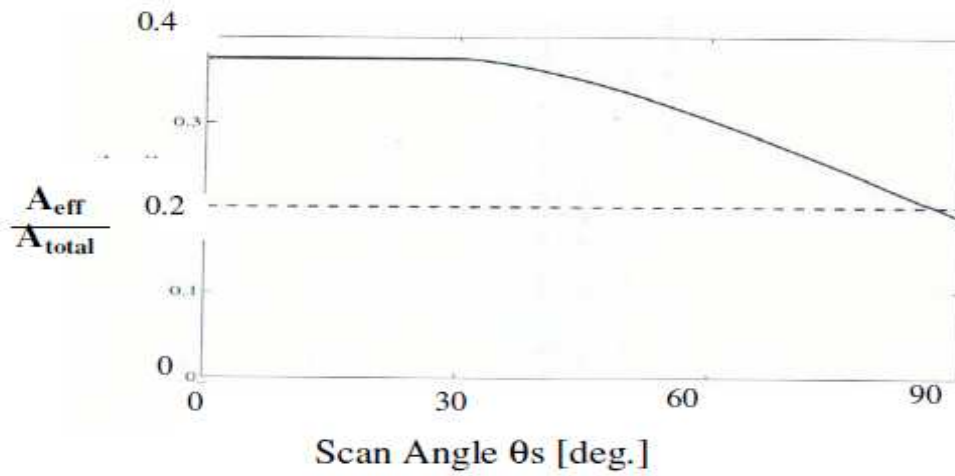


Fig.2.19. Normalized performance versus scan angle from zenith [71]

The gradual reduction in performance from the 30° scan angle and onward is due to the cutoff of the lower part of the hemisphere (Fig. 2.18). One alternative is to extend the sphere downward to make the effective area constant with scan. This significantly increases total area and, hence, the cost. Normalized performance versus scan angle from the zenith is shown in Fig.2.19. The dashed line is for an extended sphere with constant effective area. Due to hemispherical surface, gradual reduction in gain is associated as explained beyond 30° scan angle.

2.8.8 Alternative schemes for high bit rate data transmission:

Another option to transmit high data is to store the data onboard and playback at reduced data rate and transmit for longer time. However transmission is possible only during visible part of the orbit. This puts a limit on the data to be transmitted. Alternatively, data shall be down linked to more than one station. Real time transmission can not be done for this mode of data transmission.

Chapter 3

IRS satellite data transmission and reception systems

3.1 Data transmitting system:

Practical considerations mostly limit the choice of frequency band and frequency reuse. Since, remote sensing data can be received globally; compatibility of ground stations will be a major consideration in choosing frequency in the ITU allocated frequency bands and polarization.

3.1.1 Compatibility with other missions:

International missions like SPOT/ ERS satellites of Europe, JERS of Japan adopted QPSK modulation for data transmission. Landsat -7 of US has planned to transmit about 150 MBPS data at X-band using QPSK modulation. The Russian mission ALMOZ also selected QPSK modulation to transmit data rates of the order of 240 MBPS. Realization of conventional QPSK modulation is simpler compared to higher order M-ary PSK schemes. All remote sensing data reception stations globally are equipped with QPSK data reception systems. Indian Remote Sensing satellites are also configured with conventional QPSK modulation for high bit rate data transmission, compatibility with international ground stations being the added advantage. Globally and particularly in India, data reception capability at present exists in S and X-bands in RHC polarization.

For optimizing the cost of the data receiving systems, it is preferred to use same data rate as far as possible. 105 MBPS data rate is standardized for most of the IRS missions viz., Cartosat and Resourcesat series of satellites.

3.1.2 IRS data transmitting system configurations

For Cartosat-2 series, data rate to be transmitted is fixed at 105 MBPS while, Oceansat-1 transmits 20.8 MBPS data. Cartosat-1 and Resourcesat series satellites, transmit 210 MBPS data. For transmitting 105 MBPS data in Cartosat-2 series and 20.8 MBPS data in Oceansat-1, the configuration (Fig. 2.18) explained in chapter 2 is adopted. The power amplifier with 40 watts output is required for comfortable link with about 6 dB link

margin for each carrier in Resourcesat mission while 10 watts is adequate for transmitting Oceansat-1 data as can be seen from Table 3.1 which shows the link estimates for transmitting 105 MBPS and 20.8 MBPS data from Resourcesat satellite in 817 Kms orbit and Oceansat satellite in 700 kms orbit.

Table 3.1: Link estimation for Resourcesat & Oceansat missions

	Resourcesat	Oceansat
Satellite Orbit	817 Kms	700 Kms
Satellite Maximum range at 2° Ground station antenna elevation	3115 Kms	2563 Kms
Frequency	8300 MHz	8300 MHz
Path loss	181 dB	179 dB
Modulation	QPSK	QPSK
Data Rate	105 MBPS	20.8 MBPS
Tx. Power	40 watts	10 watts
Onboard loss	2 dB	2 dB
Onboard iso flux antenna gain (maximum at +/- 65°)	+7 dBi	
EIRP	21 dBw	15 dBw
Ground station G/T 7.5 mtr parabolic antenna	30.5 dB/k	30.5 dB/k
Misc. loss / pointing loss	2 dB	2 dB
Received C/No	98 dBHz	92 dBHz
Eb/No available	18 dB	19 dB
Eb/No required for 10-6 BER (theoretical)	10.8 dB	10.8
Implementation margin (predictable)	1.2 dB	1.2 dB
Additional Margin available	6.0 dB	7 dB

TWTAs are used for generating 40 watts while SSPAs are used for generating 10 watts output power.

For **transmitting data of the order of 210 MBPS** on a single carrier, high RF power (about 80 watts) is required to be transmitted involving complex design. For single carrier operation, the power amplifier can be operated at 1 dB compression or even at saturation point to get the advantage of high efficiency. It is planned to transmit

210 MBPS data on two carriers with 105 MBPS data QPSK modulating each carrier. This halves power amplifier requirement and simplifies electronics. The frequency plan adapted for Cartosat-1 and Resourcesat-1 is shown in Fig. 3.1.

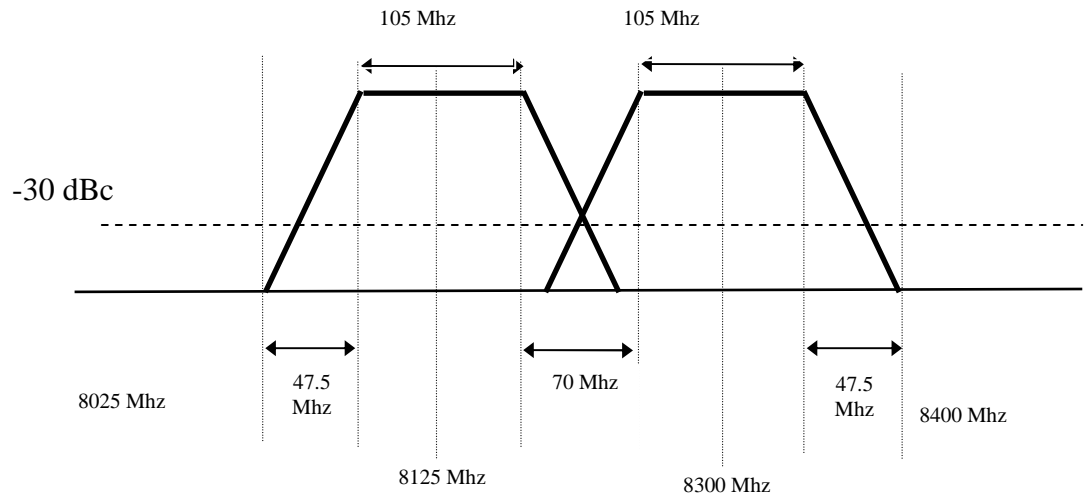


Fig. 3.1 Frequency plan for two carrier data transmission

The data transmitting system configured for transmitting 210 MBPS data by QPSK modulating two X-band carriers [191,192] is shown in Fig. 3.2. The two carriers viz., 8125 and 8300 MHz are used to transmit 210 MBPS total data, 105 MBPS on each carrier, using QPSK Modulation.

For space systems reliability is prime importance which is further strengthened with sufficient redundancy. In the developed configuration, full cold redundancy is provided to basic systems. Selection of basic system is done by powering the selected chain. Selected modulated carriers are amplified to 40 watts each by separate TWTAs. One TWTA is provided as standby for two operating TWTAs. Both amplified carriers are transmitted by separate iso-flux antennas.

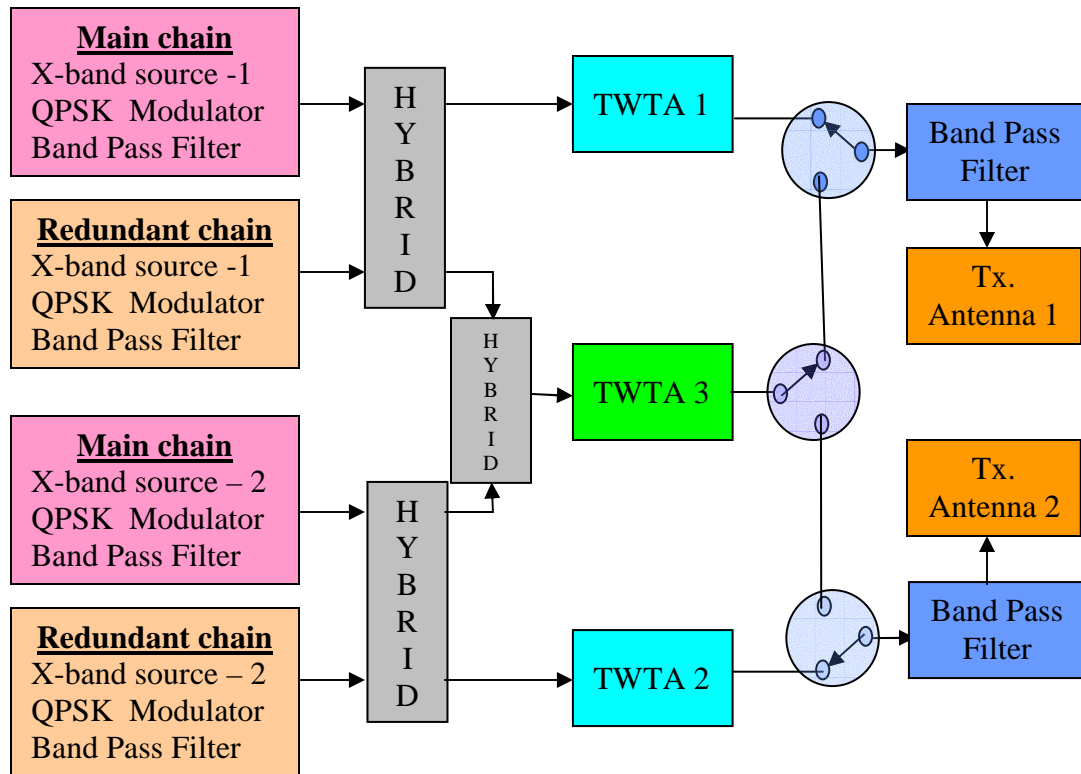


Fig. 3.2. Configuration of data transmitting system

This configuration avoids inter carrier interference generation from onboard system and power amplifiers can be operated near saturation to get the best possible efficiency from TWTA. This configuration also simplifies the design of post amplification elements like Band Pass Filters (BPF) by avoiding the requirement of handling combined RF power of 80 watts.

3.1.3 Transmitting antennas:

Iso-flux antennas are developed and used onboard IRS satellites [59, 192] so far in which, the antenna radiation (gain) pattern is shaped to compensate the path loss variation shown in Fig.2.15 for optimum utilization of onboard power through out the visible period of the orbit. The gain at $\pm 66^\circ$ look angle of onboard antenna is increased while decreasing gain at 0° to have gain pattern identical to path loss pattern over elevation angle by shaping the primary reflecting surface. Practically, the gain at $\pm 66^\circ$ is measured to be +7 dBi and the gain pattern is near equivalent to the path loss pattern. A shaped beam

antenna developed for IRS satellites and its radiation characteristic which nearly matches path loss variation is shown in Fig. 3.3.

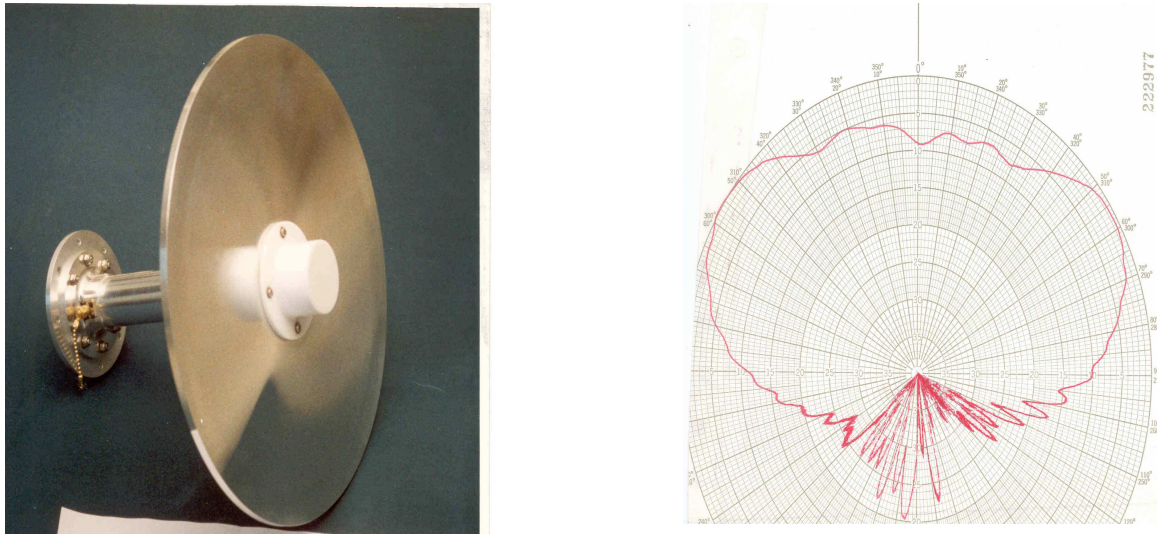


Fig.3.3. Iso-flux antenna and it's radiation pattern.

Cross polarization characteristics of an iso-flux antenna fabricated for Oceansat satellite is shown in Fig.3.4. As can be seen cross polarization isolation is as low as 3 dB in certain angles making this antenna unsuitable for frequency reuse.

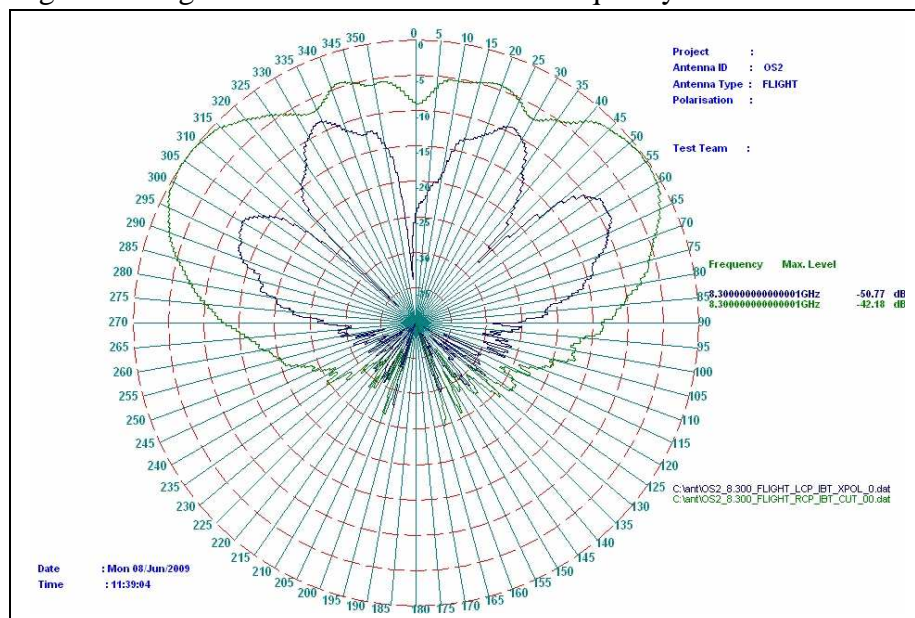


Fig. 3.4 Radiation pattern (co and cross polarizations) of iso-flux antenna.

Typical Automatic Gain Control (AGC) plot recorded at NRSC ground station on 18th April 2009 for the signal received from IRS – 1D in path no. 108 is shown in the Fig.3.5. The data transmission is made ON at 03:00:30 hrs GMT and switched OFF at 03:05:30 hrs GMT. Below 3° elevation, the signal strength variation is large due to multiple reflections due to surrounding obstacles. Above 3° elevation, signal strength is stabilized and maintained till the transmitter is switched OFF at 45.7° elevation. The path loss variation from 3° to 45.7° degrees elevation varies from 180.3 dB to 171.4 dB corresponding to the range variation of 3013 kms to 1086 kms of IRS 1D satellite which is in 817 kms orbit. Though the path loss varied by about 9 dB during the typical pass observed, the received signal strength variation is less than 2 dB as can be seen from the AGC plot. (The plot gives AGC value in volts. Vertical scale corresponds to 2 dB division approximately.)

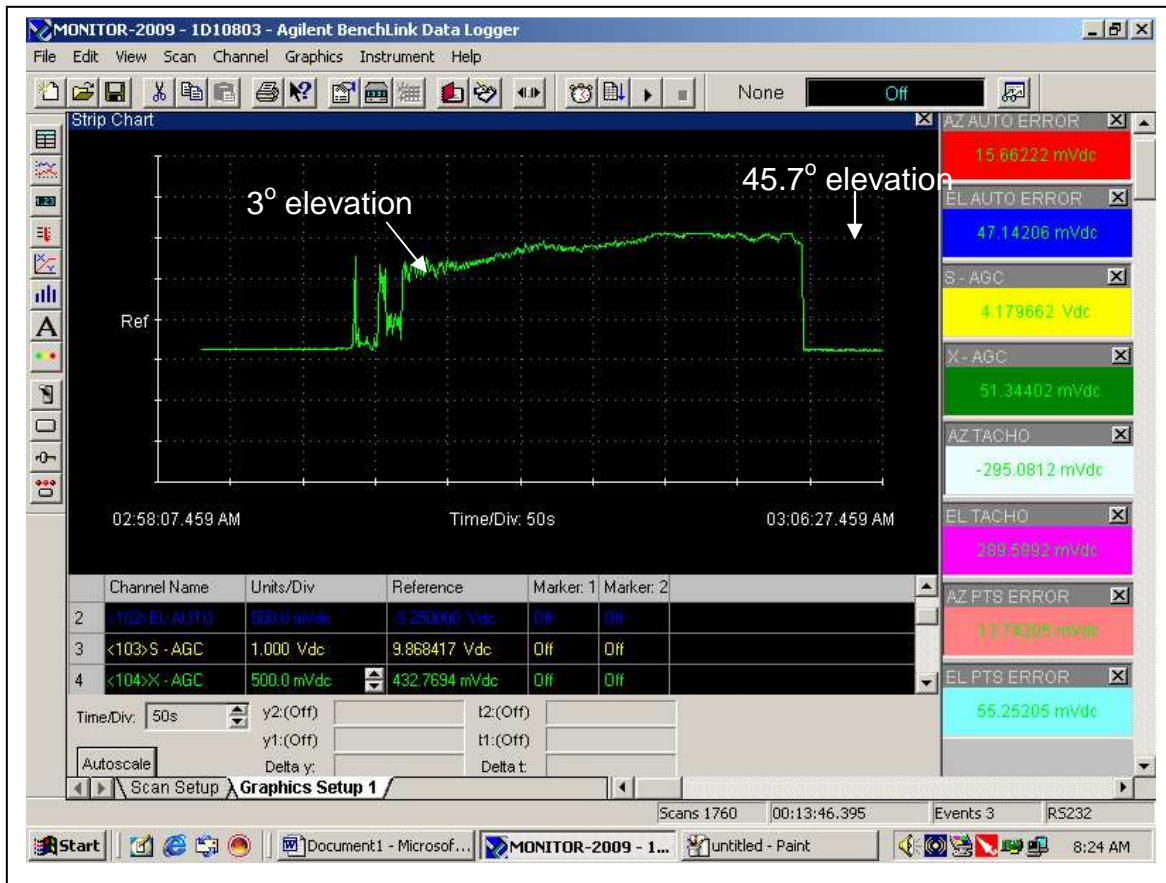


Fig. 3.5 AGC plot of IRS-1D X-band signal

3.2 Data Reception Station (DRS):

The primary function of the ground station is to acquire the data transmitted from the satellite that would be useful for further product generation. The configuration of a remote sensing satellite receive ground station is shown in Fig. 3.6. Antenna with mono pulse tracking feed and front end subsystem can receive the signals from the satellite in X-band (8 to 8.4 GHz) and S-band (2.2 to 2.3 GHz) simultaneously in RHC polarization. The received signal is converted to Intermediate Frequencies (IF) of 375 MHz and 70 MHz respectively and feeds RF/IF subsystem for demodulation and further processing. The receive station has G/T of 32 dB/K at X-band and 20 dB/K at S-band at 5° elevation. The tracking receiver generates the DC error signals corresponding to azimuth and elevation antenna offset angles to the servo subsystem.

3.2.1 Calibration:

As the satellites are visible for short periods of time, the systems validation is done offline and fine-tuned with online results.

3.2.2 Local loop test system:

End-to-end performance of the receive chain is tested in local loop before a satellite-pass. The offline assessment of the data reception systems is carried out based on BER performance of the complete RF chain by injecting the simulated data modulated spectrum into the front end Low Noise Amplifier (LNA), through a 30-dB test-coupler. BER measurements are carried out manually using internally generated pseudo random sequences of a standard sequence length before each satellite pass to ensure for proper functioning of the receive chain.

3.2.3 Bore site transmission system:

An antenna mounted on a high mast, situated at a far off distance, is used to transmit signals identical to onboard transmitting signal which are generated at ground using suitcase models or simulators, towards the ground stations' receive antennas. The bore sight measurements for the evaluation of pointing accuracies and data reception are done for characterizing total receiving system.

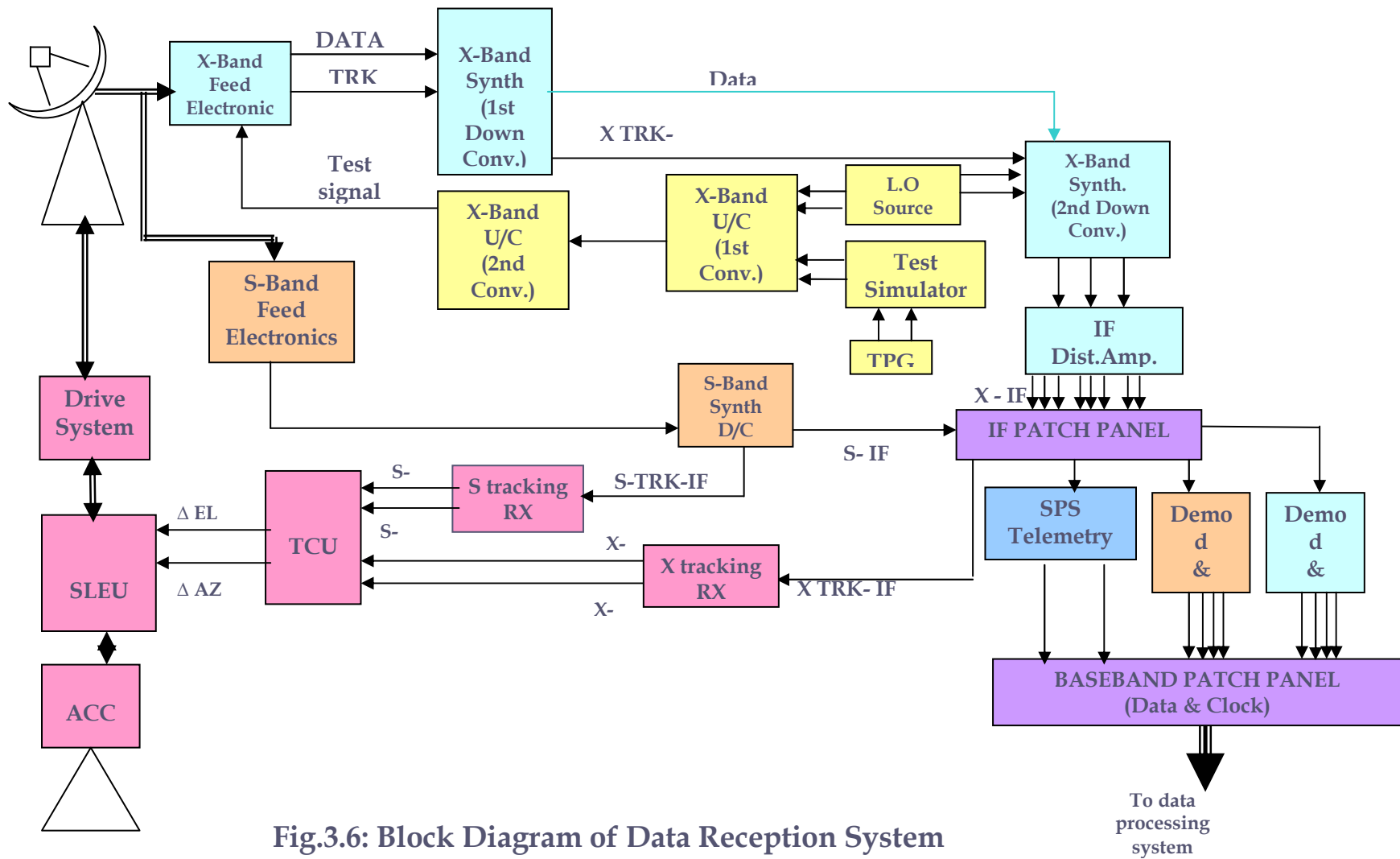


Fig.3.6: Block Diagram of Data Reception System

3.3 Issues that affect link performance:

Based on the test results, the systems are diagnosed and corrected for proper acceptable performance in real time. Uncorrectable errors contribute for the degradation of the total link performance.

The most desirable important function for all remote sensing ground stations is to have the uninterrupted data acquisition from 0 deg. to 0 deg. covering the entire visibility circle of a given station. This has to address two important issues. (a) Handling of disturbances at lower elevation angles (b) Handling of high velocity requirements at higher elevation angles.

Multiple reflections due to terrain, nearby high rise buildings or big trees, affects the signal strength considerably at low elevations making the data acquisition difficult. More over, the noise level also increases at low elevations resulting in unacceptable bit errors. Suitable site selection can improve to some extent and generally, data reception is limited to 5° .

There are difficulties with respect to tracking the satellite for higher elevation angle beyond 87 deg. Since antenna positioner is a mechanical device, some constraints will be placed on the freedom of axis motion by the positioner's physical construction. This choice of positioner coordinate system results in large azimuth velocities for tracking target trajectories that pass near the zenith position. Satellite passes having more than 87° elevation, the velocity requirement in azimuth crosses the limits specifications of the system and the positioner will fall behind the true azimuth position of the satellite until the pointing error exceeds the antenna beam width and the tracking signal is lost. Therefore such passes are required to be identified and to be handled totally by the program track mode and not by auto track mode. In program tracking approach the tracking system is driven by the pre-determined trajectory information of the satellite derived from the satellite state vectors and refined to provide least possible errors.

3.4 Characterization of receive chain:

The quality of reception depends on the signal strength and E_b/N_0 available at the input of a demodulator and hence the analysis regarding the received data quality through quantitative measurements and spectrum analysis becomes essential.

The measurement of E_b/N_0 is done by simulating the satellite transmitted spectrum by an RF simulator having the facility to provide variable signal strengths to simulate different S/N values at different data rates and spectral characteristics at receive demodulator input. The C/N_0 can be obtained from spectrum-analyzer by measuring the carrier power above noise level within the resolution bandwidth of spectrum-analyzer by switching 'OFF' the modulation. E_b/N_0 is obtained by dividing the C/N_0 with the bit rate. Spectrum-analyzer correction factor (noise power bandwidth correction) is taken into account while calculating the C/N_0 .

Real time (on-line) measurement of E_b/N_0 is not possible as there is no provision to switch-off the modulation during the satellite-pass. This measurement of E_b/N_0 on spectrum-analyzer is done only off-line, i.e., in simulated mode, before the satellite-pass. The E_b/N_0 actually available at the input of demodulators during the real time satellite-pass is estimated by comparing the spectrum with simulated spectrum stored off line on the spectrum analyzer. The method obviously leaves the scope of inaccuracy. Average value of repeated observations will reduce the error.

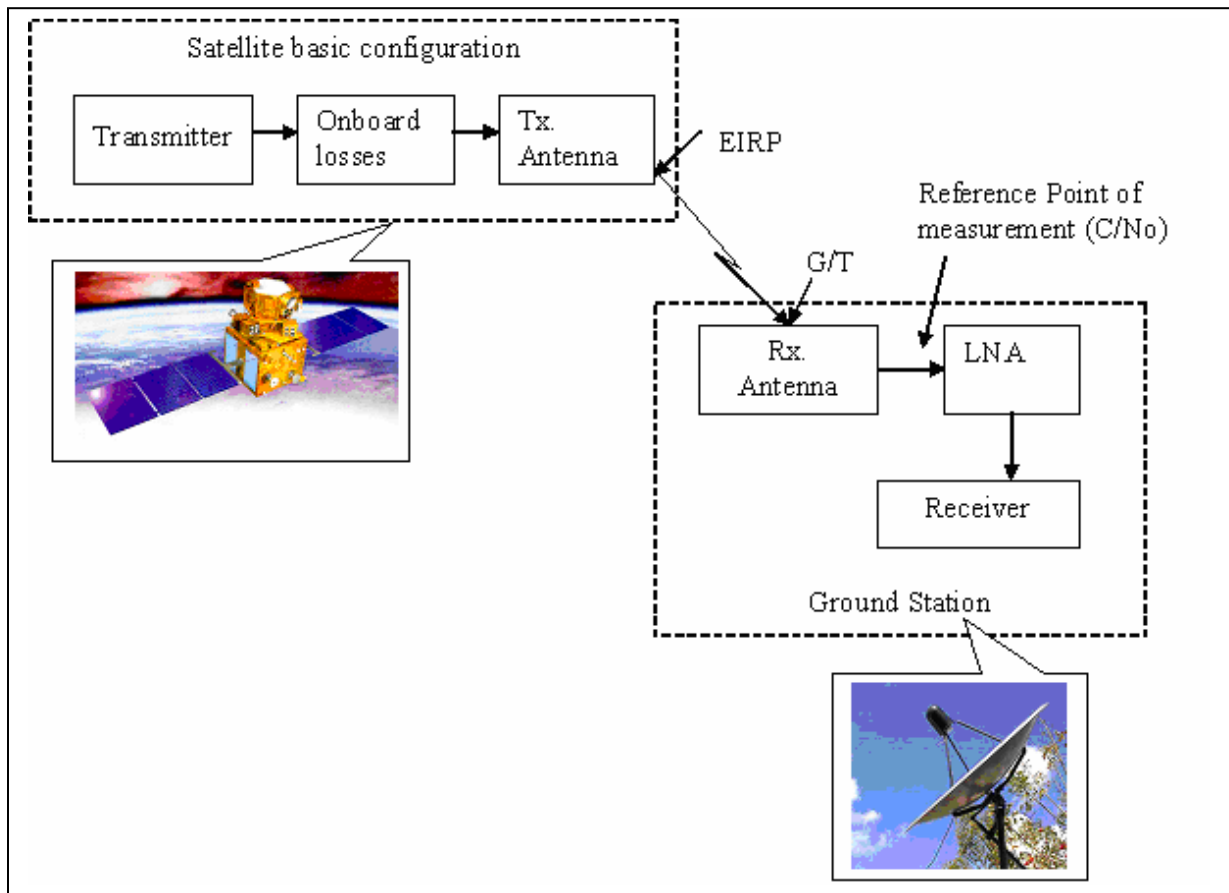
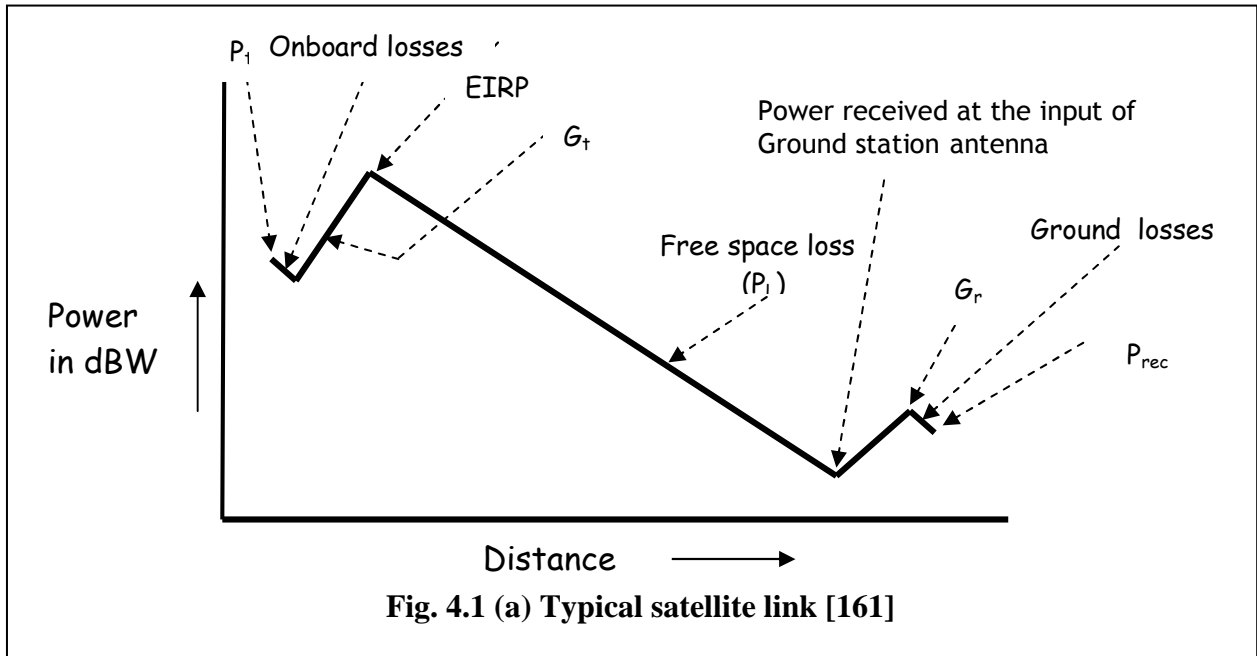
G/T, multiple reflections due to surrounding high rise buildings, trees etc will affect the signal received. Band pass filter ripples, inter-carrier interferences, Electro Magnetic Interference (EMI) and data demodulator & bit synchronizer inaccuracies like phase and amplitude imbalances of QPSK demodulator, clock instabilities, band pass filter characteristics etc, will affect the performance of the total link as explained for onboard system in chapter 4. Above described method of comparing real time received spectrum with offline stored spectrum can not identify this kind of degradation. Degradation can be estimated only by the offline BER measurement.

Chapter 4

Space to earth data transmission link considerations

The space to earth communication link basically depends on the RF frequency chosen, modulation technique, data rate, available channel bandwidth, figure of merit (G/T) of the ground station and onboard Effective Isotropic Radiated Power (EIRP) also termed as Equivalent Isotropically Radiated Power. This would help in understanding the power level requirements, sizing of ground, onboard antenna systems, and power amplifiers, for the desired data quality. Overall link budget analysis [161-164] is essential for any satellite communication system design.

An RF link sizing actually is a relatively simple addition and subtraction of gains and losses within the link. When these gains and losses of various components are determined and assumed, the result is an estimation of end-to-end system performance in the real world. To arrive at an accurate answer, factors such as the satellite onboard power amplifier gain, transmit antenna gain, slant angles and corresponding atmospheric loss over distance, receive antenna and amplifier gains and noise factors, cable losses, interference levels, and climatic attenuation factors must be taken into account. A line diagram [161] of various elements to be taken into consideration for link estimate is shown in Fig. 4.1. Various parameters associated with the satellite data transmission links are explained subsequently.



4.1 Effective Isotropic Radiated Power (EIRP.):

EIRP can be calculated from:

$$EIRP_{dBW} = P_t + G_t - L_g \quad \text{dBW} \quad \text{--- (8)}$$

where Transmitter power = P_t dBW

Transmit antenna gain = G_t dBi

Total onboard losses = L_g dB (between power amplifier and antenna)

Usually there is another parameter – Power Flux Density (PFD) linked with EIRP. PFD is generally defined as the RF power available in a reference bandwidth at the receiving station. The PFD, shall not exceed the ITU limits prescribed (Table 1.2). A satellite communication system designer shall take care of these limits which become the limiting factor for the maximum EIRP transmitted from a satellite. A limit on the EIRP also comes from the tolerable interference limit at other ground stations

4.2 Slant range & look angle:

For typical satellite earth geometry (Fig. 4.2) assuming earth to be perfect sphere, the **satellite slant range** at an elevation angle θ of ground station antenna, when pointed to satellite, with horizontal plane and **look angle** α the angle between satellite Yaw axis (line SNO) and range vector (line SG) are calculated from orbit height and earth radius as explained below:

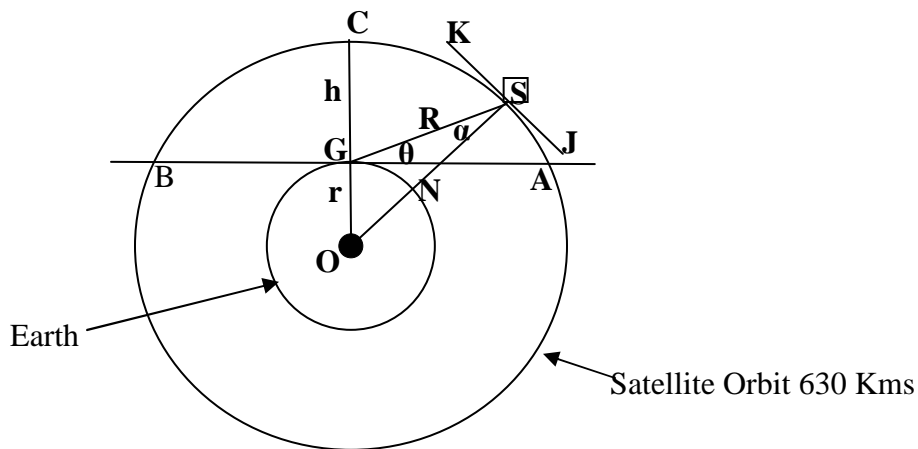


Fig. 4.2 Satellite earth/orbit geometry

In Fig. 4.2:

Satellite is at point **S**

Ground station is at point **G**

O – Centre of earth

OG = ON - Earth Radius: $r = 6380$ Kms

GC = NS - Orbit height above earth : $h = 630$ Kms (for example)

θ - ground station antenna Elevation

AGB - Tangential line at Ground station ($\theta = 0^\circ$)

JK - Tangential to orbit at S (Line OGS is perpendicular to line JK)

α - Look angle of satellite to ground station (angle between Yaw axis of satellite (SNO) and range vector (SG))

From the above figure, it can be written that

$$\frac{r}{\sin \alpha} = \frac{r+h}{\sin(90+\theta)} = \frac{R}{\sin[180-(90+\theta)-\alpha]} \quad \text{--- (9)}$$

Above expression can be reduced to

$$\frac{r}{\sin \alpha} = \frac{r+h}{\sin(90+\theta)} = \frac{R}{\cos(\theta+\alpha)} \quad \text{--- (10)}$$

By rearranging the expression and simplifying, we can get Range R and Look angle α as:

$$\text{Look angle } \alpha = \sin^{-1} \left[\frac{r \cdot \sin(\theta+90)}{r+h} \right] \quad \text{--- (11)}$$

Similarly Range R is obtained by:

$$\text{Range } R = \sqrt{(r+h)^2 - r^2 \cdot \cos^2 \theta} - r \cdot \sin \theta \quad \text{--- (12)}$$

When satellite is at point A or B, the look angle $\alpha = 65.5^\circ$

The distance between the ground station and satellite will be maximum when the satellite is at point A or B in the figure 2.3 where ground station antenna elevation is zero. At 90°

elevation, the satellite will be overhead having minimum range equal to orbit height. Accordingly, path loss (Free space loss) will be maximum when satellite is visible to ground station antenna with zero degree elevation and minimum when satellite is overhead i.e., at zenith to ground station.

4.3 Free space loss, also referred as path loss or **spreading loss**, is calculated from the equation:

$$\text{Spreading loss} = 10. \log \{ (4.\pi.R/\lambda)^2 \} \text{ dB} \quad \text{--- (13)}$$

Where λ is wave length

R is the slant range

A typical range, path loss and look angle profiles for a satellite at 630 kms orbital height above the earth are shown in Fig. 4.3:

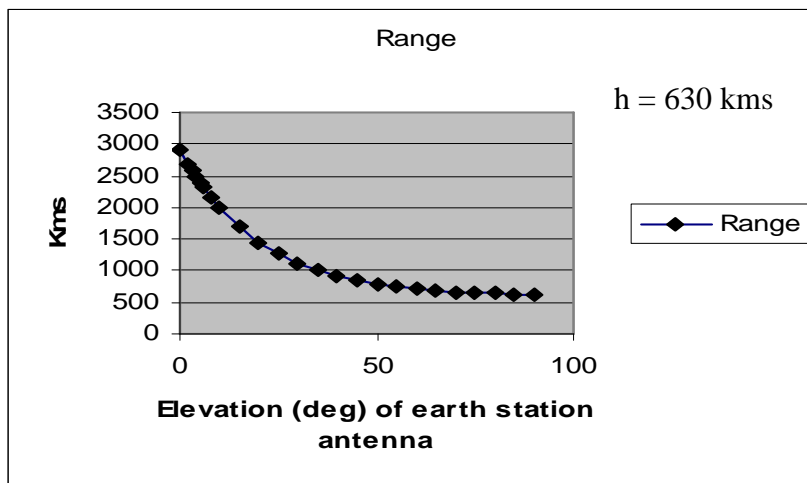


Fig. 4.3 (a). Satellite Range with respect to ground station antenna elevation

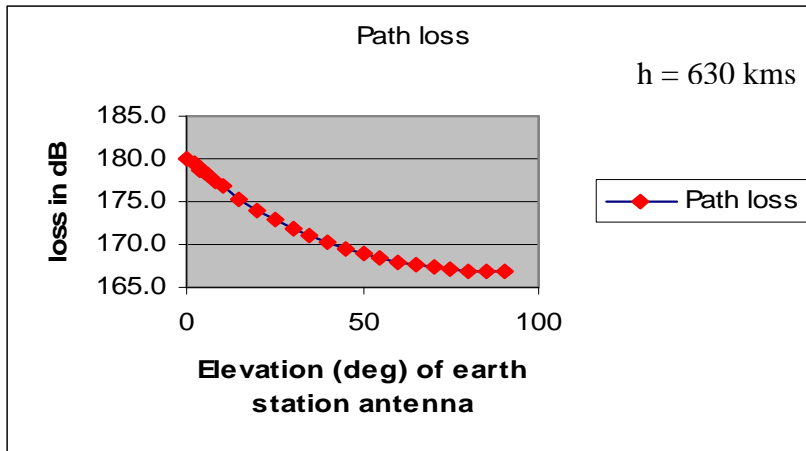


Fig. 4.3 (b) Path loss with respect to ground station antenna elevation

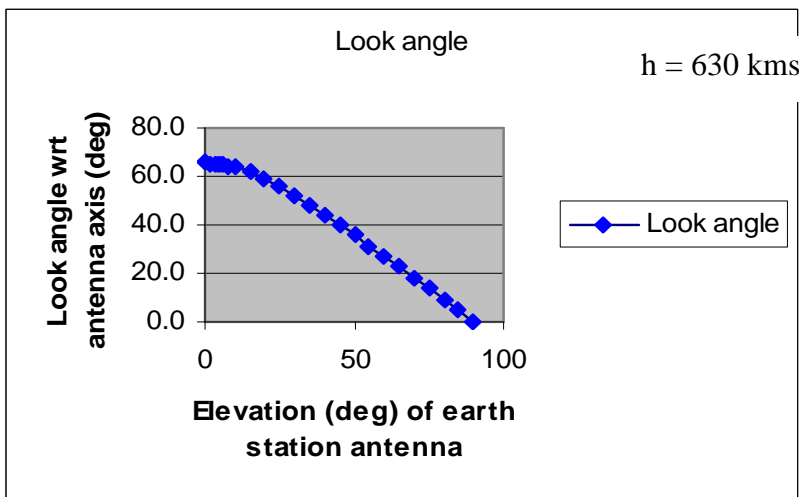


Fig. 4.3 (c) Satellite antenna look angle with respect to ground station antenna elevation

4.4 Losses other than path loss:

The “other losses” include:

- Atmospheric losses.
- Polarization loss.
- Antenna pointing loss.

Note: All links are usually worked out for 5° and above elevation. For 5° and above elevation, multipath effects are not considered.

There are many phenomena that lead to signal loss on transmission through earth’s atmosphere [37]. These include: Atmospheric absorption (gaseous effects); Cloud attenuation (aerosol and ice particle effects); Tropospheric Scintillation (a second

ionospheric effect); Rain attenuation; and Rain and Ice crystal depolarization. Rain attenuation is by far the most important of these losses for frequencies above 10 GHz. Rainfall causes the absorption and scattering to microwave signals results in severe degradation of the receive signal level. Both attenuation and depolarization come from interactions between the propagating electromagnetic waves and whatever is in the atmosphere at that time. The atmospheric constituents may include free electrons, ions, neutral atoms, molecules and hydrometers (an arcane term that conveniently describes any falling particle in the atmosphere that contains water: raindrops, snowflakes, sleet, hail, ice-crystals, graupel etc.); many of these come in a wide variety of sizes.

On most satellite links above 10 GHz, rain attenuation limits the availability of the system and, to develop an adequate link margin, the rain attenuation to be expected for a given time percentage needs to be calculated. This can be a complicated process, but there are basically three steps: (a) determine the rainfall rate for the time percentage of interest; (b) calculate the specific attenuation of the signal at this rainfall rate in dB/km; and (c) find the effective length of the path over which this specific attenuation applies. As well as causing significant attenuation, rain and ice crystals can cause depolarization. Depolarization is more difficult to quantify than attenuation. Ice crystal depolarization occurs only in severe thunderstorms and so it is a rare occurrence. At frequencies below 50 GHz, rain attenuation is mostly caused by absorption rather than by scattering of signal energy out of the path. Specific attenuation model for use in the rain prediction methods recommended by ITU is given in Annexure C. Fig. 4.4 shows typical estimated attenuation characteristics with respect to frequency due to rain.

Antenna pointing loss in auto tracking mode, with the present servo control systems, is negligible. However, this is addressed in section 3.3.

Atmospheric absorption: At microwave frequencies and above, electromagnetic waves interact with molecules in the atmosphere to cause signal attenuation. At certain frequencies, resonant absorption occurs and severe attenuation can result. These resonant absorption peaks can be seen from Fig. 4.5.

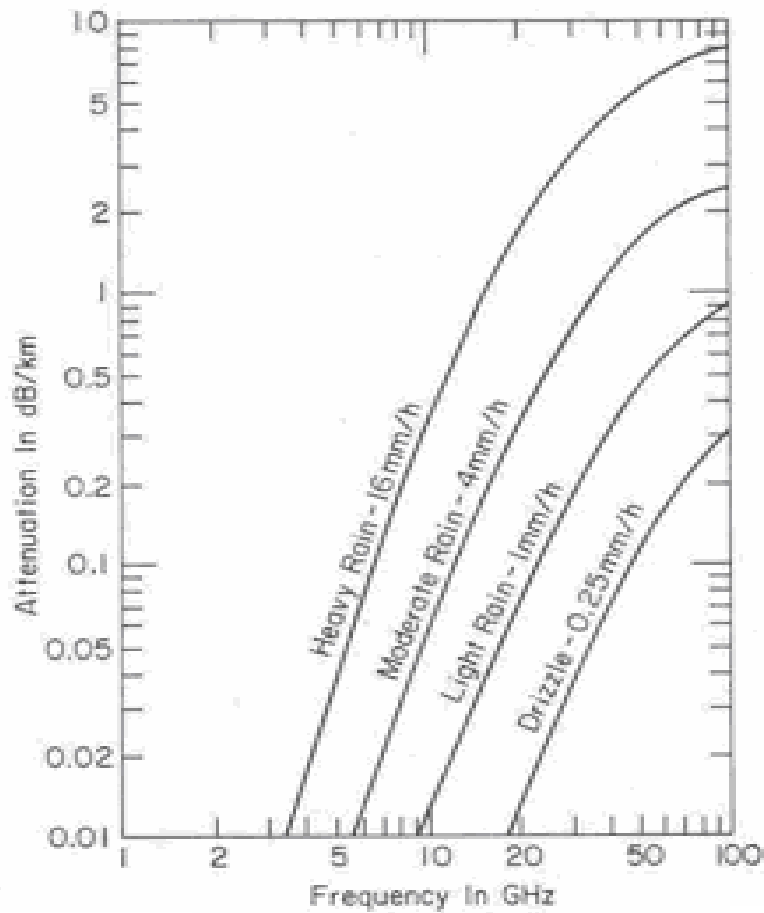


Fig. 4.4 Attenuation due to rain fall at 18deg C [170]

Any absorber with physical temperature greater than absolute Zero (0 degree Kelvin) will act as a black body radiator. The radiation is in the form of white Gaussian noise. As can be seen from the figure Fig. 4.4, heavy rain in slant path can cause attenuation above C band frequencies which attenuates the signal power and also increases the noise temperature of the receiving path [37]. Table 4.1 gives typical noise calculation for a ground station with and with out rain: Heavy rain causing 3dB rain attenuation at X-band causes over 11 dB degradation in G/T of a ground station having a 7.5 meter antenna with 80 deg K system noise temperature. In addition, Received signal will be less to an extent of rain attenuation i.e. 3 dB in this example.

Table 4.1. Comparison of G/T (Noise) with and with out Rain attenuation

	With out Rain	With Rain
Frequency	X-band	X-band
Sky noise (Fig. 4.5)	20°K	20°K
Rain attenuation (Example) L_R	0	3 dB
Noise due to rain $290(L_R-1)$	0	290_oK
Noise picked up by antenna	20°K	$(20+290)/L_R = 155_oK$
Antenna gain G (7.5 meter)	55 dB	55 dB
System Noise temperature	80°K	80°K
Total noise temperature at antenna	100°K	235°K
G/T	35 dB/k	23.7 dB

Because of this rain attenuation and its effect on antenna noise, data transmission is confined to X-band to the possible extent by adopting all new transmission techniques for sending high bit rate payload data from satellite to ground station.

4.5 G/T (Figure of Merit of the Ground station) :

To calculate the G/T of a terminal operating with the satellite, the reference plane is taken at the input to the LNA (Fig. 4.1b). G is the Gain of the receiving antenna. Ground stations in general employ Cassgrain parabolic reflector antennas. The gain of a reflector antenna is given by

$$G = (\pi d/\lambda)^2 \cdot \eta \quad \text{--- (14)}$$

Where d is antenna diameter,

λ is wavelength of the carrier frequency = (velocity of light)/frequency.

η is efficiency of the antenna

T is the total effective noise temperature T_{sys} of a receiving system, conventionally referred to the input of the receiver/Low Noise Amplifier (LNA).

T_{sys} is given as:

$$T_{SYS} = T_{ant} + T_{rec} \quad \text{--- (15)}$$

Where T_{ant} is Effective noise temperature of antenna subsystem and represents the noise picked up by antenna from Galactic or back ground sky noise. The back ground sky noise [184] is shown in Fig. 4.5.

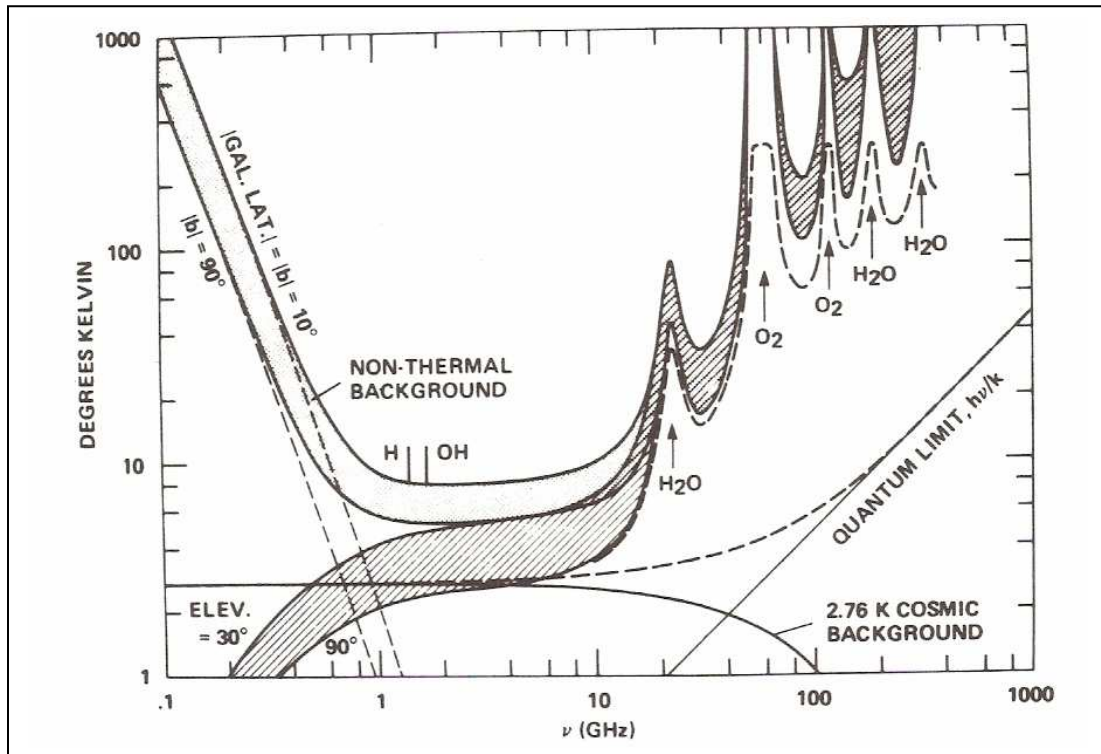


Fig. 4.5 Back Ground Radio Noise Spectrum [184]

Integrated look at the noise contribution reveals a broad quiet region extending from 1 to 60 GHz which is known as the free space microwave window. The galactic noise increase rapidly below 1GHz. The quantum noise limits impose a severe restriction above 60 GHz. Even in this region, absorption effects of water and oxygen degrade the window between 10 and 60 GHz

T_{rec} = Effective input noise temperature of receiving system. With a high gain Low noise amplifier, the receiver noise depends mainly on the noise figure of the front end low noise amplifier and is given by

$$T_{rx} = 290(F-1) \text{ degrees} \quad \text{--- (16)}$$

Where F is noise figure of Receiver which is nearly same as that of Low Noise Amplifier.

The ohmic loss components from the antenna feed to the receiver input also generate noise. Other loss producing elements are transmission lines, directional couplers, circulators, isolators, waveguide & switches. The loss factor of these components are inverse of gain ie; The respective noise temperatures would be

$$L_a = 1/g_a \quad \text{--- (17)}$$

The equivalent noise figure or noise factor

$$n_f = L_a + T_e/T_0 \quad \text{--- (18)}$$

$$\text{where } T_e = T(L_a - 1)$$

And the noise figure in dB is

$$NF_{dB} = 10 \log_{10} n_f \quad \text{--- (19)}$$

At room temperature (290 K), the noise factor equals the loss of the system

$$\text{ie; } n_f = L_a \quad \text{--- (20)}$$

G/T is measured using celestial sources like Cassopia, moon and even sun as signal sources. A typical measurement procedure reported in literature is presented in Appendice A.

Typically, a ground station like that of NRSC (ISRO) with 7.5 meter antenna will have a G/T of 32 dB/K at X-band above 5° elevation.

4.6 Estimation of C/N_0 :

C/N_0 (C/N_0 is carrier to noise density, where N_0 = noise density in 1Hz & C is the received signal power.) is a very important element in communication link. By knowing C/N_0 one can estimate the quality of demodulated signal.

Here:

$$N_0 = KT = 228.6dBW + 10\log T_{SYS} \quad \dots \text{ dB/Hz} \quad \text{--- (21)}$$

$$C_{dBW} = P_{rec} + G_{ant} - \text{line losses}(L_l) \quad \dots \text{ dBw} \quad \text{--- (22)}$$

K (Boltzmann's constant) = -228.6 dBw is the theoretical value of noise level in dBw for a perfect receiver (noise factor of 1) in 1 Hz bandwidth.

C/N_0 of a link can also be expressed as :

$$\frac{C}{N_0} = (EIRP)_{dB} - (Freespaceloss)_{dB} - (otherlosses)_{dB} + \left(\frac{G}{T_{dB/k} - K} \right) \quad \text{in dB/Hz} \quad \text{---(23)}$$

4.7 Probability of Error:

The measure of system performance for digital data communication is the Bit Error Rate or some times referred as probability of error P_E mathematically represented as:..

$P_E = \frac{1}{2} \text{erfc} \left(\sqrt{\frac{E_b}{N_0}} \right) \quad \text{--- (24)}$	E_b/N_0 is defined as the received signal energy per bit per hertz of thermal noise and is expressed in dB
---	--

$$\left(\frac{E_b}{N_0} \right) = \frac{C}{KTR} = \frac{C}{N_0} - 10\log(\text{bitrate}) \quad (\text{dB}) \quad \text{--- (25)}$$

$$\left(\frac{E_b}{N_0} \right) \text{ can also be written as:}$$

$$\left(\frac{E_b}{N_0} \right) = \frac{C}{N_0} \left(\frac{1}{R} \right) \quad (\text{dB}) \quad \text{--- (26)}$$

Where R = Bit rate, C=Received carrier power.

Fig. 4.6 shows theoretical Probability of bit error (P_e) with E_b/N_0 for PSK (BPSK & QPSK) systems [40].

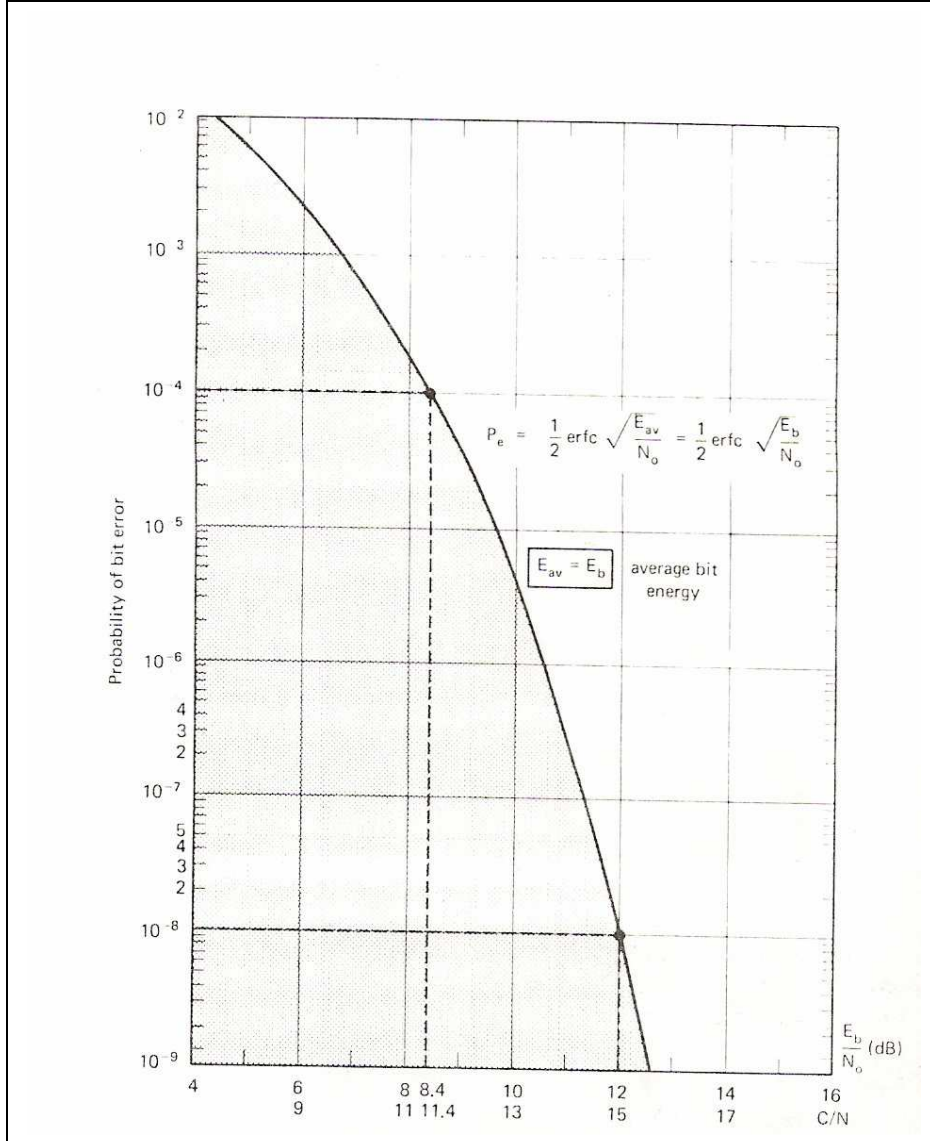


Fig. 4.6 Theoretical $P_e=f(E_b/N_0)$ performance of coherent BPSK/QPSK modems [40]

4.8 Implementation margin:

In practice, more E_b/N_0 is required for achieving the required BER over the theoretical E_b/N_0 requirement indicated in Fig. 4.5. This extra E_b/N_0 called as implementation margin is to be taken care in sizing the EIRP of the satellite. This additional margin is required to take care of various deviations causing degradation of performance.

4.8.1 Degradation due to Data quality:

Poor rise/fall time and data asymmetry causes considerable degradation in the RF performance [183]. Degradation of the total link due to increased rise/fall time and data asymmetry is shown in figures 4.7 and 4.8.

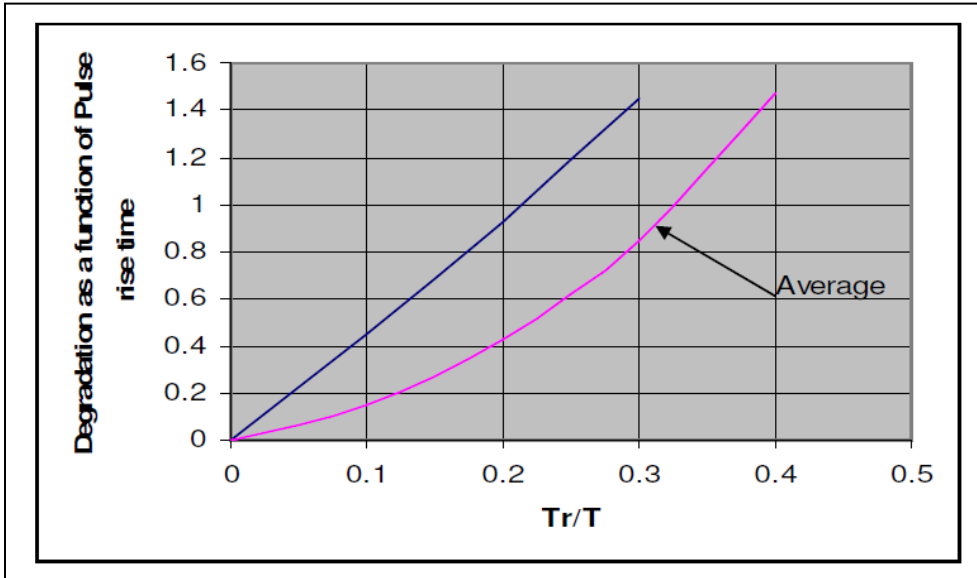


Fig. 4.7 Degradation with rise time [183]

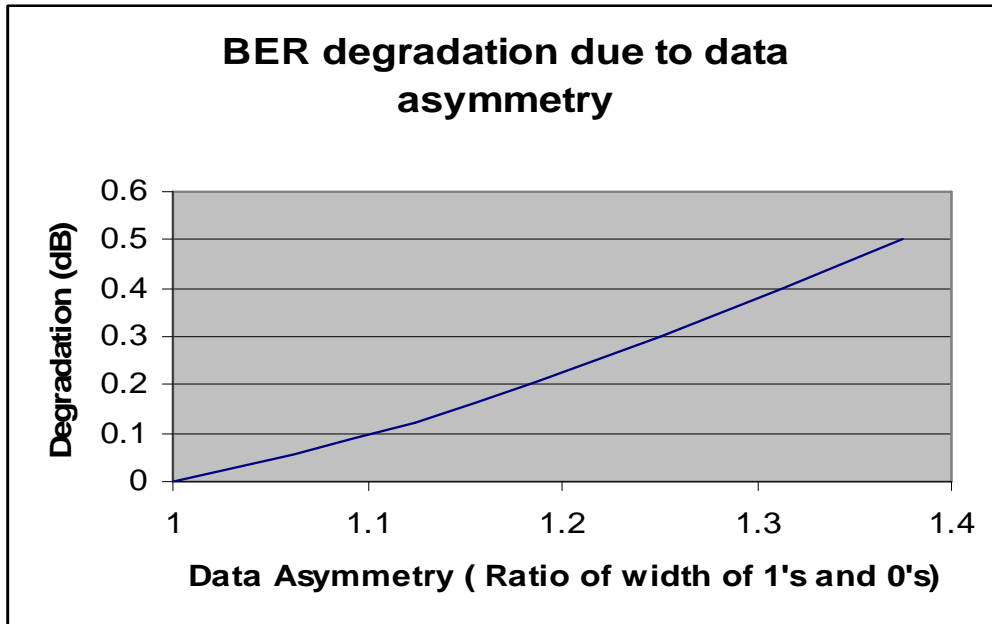


Fig. 4.8 Degradation with data asymmetry [183]

4.8.2 Degradation due to QPSK Modulator parameters [183]:

The basic parameters that affect the performance of the QPSK modulator are phase accuracy and amplitude imbalance. The phaser diagram of a QPSK signal is shown in Fig. 4.9

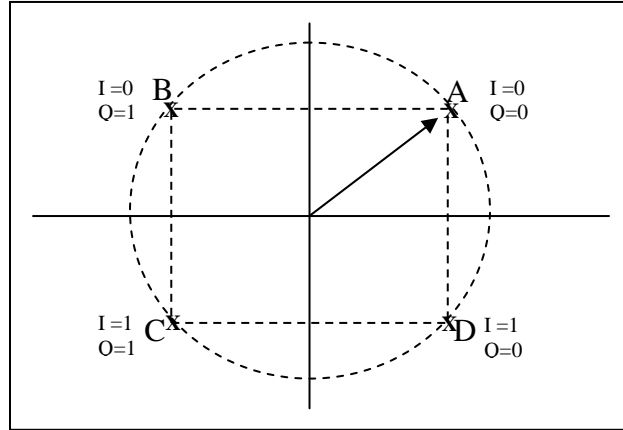


Fig. 4.9 Phaser diagram of QPSK signal

Points A,B,C,D corresponds to four phase states of 0° (reference), 90° , 180° and 270° corresponding to IQ data of 00, 01, 11, and 10 respectively. Ideally, the amplitude of the four points shall be same. Due to practical limitations of the components and circuits used to realize QPSK Modulator at X-band, phases and amplitude of the waveform at the four phase state conditions will differ from ideal values. These inaccuracies will contribute to the degradation of BER performance. Fig. 4.10 and Fig. 4.11 show the degradation in the RF link performance due to phase and amplitude errors.

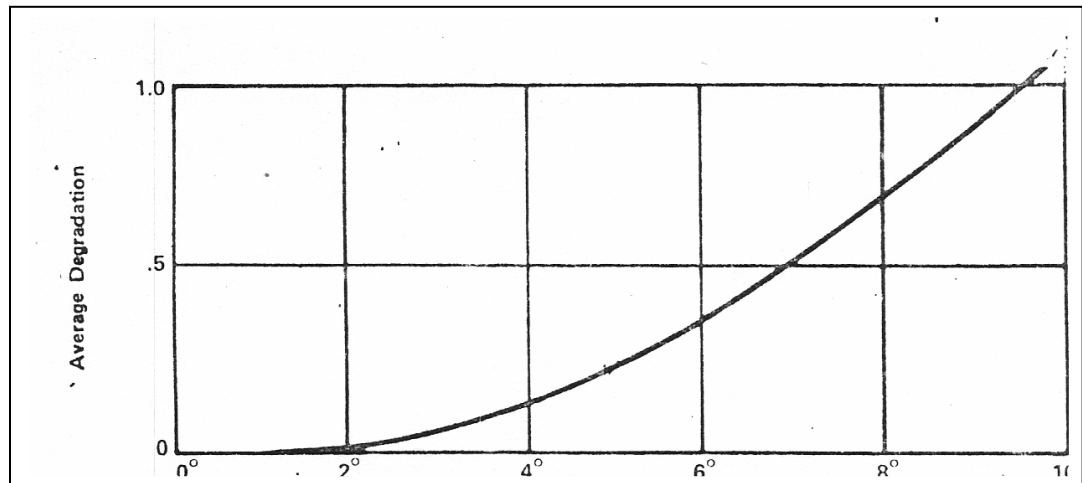


Fig. 4.10 Degradation due to Phase imbalance in QPSK modulation [183]

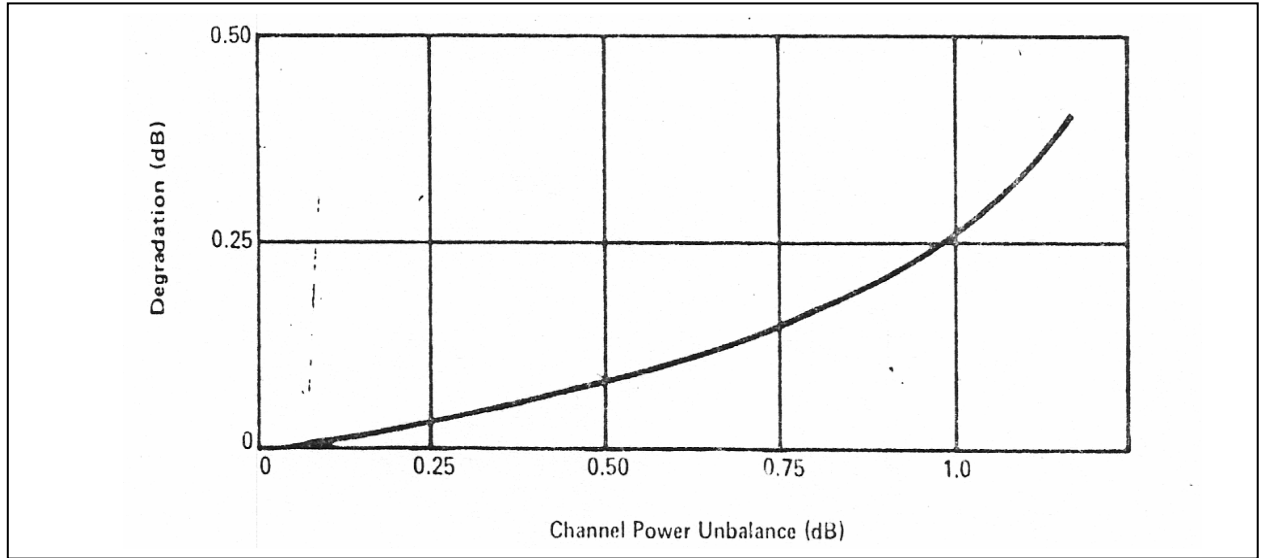


Fig. 4.11 Degradation due to amplitude imbalance in QPSK modulation
11821

4.8.3 Degradation due to AM/PM conversion in Power amplifier:

For high bit rate Data transmission, normally Traveling Wave Tube Amplifiers (TWTA) are used. The Power amplifiers are normally operated at saturation to exploit the advantage of high efficiency at saturation. The power amplifiers exhibit AM/PM transfer behaviour. Fig. 4.12 shows AM/PM characteristics of a typical TWTA given by M/s Hughes in their catalog.

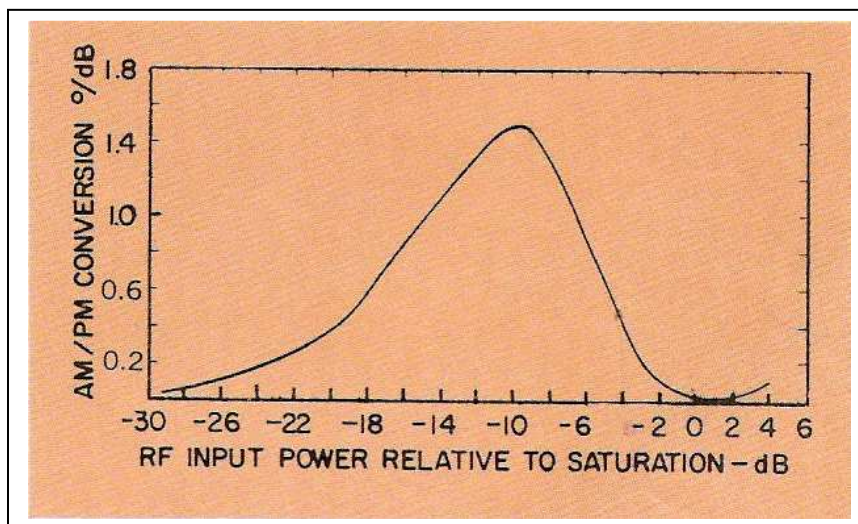


Fig. 4.12 AM/PM characteristics of TWTA.

Amplitude imbalance of the QPSK modulated signal when amplified by a power amplifier operating at saturation generates phase error depending on the AM/PM coefficient at the operating point. This phase error will add to the phase inaccuracy of the QPSK modulated signal and degradation due to phase imbalance increases. AM/PM transfer coefficient of SSPAs is better than that of TWTAs. Since, at high powers, SSPA is inefficient, TWTAs can not be replaced by SSPAs and the degradation shall be taken into account while designing the satellite link.

4.8.4 Degradation due to bandwidth limiting:

The RF spectrum, with $(\sin x)/x$ distribution, occupies infinite bandwidth theoretically. It is essential to limit the radiated spectrum to the minimum possible bandwidth. The spectrum can be restricted by pre-modulation filtering the data and also by band limiting the transmission channel. The data can be practically demodulated by restricting the QPSK spectrum to a bandwidth of 0.6 times the data rate. The effect of this filtering is to degrade system performance due to both filtering distortion and the associated inter-symbol interference [183]. It is important to determine the system performance degradation (Fig. 4.13) and trade off involved with the use of filter.

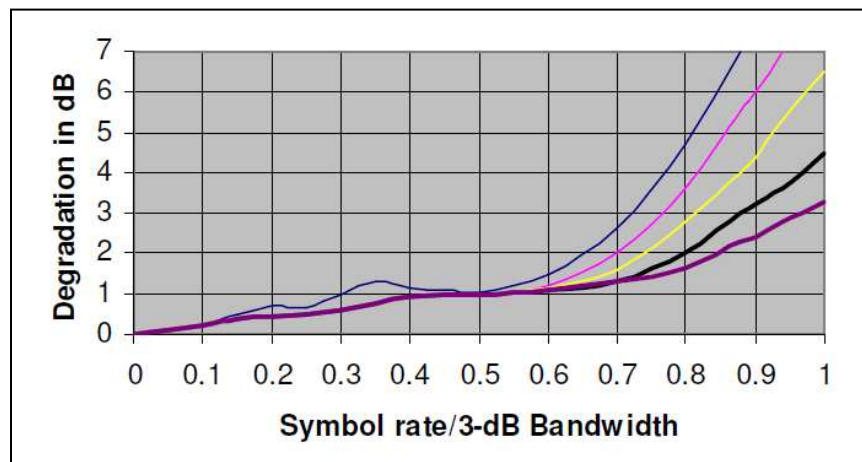


Fig. 4.13 Bandwidth limiting degradation of QPSK signals [183]

4.8.5 Degradation due to interference:

Interference of the spread of the spectrum of adjacent signals, and poor cross polarization isolation in case of transmission in dual polarisation, multiple reflections etc will cause degradation in the performance of the desired signal. Fig. 4.14 shows the degradation with respect to carrier to interference levels [183].

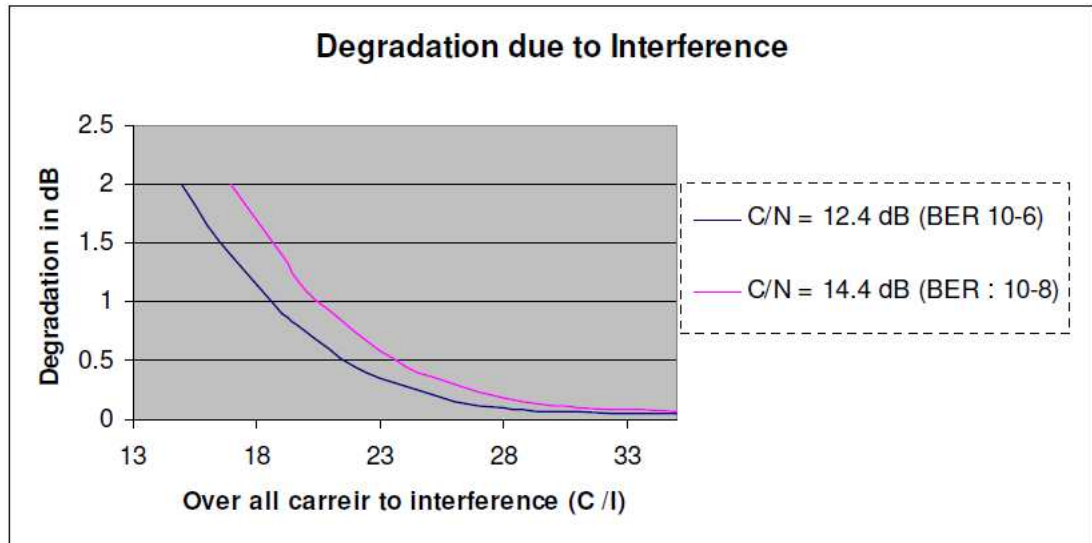


Fig. 4.14 Degradation due to interference [183]

- In general, about 1.5 dB implementation margin is found to be required for reception of 105 MBPS data QPSK modulated X-band signals of IRS at NRSC Data Reception Station.
- Adequate filtering of the modulated carriers on satellite and at ground station is essential to reduce interference degradation in case of multi carrier transmission. Generally, over all Carrier to Interference level better than 25 dB is acceptable.

Chapter 5

Performance analysis of data transmission links of IRS missions.

Any satellite is always designed to have sufficient EIRP to satisfy the performance requirements of the mission. EIRP is planned based on link performance for a given mission data rates and corresponding E_b/N_o requirement. ISRO launched application specific remote sensing satellites in various orbits (Table 1.1). Various parameters affect the performance. Some effects can be expected, based on experience, margin (implementation margin) can be provided to take care of the known performance degradations (section 4.8). Practically, about 2 dB implementation margin needs to be accounted to take care of performance degradation due to deviations of various system parameters (viz., modulator, demodulator, clock/carrier jitter, duty cycle etc.) .

$$\text{Required } C/N_o = E_b/N_o + \text{implementation margin} - 10 \log (\text{data rate}) \quad \text{--- (27)}$$

$$\text{Estimated EIRP} = C/N_o - G/T + \text{Free space loss (Path loss)} \quad \text{--- (28)}$$

Where G/T is figure of merit of the Ground Station/terminal.

The link estimate for a remote sensing satellite transmitting 105 MBPS data by QPSK Modulating an X-band carrier of 8300 MHz from 817 Kms orbit is as given in Section 3.1.2.

As per link estimation (Table 3.1), the margin for operation shall be 6.0 dB for Resourcesat-1(IRS P6) and 7 dB for Oceansat-1 (IRS P4) missions above the overall link margins accounting for degradations and implementations. During in orbit observations, this much margin could not be observed in both missions throughout the visible duration of the satellites from Shadnagar (Hyderabad) Ground station. In Oceansat-1 (IRS P4), even data loss was reported below 5° elevation. In addition various kinds of distortions in the RF Spectrum were also seen in most of the missions. In some cases, data loss, pixel dropouts and data errors, i.e., more BER, were observed due to reduction of link margins.

Possible causes for the deviations in space to earth link:

Degradation in onboard EIRP: Various factors that contribute to the reduction in EIRP are given below:

- Reduction of the power amplifier output
- Spurious generation in electronic circuits
- Detuning of band pass filters
- Onboard antenna radiation pattern
- Multipaction / corona - This problem is taken care while designing high power sections viz., band pass filters and plumbing lines in the high power path. All modules are also tested for 6dB higher power than operating power to ensure multipaction and corona free operation.

Note: These possible causes are addressed carefully during the spacecraft system development, integration and spacecraft level tests. These include thermo vacuum test, vibration and acoustic tests which take care of any detuning or degradation in overall EIRP.

- Degradation in Ground station:
 - Tracking problem/Pointing accuracy
 - G/T reduction
 - Ground noise increase - Man made noise
 - Degradation in receive systems resulting in higher Eb/No requirement
 - More implementation loss
- Rain attenuation (Annexure C) – At X-band rain attenuation is insignificant figure to be accounted.
- Spectrum distortion: Often the following deviations are observed in the QPSK modulated spectrums.
 - Onboard system modulation inaccuracies result in:
 - Phase and amplitude imbalance
 - Data asymmetry

- Carrier leakage- discrete components in the spectrum
- Spectrum distortion from conventional sync function.
- Sideband imbalance - Asymmetry in lower and upper parts of the spectrum
- Band limiting of spectrum.
- Inter carrier interference
- Non linearity increasing Inter Modulation (IM) products
 - AM/PM conversion
- Multiple reflections – predominant at low elevation angles

The analysis of the specific problems observed in some of the IRS series of satellites in orbit and during pre launch testing is discussed subsequently. The problems observed during design and testing in laboratory are also discussed. Mitigation techniques are suggested for improving the performance of the data transmission links.

5.1 IRS – P4 (Oceansat-1):

Reduction in margin was reported in almost all orbits tracked by Data Reception Station(DRS) situated at Shadnagar, Hyderabad. Total data loss was also reported in few orbits at low elevation angles.

About 7 dB margin shall exist in IRS P4 data link as per link estimation (Table 3.1). Data loss occurs only when BER increases to 10^{-4} or more indicating that signal has suffered a loss to the tune of 10 dB that includes the extra margin. It is also observed that margin starts reducing right from 20° elevation .

Analysis:

Various factors that can contribute to the problem of data reception and the causes for the loss of margin are analyzed. Conducted Test and Evaluation (T&E) of the total ground station and identified the problem.

- **Tracking problem – pointing error/accuracy:**

Dual drive system is employed in the antenna system with practically no scope for back lash. During the T&E, it has been confirmed from the error voltage recorded, that there was no scope for additional pointing error.

- **Degradation in the demodulation system:**

The E_b/N_0 requirement is independent of elevation and azimuth angles and can not reduce margin only at low elevation angles. However, demodulator's performance was found to be requiring about 13 dB E_b/N_0 for 10^{-6} BER indicating an additional E_b/N_0 of about 1.0 dB requirement. Replaced the demodulator with an alternate calibrated system.

- **Lower G/T:**

The terminal used for IRS P4 data reception was found to be having G/T of 30 dB/k even at high elevation instead of 32 dB/k. Disturbance was noticed in the feed position. The problem in the feed assembly is rectified and the G/T at high elevation angles improved but the problem at low elevation angles (below 5 degrees) still persisted. Lots of trees have grown taller around the antenna area and added to the received signal strength degradation problem at low elevation angles. Fig. 5.1 gives overall view of the DRS at Shadnagar.



Fig. 5.1 A view of Data Reception Station

When trees are trimmed to make antenna visibility clear above 2° elevation, G/T improved by about one dB.

Generally, IRS satellites data is obtained only above 5 degrees elevation and the reduction in G/T has not caused any problem for data reception. Since IRS-P4 has typical requirement of monitoring Indian ocean, Bay of bengal and Arabian sea, reception of data at low elevation angles has become necessary. Hence this problem of low G/T at low elevation angles has become predominant for the degradation in performance.

In general, G/T can decrease in certain azimuth and low elevation angles due to increase in noise temperature. The noise, thereby T, increases at low elevation angles which can be due to inband manmade noise multipath, ground conditions (wet or dry) temperature etc. Fig. 5.2 show noise temperature and G/T variation with elevation for a 5.4 meter antenna at X-band as reported by Scientific Atlanta-a well known manufacturer of space receive systems.

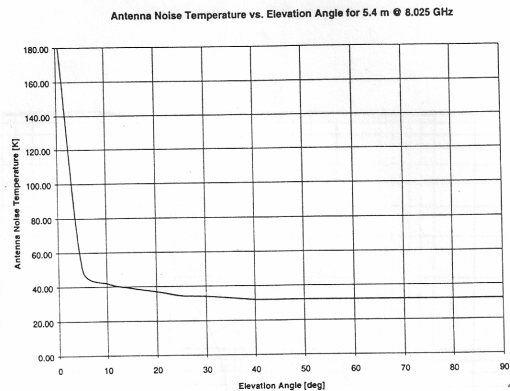


Fig 5.2(a) Noise Temperature with ground station antenna elevation

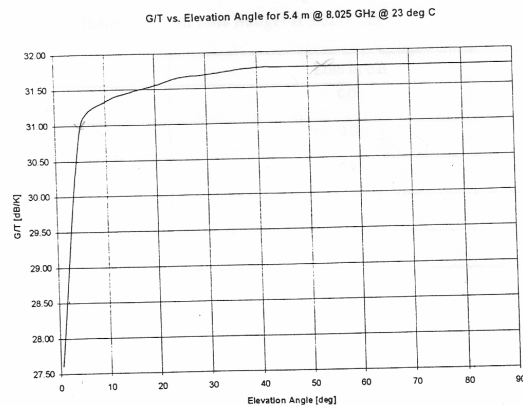


Fig. 5.2(b) G/T vs Ground station antenna Elevation angle

Noise survey is done on site at different times of the day. At different elevation angles the antenna is rotated in azimuth by 360° and noise level is measured on the spectrum analyzer (Fig. 5.3). Measured noise profile at 5° elevation at two instances, given in Fig. 5.3, is indicating an increase of noise level to an extent of 2 dB compared to the level

recorded at high elevation (45°). Fig 5.3(a) shows bursts of noise while Fig 5.3(b) shows small variation with one peak towards north of the station.

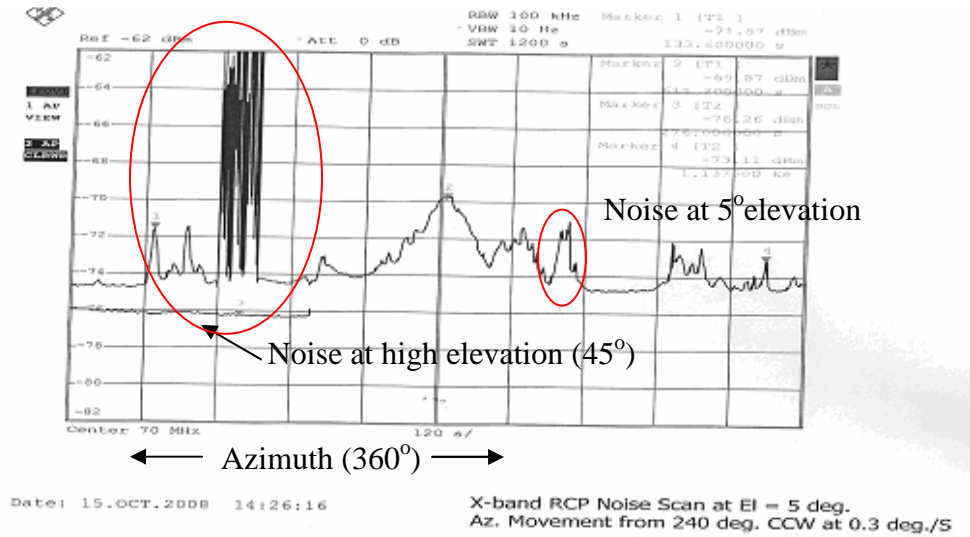


Fig. 5.3 (a). Noise temperature over full azimuth rotation of the antenna recorded on 15th October 2008.

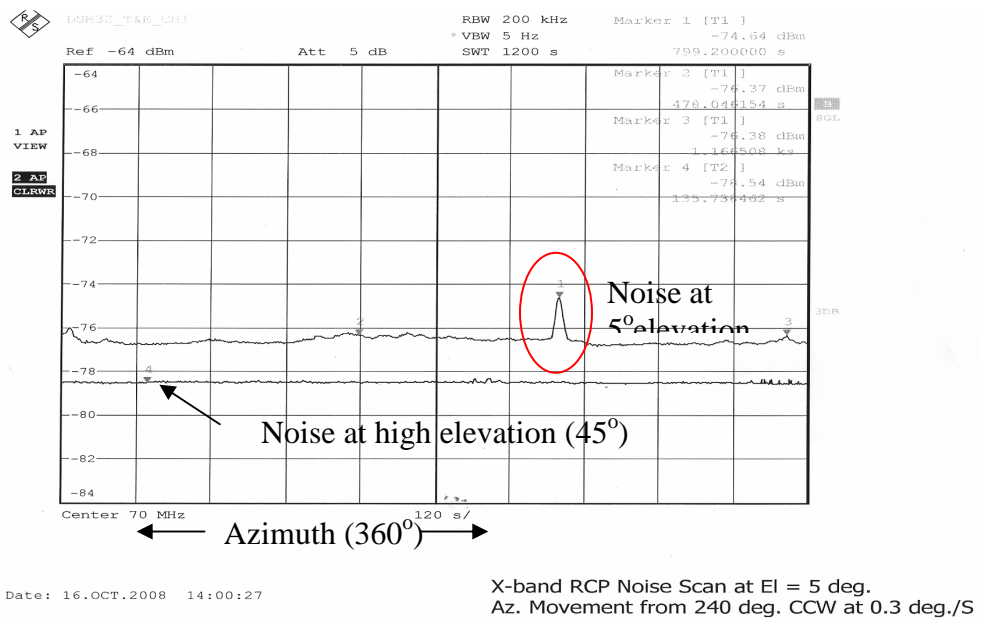


Fig. 5.3 (b). Noise temperature over full azimuth rotation of the antenna recorded on 16th October, 2008.

It is observed that a building and a mobile communication tower are in the visibility of the antenna in northern direction. The single peak which is repeating in both figures may be due to the obstruction which is in the line of sight.

The excess noise seen in fig 5.3 (a) may be due to inband man made noise observed once in a while. Ignoring the man made noise and single peak of noise in north direction, the G/T reduces by about 2 dB.

Fig 5.4 shows the atmospheric noise temperature vs frequency with respect to elevation [34]. Noise temperature increases as ground station antenna elevation is decreased. Accordingly G/T reduces at low elevation angles.

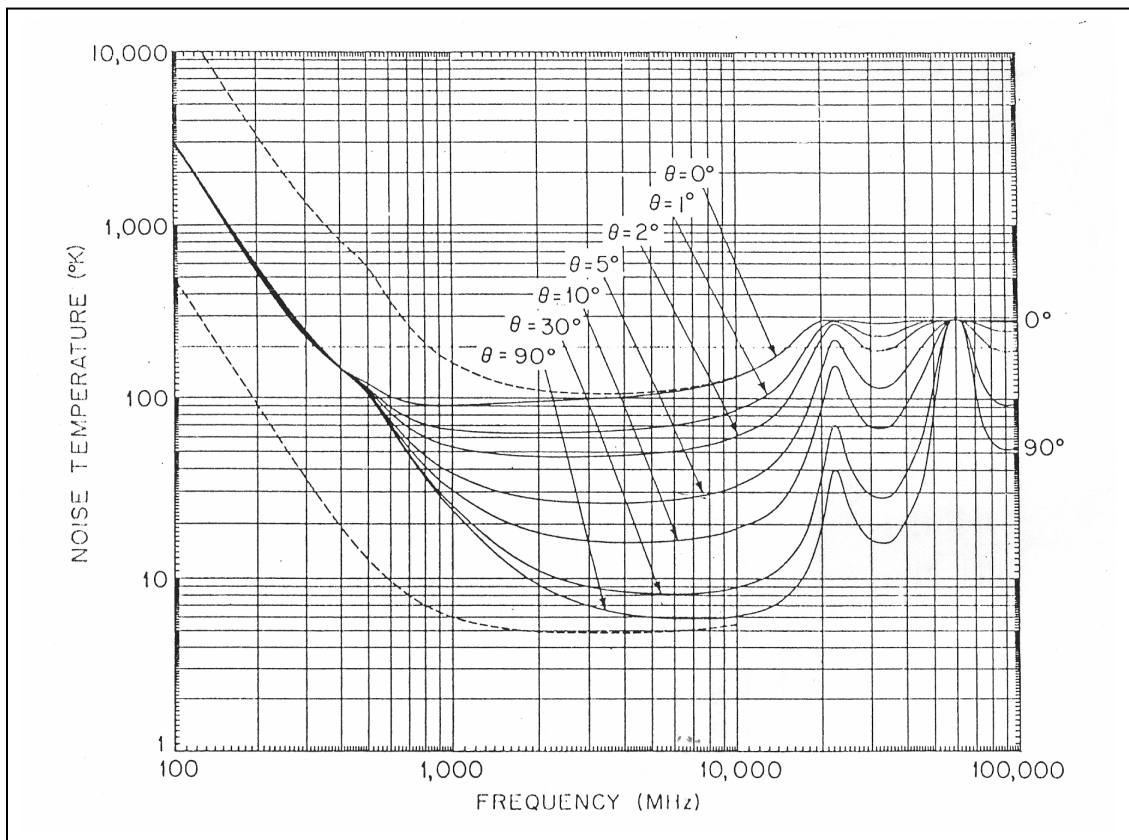


Fig 5.4 Noise temperature vs frequency for different elevations [34]

G/T measurements are carried out at different elevation angles and shown in Fig. 5.5.

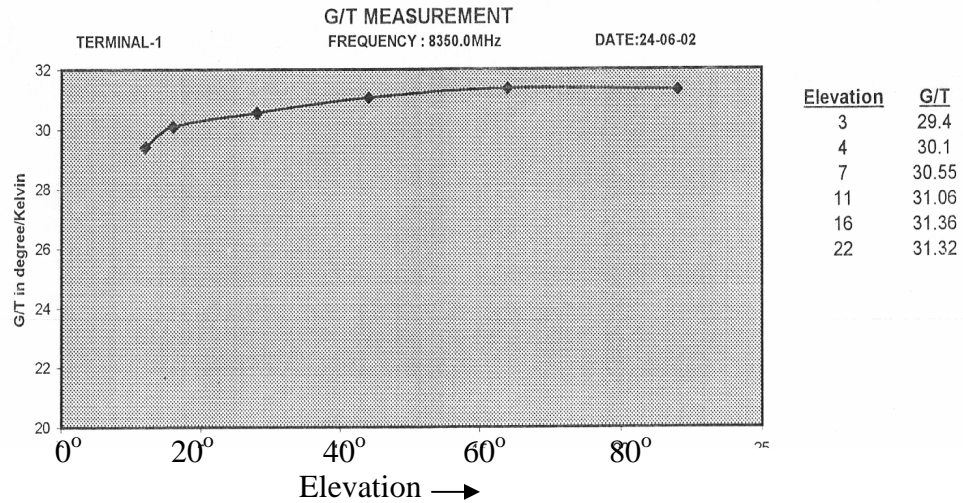


Fig. 5.5 G/T of receiving station as measured at Shadnagar.

From the above measurement, it is ascertained that the degradation in G/T due to ground noise at low elevation angles could be 2 to 4 dB in some sectors. If the noise peaks coincide with the satellite visibility angle, G/T is likely to be degraded further in those angles. The effect of this excess noise is ignored as it is not continuous. The excess margin provided in the link shall take care of this unpredictable noise if it coincides with the satellite trajectory.

▪ **Onboard antenna pattern:**

Onboard antenna radiation pattern was assumed to be axially symmetrical, but a close look on the measured results show that at certain sectors the antenna gain can be even 8 dB down (Fig. 5.6) than expected one. The gain reduction in these sectors is coinciding with low elevation pass trajectories. This reduction in gain of onboard antenna is contributing to the reduction of the margin in some sectors.

The onboard antenna, with shaping element designed for compensating path loss in 904 kms orbit of IRS 1A/1B missions that provided +7 dBi gain at +/- 61° off from the antenna axis which corresponds to 0° elevation of the ground station antenna, is

used for IRS P4 mission also. For 700 kms orbit of IRS P4, the maximum gain requirement is at $\pm 64^\circ$. More over, the antenna pattern is measured at unit level in anechoic chamber. The antenna pattern after integrating the antenna with satellite is not measured due to practical limitations.

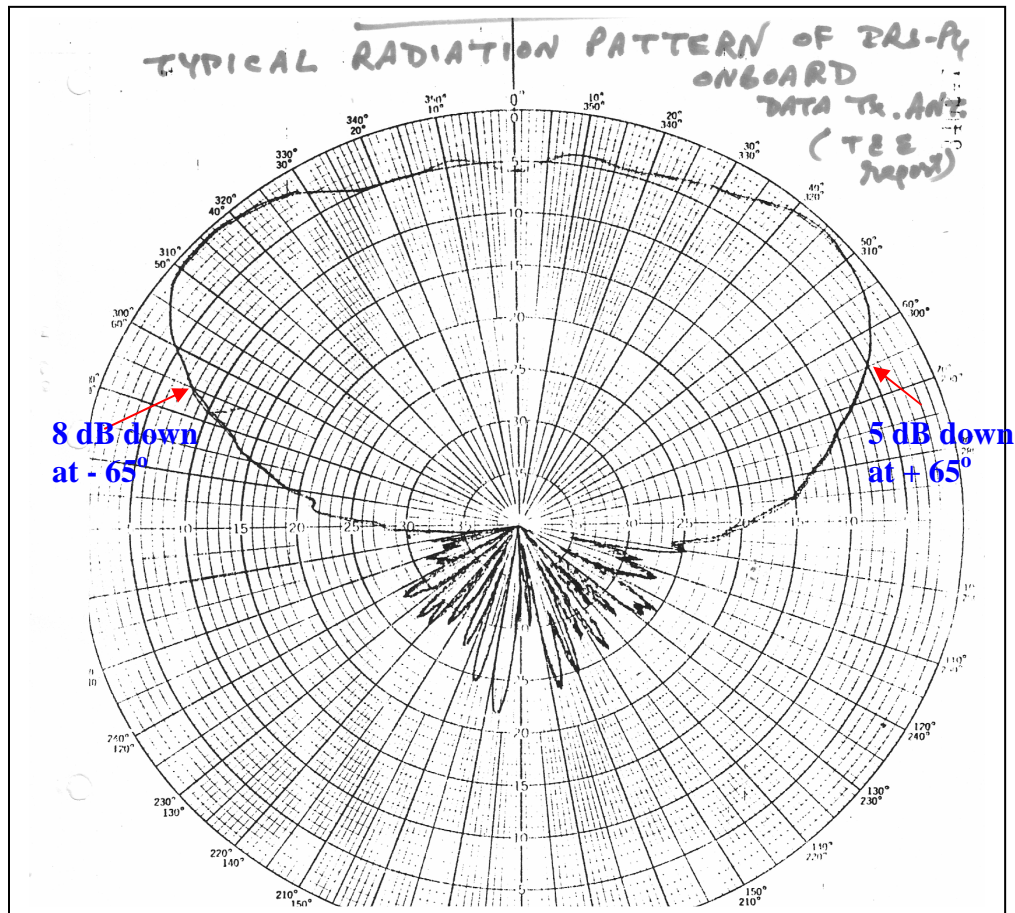


Fig. 5.6 Measured Radiation pattern of onboard (IRS P4) iso-flux antenna

From the observations, it is noted that

- i). the reduction of the expected margin at high elevations is due to the disturbance of the feed system in the receive antenna and degradation of demodulating system by about a dB.

ii) the degradation of the link below 5 deg. is due to different systems as given below:

Onboard antenna gain reduction	8 dB
Receiver BER performance degradation	1 dB
G/T reduction	> 2 dB
Total signal loss	<hr style="width: 100px; margin-left: auto; margin-right: 0;"/> >11 dB

11 dB signal loss resulted in unacceptable data quality.

5.1.1 Suggestions for avoiding signal loss problem:

- Ground station antenna situated at higher level with clear visibility shall be used for satellites requiring low elevation observations.
- Onboard antenna shaping shall ensure required mission specific gain pattern with circular symmetry in all horizontal planes.
- Field of view for the antenna onboard should be clear of all appendages and mounting structures.
- Satellite body effects shall be taken into account and radiation pattern measurement shall be carried out on satellite in compact test range.

5.2 IRS P6 (Resourcesat-1) :

The Resourcesat carried two payloads viz., LISS-3 and LISS-4 and the data is transmitted on two separate carriers viz., 8125 MHz and 8300 MHz. The RF spectrum of LISS-4 chain received from IRS P6 showed higher carrier component (carrier leakage) protruding over the data spectrum. The level observed is of the order of 5 to 6 dB during first day of X-band system operation and about 2 dB some times during regular payload operation. This behavior is not seen in LISS-3 spectrum.

Analysis [193]:

X-band QPSK modulator of LISS-4 chain got a carrier suppression of 24 dB w.r.t. unmodulated carrier while it is 30 dB in case of the modulator used for LISS 3 data modulation. Both are below the specified 20 dB value. 20 dB carrier suppression

(specification) contributes less than 0.5 dB degradation [183], which is accounted in the link margin estimation.

Carrier suppression is an inherent quality of the QPSK modulator and depends on many factors:

- 1) switching speed of the devices used in the modulator,
- 2) Rise time/fall time of the clock and data,
- 3) Duty cycle of the clock,
- 4) Asymmetry of one and zero bits in the data streams, etc.,

These parameters increase the DC content in the modulating data stream, which causes an increase of carrier leakage [39] in the data modulated RF spectrum.

For providing more clear explanation on the behavior of the data spectrum, simulations are carried out, results provided and discussed in following text, to provide answers to the doubts that are arising from the observations made in the received IRS P6 spectrums in different orbits.

▪ **Carrier leakage:**

QPSK Modulator, similar to the one used for LISS-4 chain onboard IRS P6, is used for simulation. Standard data generator is used for generating 105 MBPS (two 52.5 MBPS streams) of data. The data generator can provide 1010... type data, various length PRBS data and also programmable data.

Spectrum given in Fig. 5.7 is generated by feeding 1010... type data to have a clear idea of carrier suppression. The carrier component can be seen 24 dB down w.r.t. unmodulated carrier. Carrier leakage also results in components at all multiples of +/- 105 MHz and these are at Null points in PRBS spectrum as can be seen from Fig. 5.8.

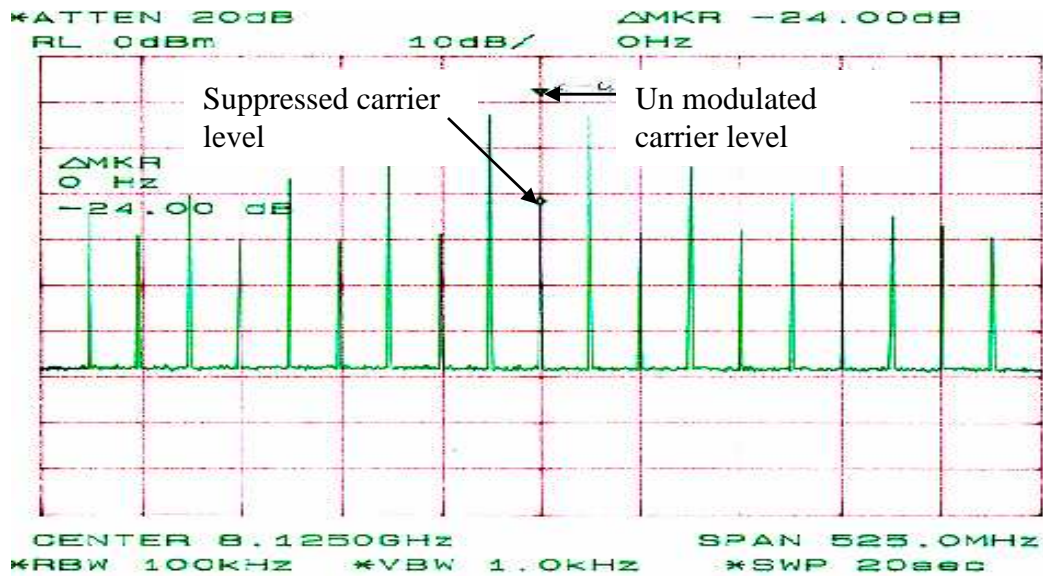


Fig. 5.7 QPSK spectrum with 1010... type data

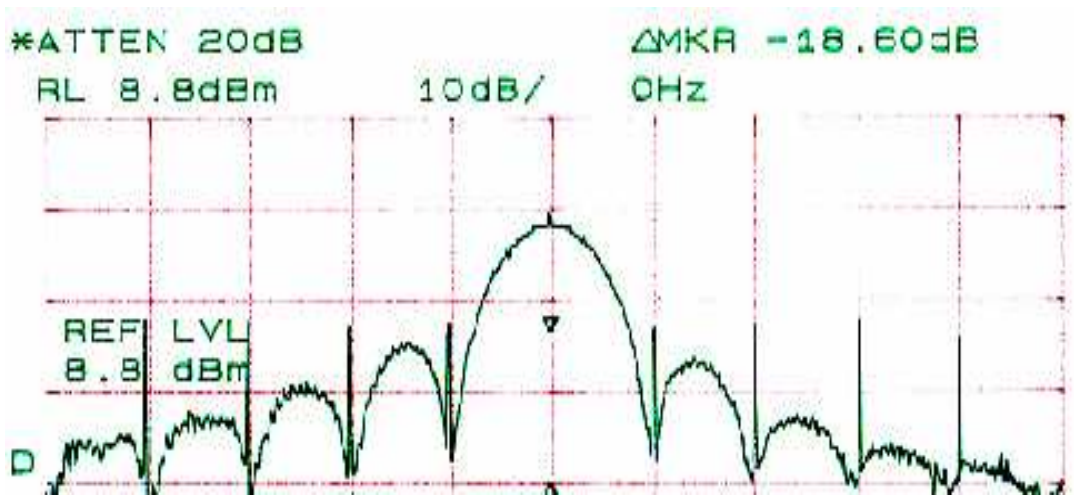


Fig. 5.8. QPSK spectrum with PRBS data.

- Carrier leakage is seen at NRSC ground station only:

The spectrum of the transmitting system during pre launch testing is observed with 1MHz resolution on the spectrum analyzer while the spectrum of the received signal (IRS P6) is observed with 100 KHz resolution bandwidth at NRSC (Fig.5.9). The main lobe envelope level of the PRBS data modulated signal depends on resolution bandwidth. The envelope level is the integrated power in the resolution bandwidth at any instant. In the upper spectrum, observed with 1MHz resolution band width, the

peak of the envelope of main lobe is down by about 20 dB from un-modulated carrier level. The carrier leakage component which is 24 dB down the unmodulated carrier level, is submerged in the envelope of the main lobe. The lower spectrum plot observed with 100 KHz resolution bandwidth where the peak of the main lobe envelope is down from un-modulated carrier level by over 25 dB. The carrier leakage component which is 24 dB down w.r.t. un-modulated carrier is seen projecting over the envelope of the main lobe.

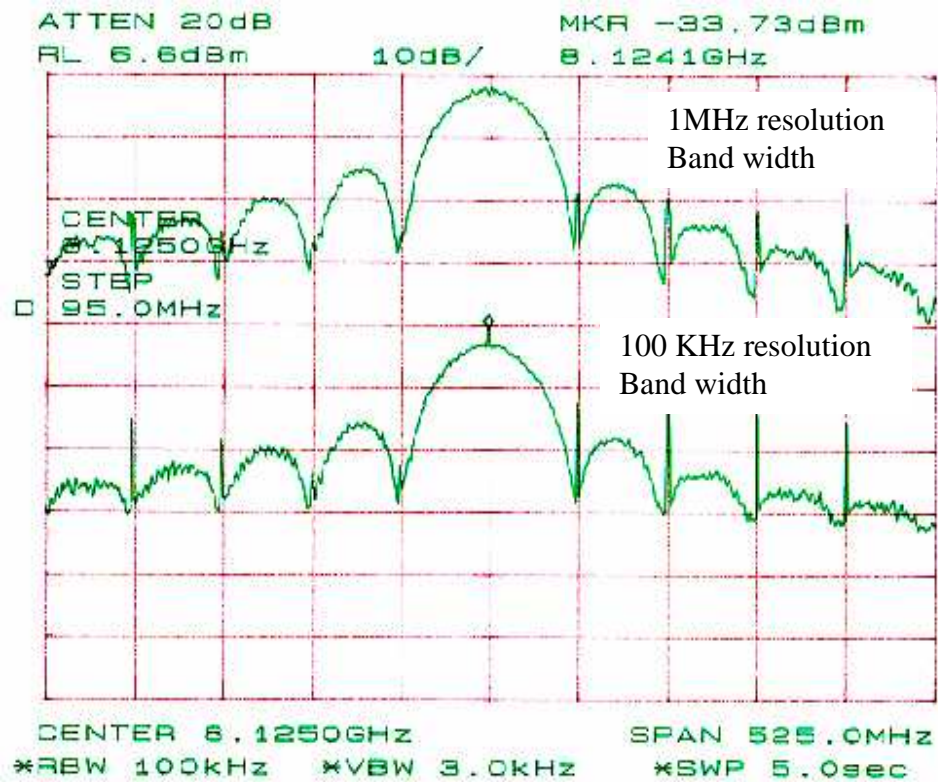


Fig.5.9 QPSK spectrums with 1MHz and 100 KHZ resolution bandwidth on spectrum analyzer

During T & E and pre launch testing, at ISAC the spectrums were always observed with 1MHz resolution bandwidth. At NRSC, the spectrums were observed with 100 KHz resolution band width to get higher dynamic range and the carrier leakage was observed at NRSC and not seen during T&E at ISAC.

- **Carrier leakage is not seen in LISS-3 spectrum:**

LISS -3 carrier spectrum did not show carrier leakage even with 100 KHz resolution bandwidth as the modulator used had 30 dB carrier suppression and the envelope level (with 100 KHz resolution band width) is down by 27 dB with respect to unmodulated carrier level. The carrier component is submerged in the envelope of the main lobe.

- **Carrier leakage is seen some times only during payload data transmission and the level is varying:**

A typical data stream is simulated to have more continuous one level bits. Spectrum is observed over some time. Spectrum plots provided in Fig 5.10 are taken at different times. Top spectrum shows more carrier leakage than lower one. Because of continuous one level bits at some places, DC content in the stream is varying with time and the carrier leakage also seen varying with time.

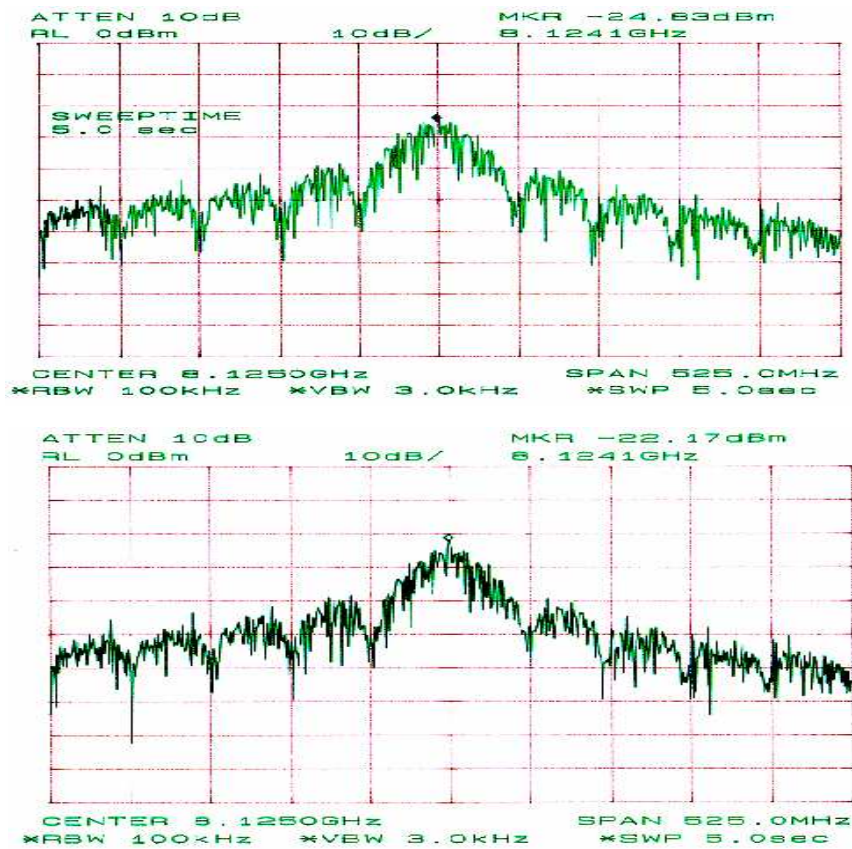


**Fig. 5.10 QPSK spectrum at different instances
(with long continuous ones in the data)**

First day after launch, the onboard, transmitting system performance is evaluated using onboard generated Pseudo Random (PRBS) data and the payload is operated in subsequent orbits. Effect of PRBS data on spectrum is studied further. Spectrum is observed with different length Pseudorandom (PRBS) data. Fig 5.11 provides spectrums observed with PRBS data of $2^{15}-1$ and $2^{11}-1$ lengths.

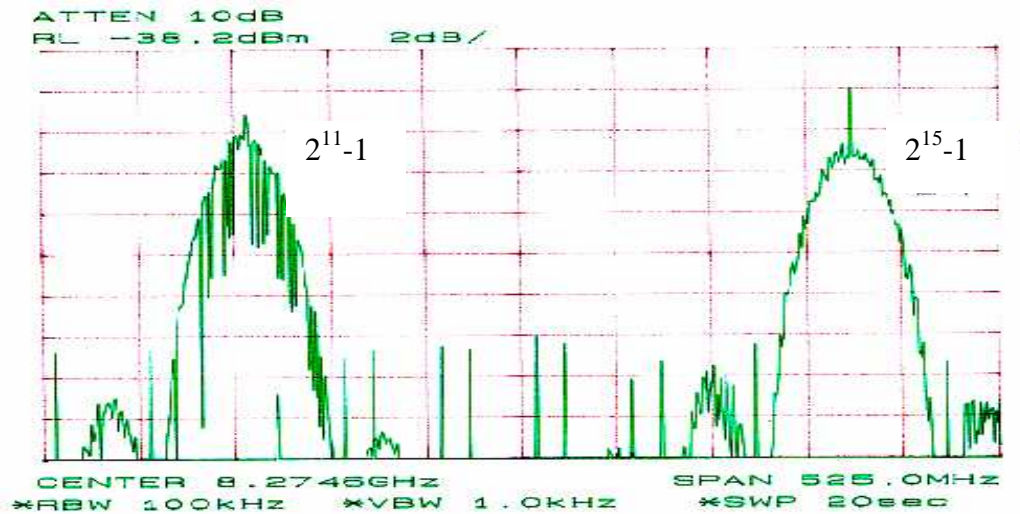


Fig. 5.11 QPSK spectrums with different length PRBS datas

Carrier leakage is more in the spectrum in which the carrier is modulated with $2^{15}-1$ PRBS data.

All these observations indicate that the spectrum and carrier leakage depend on data and provides an explanation of observing higher level carrier component on first day spectrum of IRS P6 when PRBS data was transmitted and not seen subsequently with payload data transmission.

- **Carrier leakage is not noticed in the spectrums of 1C/1D:**

IRS 1C/1D transmitted 85 MBPS data while IRS P5/P6 transmitted 105 MBPS with same 40 watts power. The peak of the spectrum envelope is less by about 2 dB in case of IRS P5/P6. Moreover, rise time and fall time of the data degrades with increasing

data rate resulting in more carrier leakage in the modulated spectrum. These two factors explain visible carrier leakage only in IRS P5/P6 spectrums at times.

- **Increase of the level of the components at nulls related to carrier level:**

Fig 5.12 provides spectrums recorded by intentionally spoiling the data quality. Spectrum at top is with normal PRBS data for comparison while the spectrum at bottom is taken by intentionally spoiling the data by loading the data path in one of the data streams with the capacitance of oscilloscope probe. Carrier leakage increased considerably as expected. The components at null points also increased along with carrier component.

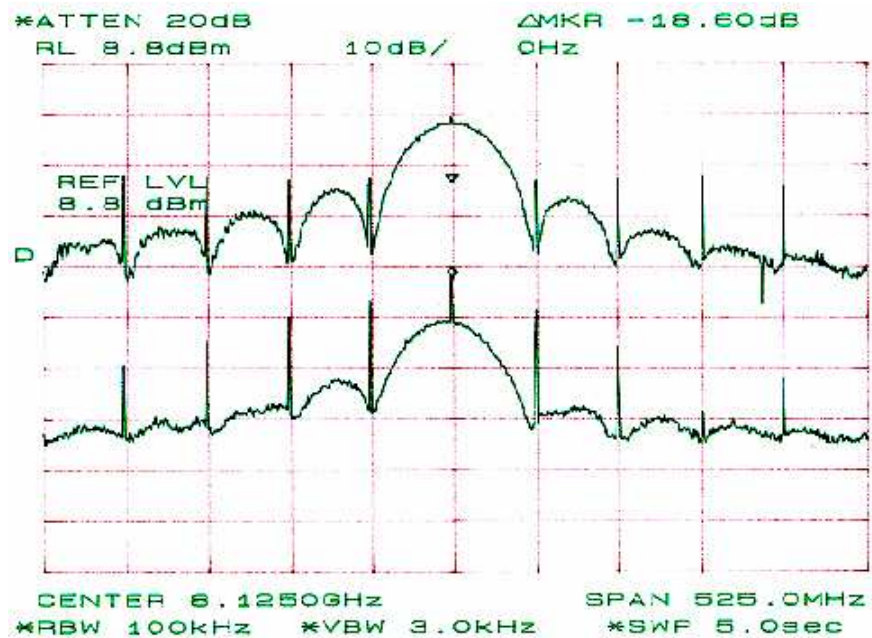


Fig 5.12 QPSK spectrum with good and poor quality data input.

This observation confirms that the level of the components at nulls is related to carrier leakage. The increase in the level of the components at nulls of the P6 spectrum when carrier leakage is seen is normal. This only results in wasting the RF power.

▪ **Degradation due to carrier leakage in the link:**

The power loss due to the increased level of the carrier leakage is calculated and given in Table 5.1. The level of the components seen in the first two nulls is assumed to be equal to the carrier component which is the worst case that can be assumed. In the observations in the P6 data spectrums, about 6 dB increase in carrier leakage is observed over normal carrier component. The degradation in worst case is not more than 0.16 dB.

Table 5.1 Degradation estimation due to carrier leakage

		Normal carrier suppression		Degraded carrier suppression	
Total power		40	watts	40	watts
Carrier suppression		24	dB	18	dB
Power in carrier+componens in two nulls		0.48	watts	1.90	watts
Useful power (90% in main lobe)		35.57	watts	34.29	watts
Power loss		-0.51	dB	-0.67	dB
<u>Degradation</u>			<u>0.16</u>	<u>dB</u>	

The behavior observed with IRS P6 data spectrums are simulated on ground and the increase in level of carrier leakage components is explained. This is not an anomaly and the spectrums observed are expected with randomized data modulation. The degradation due to this increase in component levels is less than 0.16 dB which is absorbed in the margin.

5.2.1 Suggestions to take care of the visible problematic observations in the spectrum:

- QPSK modulator design shall ensure carrier suppression more than 25 dB.
- Data quality (rise time, fall time, duty cycle) has to be maintained while transferring the data from processing digital electronics systems to modulators. Coaxial 50 ohm cables affect rise and fall times of the waveform due to the associated parasitic reactance. Low Voltage Differential Signal (LVDS) bus

interface which uses balanced line that will not degrade rise and fall times of the data severely is recommended.

- Carrier leakage results in waste of precious onboard power. This can be minimized by
 - having good isolation in QPSK modulators,
 - Proper randomization to minimize continuous ZEROs or ONEs in the data streams.
 - Minimizing parasitic reactance in the data carrying lines and ensure good rise and fall time in the data waveform.

5.3 IRS P5 (Cartosat-1)

Data loss was reported when the two X-band carriers QPSK modulated with 105 MBPS each are amplified by a single TWTA and transmitted through iso-flux antenna.

In the Indian Remote sensing satellites like IRS-1C/1D/P6, the imaging payload data is transmitted on two carriers. The two carriers are amplified to 40 watts with independent TWTAs and band limited by appropriate band pass filters independently before transmitting to ground station. A separate TWTA is provided as standby for having cold redundancy. As TWTAs are highly expensive, it was considered to transmit two carriers through one transmitting antenna system. Block schematic of the transmitting system adopted for IRS P5 is shown in Fig. 5.13. An experimental phased array with 64 elements with independent phase controlled amplifiers is used as backup transmitting antenna.

When the two carriers are transmitted through TWTA and iso-flux antenna chain, very high bit errors were reported while the reception was normal when transmitted through phased array system.

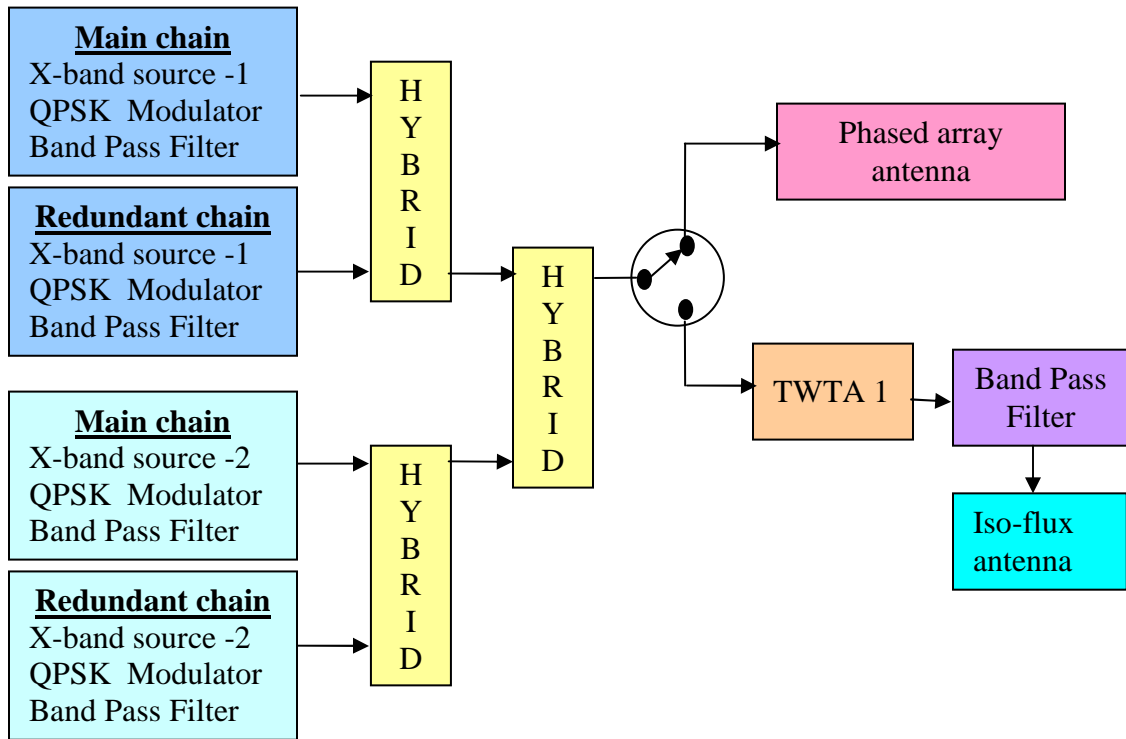


Fig. 5.13 Block schematic of data transmission system of IRS P5

Analysis [194]:

The issues of transmitting two high bit rate data modulated carriers through a single power amplifier are studied. Apparently degradation could be due to inter-carrier interference and inter-modulation products arising out of non linear power amplification and also band limiting of the signal.

Multi-carrier transmission using wideband power amplifiers like TWTAs is common in satellite communication. Inter carrier interference and inter modulation product are generated in a non linear power amplifier. These aspects are handled in communication satellites by providing input back off to the power amplifier operation. The problems are compounded in case of remote sensing satellites, like IRS P5, where very high data rates of the order of 210 MBPS needs to be transmitted in the allotted bandwidth of 375 MHz. For bandwidth and power efficiency with optimum BER performance, QPSK Modulation

scheme is chosen and power amplifiers are operated near saturation. At saturation, the amplifiers are highly nonlinear and produce inter modulation product components. These components will appear outside the allotted frequency band and causes great concern in addition to the interference problem affecting the desired carriers. Table 5.2 gives the inter modulation product levels of TWTA observed at various input levels.

Table 5.2: IM products vs Input Back Off of 40 watts X-band TWTA

Pe/Pesat(dB)		C/I (in dB)		C/I (in dB)		C/I (in dB)	
		@ F=8.0 GHz		@ F=8.2 GHz		@ F=8.4 GHz	
		TWTA	SSPA	TWTA	SSPA	TWTA	SSPA
-3		10.4	17	10.3	17	10	16
-6		13.5	20	13.5	20	12.7	19.5
-10		17.4	24	17.1	24	16.2	23
-20		32.5	35	31.7	35	31.5	35

These IM products which are of about 10 dB down with respect to the carrier level when TWTA is operated at Saturation is of great concern.

- **Simulation of onboard spectrums**

Simulation was carried out using MATLAB tools to study the spectrum spread and inter modulation products. Two carrier frequencies viz., 8125 and 8300 MHz are chosen. Each carrier is QPSK Modulated with 105 MBPS data. TWTA is operated at saturation with the two QPSK modulated carriers (8125 & 8300 MHz). At saturation the TWTA generates IM products having magnitude of about -10 dBc. Fig. 5.14 shows the combined RF spectrum of the two unfiltered QPSK modulated carriers at the output of the saturated TWTA.

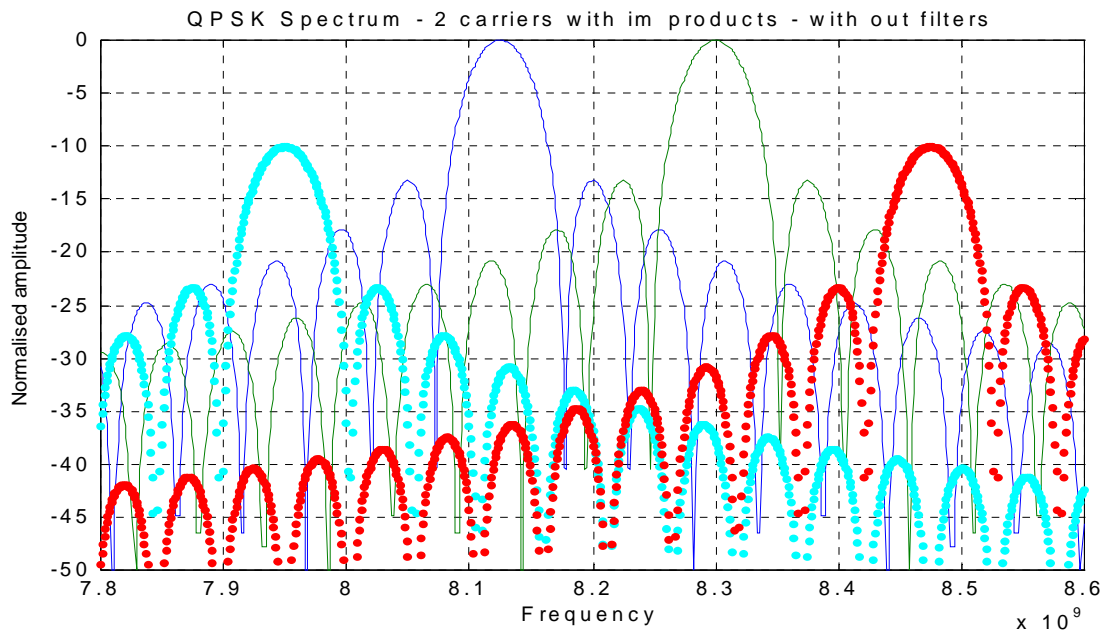


Fig 5.14 RF spectrum of two unfiltered QPSK modulated carriers at the output of TWTA.

It can be seen from the simulated figure that

- The spectrum of each carrier spreads over the second carrier spectrum and becomes an interfering signal to the other carrier.
- The two third order Inter Modulation (IM) products (7950 MHz and 8475 MHz) are outside the frequency band of interest. Spectrum of each IM product also spreads into the operating frequency band. These IM components cause interference to the required data carriers while radiating considerable signal over the adjacent frequency bands violating transmission restrictions set by ITU.

To limit the out of band radiation, a common band pass filter at the output of the TWTA is considered. A Band Pass Filter (BPF) with pass band sufficient to pass the main lobes of both the carriers and about 30 dB rejection bandwidth of 375 MHz, which can be practically realized, is considered at the out put of the TWTA for simulation purpose. Design of BPF with higher toll off characteristic causes more insertion loss and increases size and weight. More insertion loss at the out put of power amplifier is not desirable in satellite designs. Hence, simulation carried out

with practically acceptable BPF characteristics. Fig. 5.15 shows the RF spectrum at the output of TWTA after filtering.

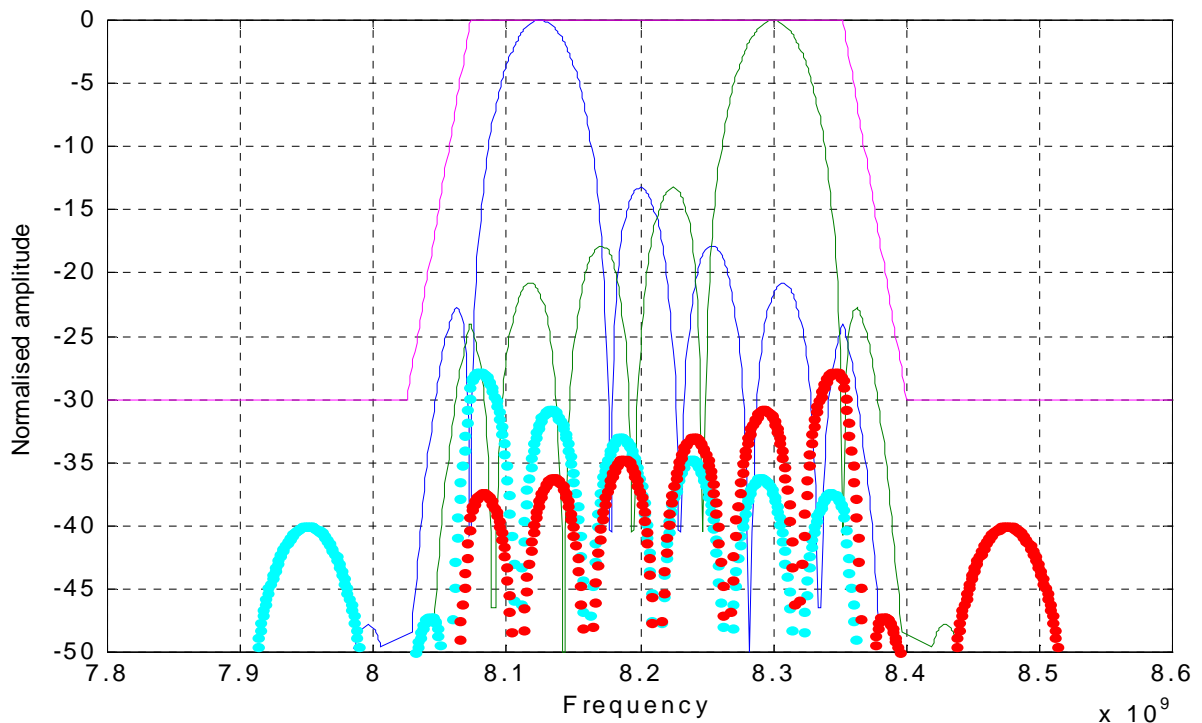


Fig. 5.15. Spectrum of two QPSK modulated carriers with common filter at the output of TWTA.

The following observations are made from this simulation:

- Reduces out of band radiation to considerable extent, but rejection is not enough to meet the ITU regulations.
- The inter carrier and IM products interference are not improved.
- The interference due to IM products on either of the two carriers is about 30 dB down whereas the inter carrier interference is only about 20 dB. This interference may still be higher as the practical spectrum may have slightly higher side lobe power than simulated spectrum.
- Typical degradation of the performance with interference [183] is shown in Fig.5.16. It can be seen that 20 dB C/I level can cause about 1 dB degradation in the overall performance.

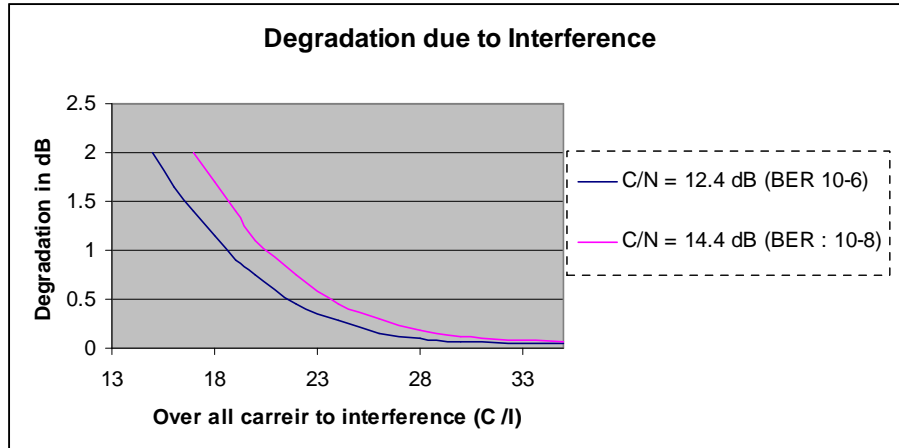


Fig. 5.16 Degradation due to interference

This problem eases with Solid state power amplifiers as IM product levels of SSPA are typically about -20 dBc at saturation. Due to poor efficiency, SSPAs are not used for high power generation in space links.

In any case, the inter carrier interference is an issue and needs be addressed. A probable solution is to filter the carriers separately and combine post amplification. The combined signals can be amplified by TWTA or can be fed to Phased array antenna for transmission. Two band pass filters with pass band to allow main lobe of the spectrum with good roll off characteristics to minimize inter carrier interference are considered for simulation.

When these two filtered carriers are amplified through TWTA operating near saturation, IM products to the level of -10 dBc will be generated as seen earlier. Fig. 5.17 shows the ideal spectrum at the out put of TWTA. Inter carrier interference and also the interference due to IM products is minimized. But, radiation outside allotted frequency band exists due to the IM products. A common band pass filter in the out of TWTA can reduce the out of band signals due to IM products produced by TWTA as can be seen in Fig. 5.18

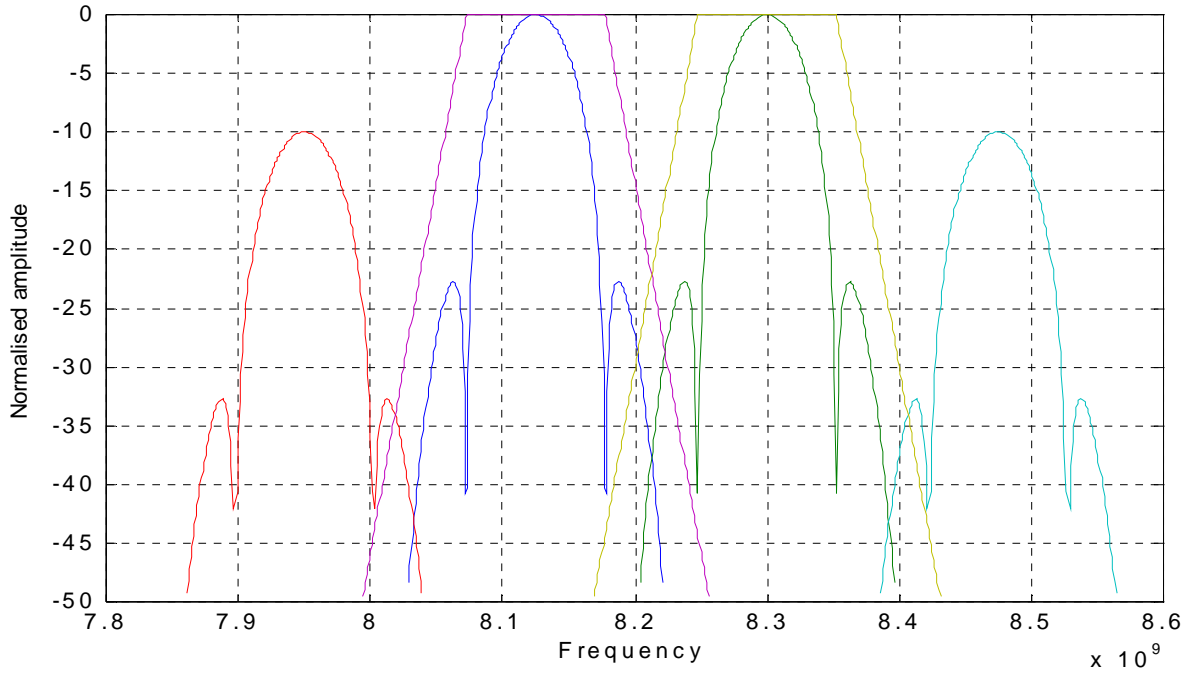


Fig. 5.17 Spectrum at the output of TWTA with two QPSK modulated and filtered carriers.

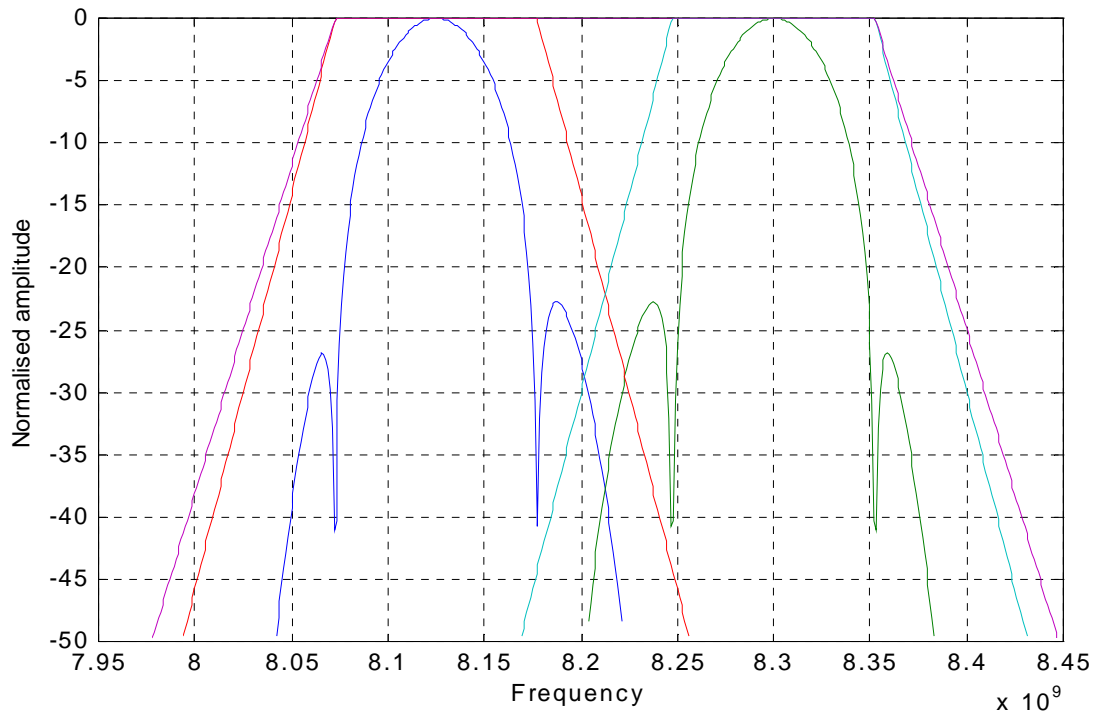


Fig.5.18 Spectrum with additional common filter at the output of TWTA.

In case of transmission through any non linear power amplifier like TWTA, as indicated earlier, IM products will exist to unacceptable levels. More over, the above observation is valid in ideal case only. In practice, the band limited QPSK modulated signal spreads its spectrum at the output of any non linear amplifier i.e., when the amplifiers are operated at or near saturation. Band limiting at the input of non linear power amplifier will not be effective. Sufficient back off can not be given with high bit rate systems as power available onboard is limited. RF spectrum of the filtered and limited QPSK signal practically regenerates its spectrum [195] as can be seen from Fig.5.19.

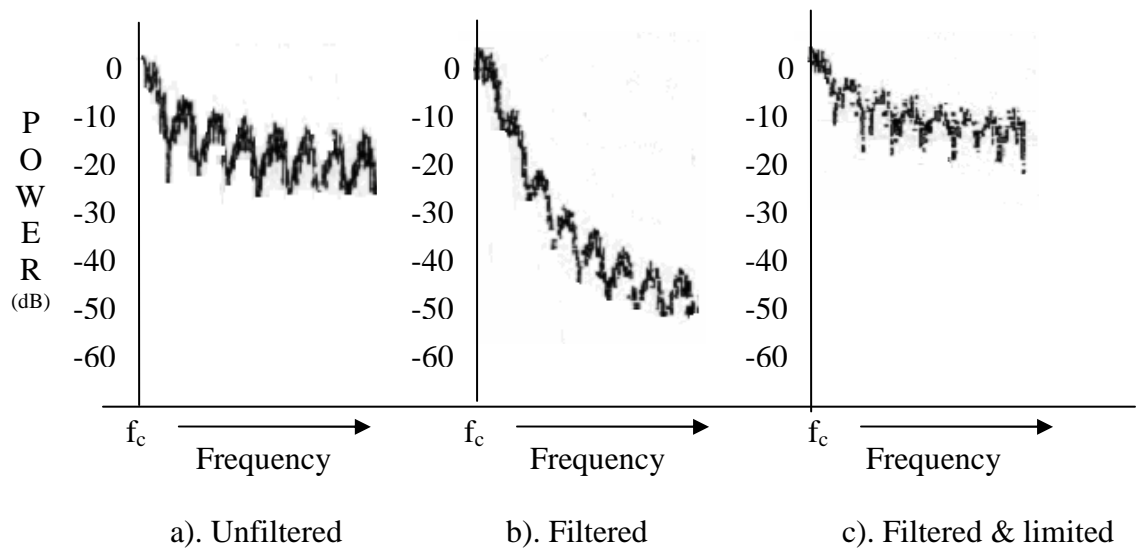


Fig. 5.19 Power spectra (normalized) of conventional QPSK signal before and after filtering and amplifying

When the two carriers are transmitted through Phased array, performance is normal while the performance degraded when transmitted through single TWTA due to high inter carrier interference and restoration of the filtered spectrum due to operation of the TWTA at saturation.

5.3.1 Mitigation techniques:

- For transmitting two carriers either through single non linear power amplifiers like TWTA, the effect of inter carrier interference has to be minimized.

- Appropriate filtering of the two QPSK modulated signals prior to amplification is essential.
 - High power TWTA operating with heavy back off will reduce the IM products when TWTA is used for transmitting two carriers. But, operating a TWTA with back off is highly inefficient and consumes more DC power making it unsuitable option for satellite applications.
- An alternative **solution to this problem is to adopt Offset Quadrature Phase Shift Keying (OQPSK) modulation technique** [195] instead of QPSK. In OQPSK modulation technique, one stream of data is delayed by half bit with respect to second stream of the data to avoid 180 degree transition in the modulated carrier. With this modulation scheme, the output of TWTA will retain filtering effect unlike QPSK signal. This can be seen from Fig.5.20.

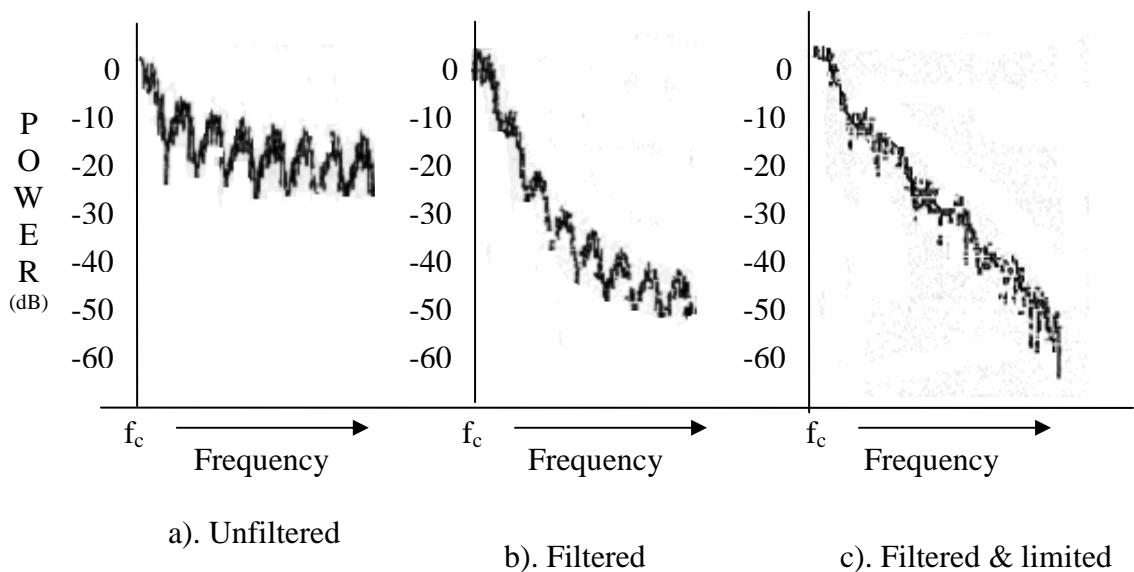


Fig. 5.20 Power spectra (normalized) of OQPSK signal before and after filtering and amplifying

- Phased array using small signal amplifiers in each radiating element is another suitable option. It will not create much degradation as inter carrier interference is less due to the use of low power solid state amplifiers. Fig. 5.21 shows the RF spectrum of the Phased array antenna which is used for IRS P5 mission. As can be seen from the figure, IM products cause problem for out of band radiation

only. The low power amplifiers used to excite the radiating elements normally have IM product levels better than -20 dBc at 1dB compression point.

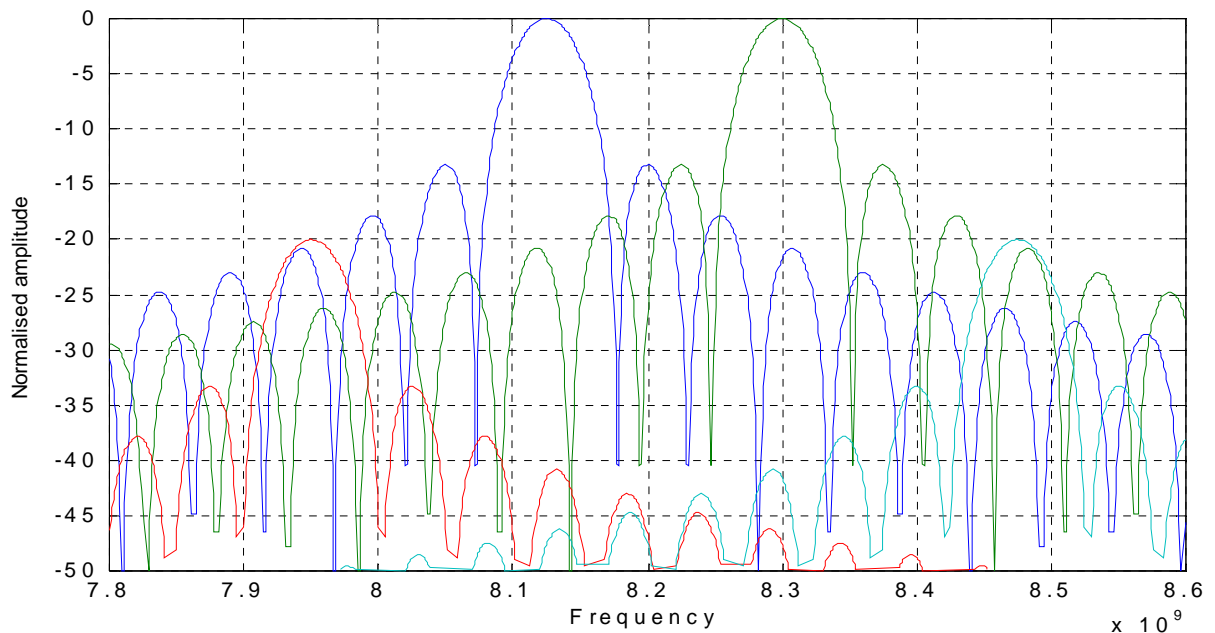


Fig. 5.21. Spectrum of two QPSK carriers, with IM products and without filter, radiated by Active Phased Array Antenna.

IM products level in pass bands is better than -40 dBc and causes practically insignificant degradation in the performance. However, IM products cause problem for out of band radiation. It is not possible to reduce IM products by filtering as number of filters required is as high as radiating elements. Power consumption of low power solid state amplifiers does not increase considerably with input back off. Hence, sufficient back off can be provided to reduce IM product level. Inter carrier interference can be minimized by filtering the spectrums of both carriers individually before combining for transmission by Phased array.

5.4 Effects of high bit rate data on QPSK spectrum:

When low bit rate data is modulating a carrier, the spectrum will be near ideal $(\sin x)/x$ profile. But practically, the spectrum will be far from ideal spectrum at high data rates.

A typical RF spectrum measured on spectrum analyzer is given in Fig.5.22. Unwanted discrete line components, asymmetry and distortion of the spectrum found to be increasing with increasing rise and fall times.

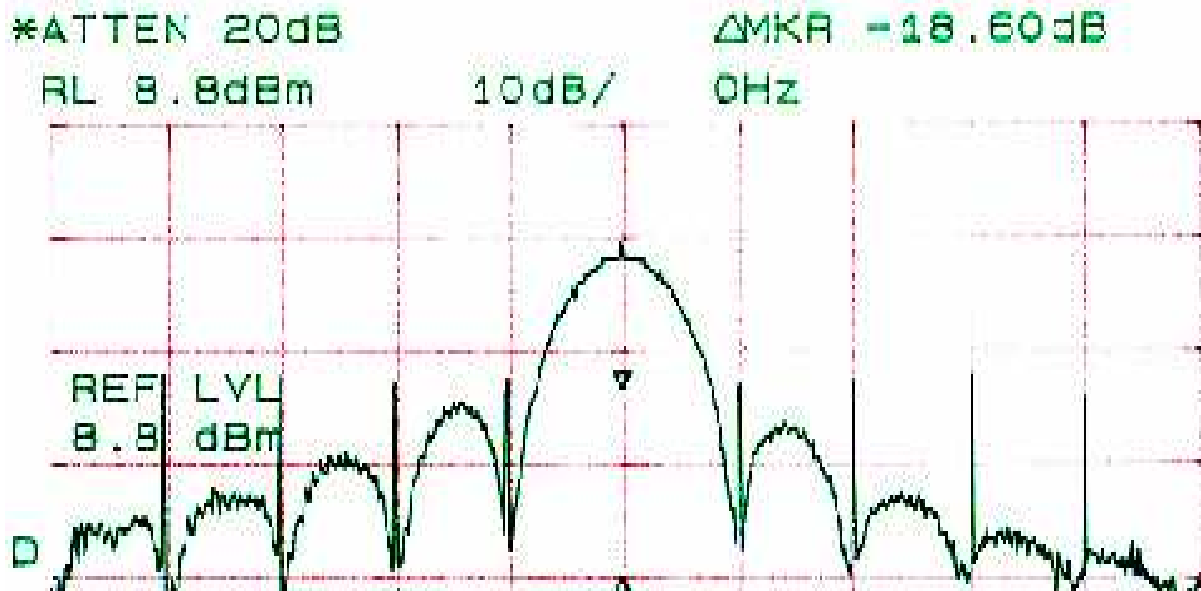


Fig.5.22. Practically observed QPSK spectrum

Various factors affecting the spectrum and their effects are discussed along with simulation using MATLAB tools in the following sections.

Major factors limiting high bit rate data transmission [196]:

The power spectral density of an unfiltered BPSK signal when carrier f_c is modulated by NRZ random data is given by [39, 40]

$$S_i(f) = 2.k.A^2.Tb.\left[\frac{\sin(\pi.(f - f_c).T_b)}{(\pi.(f - f_c).T_b)}\right]^2 \quad \text{---(29)}$$

The QPSK signal is generated by linear addition of two quadrature (one shifted by 90 deg.) BPSK signals which can be represented as

$$S_{\text{qpsk}}(f) = S_i(f) + j . S_i(f) \quad \text{--- (30)}$$

For random equiprobable input data, equation (30) represents the power spectrum of unfiltered QPSK modulation.

Fig.5.23 shows a typical unfiltered ideal RF spectrum of an X-band carrier modulated with 105 MBPS randomized data.

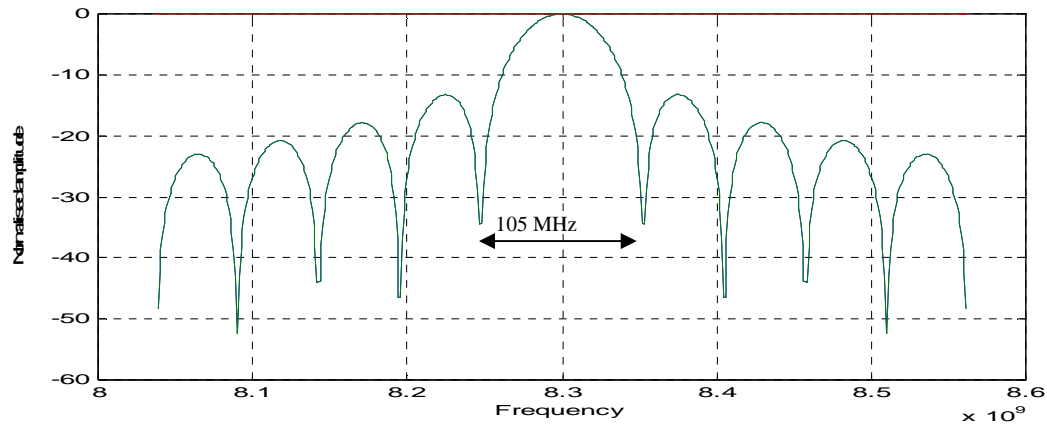


Fig.5.23 Typical ideal QPSK spectrum (simulated)

- **Data quality:**

The data of the imaging sensors used onboard remote sensing satellites is formatted, randomized to avoid continuous states of one or zero in the data which is an essential requirement for clock recovery in the demodulation process, differentially encoded to take care of phase ambiguities for correct demodulation of the data. The active elements used in handling the data before modulation got an upper frequency limit. More over, due to accommodation limitations on the satellite, the image sensing system, digital data handling systems, RF systems including modulators, power amplifiers and transmitting antennas are accommodated in spatial separation. The data from base band systems is fed to modulator through co-axial cables. The parasitic reactance (capacitance of co-axial cable etc) affects the rise/ fall time of the data and also duty cycle. The switching will have different turn ON and turn OFF times due to diffusion capacitances. All the parasitic reactance will spoil the shape of the data pulse. The wave form can be approximately represented by trapezoidal pulses as shown in Fig. 5.24

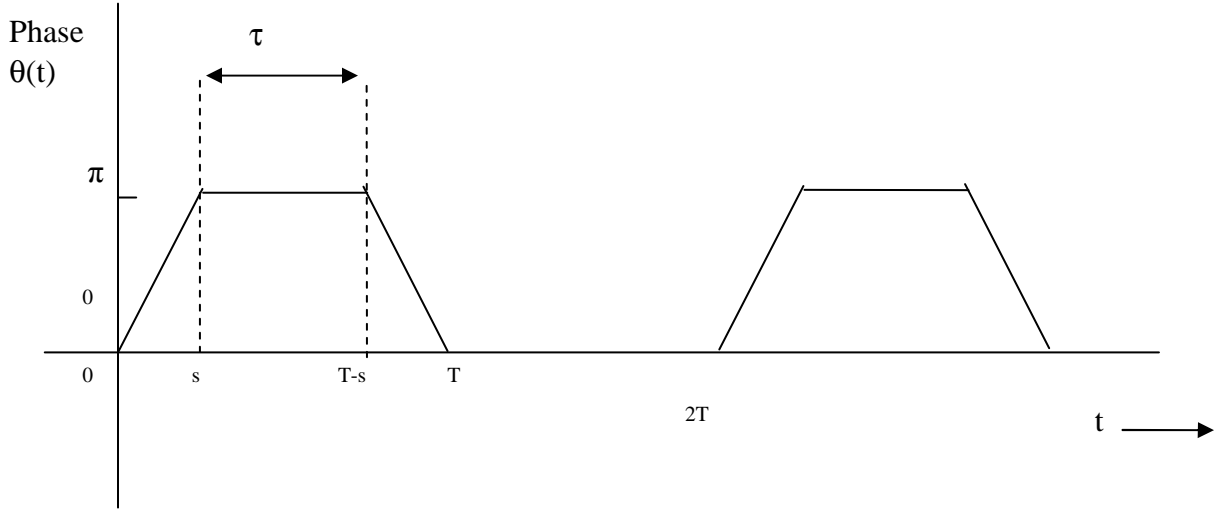


Fig. 5.24 Data pulses of finite rise/fall time.

- **Effect of rise / fall times**

Poor rise time and/or fall time will affect the modulated RF spectrum which can be simulated. Equation (29) gets modified for the power spectrum for antipodal PSK modulation [39] by data with waveform period T , rise and fall times s , there by the top of the pulse having width $\tau = T-2s$, as

$$G(f) = \frac{T}{4} \left(\frac{\pi}{4} \right)^2 \left\{ \frac{\frac{\tau}{T} \frac{\text{Sin} \pi(f_c - f)\tau}{\pi(f_c - f)\tau} + \frac{s}{T} \cos \pi(f_c - f)T}{[(f_c - f)s]^2 - \left(\frac{\pi}{4} \right)^2} \right\}^2 \quad \text{--- (31)}$$

where f_c is carrier frequency.

The spectrum is simulated for different rise and fall times in the data waveform. Fig. 5.25 shows spectrums for different rise and fall times. Rise and fall times are assumed to be identical. As rise and fall time increases, the spectrum gets distorted. From the figure, it can be seen that main lobe of the spectrum gets distorted with increase of rise and fall times equally. Fig. 5.26 shows spectrums with different rise and fall times. As can be seen from the spectrums, with increasing rise or fall time,

discrete carrier components are seen increasing in level. When rise time and fall time are equal, net DC content in the data is zero and spectrum distortion only is seen with out discrete carrier components.

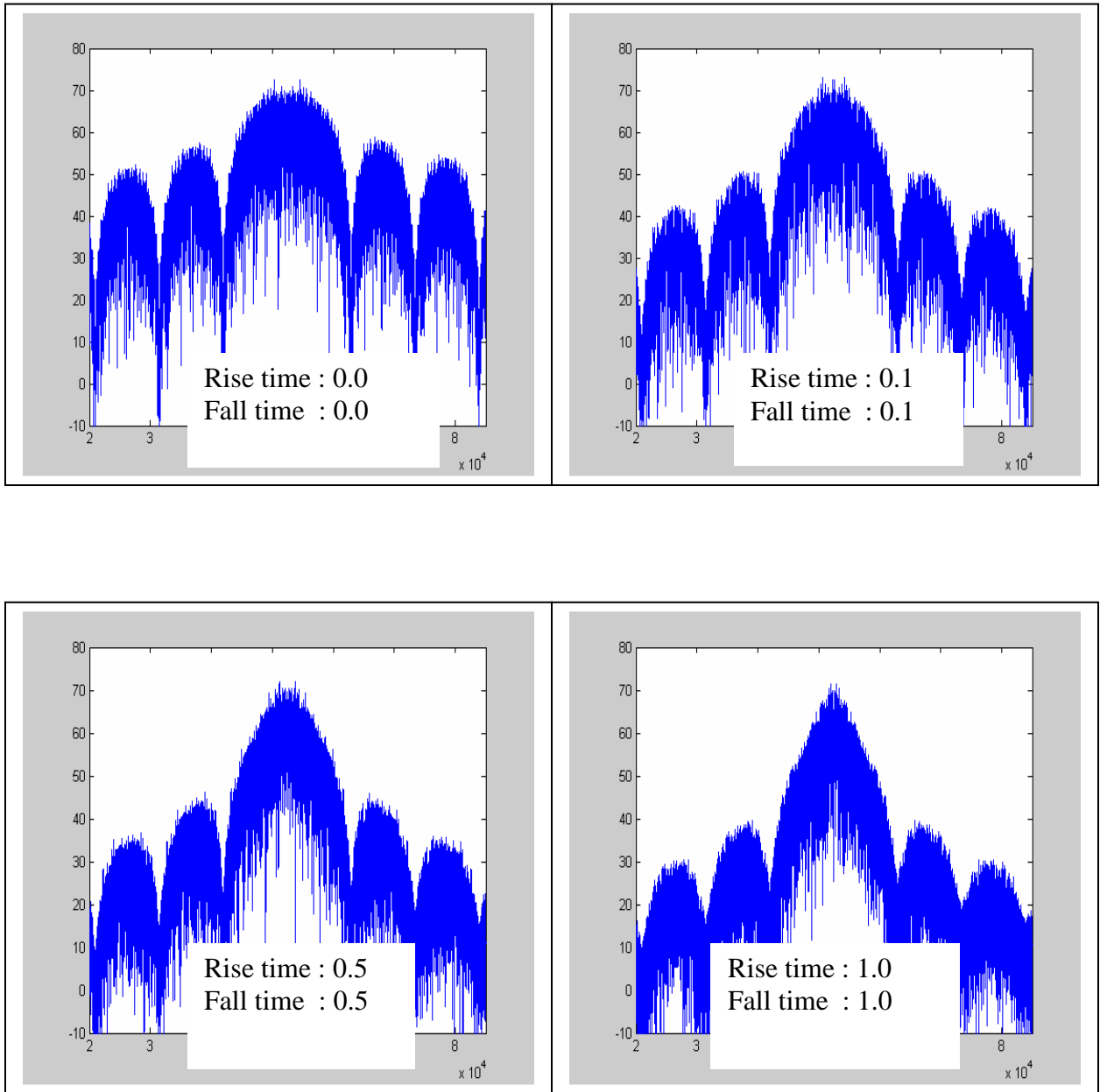


Fig. 5.25 Simulated spectrums with different equal rise/fall times of data

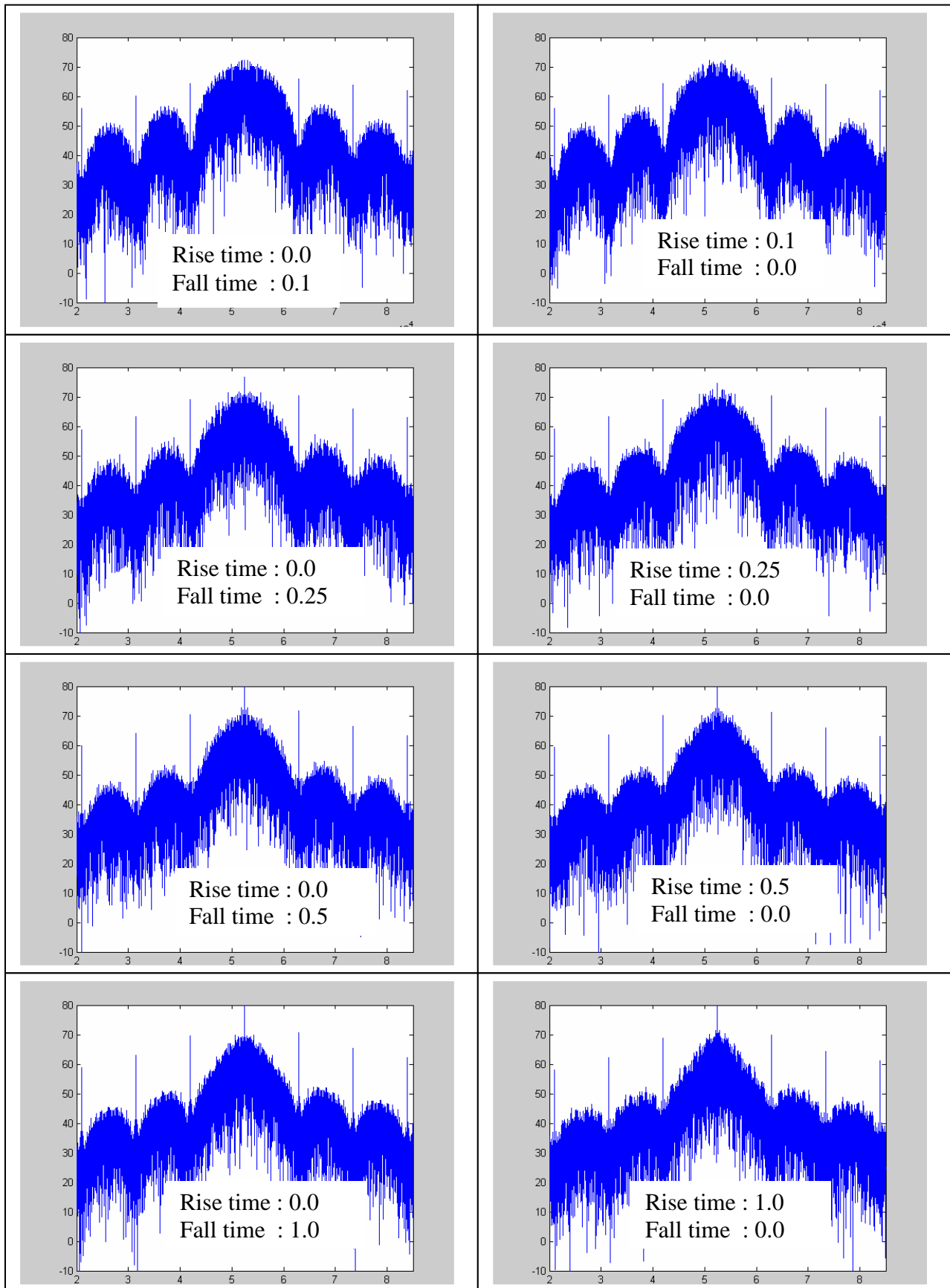


Fig. 5.26 Simulated spectrums for different un equal rise and fall times of data

- **Effect of duty cycle and DC current in data:**

Spectrum is simulated (Fig. 5.27) by adding DC component to the data before QPSK modulating the carrier. Top spectrum plot in the figure shows QPSK spectrum without DC and the other two figures show with increasing DC content in the data. It can be seen from the figures that with increasing DC, the discrete carrier components increase corresponding to DC content in the data. Balanced data (equal duration for one and zero bits) will have zero average current DC content increases in a data stream when there is data asymmetry i.e., duration of bit one is different from duration of bit zero and number of ones and zeros in a data stream are not equal. This affects the performance of the link as the discrete components in the spectrum do not contribute for information.

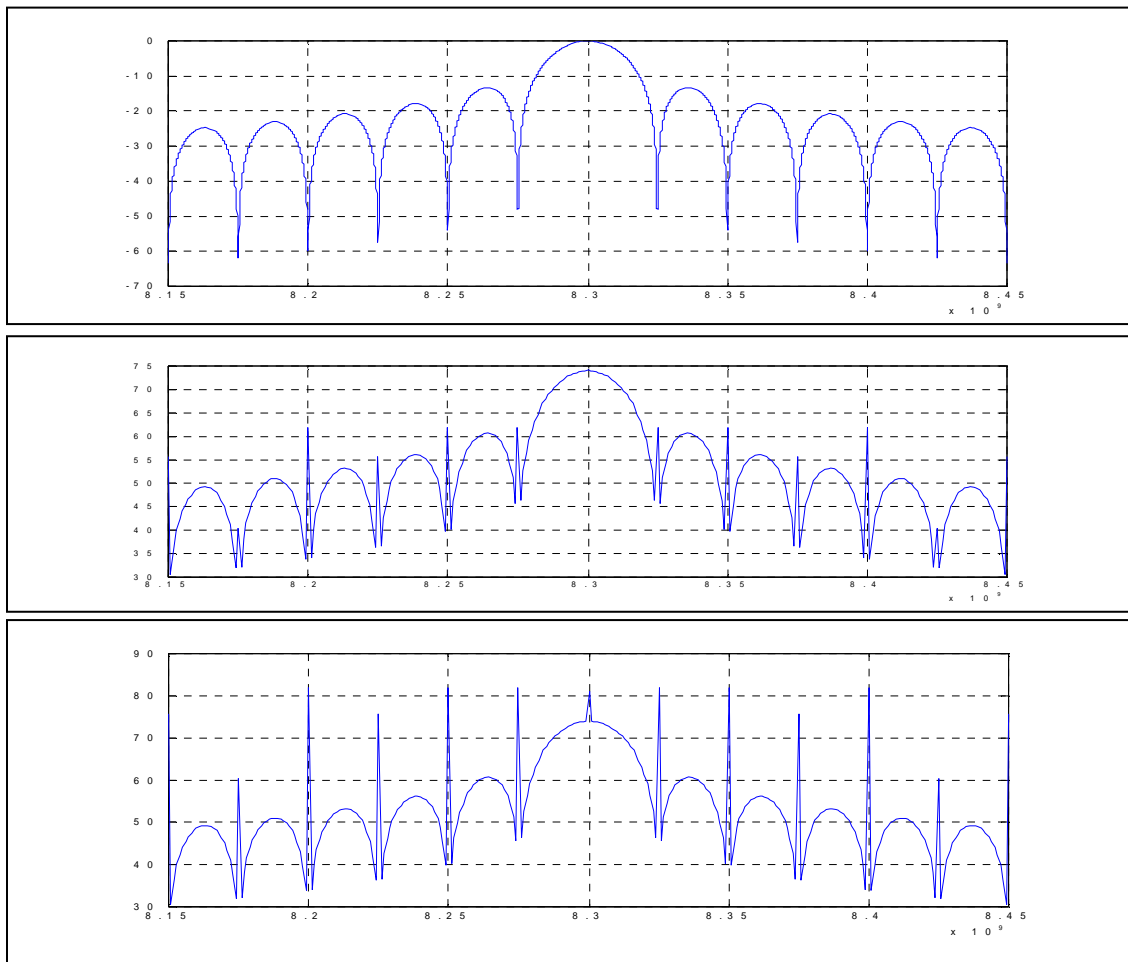


Fig. 5.27 Simulated QPSK spectrum with increasing DC content in the data

Poor rise/fall time and data asymmetry causes considerable degradation in the RF performance. Degradation of the total link [183] is estimated from Fig. 4.7 & 4.8.

- **Degradation due to QPSK Modulator parameters:**

The basic parameters that affect the performance of the QPSK modulator are phase accuracy and amplitude imbalance. The phaser diagram of a QPSK signal is shown in Fig. 5.28, should be a perfect circle.

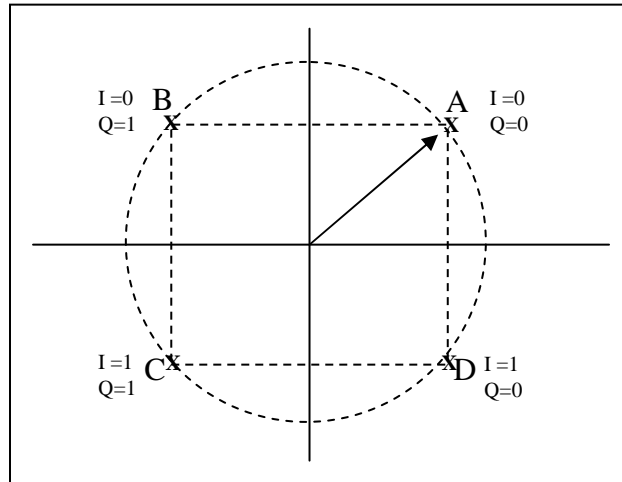


Fig. 5.28 Phaser diagram of QPSK signal

Points A,B,C,D corresponds to four phase states of 0° (reference), 90° , 180° and 270° corresponding to IQ data of 00, 01, 11, and 10 respectively. Ideally, the amplitude of the four points shall be same. Due to practical limitations of the components and circuits used to realize QPSK Modulator at X-band, phase and amplitude of the waveform at the four phase state conditions will differ from ideal values. These inaccuracies will contribute to the degradation of BER performance and can be estimated from curves depicted in Fig. 4.10 & Fig. 4.11 [183].

- **AM/PM conversion in Power amplifier:**

For high bit rate Data transmission, normally Traveling Wave Tube Amplifiers (TWTA) are used. The power amplifiers exhibit AM/PM transfer behaviour. This adds to the degradation as explained in section 3.5.1.4. AM/PM transfer coefficient of SSPAs is better than that of TWTAs. Since, at high powers, SSPA is inefficient,

TWTAs can not be replaced by SSPAs and the degradation shall be taken into account while designing the satellite link.

- **Spectrum limiting:**

Since power spectra of QPSK signals exhibit side lobes that may interfere with adjacent channels, certain amount of filtering is necessary at the transmitter. This filtering results in an increased amount of envelope fluctuation in the signal, which leads to spectrum spreading due to AM/PM and AM/AM non linear effects of the transmitter high power amplifier (HPA). These non linearities tend to restore the spectral side lobes that have been previously removed by filtering. To operate the transmitter's high power amplifier in a power efficient mode, the power amplifier must be operated in saturation. For near linear mode of operation, about 5 dB output back off would be required. Alternatively, Band Pass Filters (BPF) located after the saturated power HPA could restrict the spectrum and reduce interference into adjacent channels. It is not practical to design an ideal linear phase band pass filter. Filter design will become very complex. Post amplification filtering dissipates considerable amount of RF power. Hence, stringent post HPA filtering is not a desirable design approach. To overcome this, HPA has to operate at approximately 3 to 5 dB output back off or fairly expensive HPA linearizers (LTWTA) will have to be used. In such a case, pre amplification filter can be used. Because of this problem, for many power efficient and spectral efficient applications, QPSK does not seem to be a very attractive modulation technique when spectrum needs to be tightly filtered.

Minimum Shift Keying (MSK) and Offset Keyed Quadrature Phase Shift Keying (OK-QPSK) modulation techniques are proposed for use on non linear, severely band limited communication channels because both techniques retain low side lobe levels on even non linear channels, while allowing efficient detection performance. Either MSK or Offset QPSK waveform is band limited and then hard limited, the degree of regeneration of the filtered side lobes is less than conventional QPSK. However, any band limiting results in power wastage and requires additional margin. Effect of band limiting can be estimated from Fig. 4.13.

- **Degradation due to multiple reflections:**

The receive antenna at ground station receives signal from satellite along with the signals reflected by nearby structures and terrain. Particularly at low elevation angles, these reflected signals can also be picked up through side and back lobes of the receiving antenna. The reflected signals will combine with directly received main signal in different phases and the amplitude of the composite signal varies. When they are out of phase, the direct signal level gets reduced. The spectrum gets totally distorted and fluctuates in level beyond acceptable limits at low elevation below 5° .

Fig. 5.29 shows the AGC plot recorded during one of the passes of Oceansat-II at NRSC Data Reception Station (DRS). The onboard transmission is switched on at 9.6° elevation and switched off at 2° elevation in descending phase. The AGC recorded shows considerable variation of signal strength at low elevation angles. In addition to the reduction of G/T at low elevation angles due to noise, this variation of signal level makes the RF link unusable. The receive antenna shall be designed to have minimum possible side lobe and back lobes. However, signal received by multiple reflections directly by main lobe cannot be avoided. Care shall be taken to locate the terminal avoiding high-rise structures around and to place the antenna on a pedestal of maximum height practically possible. Further effects shall be taken care in designing the total transmission link.



Fig. 5.29 AGC plot of Oceansat-II

5.5 Frequency Reuse:

Frequency reuse techniques enhance the data transmitting capability in the same bandwidth. One method of obtaining frequency reuse is to transmit two signals on the same frequency band by placing each on orthogonal polarizations; thereby doubling the information capacity carried by the satellite. A fundamental requirement of dual polarized transmission is to maintain a good level of isolation between two polarizations. Poor cross polarization isolation give rise to cross talk and results in interference that degrades the performance of the data link and can be estimated from Fig.4.14.

5.6 Observations and recommendations:

- Practical considerations mostly limit the choice of frequency band and frequency reuse. Since, Remote sensing data can be received globally; compatibility of ground stations will be a major consideration in choosing frequency band and polarization. Globally and particularly in India, data reception capability at present exists in S and X-bands in RHC polarization. So, till now, all remote sensing missions are planned to transmit data in either S band or X-band with RHC polarization. To meet the demand for transmitting higher and higher data rates, consideration of frequency reuse and even shifting to Ka band is becoming essential and is being implemented.
- As data rate increases, the waveform shape gets altered due to increasing parasitic reactance resulting in asymmetry of the duration of one and zero bits in the data stream. This increases DC content in the data contributing for carrier leakage. The power in the carrier leaked components does not contribute for information and results in link degradation. Care should be taken with design of the RF systems particularly in the layout and interface sections to ensure good quality data at the input of modulator. Proper pre modulation filters [197] not only limit the spectrum occupancy but also minimizes the asymmetry due to rise time and fall time variations in the modulating data.
- Transmitting high rate data requires higher EIRP and also demands wide band width operation. It is always preferable to transmit the same data on multiple carriers with low EIRP in each carrier. Proper carrier spacing with adequate spectrum filtering becomes important system design [198].

- Multi carrier operation can cause inter carrier interference and IM product generation which degrades the performance. Adequate filtering before power amplification minimizes inter carrier interference. Sufficient back off is required in the power amplifier to reduce the spectrum restoration. It is not always possible to achieve this as high power requirement calls for operation near saturation. Though SSPAs got better IM product generation, they are highly inefficient for high power generation. Power amplifier with higher third order intercept point which provides less IM products shall be preferred by scarifying some efficiency.
- Proper filtering at the output of power amplifier can reduce unwanted out of band radiation, but the power in the IM products and loss due to insertion loss of the final filter, contributes to the reduction of EIRP. This needs to be accounted while designing space to earth data transmission link.
- Spectrum regeneration occurs when filtered modulated signals are amplified by high power amplifiers operating at saturation. **Offset QPSK provides a solution for this problem [195]**. Hence, OQPSK modulation technique is strongly recommended for high data rate filtered multi carrier transmission.
- Satellite body affects the radiation pattern of wide beam antennas. Proper positioning with adequate field of view for the antennas on the satellite, careful analysis and measurements are essential to ensure circular symmetry in the radiation pattern of the onboard antenna.
- Reception of the signal at low elevation angels is always a problem due to multiple reflections and increased ground noise in some sectors. Ground station antennas shall have very low side lobes and shall have clear visibility at low elevation angles. Site selection free of obstructions is very important. No concrete platform around antenna shall exist, instead grass terrain helps to reduce reflections.
- Adequate link margin shall be provided to take care of the degradations due to the deviation of characteristics of various elements in the data transmission systems which can not be controlled and accounted beyond a point. After taking care of known

deviations with proper system design, about 2 to 3 dB clear link margin will ensure proper data reception with out loss of signal and data quality.

- It is strongly suggested to use OKQPSK modulation scheme particularly when data is transmitted by multiple carriers. However, conventional QPSK modulation scheme is a preferable choice for single carrier transmission. 8-PSK modulation and even migrating to Ka band shall be considered for transmitting very high data rates (>640 MBPS) of high resolution imaging missions.

Chapter 6

Onboard high gain antenna systems with directional beams

High gain, directional beam antenna systems overcome the limitations of iso-flux antennas [Refer Chapter 3]. It is more appropriate to have high gain directional beam, which can always be pointed towards the required ground station independent of satellite flat form orientation. Paraboloid antenna or planar phased array provides high gain with narrow beam necessitating mechanical beam steering. Here the beam steering is accomplished by dual gimbal mechanism. To overcome mechanically induced jitter, electronically steerable antennas are preferred to provide the required EIRP over the full hemisphere. These antennas along with design concepts are briefed in the subsequent sections.

6.1 Mission requirements:

For typical IRS satellite in ≈ 600 Kms orbit providing a daily revisit to the interested region, spacecraft platform biases are applied to get the required across-track resolution to make the camera to trace the earth surface at an intended rate. This requires the spacecraft to rotate over Pitch axis at a rate of about 1 degree/second with spacecraft Pitch biases ranging between $\pm 45^\circ$. Spacecraft Roll bias is planned to the extent of about ± 45 deg, nominally limiting to $\pm 26^\circ$, to have imageries of regions separated from the spacecraft path to the extent of about 250 Kms.

In summary the spacecraft biases will be in the range :

Yaw : 0 to -45° .

Roll : $\pm 45^\circ$ (desirable) ,
 $\pm 26^\circ$ (nominal)

Pitch : $\pm 45^\circ$

The maximum rate variation over Roll/Pitch axes can be to the extent of about 1 deg/sec.

The data transmitting antenna with Field Of View (FOV) of $\pm 90^\circ$ is planned to be mounted along the spacecraft body Yaw axis. Beam along which payload data transmission is planned has about ± 8 deg width, being steerable anywhere within antenna FOV. The steering is selectable by means of two angular orientations. One angle called azimuth measured in Roll-Pitch plane of spacecraft from negative Roll towards negative Pitch on + angle. The other angle is with respect to spacecraft Yaw axis. The coordinate system followed for high gain antennas is shown in Fig. 6.1.

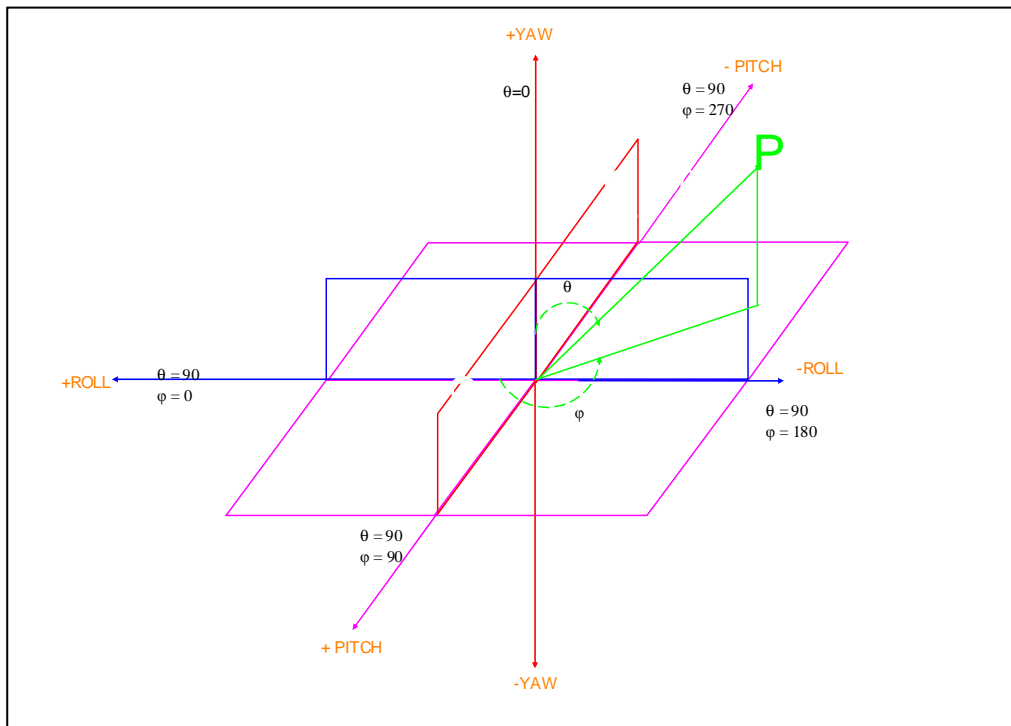


Fig. 6.1 Co-ordinate system for high gain antenna

The antenna needs to generate +19 dBW EIRP to ensure reliable link performance for transmitting 105 MBPS data. Link estimate is given in table. 6.1

Table. 6.1: Link Estimate for data transmission from IRS satellite in 600 Kms orbit.:

Carrier frequency	: 8125 MHz	
Modulation/Data rate	: QPSK /105 MBPS	
Tx. EIRP.	: +19 dBW	
Half power beam width (HPBW)	: 16° (Typical)	:
Orbit	: 600 Kms	
Elevation	: 5°	
Max. range	: 2329 Kms	
Path loss (@ 8300 MHz)	: 178 dB	
Miscellaneous loss	: 2 dB	
Ground station G/T at 5° elevation	: 30.5 dB/degK	
Received C/No	: 98 dB/Hz	
Available E_b/N_o	: 17.8 dB	
Required E_b/N_o for 10^{-6} BER	: 10.8 dB	
Implementation margin	: 2.0 dB	
Available margin	: 5.0 dB	

Under nominal conditions, for the planned orbit, the onboard antenna beam axis subtends a maximum angle of about 66° corresponding to an elevation of 5° of the ground station antenna. When the biases are applied (Pitch, Roll, Yaw) for changing the orientation of spacecraft for special imaging sessions, the resultant angle subtended can change from 40° to 90°. Thus it is desirable to maintain peak EIRP of 19 dBW in the range 40° to 90° off array axis. For angles less than 40°, the slant range being less, the EIRP can be less to that extent of path loss advantage.

6.2 High gain antennas:

Use of high gain antennas for transmitting high bit rate data has significant advantages [section 2.8.4]. Due to narrow beam width associated with high gain, the beam needs to be steered. Conventionally, antennas are steered either mechanically or electronically.

6.2.1 Mechanically steered high gain antennas:

In satellite communications systems, the antenna architecture has been to attach the entire antenna, (paraboloid reflector antenna comprising a parabolically curved main reflector, a feed horn, and a subreflector, or a planar patch array) to a positioning mechanism, such as a gimbal which moves the entire antenna to position or scan the antenna beam over the earth. Mechanically steered antennas require a positioner for mechanically rotating the antenna and for supplying the necessary electrical signal thereto. For example, conventionally positioners include azimuth and elevation drive motors for rotating the antenna and a rotary joint for supplying the electrical signals to the antenna. Paraboloid reflector antenna as well as planar phased array antenna developed for Chandrayaan and Cartosat-2/2A spacecrafts are described subsequently:

- **Paraboloid antenna:**

The data transmission antenna developed at X-band is a 0.7m axially displaced ellipse, commonly known as ADE reflector. The main reflector is fabricated out of composite material and the sub-reflector feed and the polarizer are made out of aluminium. This antenna is mounted on a dual gimbals system to provide the required beam pointing towards the ground station. The antenna fabricated and flown onboard Chandrayaan spacecraft is shown in Fig. 6.2.

The RF connectivity at the axis of rotation is provided by the usage of co-axial rotary joints. The feed for the antenna system is a corrugated horn and capable of transmitting in both left hand circular polarization (LHCP) and right hand circular polarization (RHCP). The axial ratio of the polarizer is better than 1dB and having the cross polar isolation of better than 20dB. The overall specifications of the data transmission antenna are given in table 6.2



Fig. 6.2 : Dual gimbal controlled paraboloid antenna

Table 6.2 Specifications of dual gimbal antenna of Chandrayaan.

Configuration	0.7 m high efficiency ADE reflector
Frequency	8.45 GHz to 8.50 GHz
F / D	0.38
Polarization	RHCP / LHCP
Peak gain	+ 33 dBi
Half power beam width	3.4 °
Axial ratio	2.0 dB (max.)
Weight	5 Kgs

- **Planar phased array**

Two factors contribute to the heavy weight of paraboloid antenna system. First, to maneuver a large mass and therefore the momentum, a heavy duty gimbal system is necessary. Second, to secure the entire antenna assembly in place during the launching vibration requires the use of a heavy latching structure during launch. One antenna that addresses the above concerns is planar phased array.

A planar patch array antenna shall be mechanically steerable with a dual axis positioner for rotating the array about azimuth and elevation axes over full hemisphere.

Fig. 6.3 shows a planar phased array mounted on dual gimbal mechanism developed for Cartosat-2/2A spacecrafts.



Fig. 6.3 Dual gimbal mounted planar phased array antenna of Cartosat-2

6.3 Electronically steerable antenna:

Conventional phased array with elements driven by controlled phase shifter amplifiers provides high gain directional beam with cosine scan behaviour and is not suitable for wide angle scanning. Spherical phased array provides a solution for the deficiency associated with mechanically steered antennas as well.

6.3.1 Spherical phased array:

The spherical array consists of a number of radiating elements that are arranged on spherical surface to enable beam steering without significant directivity degradations. A suitable antenna element distribution is selected to maintain uniform pattern while scanning, ideally to accomplish this element distribution should appear same from any far field observation. Among the various configurations like geodesic, icosahedron etc., the sphere is configured with multi-face polygon supporting the radiating elements.

In order to maintain maximum EIRP of 19dBW through 40° to 90° elevation angle, more number of elements are to be accommodated in that direction. Icosahedron geometry having 20 faces and 12 vertices and each face being an equilateral triangle, all the elements can be accommodated with uniform spacing maintained between all the elements. On the surface of sphere, this configuration has the additional advantage of flexibility to maintain desired element spacing for any diameter of the sphere.

- **Geometrical considerations:**

The spherical coordinate geometry used and the orientation of the spherical surface ($r = a$) are as shown in Fig.6.4

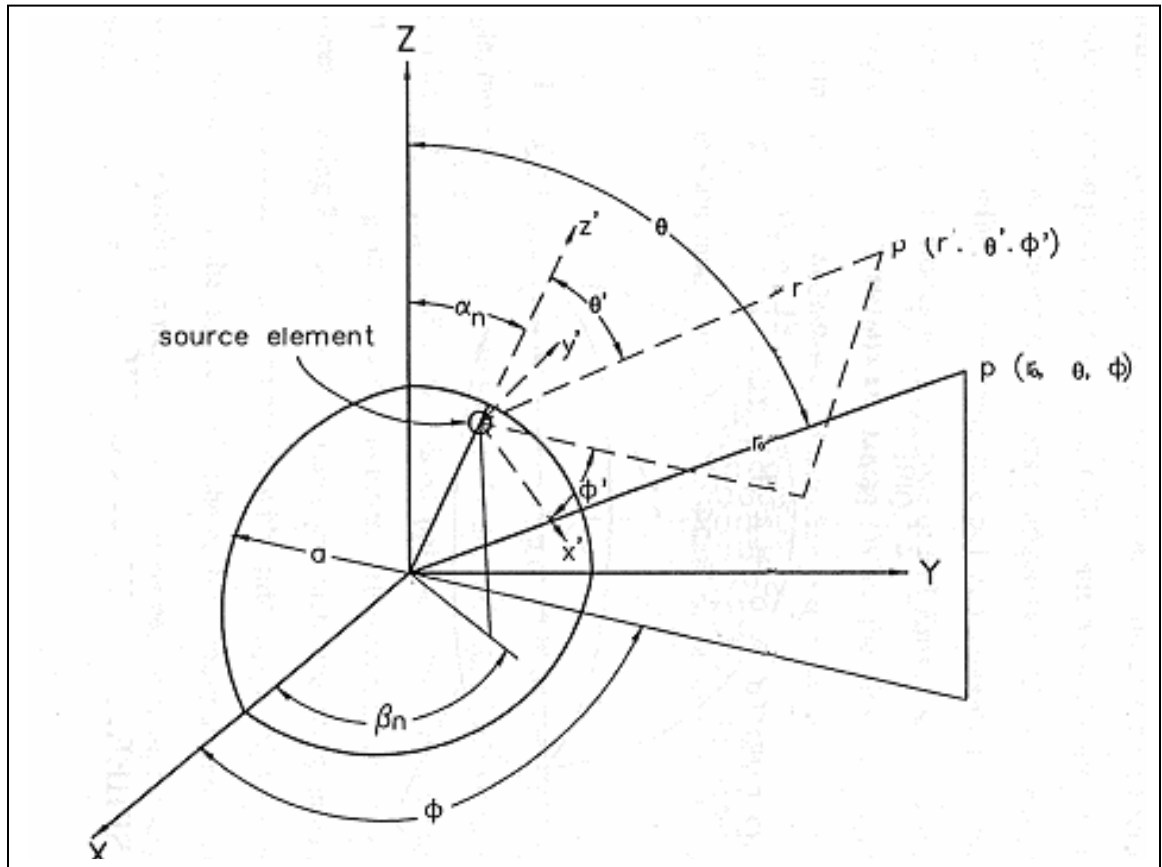


Fig. 6.4 Coordinate system for spherical array

The orientation of the spherical surface ($r = a$) is as shown in the Fig. 6.4. The coordinates of each element are α_n and β_n and those of far field are $P(\gamma_0, \theta, \phi)$. The values of α_n, β_n are determined by element distribution. Each antenna is assumed to generate circularly polarized pattern and is oriented so that maximum direction of the pattern coincides with the radial direction. All the elements are excited with uniform amplitude but they are phased such that there is a maximum in the radiation pattern produced by the array, in the direction θ_0, ϕ_0 .

The icosahedron type of element distribution is given by the following expression:

$$\alpha_n = 90^\circ - (p * 15^\circ) \quad \text{--- (32)}$$

where n is an integer in the range $-6 \geq n \leq 6$,

$$\begin{aligned}
\beta_n &= 72^\circ * q / (6 - |p|) \text{ for } p = 5, 4, 3, 2 \text{ and} \\
\beta_n &= 180^\circ + 72^\circ * q / (6 - |p|) \text{ for } p = -5, -4, -3, -2 \\
\beta_n &= 0 \text{ for } p = +/- 6 \qquad \text{--- (33)}
\end{aligned}$$

where q is a positive integer ranging from 0 to a value M(p) which depends on p.

In this arrangement, there are 182 elements distributed over the entire spherical surface. For an hemispherical surface ($0 \leq p < -6$) the total number of elements used is 91.

As per the above formulation, radiating elements are mounted in various bands. Each band is identified by the elevation angle α . Where $\alpha = 0^\circ$ corresponds to zenith and $\alpha = 90^\circ$ to horizon. For any other value of α , a circle is available with radius ranging from 0 to a. In each of the bands, depending on the circumference available, radiating elements can be located. A single element can be located at the zenith ($\alpha = 0$) and approximately 20 – 30 elements on the great circle ($\alpha = 90^\circ$) depending on the radius of the sphere.

6.3.2 Design and analysis [199]:

Spherical array is analyzed in a fashion as that of planar arrays with suitable changes on account of the spherical configuration. For a far field point P(θ , ϕ) the phase of a particular element needs to be accounted considering the spherical curvature on which the element is located. Since the far field point P(θ , ϕ) does not subtend the same angle for all the elements, the contribution of different elements is not the same and hence appropriate co-ordinate transformation is carried out.

A beam in a given direction is generated by exciting a conical portion of the sphere with semi cone angle of α_c about the beam direction (θ_0 , ϕ_0). For such an excited spherical surface centered at θ_0 , ϕ_0 and angular size $2\alpha_c$, the on-off condition δ_n is given by,

$$\begin{aligned}
\delta_n &= 1 \text{ if } [\cos \theta_0 * \cos \alpha_n + \sin \theta_0 * \sin \alpha_n * \cos (\phi_0 - \beta_n)] > \cos \alpha_c, \\
&= 0 \text{ other wise} \qquad \text{---(34)}.
\end{aligned}$$

Physical meaning of this equation is that only those elements falling within α_c degrees of the direction (θ_0, ϕ_0) and at the same time visible from the far field point P will contribute to the pattern.

The phase values of each element is calculated from the element location (α_n, β_n) and beam direction (θ_0, ϕ_0) with the position of active elements and their respective phase, the radiation pattern can be computed. The formulation to compute radiation pattern is simplified by the assumption that the radiation pattern of the array elements is $\text{Cos}^n(\theta)$ type.

Array analysis algorithms are developed to compute 3D radiation pattern and directivity / EIRP values. The inputs for the programme are the following:-

- Element location (α_n, β_n)
- Element radiation pattern - approximated
- Radius of the sphere (a)
- Semi-cone angle (α_c)
- Beam direction (θ_0, ϕ_0)

The active elements are identified from equation 3 by applying the necessary conditions. The second step is to estimate the phases to be incorporated from pointing the beam in required direction.

The phase to be given for an element located at α_n, β_n on the hemisphere to form in a direction θ_0, ϕ_0 is given by

$$\psi = 2 * \Pi * a * \Delta_n - \eta_n \quad \text{--- (35)}$$

Where

$$\Delta_n = \text{Cos } \theta_0 * \text{Cos } \alpha_n + \text{Sin } \theta_0 * \text{Sin } \alpha_n * \text{Cos } (\phi_0 - \beta_n)$$

$$\eta_n = \tan^{-1} \frac{(\text{Cos } \alpha_n + \text{Cos } \theta_0) * \text{Sin } (\phi_0 - \beta_n)}{\text{Sin } \alpha_n \text{ Sin } \theta_0 + (\text{Cos } \alpha_n * \text{Cos } \theta_0 + 1) * \text{Cos } (\phi_0 - \beta_n)}$$

Equation 4 is computed in a processor and appropriate TTL output pulses are generated for setting the phase shifter. The control circuitry in MMIC module shall convert TTL output to corresponding bias values for the phase shifters. Once the active elements with appropriate phases are derived, the analysis can be carried out for radiation pattern. Array factor at various far field observation points (θ, ϕ) is calculated using

$$E(\theta, \phi) = \sum \sum \delta_n \psi_n \exp [i (ka (\psi_n - \Delta_n) - (\xi_n - \eta_n))] \quad \text{--- (36)}$$

Where

$$\psi_n = \cos \theta * \cos \alpha_n + \sin \theta * \sin \alpha_n * \cos (\phi - \beta_n) \quad \text{---(37)}$$

$$\xi_n = \tan^{-1} \frac{(\cos \alpha_n + \cos \theta) * \sin (\phi - \beta_n)}{\sin \alpha_n \sin \theta + (\cos \alpha_n * \cos \theta + 1) * \cos (\phi - \beta_n)} \quad \text{---(38)}$$

The contributions from each of the active radiating elements at the far field observation point is vectorially added after considering appropriate coordinate transformation for each element. The resultant radiation pattern is the product of the element radiation pattern and array factor. Pattern analysis is done for various beam pointing directions observing EIRP and side lobe level values. It is repeated for different combinations of sphere radius and element distributions.

A chosen set of elements is generally used to steer the beam about the center of the elements to an extent of approximately $\pm 12^\circ$ in both elevation and azimuth planes by varying the phases of elements. During phase change the directivity remains same. The directivity is mainly obtained by the subset of elements which subtend low angle (less than 12°) at the beam direction contributing 100%. As the subset angle increases their contribution reduces; however they contribute for EIRP with the increased RF power. The set of element changes as the beam angle changes by more than 12° to 15° in one of the planes. The change over of elements occurs at the foot- print of the cone on the spherical surface. An element is off when its contribution is nil and on when it is significant for directivity. Its contribution increases with the beam direction approaching

the element location, an element's contribution being maximum when the beam direction matches with that of element location. As the beam is scanned, the foot- print of the cone also moves in the direction of the beam resulting in some of the elements made off and a new element becoming on.

The above configuration is able to meet the design goal of 19 dBW EIRP for the 40° – 90° sector in elevation for all azimuth angles excepting the side lobes structure for various configuration. Directivity in 90° scan angle is of importance but this has been low, due to the fact that there are no active elements beyond 90° in the hemisphere, which results in minimum number of elements. To improve, the elements are located till 100°, thus the effective number of elements increased in 90° direction maintaining the directivity and EIRP

6.3.3 Simulation

The directivity of the spherical array can be computed from the radiation pattern by equation 6 and integrating over θ and ϕ . Directivity is given by

$$Directivity D = \frac{4 * \pi * E_{max}(\theta, \phi)}{\int_0^{2\pi} \int_0^{\pi} E(\theta, \phi) \sin \theta d\theta d\phi} \quad \text{--- (39)}$$

The integration for the directivity is carried out on 2178 points in the radiation sphere. This is selected from the computation time point of view. Integration was also carried out by taking 4320 points and the value was found to be matching within ± 0.1 dB.

Mission requirements of 19 dBw EIRP is met for cone angle values of $\alpha_o > 45^\circ$ and the variation of the EIRP for a given θ_o with ϕ_o is within a dB. Maximum EIRP is achieved in the region of θ_o over 45-65° and this is obvious from the fact the number of active elements available in this region is maximum. As θ_o approaches 90° the EIRP slightly droops in spite of the packing of more elements in the high α_n regions and this due to the truncation of the sphere at $\alpha_n=90^\circ$ (hemispherical configuration). Since the satellite is moving, with changing look angles of beam whereby sidelobe levels also change

depending upon the number of elements excited and their phases, the levels of the sidelobes (max -10 dB and -15 dB typical) are not of much significance.

Increase in the radius of the sphere can increase the directivity if the side lobe levels are maintained low (below -15 dB) and pseudo grating lobes formation is avoided. This can be met only if inter element spacing is maintained within 0.8λ . To achieve this, more number of elements are needed if sphere is made larger. To properly distribute the elements on sphere, number of bands to be increased maintaining the inter element spacing less than 0.8λ . In order to maintain maximum EIRP through 40° to 90° elevation angle, more number of elements are to be accommodated in that direction. It is found by simulation that 64 elements mounted in 5 bands at $22, 40, 58, 76$ and 94 degrees with respect to vertical axis with 4, 12, 12, 18 and 20 elements in corresponding bands (in five bands respectively starting from vertex) on an hemisphere are needed for getting the required EIRP. With the above elements distribution, various hemisphere sizes are considered and radiation patterns are simulated. Radiation patterns for hemispheres of radius $2.5\lambda, 3\lambda, 3.5\lambda, 4\lambda, 4.5\lambda,$ and 5λ are shown in Fig. 6.5.

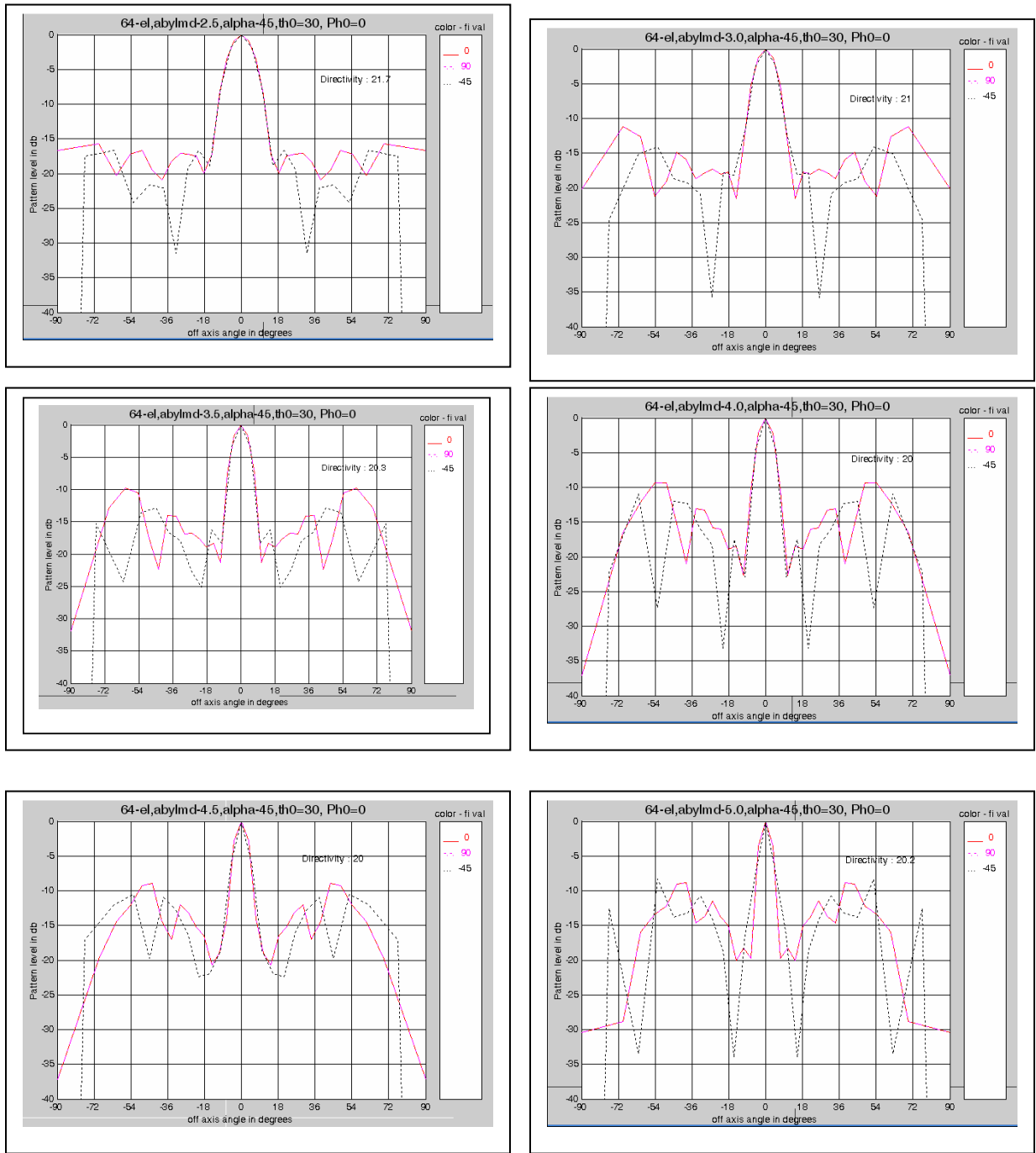


Fig. 6.5 Simulated radiation patterns for different size hemispheres

Directivity, computed for different radius of the sphere (a/λ) for different cone angles (α_c), is given in table 6.3 and is shown pictorially in Fig. 6.6.

Table 6.3 Directivity for hemispheres of different radius –simulation results

a/λ	Directivity (dBi)			
	$\alpha_c = 45$	$\alpha_c = 60$	$\alpha_c = 75$	$\alpha_c = 90$
2	18.66	20.58	20.58	20.28
2.5	19.8	21.72	21.72	22.2
3	19.89	21.01	21.01	21.56
3.5	19.78	20.32	20.32	19.81
4	19.8	20.06	20.06	19.4
4.5	19.8	20.01	20	19.47
5	19.8	20.29	20.29	19.62

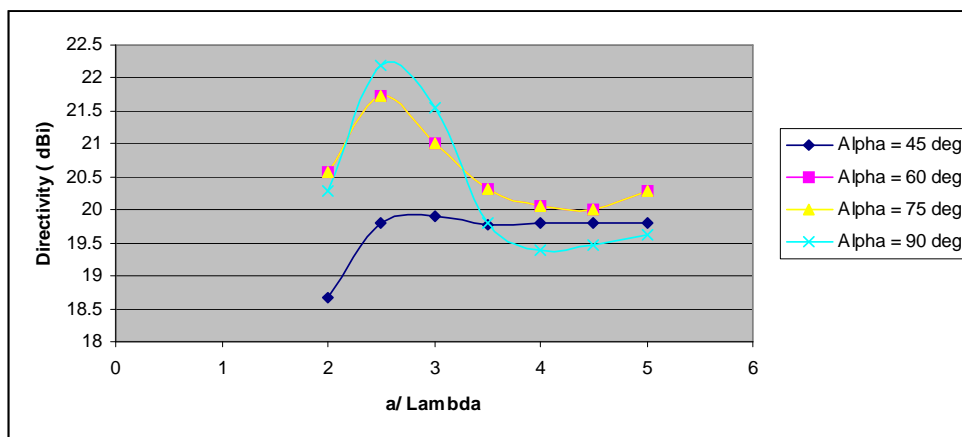


Fig. 6.6 Directivity vs a/λ for different cone angles

As diameter/radius (a/λ) of hemisphere is varied, initially the directivity increases and decreases with further increase in a/λ and saturates as seen from Fig. 6.6. When radius is increased beyond this point, the directivity fluctuates. The half power beam width keeps on reducing with increasing radius (a/λ). Theoretically, with reduction in half power beam width, the directivity should increase, but this does not happen due to increase of side lobes or due to generation of pseudo-grating lobes of significant levels. This implies that for a given diameter of the sphere with appropriate number of elements has a limitation on the realizable maximum directivity. Hemisphere with 2.5λ radius is found to be best trade off with respect to the directivity, radiation pattern and grating/side lobe levels.

It is to be noted that half power beam width (HPBW) decreases with the increase in sphere radius. Radiating elements located on spherical surface using icosahedron can accommodate any number of elements. As the beam direction (θ_0, ϕ_0) changes the

number of excited elements vary as much as 10% for a fixed value of α_c . This variation in number of active elements depends on the element distribution. This 10% of the elements are generally on the foot point of the cone on the sphere, due to which these elements are pointing away from the beam direction. Hence, they do not contribute significantly for the gain in the beam direction resulting in nearly constant beam width. However, these elements contribute to the wide angle side lobes.

The maximum value of directivity depends on the semi cone angle α_c and is generally above 60° . For angle exceeding 60° , the number of active elements increases significantly however the directivity does not increase proportionately due to the fact that for a given beam direction from spherical nature of surface, the contributions from all the elements is not the same in that direction. In an icosahedron, it is observed that for a beam along the Pole ($\theta_0=0$ and $\phi_0=0$) of the sphere, an increase of α_c from 75° to 90° , the number of elements increase by 20% with an increase in gain of about 0.5dB. For the application there is no specific figure for the directivity but the EIRP requirement of 19 dBW is the criteria. In an active array configuration, more number of active elements leads to an increase in RF power leading to higher EIRP. This indicates that though there is no significant improvement in directivity, by increasing α_c , there is a considerable increase in EIRP due to higher RF power generated.

The number of active elements executed by semi-cone angle α_c needs to be controlled, for two reasons. First with an increase in α_c , no significant change in directivity but significant increase in wide angle side lobes occurs. From mission point of view, the wide angle side lobes shall be below -15dBc . The second is the DC power requirements and power dissipation aspect. Each element has a MMIC block switched on, consuming a DC power of 4 watts of which only 100mw of RF power is generated. Hence the remaining 3.9 watts of power is dissipated as heat. Thus with increase in number of excited elements DC power goes up and power dissipation also goes up resulting in temperature increase of SSPA thereby asking for a complex thermal control system. There is an optimum limit on number of elements excited without sacrificing total EIRP

figure of 19 dBW. However, for a requirement of higher EIRP the sphere diameter, and number of elements can be increased.

The elements, which contribute significantly to form radiation beam in the desired beam direction only need to be excited. Elements falling in the area are excited with proper computed phase. The maximum value of the directivity depends on the semi cone angle- α_c . Fig. 6.7 shows the simulated radiation patterns of the hemispherical array for different cone angles. Table 6.4 provides simulation results.

Table 6.4. Directivity versus cone angle - simulation results

Semi Cone angle (deg.)	No. of elements	Directivity (dBi)	Side lobe level w.r.t. main lobe. (-dBc)
15	1	10.1	--
30	5	16.5	10.5
45	17	19.8	13
60	29	21.7	16
75	29	21.7	16
90	45	22.21	12.5

No recognizable beam

[$a/\lambda = 2.5$, $\alpha_c = 15^\circ$]

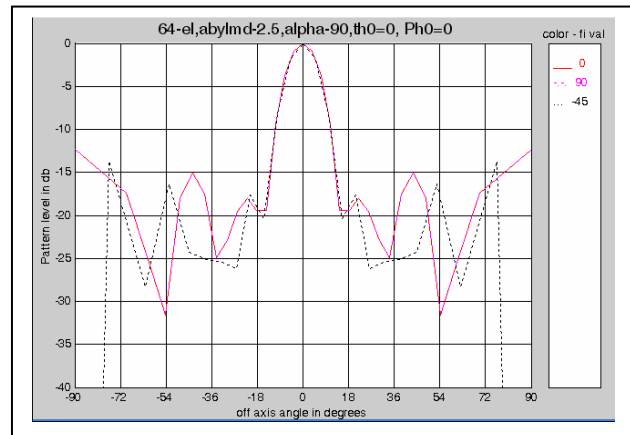
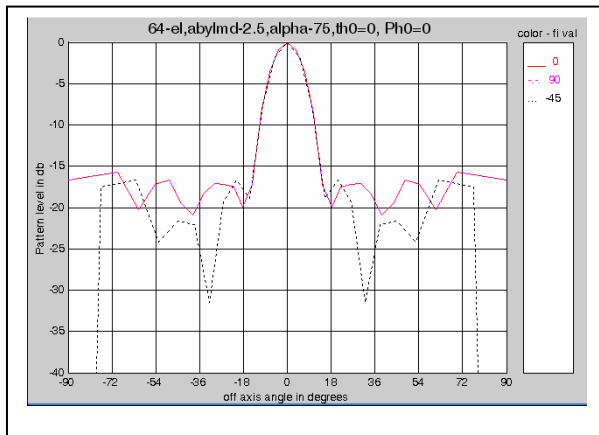
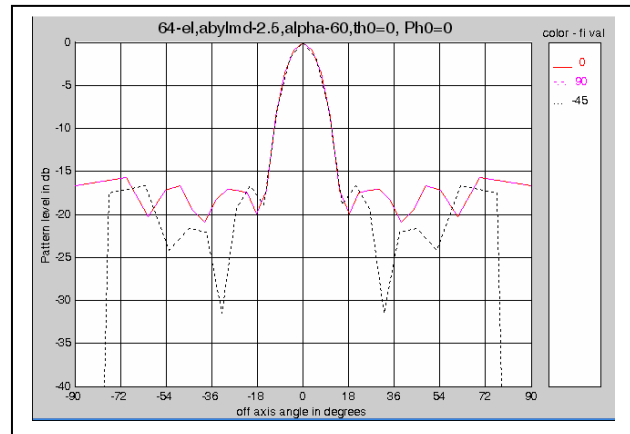
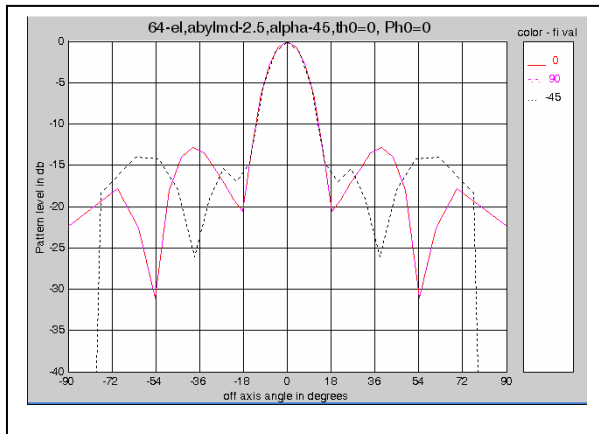
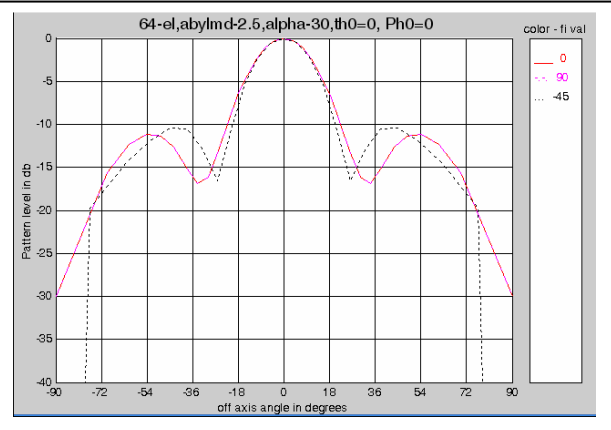


Fig. 6.7 Simulated radiation patterns for different cone angles

It can be seen from the simulation results that excitation of radiating elements in 60° cone angle provides optimum performance.

6.3.4 Spherical active array configuration:

In the active array configuration, a 5 bit phase shifter along with a solid state amplifier is included. The drive for all the amplifiers is always present, with a provision to switch on/off by applying the bias for the particular element. The active array configuration is as shown in Fig.6.8. It is proposed to implement Monolithic Microwave Integrated Circuit (MMIC) modules consisting of phase shifter, amplifier and control circuit for each of the element. A processor unit which is a part of the antenna system, estimates the phase shifter settings and on/off state (amplitude) of the amplifier. MMIC module is interfaced to processor units. The overall design optimization is necessary to minimize the number of radiators and to reduce interfacing connectors. Additionally in order to reduce the total cost of the system the design is to be optimum with minimum no of elements.

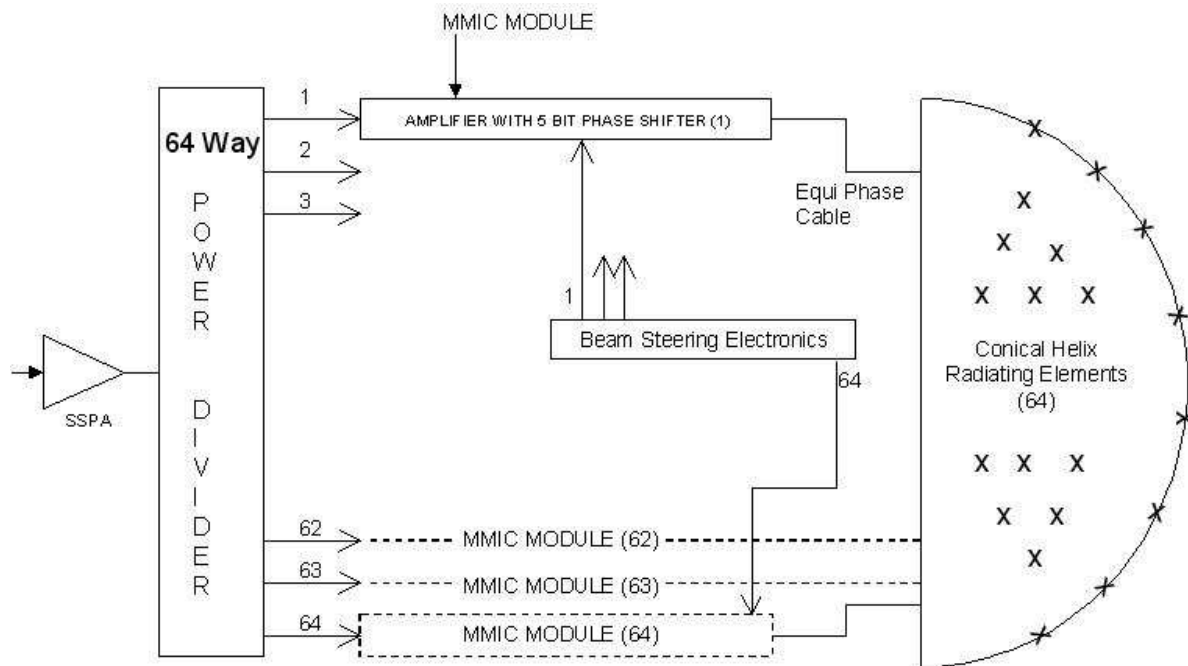


Fig.6.8 Conventional Spherical Array Configuration

6.3.5 Simulation results

The element distribution followed is given in Table 6.5 and shown pictorially in Fig. 6.9. The element pattern was approximated with $\cos^2(\theta)$ (directivity of 9dBi). The 3D contour plots for the beams scanned at different beam directions are as shown in Fig.6.10. The radiation pattern is plotted about the peak beam center (θ_0, ϕ_0) . The number of active elements and their phase, directivity and EIRP values are also included in the figures. 100 mw RF drive to each radiating element is considered for estimating EIRP

Table 6.5 Element distribution on hemisphere

Elevation (in Deg)	Number of Elements	Angle Interval	Offset (in Deg)
22	4	90	
40	12	90	0
58	12	30	0
76	16	22.5	11.25
94	20	18	0

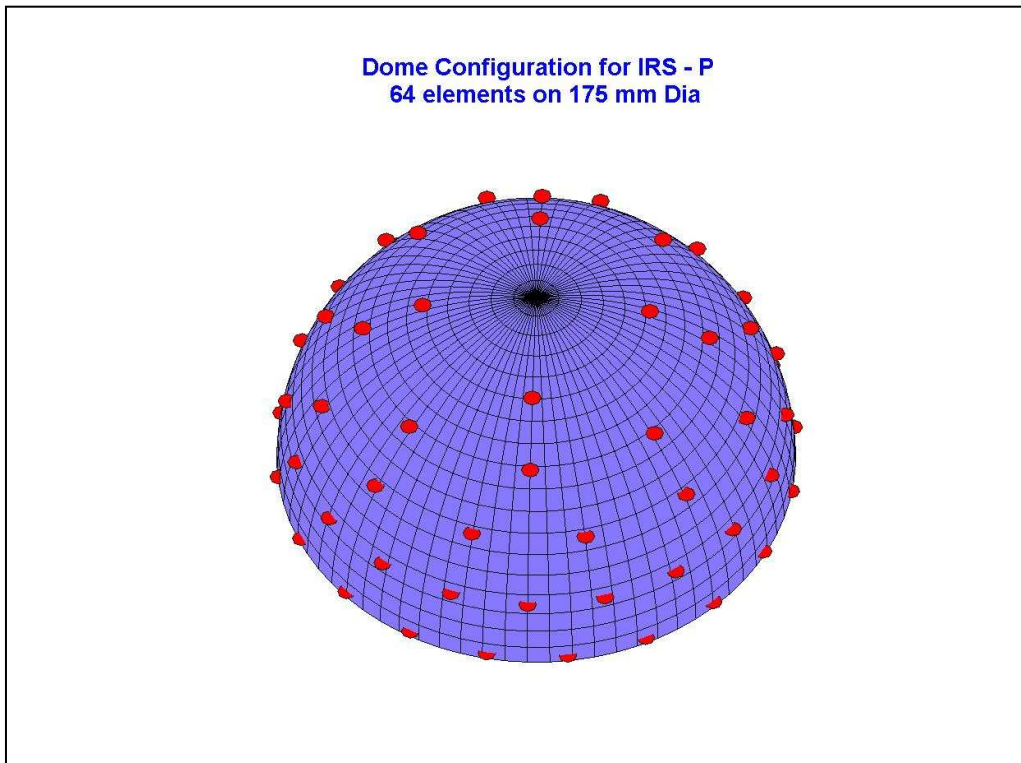


Fig. 6.9 Element distribution on 175 mm dia hemisphere.

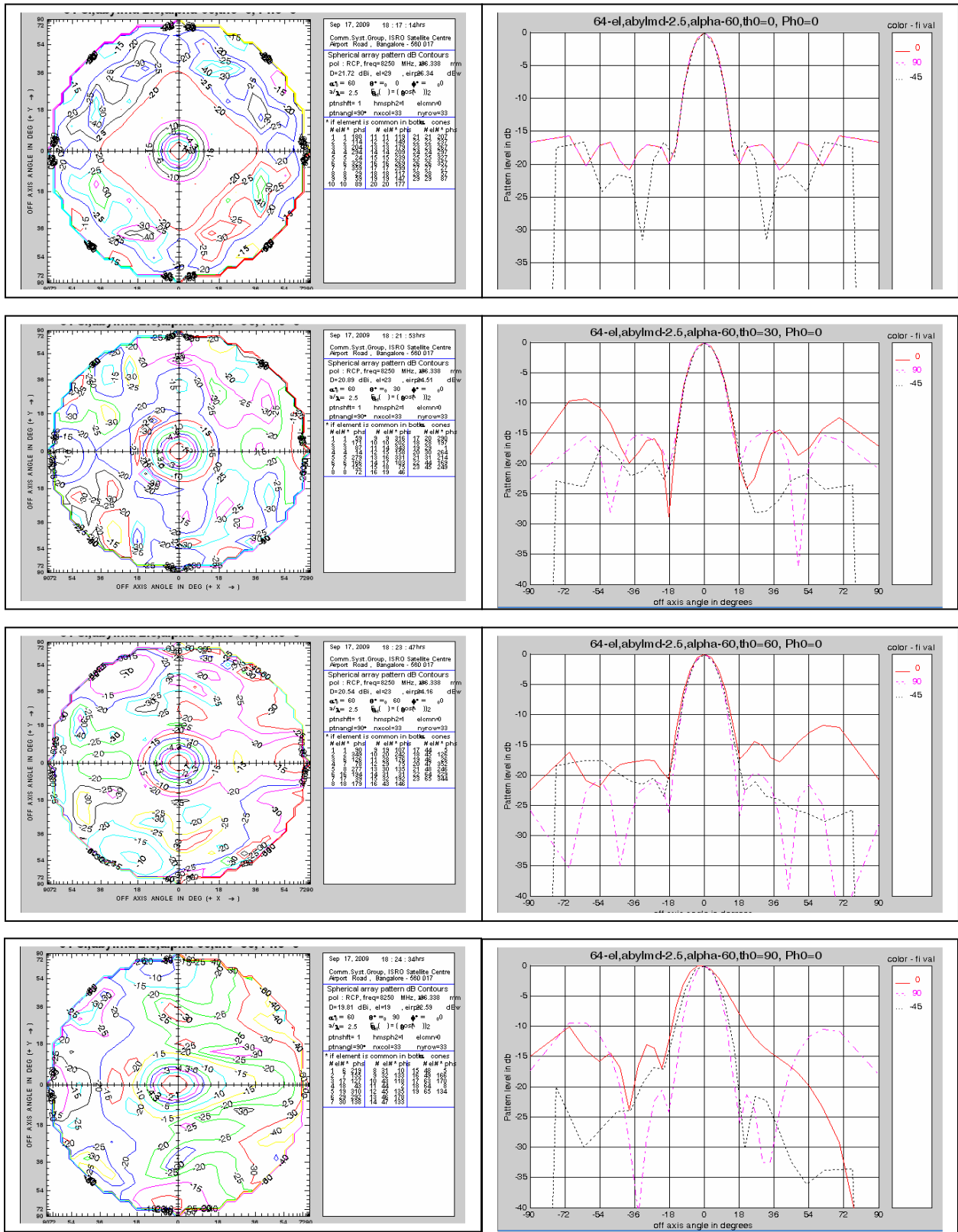


Fig. 6.10 Radiation patterns at different elevation angles

6.3.6 Element failure analysis

In any antenna array the final performance of the system is dependent on the successful functioning of all the radiating elements and drive amplifiers. In the event of failure of one of the elements, the other elements contribute for the performance and hence the degradation is graceful. This is one of the major advantage of antenna arrays. In an active array the EIRP is the addition of the antenna gain and the RF power generated by the array. In the event of failure of an element the RF power generated by the array gets reduced to the extent resulting in a further reduction in the EIRP of the array. In the case of spherical array which operates in the active array mode this is of concern and hence needs to be considered.

Spherical analysis was carried out taking into account failure of one element. Simulation indicates that there is a drop of 0.4 dB in the gain of the array. The RF power generated reduces. Overall, the EIRP reduces by 0.7 dB in the event of failure of any one of the elements. The analysis was performed for the failure of various elements and this reduction is observed within ± 0.1 dB. A typical case of one element failure on the EIRP over elevation is shown in Fig. 6.11

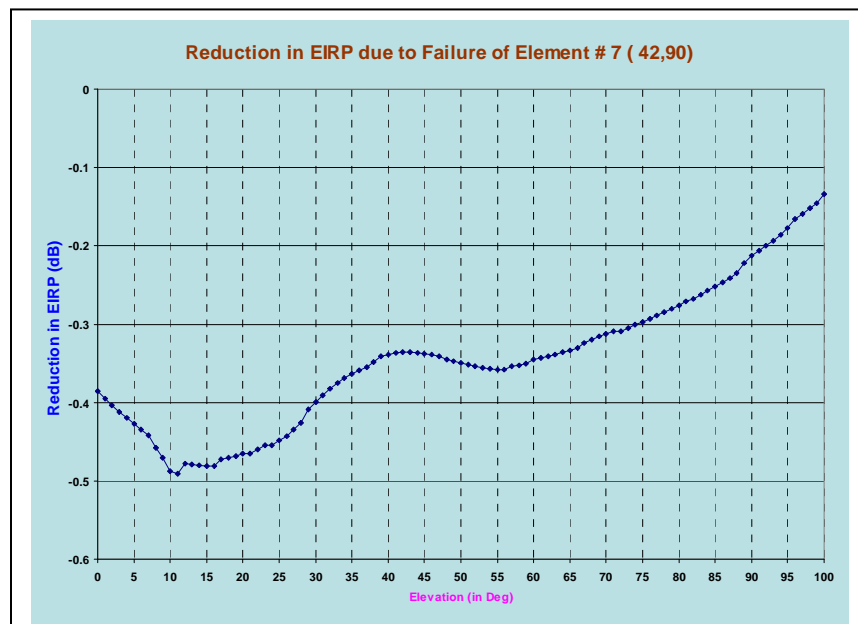


Fig. 6.11 Degradation of EIRP over elevation at a typical azimuth angle of 90° for one element failure

6.4 Phased array antenna configuration for Cartosat-2:

Weight of the phased array antenna to produce and steer the beam over full hemisphere is generally higher compared to the mechanically steered (dual gimbal system) and is of concern. A novel approach is proposed which is capable of generating single beam with significant weight reduction.

The spherical phased array antenna has radiating elements distributed almost uniformly on a hemispherical surface as explained earlier. It generates a beam in the required direction by switching 'on' only those elements, which can contribute significantly towards the beam direction. Typically to generate a single beam the antenna uses only about 1/4 to 1/3 of the total number of elements. As per simulation, the phased array antenna requires about 64 radiating elements with 100 mw drive for generating single beam with 19 dBw EIRP for Cartosat-2 spacecraft. For seamless beam generation over the hemisphere, the PAA operates in the active array mode where each of the radiating elements is fed by a MMIC module that consists of a 5-bit phase shifter and amplifier. Hence, phased array in general uses as many MMIC modules as the number of radiating elements. However, due to the basic concept of beam generation, at any given time only one third of these amplifiers are switched on and the remaining $2/3^{\text{rd}}$ are kept off. The MMIC modules along with the associated control electronics, harness and housing is a major contributor to the overall system mass. Apart from the self mass it also calls for use of as many coaxial input and output cables and control harness which in turn adds to the mass. DC power requirement for use of 64 MMIC modules is also higher. Considering these aspects, a new configuration is developed to realize a light weight, efficient phased array antenna which uses reduced number of MMIC amplifiers. In this configuration, only 16 MMIC modules are used and each of the MMIC is shared between four radiating elements using a SP4T switch as shown in Fig. 6.12

Single Beam 64 element Spherical Phased Array

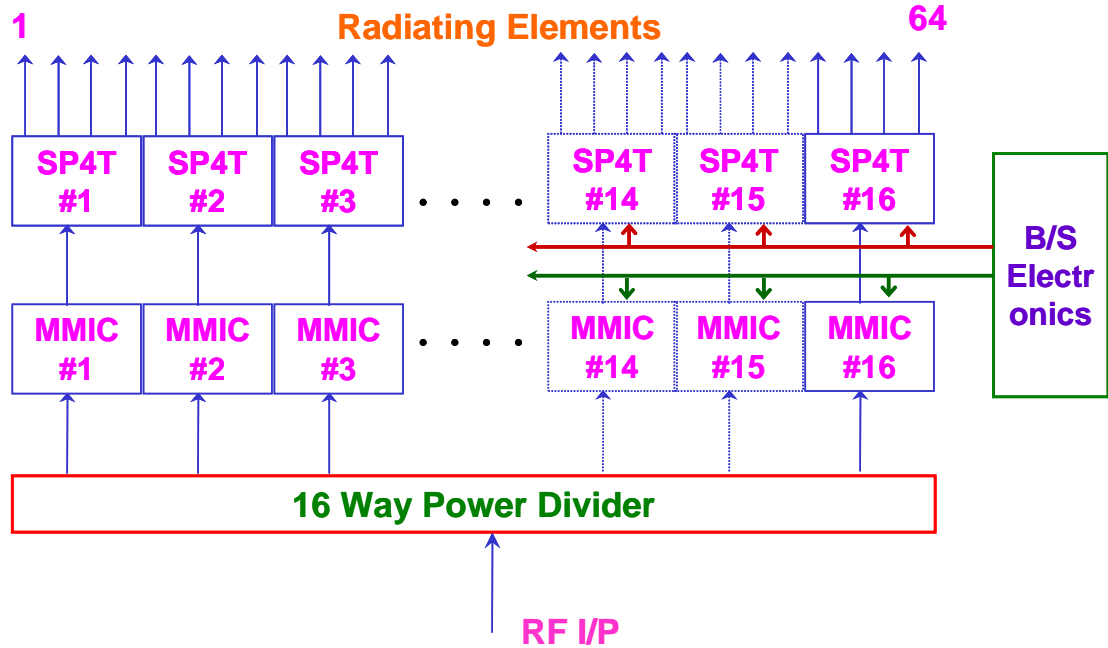


Fig.6.12. Single beam spherical array with 64 elements and 16 unit amplifiers

The information regarding sharing of the MMIC amplifiers by the radiating elements in the form of a look up table (Table 6.6) is provided to the beam steering electronics which enables the control of the SP4T switch by the beam steering electronics. Apart from estimating which of the radiating elements are to be made ON, the beam steering electronics using the look up table data selects the SP4T switch settings so that the radiating elements are correspondingly connected to the MMIC modules.

The predicted EIRP performance over different elevation angles (for an azimuth angle of 0°) with 100 mW output at MMIC is as shown in Fig.6.13. EIRP is estimated on the basis of 100mw RF output from MMIC modules. Analysis further indicates that this performance is maintained to within ± 0.5 dB for all other azimuth angles. Accounting overall system loss of 0.5 dB for RF cables, the EIRP is better than 20 dBW for elevation angles beyond 45° while the minimum value is 19 dBW around 30° . The element distribution on the dome is specifically configured for this kind of performance where at low elevation angles there will be advantages in the link due to the slant range reduction. It should be noted that for all the beam directions the number active elements (elements which are ON) are uniformly maintained at 16.

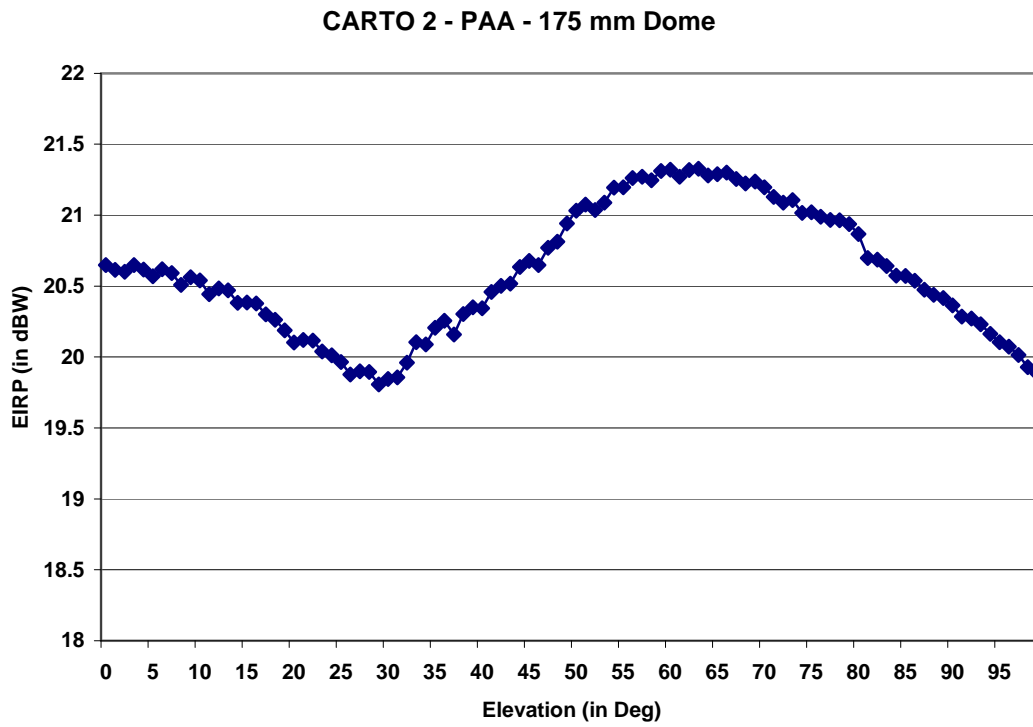


Fig. 6.13 Simulated EIRP vs. Elevation angle

Table 6.6 Element location and unit amplifiers distribution data
(175 mm Dome diameter - 64 elements - 16 unit amplifiers)

Element number	Alpha (deg)	Beta (deg)	MMIC ID	output port ID
1	22	0	1	1
2	22	90	2	1
3	22	180	3	1
4	22	270	4	1
5	40	0	5	1
6	40	30	6	1
7	40	60	7	1
8	40	90	8	1
9	40	120	9	1
10	40	150	10	1
11	40	180	11	1
12	40	210	12	1
13	40	240	13	1
14	40	270	14	1
15	40	300	15	1
16	40	330	16	1
17	58	15	3	2
18	58	45	4	2
19	58	75	1	2
20	58	105	16	3
21	58	135	3	3
22	58	165	4	3
23	58	195	1	3
24	58	225	2	2
25	58	255	3	4
26	58	285	4	4
27	58	315	1	4
28	58	345	2	3
29	76	0	7	2
30	76	22.5	8	2
31	76	45	9	2
32	76	67.5	5	2
33	76	90	6	2
34	76	112.5	7	3
35	76	135	8	3
36	76	157.5	9	3
37	76	180	5	3
38	76	202.5	6	3
39	76	225	7	4
40	76	247.5	8	4
41	76	270	9	4
42	76	292.5	13	2
43	76	315	5	4
44	76	337.5	6	4
45	94	9	14	2
46	94	27	15	2
47	94	45	16	2
48	94	63	2	4
49	94	81	10	2
50	94	99	11	2
51	94	117	12	2
52	94	135	13	3
53	94	153	14	3
54	94	171	15	3
55	94	189	10	3
56	94	207	11	3
57	94	225	12	3
58	94	243	14	4
59	94	261	15	4
60	94	279	16	4
61	94	297	10	4
62	94	315	11	4
63	94	333	12	4
64	94	351	13	4

6.4.1 Realization:

Mission requirements given in section 6.1 translates to an antenna pattern, which is hemispherical. There is a need to scan the beam in elevation up to 90° and over 0 to 360° in the azimuth. To achieve the required EIRP for various directions with minimal variation, an active spherical array configuration is developed. The active array configuration developed to meet the above requirements based on the design/simulation as explained in earlier sections, is shown in Fig. 6.14.

The radiating elements are distributed on a 175 mm dia hemispherical dome as per the angular locations given in table 6.7. and is shown in Fig. 6.15

The beam direction from the satellite to the designated ground station is computed from the orbit parameters every second in the spacecraft. The beam direction is updated every second to have a smooth scanning of the beam. A set of radiating elements, in a 60° cone around the desired beam direction, which contribute for the radiation of signal in the desired direction, are selected. Each element is excited by phase controlled amplified signal of 100 mW power.

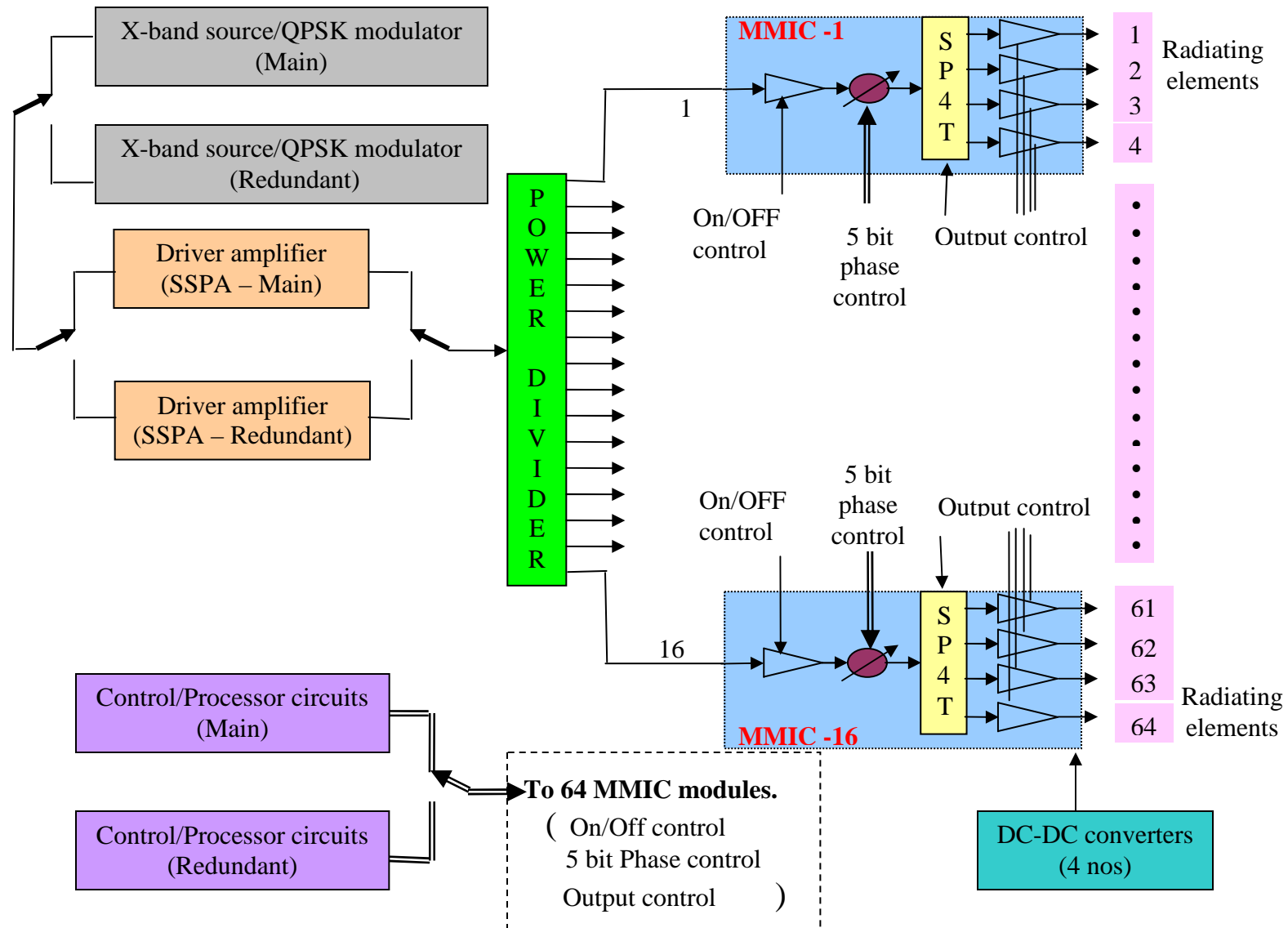


Fig. 6.14 Block schematic diagram of phased array antenna of Cartosat – 2

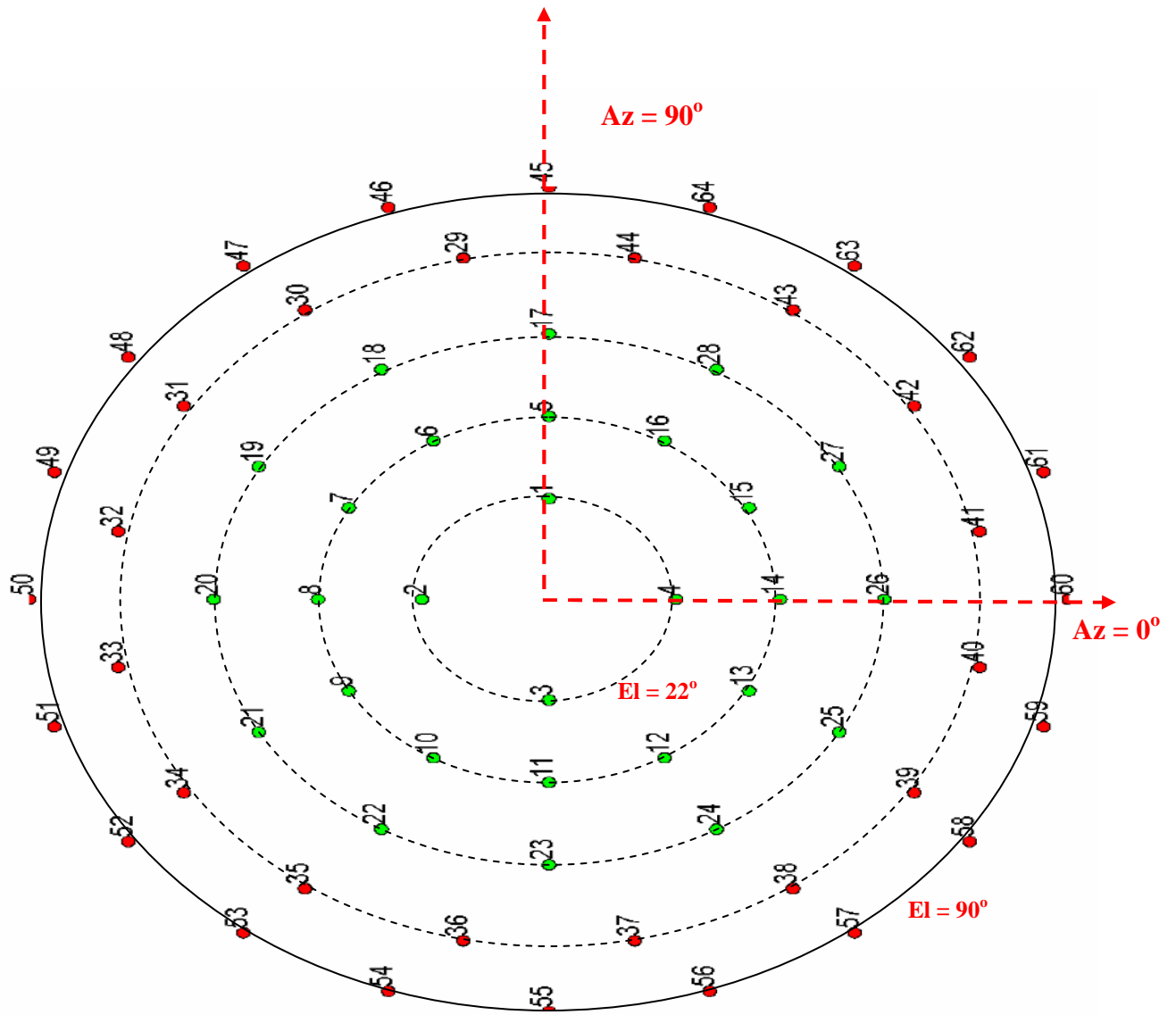
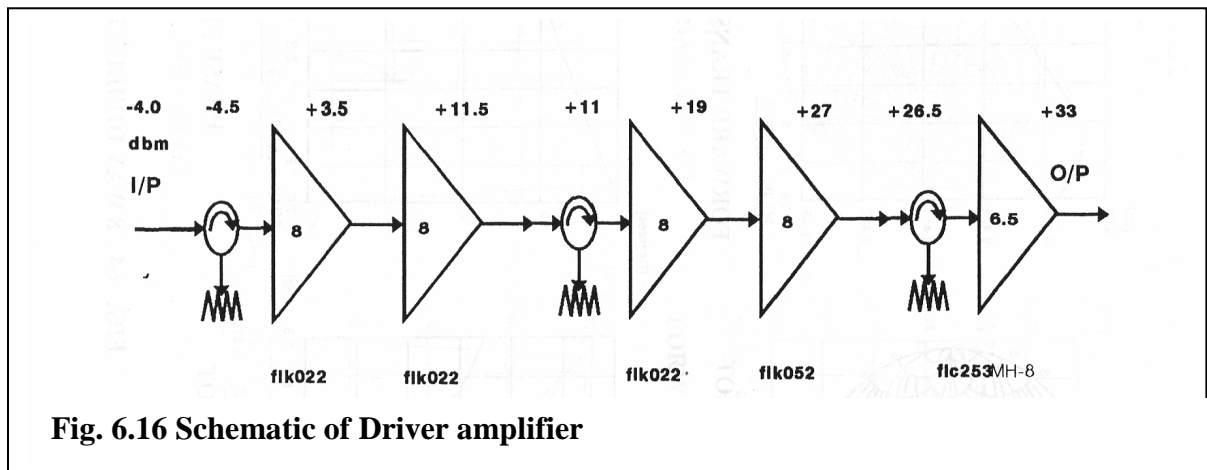


Fig. 6.15 Element location on the hemisphere dome

6.4.2 Driver amplifier:

A 2 W Amplifier is designed to drive MMIC amplifier blocks feeding 64 elements of phased array antenna system..

Fig. 6.16 shows the schematic of the amplifier. A cascade of five-amplifier stages amplifies the input X-band signal to +33 dBm. From the available lot of devices the lineup/individual amplifiers have been selected to optimize overall efficiency.



In order to keep overall dimensions to a minimum, the amplifier is designed for MIC realization on alumina substrates. All amplifier stages are housed in a single package. With this layout, interconnection losses are minimized. In order to prevent any unwanted feedback, isolators are provided after every two stages of amplification. Further isolation between individual stages is achieved by use of “walls” on cover plate, which also cut out any cavity resonance in desired band. To facilitate modular approach and testing of individual stages before final assembly, each amplifier stage is matched independently to 50 ohm both at input and output using microstrip lines. The photograph of the realized amplifier is shown in Fig.6.17. The SSPA is operated with +9 volt supply and gate voltage is derived from -5 volt supply. The switch ON and switch OFF sequences are taken care in power supply design.

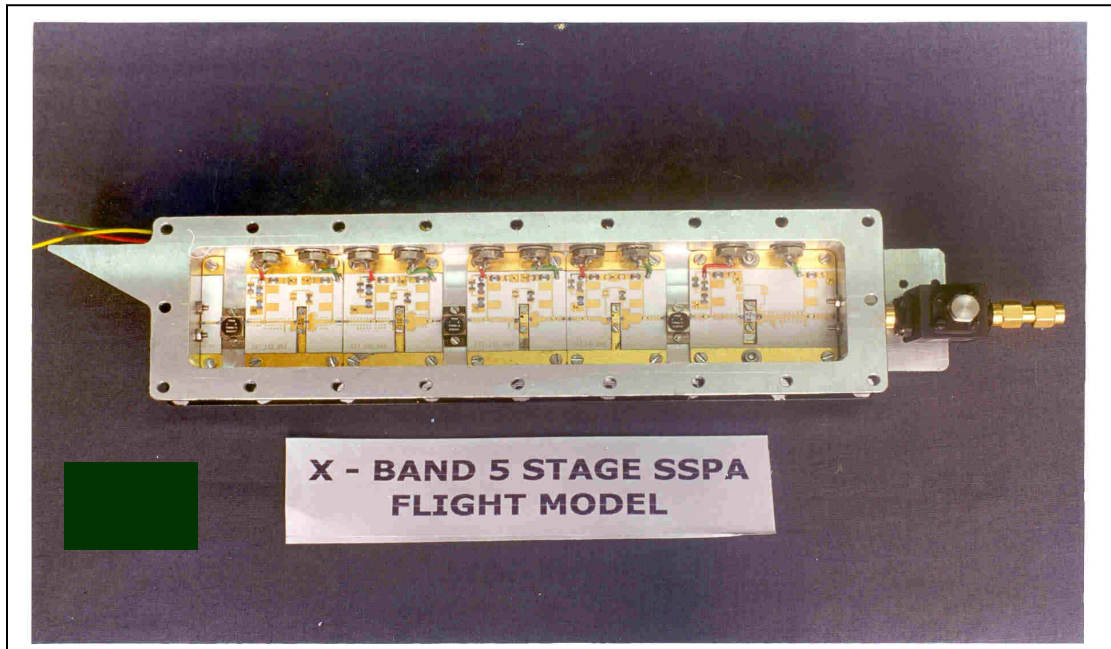


Fig. 6.17 Photograph of the realized X-band driver amplifier

The break up of power gain and operating levels of various amplifier stages is shown in table 6.7. To ensure high reliability, the amplifier is configured to keep the junction temperature of all active devices within 110°C. About 5°C rise is assumed due to thermal resistance in the heat flow path from heat sink to device case (θ_{ch}). Table 6.8 gives an estimate of junction temperatures of various stages. All passive components are operated well within rated parameters and meet all derating requirements. Fig 6.18 shows the frequency response of the amplifier assembly.

Table 6.7. Operating levels of various amplifier stages

Sl No	Amp stage	Pin DC(W)	Pin RF(dBm)	Pout RF (dBm)	Gain
1.	XPA-02*	0.65W	-4.0	+3.5	7.5
2.	XPA-03	0.65W	+3.5	+11.5	8.0
3.	XPA-04*	1.35W	+11.0	+19.0	8.0
4.	XPA-05	1.35W	+19.0	+27.0	8.0
5.	XPA-06*	6.5W	+26.5	+33.0	6.5

* includes isolator loss

Total D/C power - 11W
 Final O/P power - 2W
 η over all - Better than 18%

TABLE 6.8. Power dissipation and junction temperature details

Amp Stage	SSPA 05	SSPA 04	SSPA 01/02/03
Device	FLC253MH8	FLK 052 WG	FLK022WG
I/P dc power	6.5 w	1.35 w	0.65 w
I/P RF Power	0.4 w	0.08 w	-
O/P RF power	2.0 w	0.4 mw	-
Power dissipated	4.1 w	1.04 w	0.65 w
θ_{jc} (Junction to case)	32.8°C	20.8°C	24°C
θ_{ch} (case to heat sink)	5°C	5°C	5°C
Heat sink temp °C	50°C	50°C	50°C
Junction temp °C	87.8	75.8	79.0

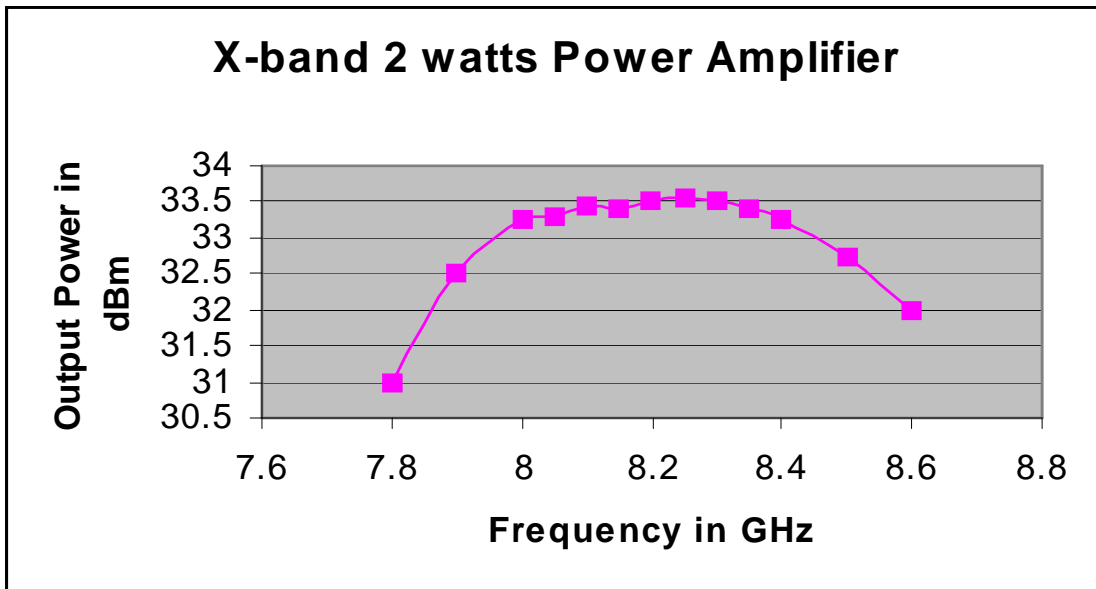


Fig. 6.18 Frequency response of X-band 2 watts driver amplifier

6.4.3 Phased Array Electronics assembly:

Phased array electronics system consists of power divider, MMIC modules, beam steering electronics (microprocessor based beam control system) and DC-DC converters to power all active circuits. The mechanical assembly of the Phased Array electronics system is shown in Fig. 6.19. The individual subsystems are explained in subsequent sections.

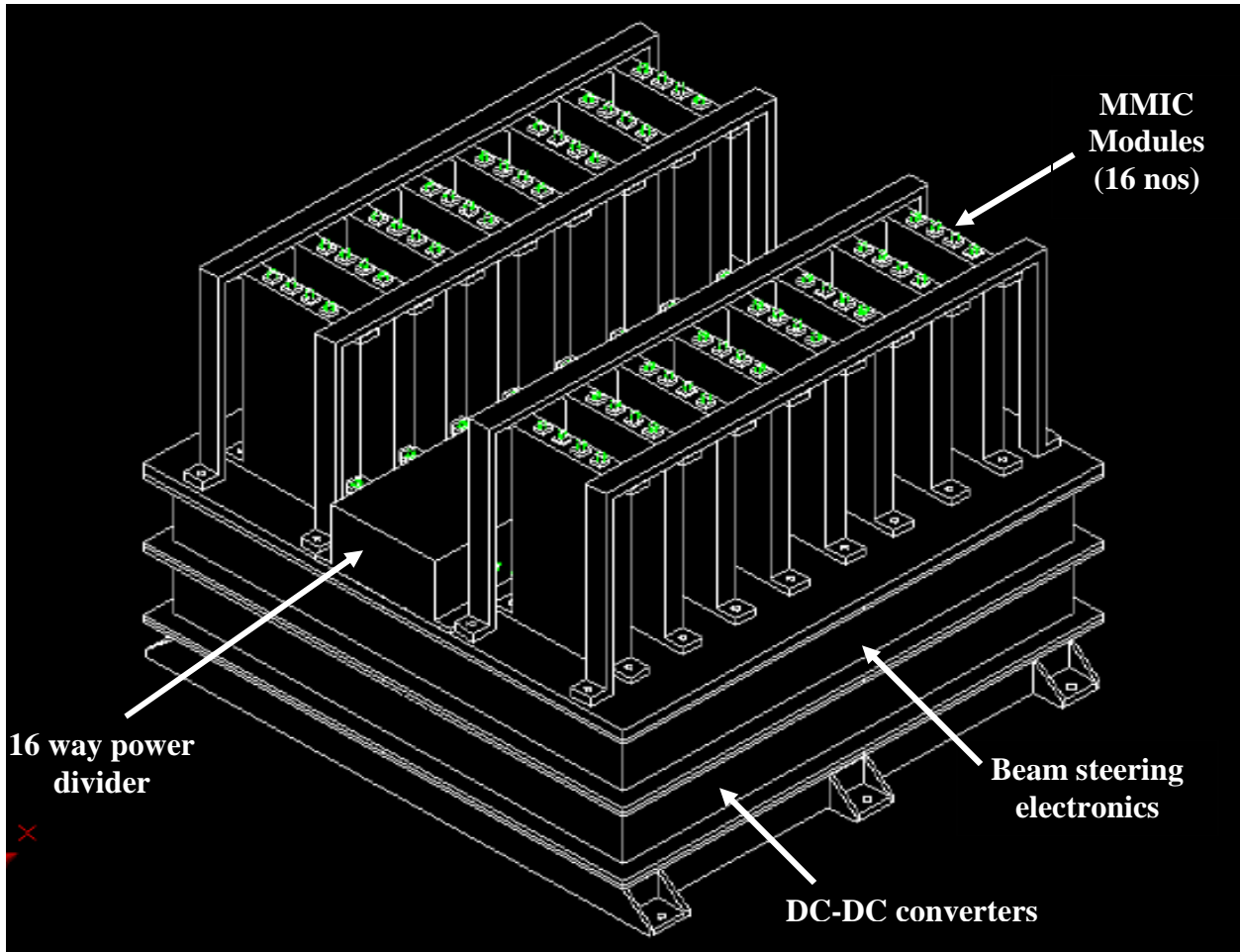


Fig. 6.19 Assembly of Phased Array electronics

- **Microstrip Power Divider:**

The RF interface to the array is through a power divider, which divides the Driver amplifier output RF signal (QPSK Modulated) fed to the PAA so as to provide the drive for all the MMIC phase shifter modules. As there are 16 MMIC modules the power needs to be split to 16 equal ways maintaining the same phase relationship to all the output ports. A microstrip power divider on 30 mils RT Duroid 6002 substrate is selected for this purpose. The basic requirement of equal power division and equal phase characteristics is achieved with the system explained, meeting all the requirements. The necessary power division is realized basically with corporate feed network technique using simple T-junctions at appropriate locations, maintaining equal phase characteristics with proper transmission line lengths. As phase uniformity is to be maintained a corporate feed structure is incorporated. All these exercises are carried-out using LINMIC software for simulations, on RT Duroid substrate of $\epsilon_r = 2.94$, 30 mils thick. The final size arrived is 200mm x 65mm. All the output ports (16 numbers) of the divider are SMA connectors accommodated on the two sides of the divider box and the input port is at the centre of the box with SMA interface. The finalized layout is shown in Fig. 6.20. and its measured return loss characteristics is shown in Fig. 6.21 respectively. The insertion loss of the power divider is measured to be 2 dB. The amplitude & phase imbalances are ± 0.5 dB and $\pm 4^\circ$ respectively.

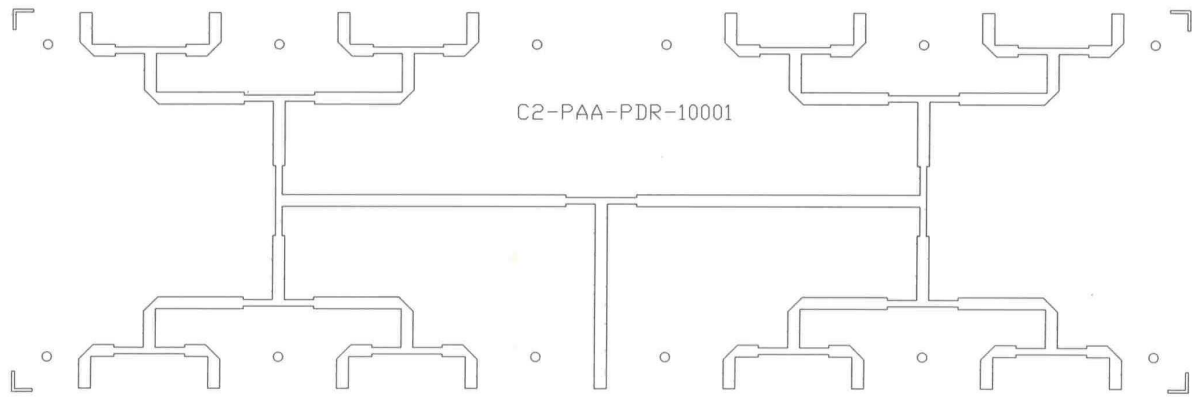


Fig. 6.20 Layout of 16-way microstrip power divider

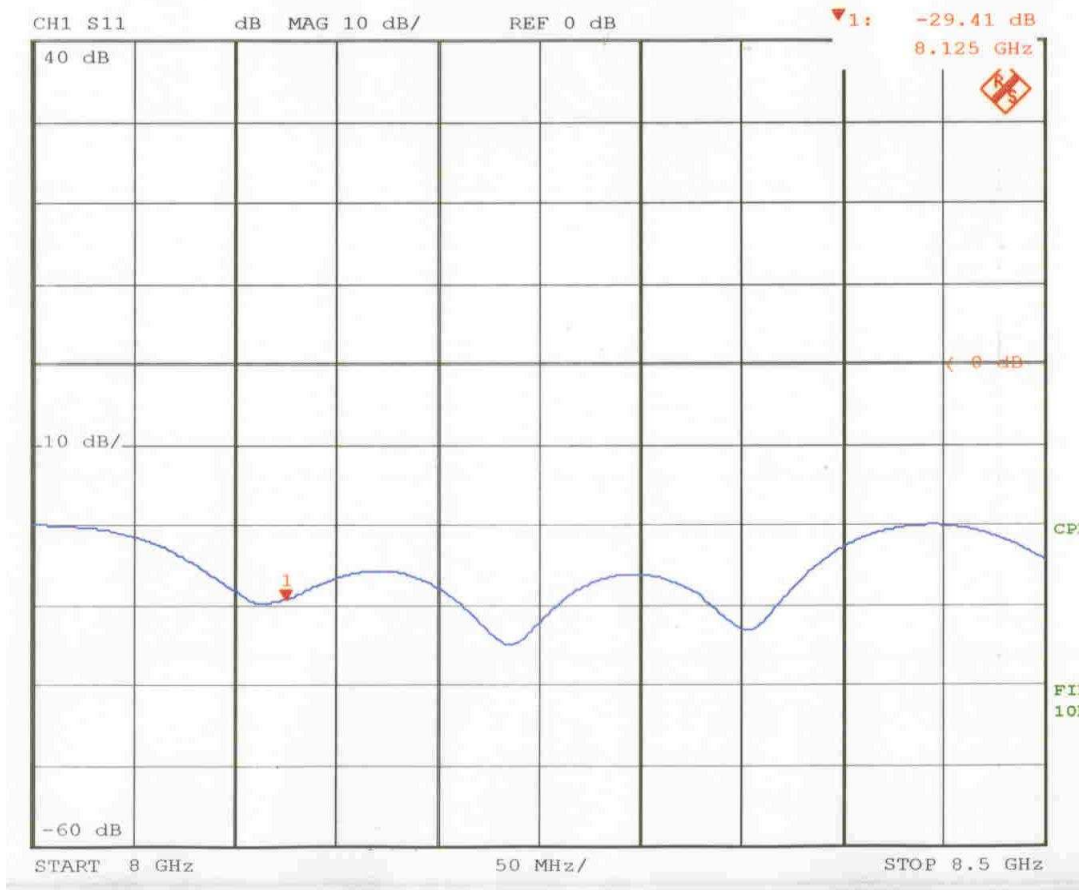


Fig. 6.21 Return loss response of microstrip power divider

- **MMIC Phase shifter/amplifier/switch module:**

MMIC module consists of a small signal amplifier, 5 bit digital phase shifter, SP4T switch and Four +20 dBm power amplifiers. The schematic is shown in Fig.6.22.

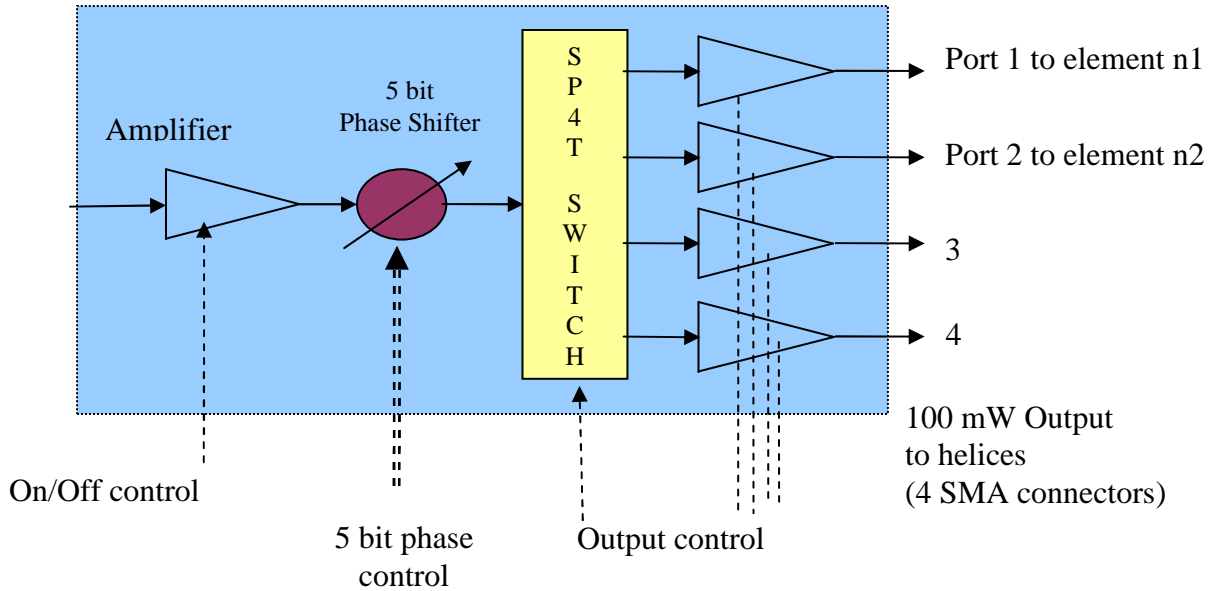


Fig. 6.22 Schematic of MMIC amplifier-phase shifter module

Beam steering electronics provides control signal to the module. At a time only one out of the four power amplifiers is active. Inactive amplifiers are switched off to save DC power. Beam steering electronics also provides 5 bit phase control signal to set the phase of the channel.

The test results of one of the 16 amplifier-phase shifter-switch assemblies are given in Table 6.9.

Table: 6.9 Test results of amplifier-phase shifter assembly

Amplifier Serial No: 36		+8V Reset Current		358 ma	
Frequency:	8.125GHz	-6.5V Reset Current		60	
Phase bits	10000	+8V On Current		501	
Spec on O/P power	20dBm	-6.5V On Current		80	

Input Power	Port 1		Port 2		Port 3		Port 4	
	Output Power (dBm)	Gain (dB)	Output Power (dBm)	Gain (dB)	Output Power (dBm)	Gain (dB)	Output Power (dBm)	Gain (dB)
-15	14.94	29.94	14.43	29.43	14.7	29.7	14.71	29.71
-13.9	15.86	29.76	15.36	29.26	15.6	29.5	15.7	29.6
-12.9	16.81	29.71	16.36	29.26	16.6	29.5	16.7	29.6
-11.9	17.7	29.6	17.25	29.15	17.5	29.4	17.54	29.44
-10.9	18.55	29.45	18.1	29	18.3	29.2	18.4	29.3
-9.9	19.4	29.3	18.94	28.84	19.15	29.05	19.23	29.13
-9.4	19.78	29.18	19.33	28.73	19.56	28.96	19.56	28.96
-9	20.2	29.2	19.72	28.72	19.93	28.93	20.03	29.03
-8.5	20.6	29.1	20.11	28.61	20.3	28.8	20.4	28.9
-8	20.9	28.9	20.47	28.47	20.6	28.6	20.67	28.67

- **Control unit for phased array antenna (Beam steering electronics):**

The phased array antenna, as already mentioned, consists of 16 amplifier/phase-shifter/switch units. Each unit requires one bit (TTL compatible) for ON/OFF control, five bits (TTL compatible) for phase control and two bits for switch control. The main function of the control unit is to provide TTL control signals to the amplifier/phase shifter/switch units. The ON/OFF condition and phase shift values are computed from an algorithm.

The basic input to the algorithm is the beam direction , which is provided onboard by Attitude and Orbit Control Electronics (AOCE) system. The control unit reads the beam direction information from AOCE and carries out real time computation of the algorithm at specified intervals of time using a microprocessor system.

The system employs the INTEL 80C86 microprocessor and has 32K of ROM memory and 16K of RAM memory. The I/O space is decoded to provide access to 128 I/O devices. Of these, 96 are latches, which are used for storing the ON/OFF and phase shift and switch position information required for the modules. The block schematic of the beam steering /control system is given in Fig.6.23. The algorithm flow chart is given in Annexure A.

Total insertion phase (from power divider input to individual radiating element input) is measured and stored in a PROM as a lookup table. This phase information will be used as bias while calculating actual phase shift requirement for each element.

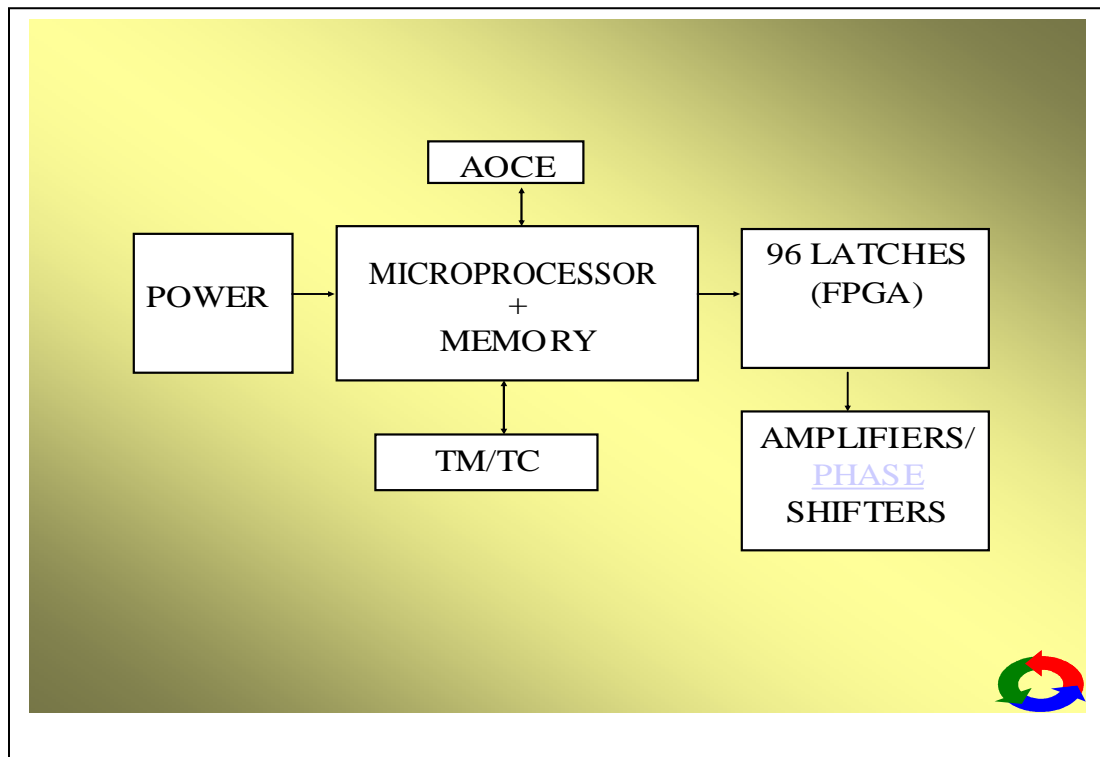


Fig. 6.23 Block schematic of beam steering electronics.

The microprocessor module, memory modules (both RAM & PROM), TM/TC/AOCE interface circuits, output latches interface circuit are accommodated in one PCB. Full passive redundancy has been planned. The output latches of both main in and redundant chains are realized in FPGAs. The outputs of main and redundant latches are shorted. The selected system will provide the control signal while the output latches of the deselected chain will be in tristate. The main and redundant latches are powered by separate DC/DC converters to enable the tristate logic gates to provide the control signal from the selected (powered ON) main or redundant processor system. This assembly will form the base for the other phased array modules. The control unit has interface to Telecommand, Telemetry, power, AOCE and amplifiers to carry out the various functions. Fig. 6.24 shows the beam steering electronics package.

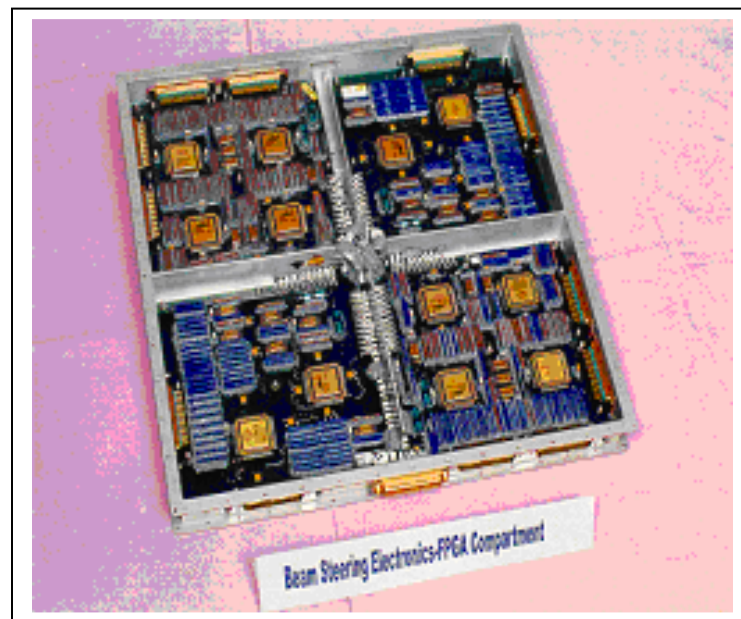


Fig. 6.24 Beam steering electronics package

6.4.4 Radiating elements:

The radiating element selection is one of the important design choices among various available options. Several types available, to mention a few, are dipole, horn, patch, helix, slots etc., Based on the application, particular element type is chosen. For satellite based active phased array antenna, several compromises are made in selecting the element. The overall weight and power consumption is the main criterion for satellite applications, particularly for the array under consideration involving 64 elements. Another aspect is accommodating all these elements in the available hemi-spherical surface and volume. In order to accommodate the radiating elements of 64 numbers on the surface is a big task meeting the electrical spacing separation. So, a smaller size and light weight element is preferred that has moderate gain and having inherent characteristics of generating circular polarization. Additional devices like hybrids and feed networks are required to generate circular polarization for many configurations like patches, horns etc. The power handling capability of the element is not of concern in this particular application since it handles low power of 100 mw through each element as overall power is shared by the array. Basically, a conical helix element antenna is chosen as it meets the basic requirements (Table 6.10) viz., minimum size, gain, self generation of circular polarization.

Table 6.10 Specifications of radiating elements:

Centre frequency	8.2 MHz
Bandwidth	400 MHz
Polarization	RHCP
Axial Ratio	< 2 dB
Return Loss	> 20 dB
Gain	+7 dBi
Power handling capability	1 Watt

Conical helical antenna is used as radiating element for spherical array to be operated at X band. The basic design parameters considered are HPBW, axial ratio and impedance. Solid Teflon former is used here for the rigidity of the structure as well as to reduce the axial length and diameter of the helix. C (the circumference of the helix) is chosen to be

0.9λ (31.4 mm) and S (the pitch) is chosen to be 0.1λ (3.5mm). The former is wound with the silver plated copper wire of dia 0.5 mm.

A tapered design is chosen (Fig. 6.25) to achieve good axial ratio over wide angles. A tapered helix is assembled by tapering the top four turns which results in a tapered helix consisting of a uniform section of two turns (0.27λ diameter) and a tapered section of four turns from 0.27λ to 0.05λ . This corresponds to a taper angle of about 16° . The axial length of the helix comes to 21mm. To suppress the side lobes and back lobes a conical ground plane with 0.55λ diameter and height 0.12λ is selected. SMA (jack) interface connector is off centered to the base to suit the starting point of the helix. The terminal impedance is matched to 50 ohms by a metal strip transforming section.

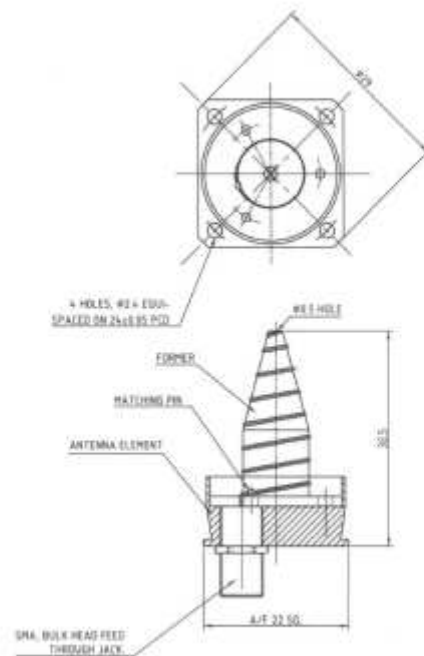


Fig. 6.25 Assembly of the radiator (Helical antenna)

Testing of the antenna elements:

Detailed tests are carried out on the conical helix in the frequency band 8.0 to 8.4 GHz.

The measurements are conducted in anechoic chamber for the following parameters:

1. Return loss
2. Radiation pattern
3. Axial ratio

Detailed response plots of the element are presented here.

Fig.6.26 shows the return loss characteristics over full band.

Return loss is better than 20 dB.

Fig.6.27 shows radiation pattern plot at 8.2 GHz

Fig.6.28 shows axial ratio plot at 8.2 GHz

Axial ratio is better than 1 dB

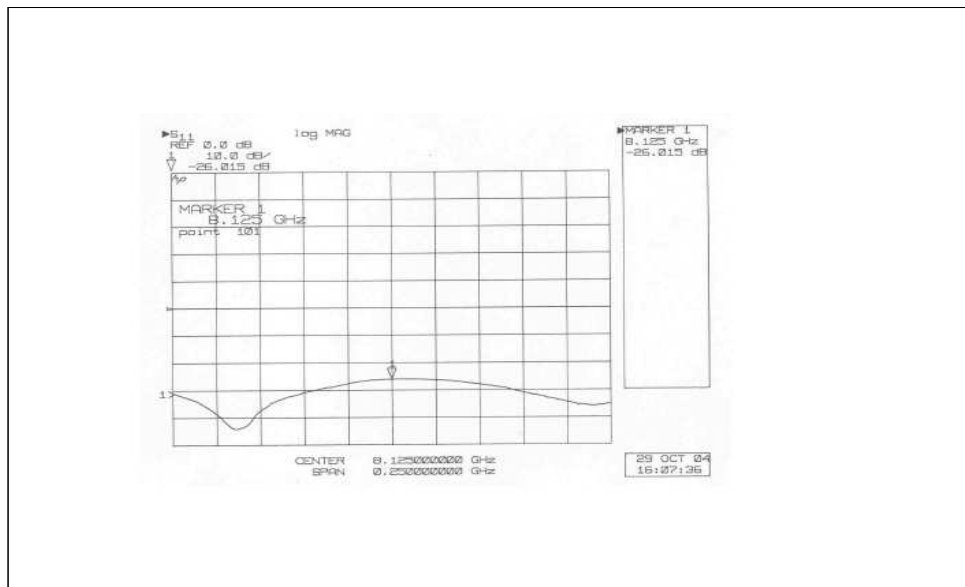


Fig. 6.26 Return loss response of helical antenna

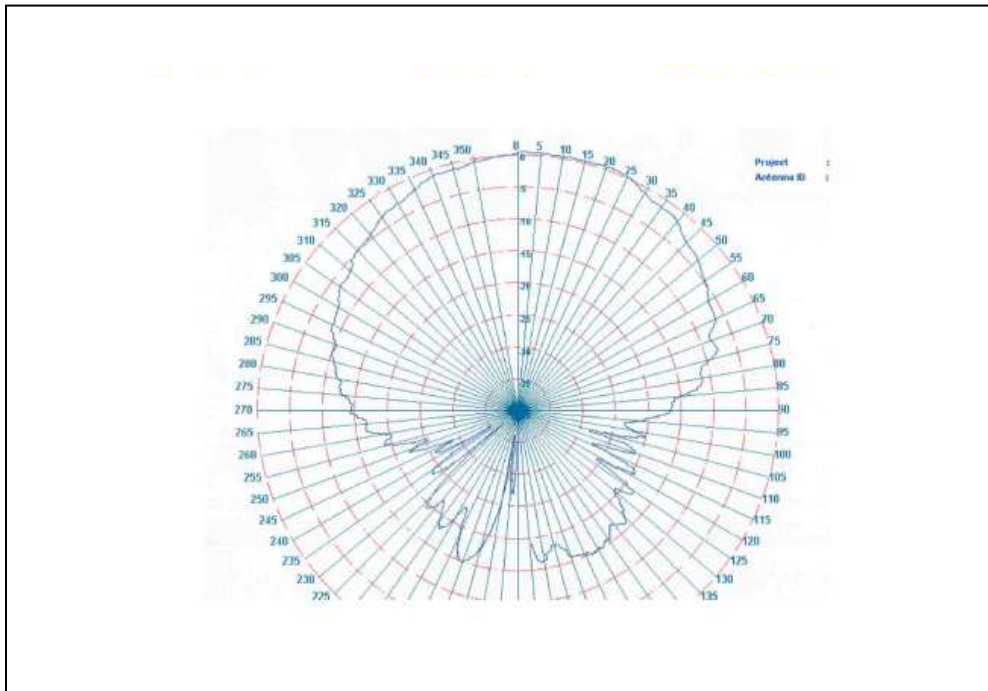


Fig. 6.27 Radiation pattern of helical antenna

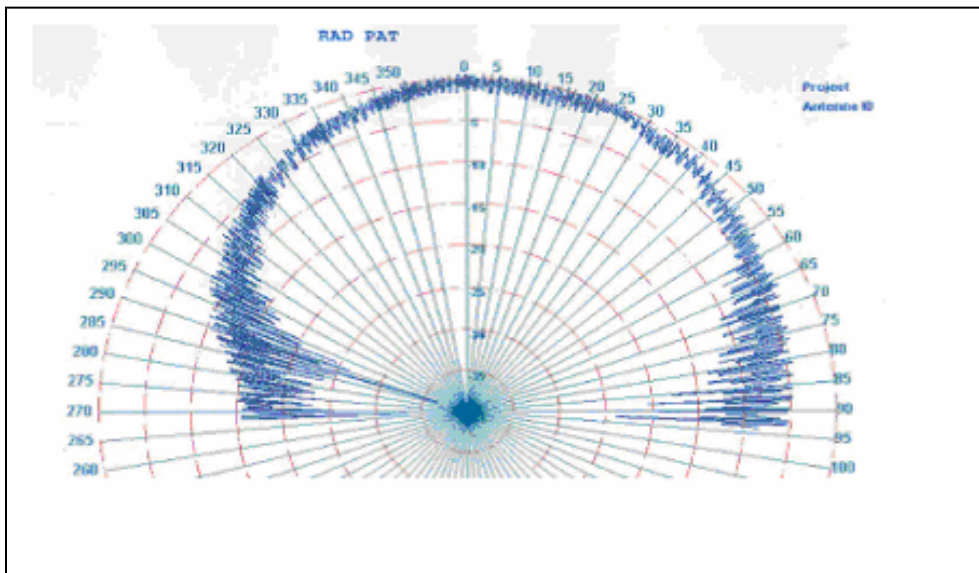


Fig. 6.28 Axial ratio of the helical antenna

6.4.5 Assembly and integration:

After testing the performance of various components such as the MMIC modules, beam steering electronics, power dividers and interconnect cables, the total system is integrated as detailed here. The 16 outputs of the power divider assembly are assembled to 16 channel phase shifter amplifier assemblies. 64 near equi-phase cables are connected to the 64 outputs of the assembly. In the integrated array, calibration was carried out for both amplitude and phase. The power output of the MMIC amplifiers were adjusted to 20 dBm using fixed attenuators in the power divider amplifier assembly interface.

After calibrating all 64 outputs, look up table for phases is generated and PROM of the beam steering electronics is fused and the package assembled with DC-DC converters (power supply) package. The RF assembly (power divider and amplifier assemblies) is stacked on the beam steering electronics package (Fig. 6.19). 64 outputs of the 16 amplifier assemblies are connected to the radiating elements on the dome and the dome assembly is fixed over the amplifier assemblies with proper supports. The radiating elements are covered with Quartz wool thermal blanket for protection from extreme cold and hot environments of the space. All tests on the integrated assembly as per quality assurance plan were conducted with the thermal blanket. Final phased array antenna is shown in Fig. 6.29.

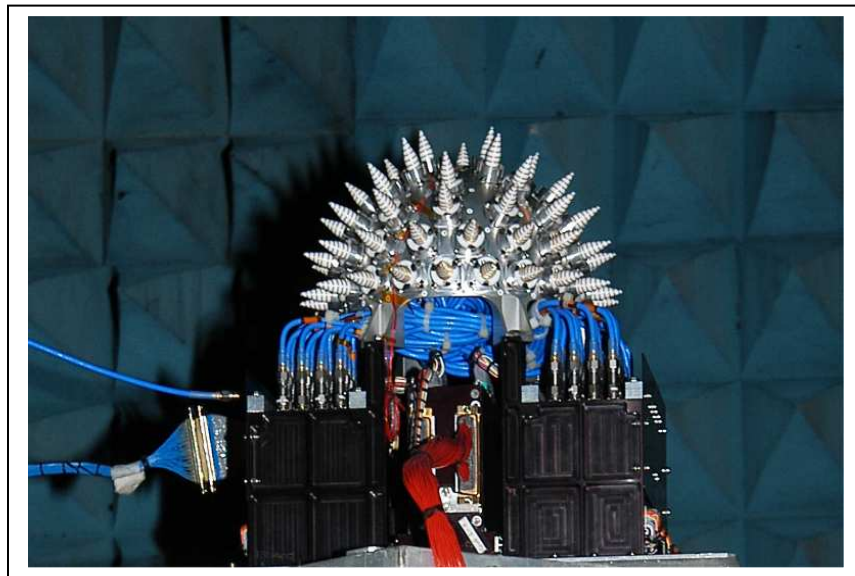


Fig. 6.29 Final Assembly of spherical X-band, 64 element phased array

6.4.6 Redundancy and Quality Assurance (QA) aspects:

Passive redundancy has been provided to driver amplifier. Out put of the selected Amplifier will be selected by a co-axial transfer switch. Passive redundancy is provided to beam steering electronics. Separate DC-DC converter is used to power beam steering electronics.

The 16 amplifier/phase shifter assemblies are powered by 8 DC/DC converters. Each converter will be powering 2 phase shifter/amplifier units. No additional redundancy is planned for phase shifter amplifier assemblies and radiating elements as failure of channels will cause only graceful degradation to EIRP. Failure analysis has been carried out to estimate the EIRP reduction due to elements failure. Failure of one DC/DC converter is taken for analysis as each converter failure affects four channels and there will not be radiation from four elements located spatially apart. Degradation of 0.7 to 1.0 dB (max) in EIRP is measured with the failure of any one converter.

6.4.7 Test philosophy:

The characterization of active phased array is planned in two phases.

- **Phase-1: Testing of modules**

In phase 1 the testing of all the elements like antenna elements, SSPA/Phase shifter modules, 1: 16 Power Divider, Driver Amplifiers, Control circuits etc. constituting the phased array are characterized as per the normal Test and Evaluation (T&E) plan before integrating all the units.

- **Phase-2 : Integrated testing of the active phased array**

On completion of phase 1 tests, the modules are assembled and further tests are conducted. As the array is used in 'transmit' mode in the actual application all the measurements are planned to be carried out in this mode in an Anechoic Chamber. The measurement set-up used is shown in Fig. 6.30. A static helix on the other end of the range receives the signal from phased array antenna. Signal is divided to two, one for the pattern measurement setup and the other to a spectrum analyzer for EIRP measurement.

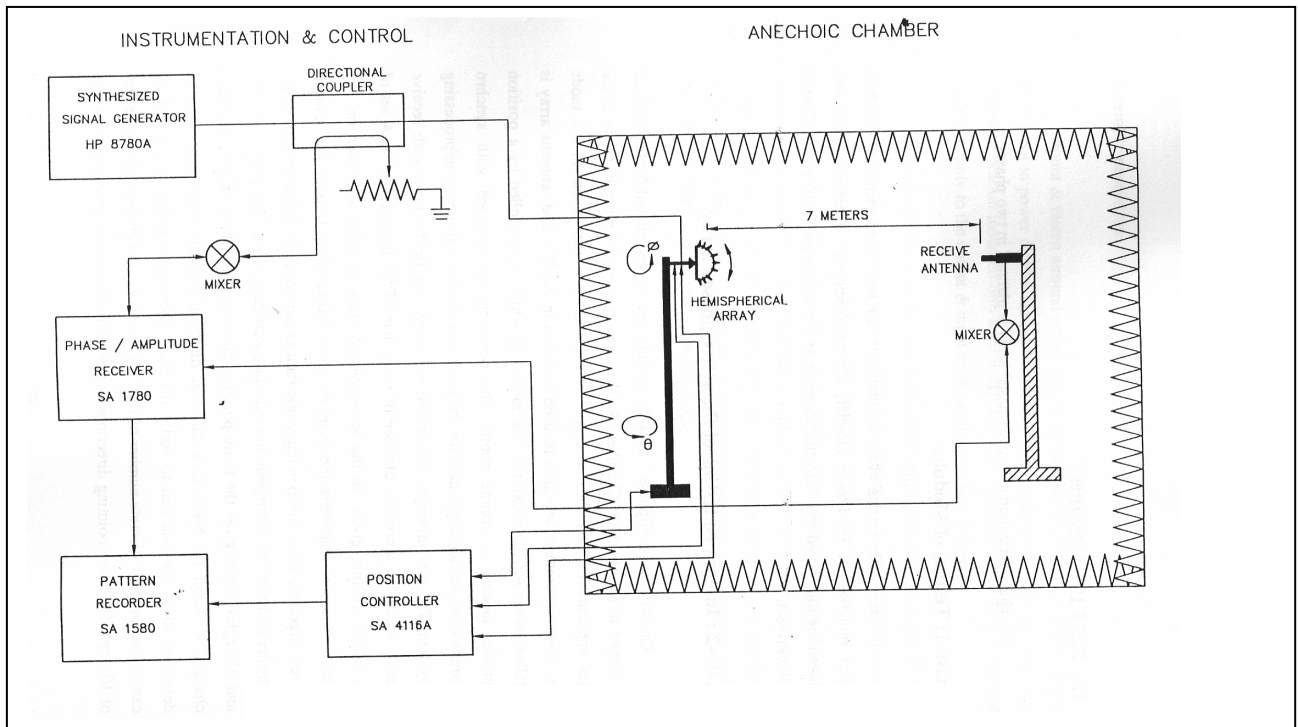


Fig. 6.30 Radiation measurement set up

PAA was tested in the anechoic chamber using the test console/ simulator for the following measurements.

- Single Beam characteristics
- EIRP
- Orbit simulation
- Radiation Pattern over bandwidth
- Effect of quartz wool thermal cover
- Effect of phase and amplifier switching on QPSK modulated signals

The antenna array is installed on an azimuth/elevation (Az/EI) positioner, the motion of which is controlled by a position controller located in control room. The positioner is equipped with synchro transmitters to provide angle data for the position indicator and recording/processing subsystem. The measurements are carried out using far field criteria with receive antenna located at a nominal distance of more than $2D^2/\lambda$ from the Array on

test. Fig 6.31 shows photograph of the spherical phased array under radiation test in anechoic chamber.

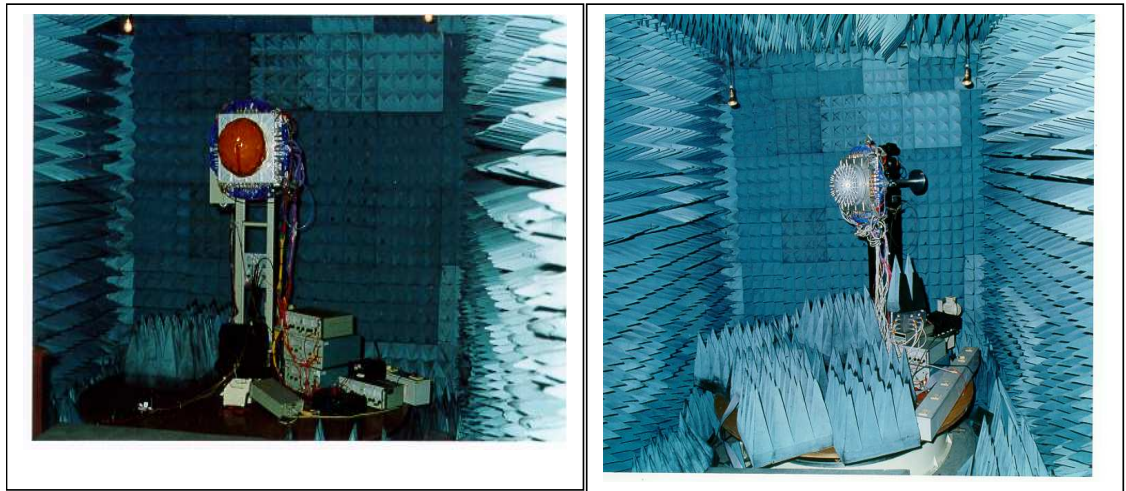


Fig. 6.31 Spherical phased array with and without Quartz wool blanket under radiation test in anechoic chamber

A set of bias values are first given to the active phased array in order to 'switch on' the required number of amplifiers and to set the phase shifter values to point the beam in a given direction. The corresponding angle data as per design is fed to the positioner controller to direct the beam peak towards the receiving antenna. The positioner Az and El angles values gives the beam pointing direction. The phase shifter control is changed to direct the beam to a different direction and the same procedure as described above are followed to verify the beam pointing direction. This check is carried out for a few discrete number of sets, say Az in steps of 20 deg and El in steps of 10 degs. The beam pointing directions as per measurement are compared with the expected ones (for given bias values) to validate the design of the antenna array.

The total beam characteristics for a particular beam direction are obtained by 3D radiation pattern measurements and EIRP values are obtained from the measured gain and power levels. The 3D radiation measurement results are in accordance with the simulation. Fig. 6.32 shows the radiation patterns obtained, at different beam directions over the hemisphere.

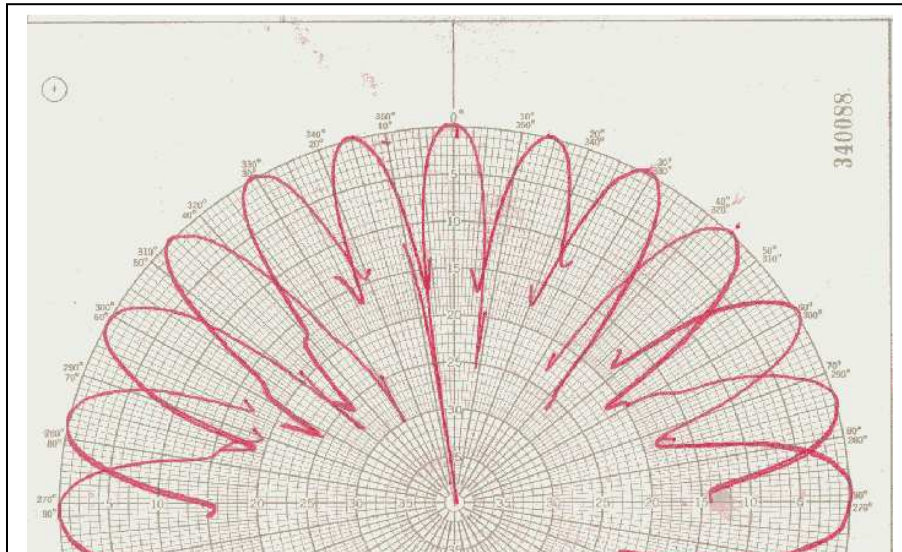


Fig. 6.32 Radiation patterns of single beam at different directions.

- Vibration test:** Total assembly was subjected for sine and random vibration test to the levels specified by Environmental test level specifications of Cartosat-2 satellite. Fig 6.33 shows the phased array on the vibration table. To ensure the integrity of the system, only DC supply is given and currents are observed during vibration test. Pre and post vibration tests were done in detail including radiation measurement. No degradation in performance is observed due to vibration test.

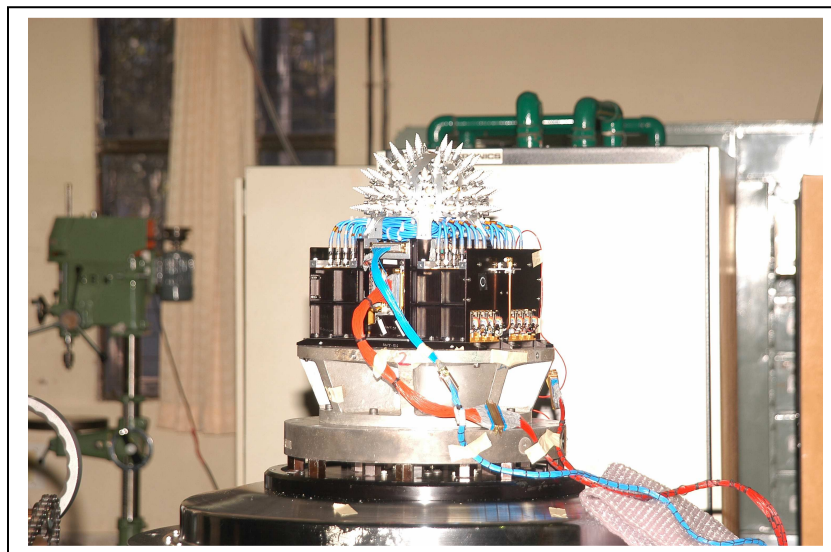


Fig. 6.33 Phased Array on Vibration Table

- **Thermovacuum test:** Active thermovacuum test conducted to evaluate end-to-end performance of the phased array. A special fixture (Fig.6.34) with pickup probes fixed in 16 directions about the phased array antenna reference axis is used. Beams were generated along one of the pickup probe directions. Signals from all pickup probes are measured and confirmed that the beams are generated in the intended direction. Measurement was carried out twice in long cold soak and twice in long hot soak. Fig 6.35 shows loading of phased array mounted on special fixture into 4 meter thermovacuum chamber.

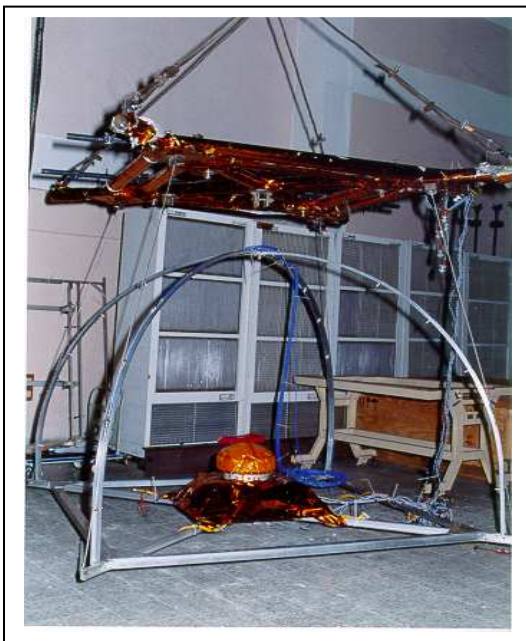


Fig. 6.34 Phased array mounted in a special fixture with receiving probes mounted in different directions.

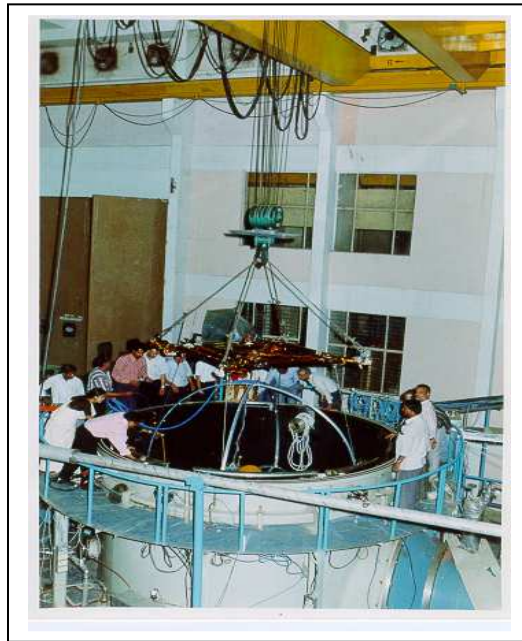


Fig. 6.35 Phased array being loaded into thermovacuum chamber

- **Orbit simulation:** The beam pointing locations as per mission requirements for satellite passes in high elevation, low elevation and nominal are also validated by giving the appropriate bias signals, aligning the beam peak to the receive antenna and noting the change in the Az and El angles. This is done mainly to gain confidence in the system.

Programmable positioner was moved as per the orbital data for 210 seconds and simultaneously phased array is commanded to generate the corresponding beam directions. The received signal was continuously logged at 1 sec interval and EIRP during orbit was estimated. Fig. 6.36 shows the EIRP measured along with elevation and azimuth angles for a typical orbit of 210 seconds simulated for Hyderabad(Shadnagar) ground station.

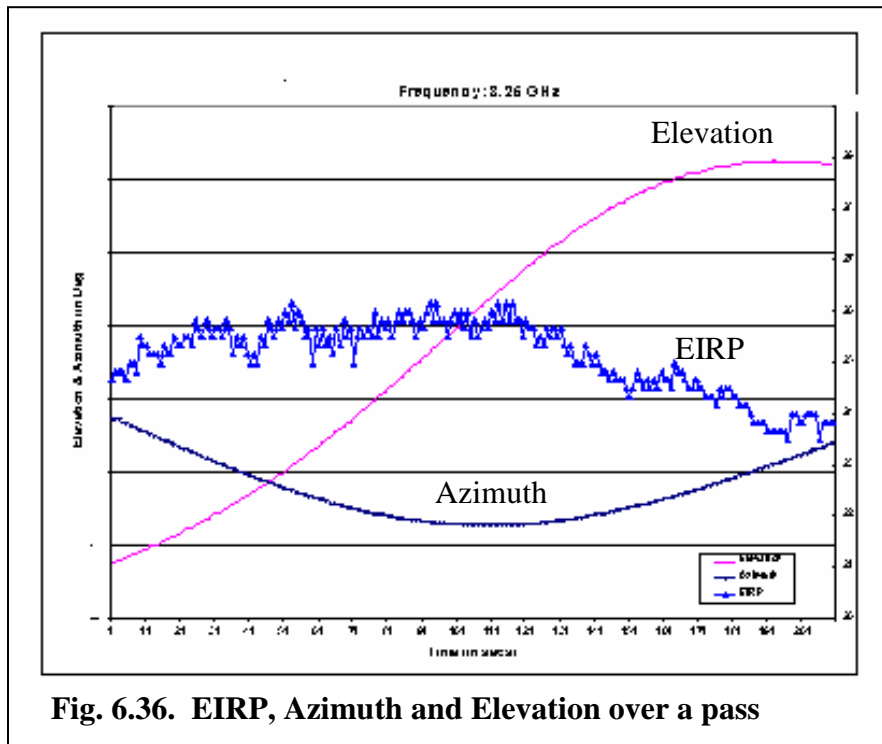


Fig. 6.36. EIRP, Azimuth and Elevation over a pass

- Effect on QPSK modulation:** QPSK modulation is accomplished by switching the carrier phase in accordance with the data levels. Any phase and amplitude errors induced in the modulated carrier will affect the performance. Since beam steering in Phased array is accomplished by switching various amplifier units and by switching the phase of the carrier in different channels, the effect of switching the carrier through phase shifters and amplifiers on the QPSK modulated carrier are tested. The radiation test is repeated by replacing the signal generator with the actual X-band QPSK transmitter and BER

measurement carried out to assess the impact of phase switching in channel amplifiers on the performance of QPSK modulation. No BER degradation was noticed in the representative pass simulations corresponding to high elevation, low elevation and normal orbit passes. This measurement confirmed that the phase switching and channel amplifier inclusion and exclusion during a pass has no effect on far field radiation pattern. In orbit performance also confirmed this aspect.

- **Effect of Quarz wool blanket on the radiators:** The EIRP measurement was carried out with and without Quartz wool blanket (Fig.6.31). EIRP degradation of about 0.1 dB only could be observed which is negligible.
- **Performance over full bandwidth:** The phased array is used to transmit two carriers; each is modulated with 105 MBPS data. This practically occupies full bandwidth. The response of the phased array over the full beam width is important as unequal radiation causes spectrum distortion and causes performance degradation. The radiation test repeated by transmitting different frequency carriers to characterize the performance of the phased array. Fig.6.37 shows radiation characteristics measured at different frequencies covering full X-band band width by simulating a typical orbit period. maximum imbalance of 1 dB is seen over the frequency band. This can not be reduced. The degradation due to this unequal transmission of the spectrum causes little degradation which need to be taken care by sufficient margin.

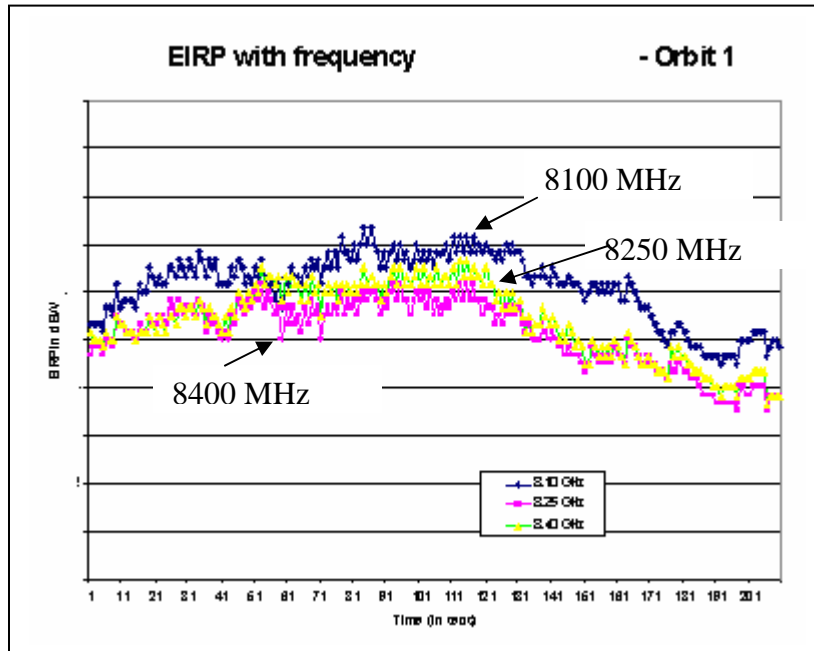


Fig. 6.37 EIRP with frequency over a typical visible orbit

- **Pre launch Test:**

The Phased Array after integration onto the spacecraft is tested in radiation mode with RF absorber panels surrounding the spacecraft. The beams generated by choosing different bias states are checked with the fixture used for thermovacuum test. Beam directions are commanded through spacecraft telecommand system and beam generation in the required directions are verified. This test is mainly to verify all the interfaces viz., power, telemetry, telecommand and AOCE system onboard the spacecraft.

Measured results:

Weight : 12.5 Kgs.

Total DC power : 60 watts.

EIRP : +19 dBW minimum

Beam width: +/- 8° (0n axis) to +/-10° (at +/- 65° from on axis)

- **In orbit Test:**

- (i) Fig. 6.38 shows the recorded spectrum of the signal received from Cartosat-2A.
- (ii) continuous recording the AGC of the receiver (Fig. 6.39) which is calibrated to incoming signal strength in the ground station during various typical passes of the satellite.
- (iii) Pre-positioning the Ground Station antenna beam and monitoring the same at the expected time. Expected signal strength recorded through out pass confirming the tracking predictions.

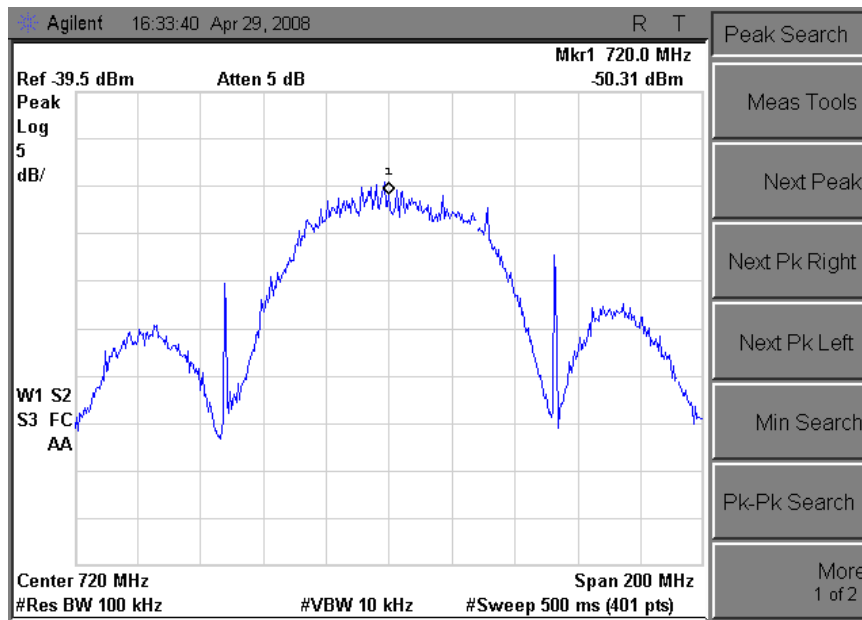


Fig. 6.38 Recorded spectrum of the signal received from Cartosat-2A

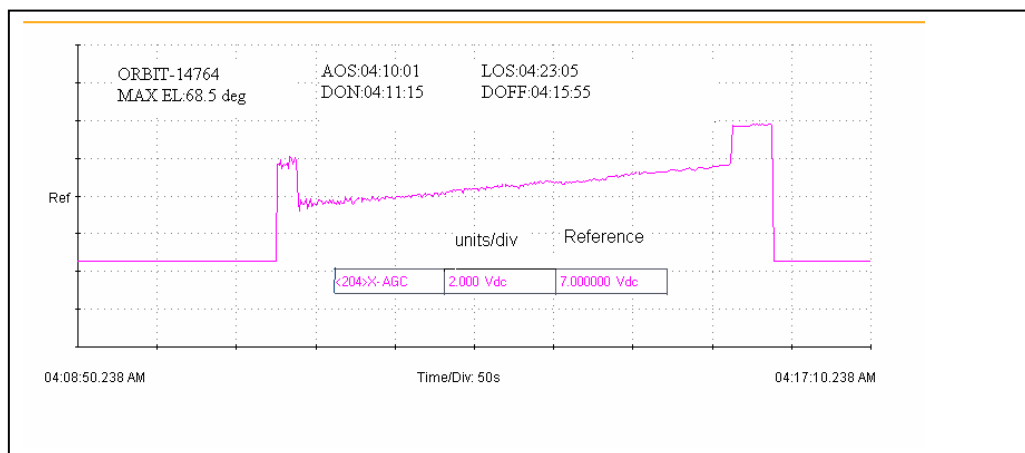


Fig. 6.39. AGC plot indicating signal strength of Cartosat -2 over a typical pass.

- **Multi carriers transmission:**

Multiple carrier transmission becomes mandatory from spacecraft due to various constraints and for easy realization of data handling systems. Multi carrier transmission, particularly with QPSK modulated carriers, becomes a challenge for the system designers. Effect of transmission of multiple carriers through active spherical phased array are investigated. Radiation test repeated by transmitting two QPSK modulated carriers of 8125 and 8300 MHz simultaneously. BER test was conducted on each carrier with and with out second carrier. BER degradation of 0.5 to 0.6 dB was noticed in the presence of second carrier. This corresponds to the IM products generated by Phase shifter amplifiers. Channel amplifiers are operated to give 20 dBm output which corresponds to 1 dB compression. At this operating point IM products measured on the channel amplifiers is about -25 dBc. Estimated degradation due to this level matches with the measured BER degradation.

6.5 Summary:

High gain antennas developed for onboard Cartosat-2 satellite are described. Configuration of spherical phased array along with design concepts are explained. A new Spherical phased array developed with a technique to reduce onboard power consumption and weight is presented along with test results. The system is flown onboard Cartosat-2/A satellite and the performance is quite satisfactory.

6.6 Dual beam generation - concept:

The phased array developed to generate single steerable beam with new technique of sharing MMIC amplifier with four radiating elements, explained above, has resulted in optimum configuration with respect to weight and onboard power consumption. This phased array is flown onboard Cartosat-2/2A satellites along with mechanically steered planar phased array antenna as back up. IRS data reception stations are situated at Shadnagar (Hyderabad) and Delhi and some missions, like Resourcesat and Cartosat-1 series of IRS satellites, require transmission of the imagery data at 210 MBPS rate to the two stations simultaneously. For both the stations viz., Delhi and Hyderabad to receive the data, two steerable beams with +22 dBw EIRP are to be generated (Fig.6.40). A possible concept to generate two beams to enable the reception of satellite data transmission at any two predefined stations is described here.

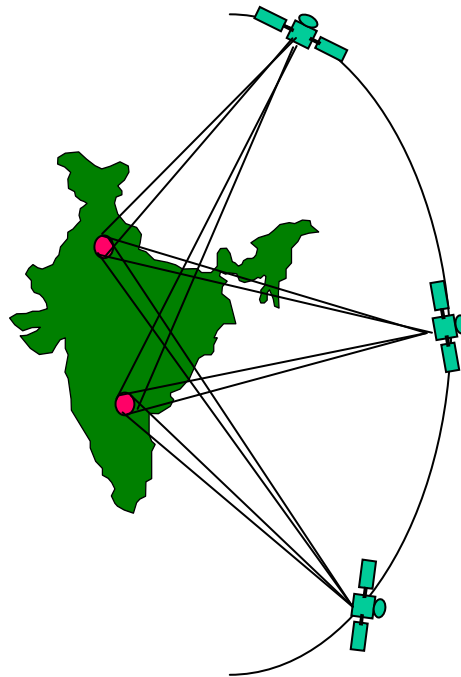


Fig. 6.40 Dual beams from satellite in LEO orbit

It is found by simulation that 96 elements mounted in 7 bands at 12,24,36,48,60,78,90 degrees with respect to vertical axis with 3,5,10,15,18,22,23 elements in corresponding bands on an hemisphere are needed for generating two beams with the required EIRP. With the above element distribution, various hemisphere sizes and cone angles are considered and simulated the radiation pattern as explained earlier in section 6.3 for single beam generation with 96 elements.

The Directivity of 96 element hemispherical array is computed for semi cone angle of 60° and shown in Fig. 6.41

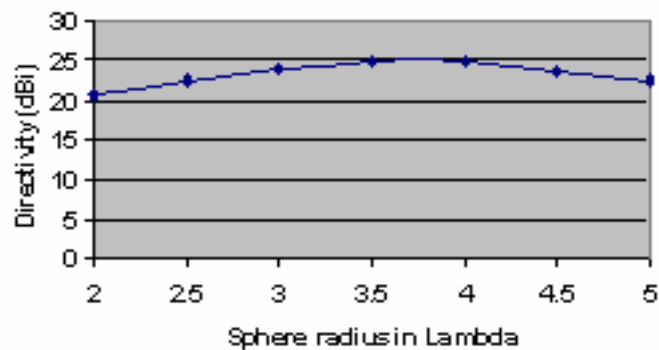


Fig.6.41 Directivity versus hemisphere radius (in Lambda)

Hemisphere with 3.5λ radius is the best trade off with respect to the directivity, radiation pattern and grating/side lobe levels. Simulated radiation patterns for different cone angles of the hemispherical array of 3.5λ and the results are given in Table 6.11.

Table 6.11. Directivity versus semi cone angle - simulation results

Semi Cone angle (deg.)	No. of elements	Directivity (dBi)	Side lobe level w.r.t. main lobe. (- dB)
15	4	15.2	9
30	10	19.1	10
45	20	21.7	16
60	56	24.9	20
75	76	25.4	18
90	96	25.4	18

Simulation results indicate that the excitation of radiating elements, on 3.5λ radius hemisphere, in 60° semi cone angle provides optimum performance.

when separation between the two beam directions is less than one cone angle, it is found that there are elements common to both the beams (Fig. 6.42) that need to be assigned two phase values viz. ρ_{n1} (phase of n^{th} element) for beam direction 1 and ρ_{n2} (phase of n^{th} element) for the second beam. As there is only one phase shifter provided per each element, there can only be one phase value that can be assigned. Therefore the dual phase assignment ambiguity needs to be resolved. It is important to note that the resolved phase should result in the proper beam formation in the two desired beam directions and the minimum EIRP requirement should also be met.

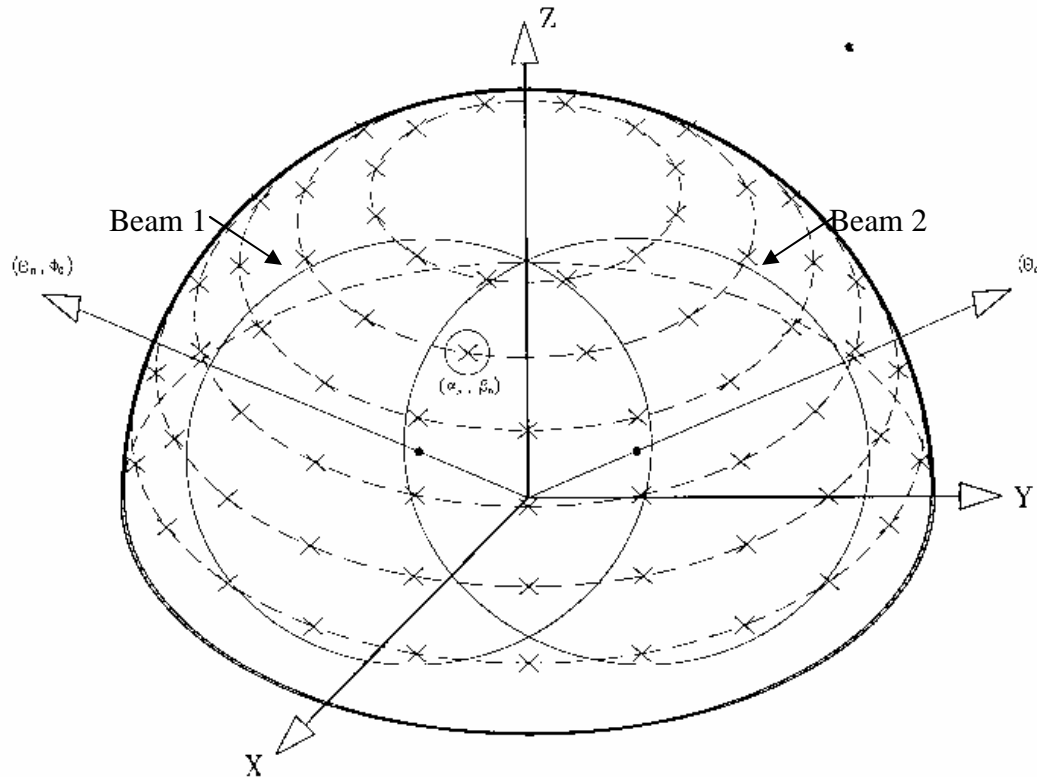


Fig. 6.42 Hemi sphere showing common elements of two beams

Initially, average values of the two phases are assigned to the common elements. The phase for a common element n is given as

$$\rho_n = (\rho_{n1} + \rho_{n2})/2 \quad \text{--- (40)}$$

Spherical array analysis was carried out for many combinations of the two beam directions and preliminary results indicated that the gain requirements are not met in many directions. Hence a weighting factor was introduced for the two-phase values and the analysis was performed for various weighting coefficients.

$$\rho_n = (w_1 * \rho_{n1} + w_2 * \rho_{n2})/2 \quad \text{--- 41)}$$

To start with w_1 and w_2 are assigned 0.5 and detailed analysis was carried out for a given beam direction by generating the second beam at various azimuth and elevation angles in 5° intervals. The zones where the EIRP specifications are not met are identified and the weighting factors are modified only in this region to improve the EIRP. There remained still some combinations where the mission requirements could not be met. To overcome this, the reference phase of the signal exciting radiating elements is considered as a variable. A combined analysis where the weighting factors (w_1 , w_2) and reference phases are changed is carried out and EIRP is estimated. Identifying the various regions for different sets of weighting factors and reference phase, fine-tuning of w_1 and w_2 in these regions were carried out and this resulted in meeting EIRP requirement over nearly 95% of the beam combinations.

The simulated contours are shown in Fig. 6.43. Top figure shows two beams widely separated and the second figure shows when the two beams are very closely separated.

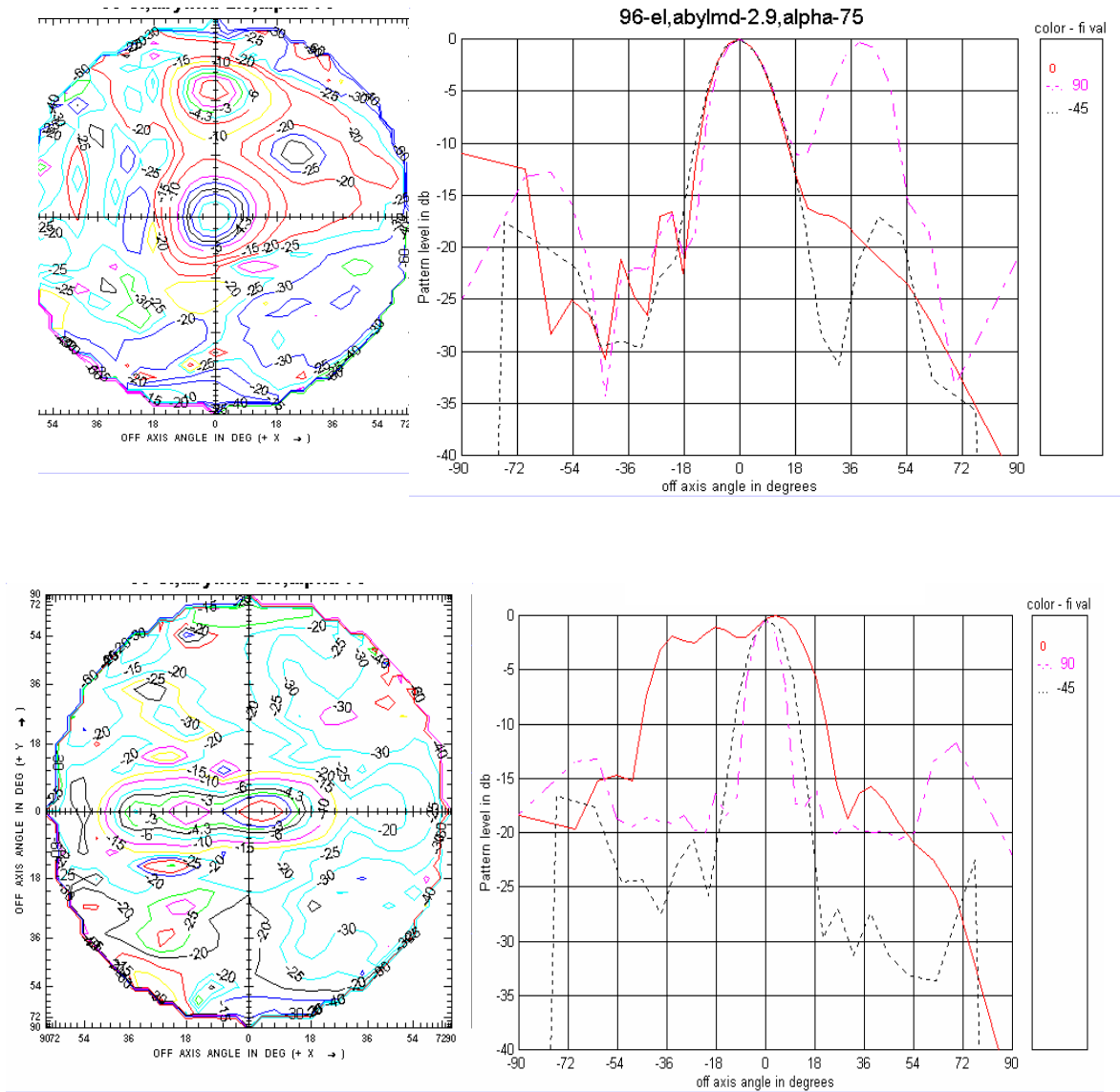


Fig. 6.43 Simulated contours of two beams

It is found that when separation of the beams is above half power beam width, two distinct beams are formed. As beams separation reduces, a single beam is formed (Fig. 6.40).

Fig. 6.44 shows a configuration for an active spherical phased array to generate two steerable beams.

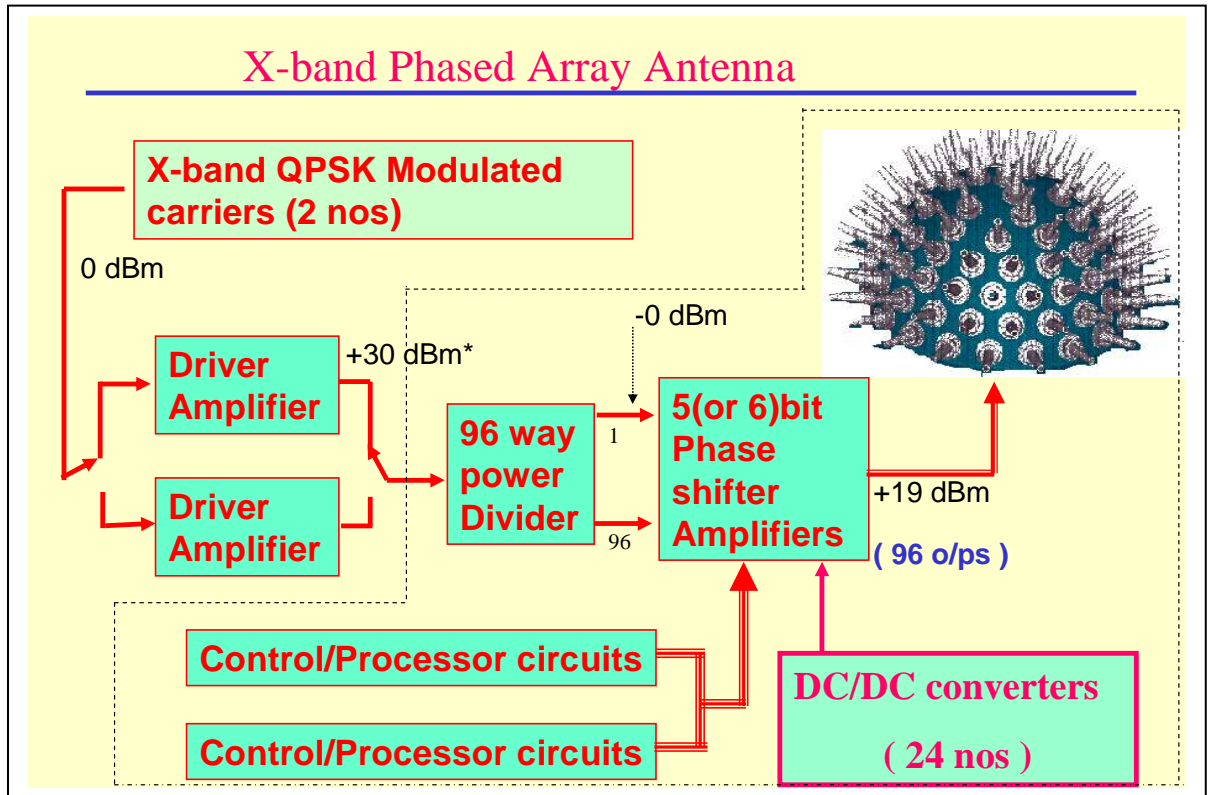


Fig. 6.44 Schematic block diagram of spherical active phased array antenna generating dual beams.

The above concept can be extended to generate more number of independently steerable beams.

Chapter 7

Summary, outcome of the present work and Specific contributions

7.1 Summary and outcome of the work:

The basic requirements for effective transmission of high bit rate data from remote sensing satellites are studied and appropriate techniques worked out for meeting the increasing demand for higher rate data transmission. The effects of various parameters that affect the basic high bit rate communication link are studied. Answers are provided to the questions that arose periodically with high bit rate data transmission from the Indian Remote Sensing (IRS) satellites launched so far. The problems reported with the performance of data transmitting system on orbit and during check out operations of IRS satellites are taken as case studies. Causes for link performance degradation are identified and possible mitigation techniques are suggested. The parameters which cause performance degradation and are beyond control of the system designers are also identified. The effect of these parameters is to be compensated by providing appropriate margin in the link budget.

Indian Remote Sensing satellites generally configured with shaped beam antennas to facilitate iso-flux signal reception on ground. The shaped radiation pattern does not always compensate path loss perfectly. Due to satellite body effects, which are usually beyond designer's control, true iso-flux antennas could not be realized. Considerable variation in the signal strength received at ground station is observed in quite a few missions. In addition, shaped beam antennas are associated with the following important problems:

1. Signal is radiated over very wide area (about +/- 65degrees cone) from satellite. This is not acceptable always, particularly for transmitting surveillance/ sensitive imagery data.

2. Necessitates the use of high power amplifiers like TWTAs, due to associated lower antenna gain, which requires careful handling of power and thermal issues.
3. Does not support frequency reuse due to poor cross polarization isolation property.
4. Beam width is not adequate to support agile satellites having Step and Stare control and requiring tilting of the satellite to enhance imaging area.

To overcome all these issues, a novel active spherical phased array antenna system has been considered. The design concepts, trade offs, simulation results are presented. A new phased array design / configuration is realized by developing an innovative technique of sharing the power of amplifier/phase shifter between four radiating elements for optimum utilization of the power. The phased array is developed and qualified for space use and flown onboard Cartosat-2/2A Satellites. The performance is quite satisfactory and provided confidence to fly similar phased array systems onboard future Cartosat/IRS series satellites.

The basic design of the phased array is extended to generate two simultaneous beams which can be steered independently for transmitting the X-band QPSK modulated signals to two ground stations simultaneously. The issues involved in generating two beams in a spherical phased array, mainly sharing the radiating elements which are common to two beams is addressed to have optimum performance.

All the studies and research/development activities are published in leading journals and presented in conferences (Refer Publications/presentations of the author).

Successful demonstration of the phased array has led to the development of :

1. Use of single beam phased arrays for all Cartosat satellites meant for strategic applications.
2. Development of spherical phased array to generate radiating beam steerable over full sphere for Astrosat mission.
3. Development of spherical phased array to transmit in dual polarization to increase data transmitting capacity in RISAT mission.
4. The development of multi beam multi panel phased array antenna for tracking MEOSAR (Middle Earth Orbit Search and Rescue system) satellites for search and rescue operations. This state of the art design is proposed to replace the conventional system with about six independent reflector antennas being followed by international space agencies.

7.2 Specific contributions

1. Studied data transmitting configurations:
Various factors and configurations for high bit rate data transmitting systems are studied and best suitable configuration for IRS Satellites recommended for implementation on Satellites.
2. Critically examined space to earth links:
 - a. Studied link analysis and identified various parameters that effect link performance.
 - b. Identified correctable and non correctable degradations.
 - c. Analyzed the problems reported from Indian Remote Sensing satellites in connection with data transmission systems and suggested possible mitigation techniques to take care of the problems in future missions.

3. Carried out the design, simulation, realization and testing of X-band spherical active phased array antenna systems.
 - a. Provided solution to many issues coming out of shaped beam iso-flux antennas.
 - b. Design tradeoff based on simulation and testing discussed.
 - c. Graceful performance degradation due to failure of active components is estimated.
4. Carried out optimization in terms of power, weight and size. The system developed with optimization technique of sharing active elements between radiating elements, is qualified and flown onboard Cartosat -2/2A Satellites. The performance is quite satisfactory. Based on the satisfactory performance, the phased array is slated for use in all future Cartosat series satellites.
5. Based on the successful development of single beam phased array antenna system, the design is extended to the development of spherical phased array to generate two beams for transmitting the data to two ground stations simultaneously. by developing new techniques for sharing radiating elements.
6. Identified the scope for further research and development in data transmitting systems for remote sensing satellites.

Chapter 8

Scope for further studies:

Based on the present work, the author feels that there exists ample scope for further studies to be carried out by researchers in the field.

Some of these areas are:

1. Higher order Phase Shift Keying modulation techniques to increase data rate throughput in the limited band width needs to be developed for future missions.
2. Data rate can be increased further by transmitting in dual polarization. Generating dual polarized radiating beams is a challenge for designing spherical active phased array, hence needs further study.
3. Another problem associated with spherical phased array is the generation of unwanted radiation due to spurious and side lobes in the radiation patterns. This needs further investigation.
4. Various issues affecting the performance of the QPSK modulated carriers transmitted in spherical array with dual polarization can be studied for cross talk effects.
5. Since the system is for onboard spacecraft use, reduction of size and weight is very important. The active unit modules containing MMIC Amplifiers, Phase shifters can be integrated with radiating elements. Effects of the reduction of size on thermal and electrical performance can be studied.
6. EIRP of the radiating beam can be reduced to take the advantage of path loss variation in a visible pass. Optimum distribution of elements and/or changing the drive levels to radiating elements dynamically can be studied and implemented.
7. Missions like Astrosat needs steering of the transmitting beam over full sphere. There is scope to carry out detailed study and development to meet this requirement.

8. Based on the concept explained for dual beam generation, more analysis and work can be carried out further to realize a space qualified system and conduct more experiments to study various effects on the beams.
9. The spherical phased array concept can be extended to track multiple satellites simultaneously for Telemetry, Tracking and Command (TT&C) purpose. To meet this requirement, the phased array needs to be realized with Transmit and Receive (TR) modules. This concept can be further studied and developed.
10. In place of spherical phased array, depending upon the orbital geometry & payload requirements, even conical or cylindrical phased arrays show a promise which could be studied in detail.
11. Multi panel arrays mounted on a spherical surface can be used for receiving signals from multiple satellites like the cluster of satellites in Middle Earth Orbit (MEO) for supporting Search and Rescue (SAR) system. This calls for tracking a satellite with multiple panel arrays with smooth change over between the beams of adjacent panels to provide continuous tracking of a satellite. Sharing of panels for receiving data from multiple satellites is an involved development. This needs detailed study.

Chapter 9

References

- [1] Krieger F.J. Announcement of the First Satellite-Behind the Sputniks, Pravada, October 5, 1957, (Washington, DC: Public Affairs Press, 1958), pp. 311-312. Source: Historical Reference Collection, NASA History Division, NASA Headquarters, Washington, D.C.
- [2] Data Sheet, Department of Astronautics, National Air and Space Museum, Smithsonian Institution. Source: <http://www.jpl.nasa.gov/explorer/>
- [3] The explorer programme.
Source: http://news.eoportal.org/didyouknow/041203_explorer.html
- [4] Estes J.E., Hemphill J.J. U.S. Government land remote sensing program and coordinated operations of Landsat 5 and &, IEEE International symposium 2001 on Geoscience and Remote Sensing, IGARSS-01. Volume3, Issue 2001, pp 1475-1477.
- [5] Mowle E.W., Dennehy C.J. The Landsat-6 satellite: an overview. IEEE Aerospace and Electronics Systems Magazine, 1991, June, Volume 6, Issue6, pp.18-23.
- [6] JPL Publication information.
Source: <http://southport.jpl.nasa.gov/scienceapps/seasat.html>.
- [7] The Almaz programme. Source: <http://www.russianspaceweb.com/almaz.html>
- [8] CNES Programmes. Source: <http://www.cnes.fr/web/CNES-en/1415-spot.php>.
- [9] Duchossois G., Honvault C. The First ESA Remote Sensing Satellite (ERS) – The Programme and the System., OCEANS, 1981, September, Volume 13, pp.1014-1018.
- [10] Mohr J.J., Madsen, S.N. Geometric calibration of ERS satellite SAR images, IEEE Transactions on Geoscience and Remote Sensing, 2000, April, Volume 39, Issue 4, pp. 842 – 850.
- [11] Attema E.P.W., Duchossois G., Kohlhammer G. ERS-1/2 SAR land applications: overview and main results, Proceedings of IEEE International Symposium on Geoscience and Remote Sensing, IGARSS '98. 1998, Volume 4, pp. 1796-1798.
- [12] Igarashi T. Overview of NASDA's earth observation remote sensing, Advances in Space Research, 2002, June, Volume 29, Issue 11, pp. 1619-1624.

- [13] Ouchi K., Mitsuyasu H. Applications of JERS-1 SAR data to the determination of the directional spectra of ocean waves using weighted cross-spectra, Proceedings of IEEE International Symposium 1999 on Geoscience and Remote Sensing, IGARSS '99. 1999, Volume 2, pp. 1004-1006.
- [14] Kiyoshi Tsuchiya, Kohei Arai, Tamotsu Igarashi. Present status and future plans of the Japanese earth observation satellite program. Advances in Space Research, 1989, Volume 9, Issue 1, pp. 217-224.
- [15] Yukio Haruyama. Progress of Japan's earth observation satellites. Advances in Space Research, 1994, January, Volume 14, Issue 1, pp 21-24.
- [16] Yong Xue, Yingjie Li, Jie Guang, Jianping Guo, Xiaoye Zhang. Small satellite remote sensing and applications-history, current and future. International Journal of Remote Sensing archive, 2008, August, Volume 29, Issue 15, pp. 4339-4372.
- [17] Jianxiang Chen. Weigen Huang; Jingsong Yang. Satellite remote sensing of the oceanic environment in China. Proceedings of IEEE International Symposium on Geoscience and Remote Sensing. 2005, July, Volume 2, pp. 1018 – 1020.
- [18] Xingling Wang, Gang Wang, Yan Guan, Quan Chen, Lianru Gao. Small satellite constellation for disaster monitoring in China. Proceedings of IEEE International Symposium on Geoscience and Remote Sensing. 2005, July, Volume 1, pp. 25-29.
- [19] Radarsat Data Overview. Source: <http://nsidc.org/data/radarsat/index.html>
- [20] Chandrasekhar M.G. Remote Sensing Applications Scenario in India for IRS 1A to 1C. Journal of Spacecraft Technology, 1995, July, Volume 5, No.2, pp 1-15.
- [21] Kalyanaraman S., Rajangam R.K. IRS-1C Spacecraft Configuration, Technology and Realization aspects. Journal of Spacecraft Technology, 1995, July, Volume 5, No. 2, pp 16-28.
- [22] IRS-P4 (Oceansat). Source: <http://www.csre.iitb.ac.in/isro/irs-p4.html>.
- [23] IRS Earth Observation Satellites.
Source: <http://www.isro.org/satellites/earthobservationsatellites.aspx>.
- [24] Chandrayaan-1, India's lunar space craft to Map the Moon.
Source: <http://www.chandrayaan-1.com/>.
- [25] Goswami J. N., Annadurai M. Chandrayaan-1: India's first planetary science mission to the moon. Current Science. 2009, February, Volume 96, No. 4, pp. 486-491.

- [26] ISRO-CNES Megha-Tropiques weather satellite.
Source: <http://knol.google.com/k/vijainder-k-thakur/isro-cnes-megha-tropiques-weather/yo54fmdhy2mq/9#>.
- [27] ASTROSAT-An “Indian Multi wavelength Astronomy Satellite, Source: <http://meghnad.iucaa.ernet.in/~astrosat/>.
- [28] Nasta, Rodolphe, Tonello, Emile. Method of high and low bit rate transmission on the command link of a satellite. United States Patent 6829310, 12/07/2004.
- [29] Nagura R. Optimum data transmission and imaging method for high resolution imaging from Earth observation satellite. IEEE Workshop on Advances in Techniques for Analysis of Remotely Sensed Data, 2003, 2003, October 27-28, pp.163 – 172.
- [30] Froehlich F.E., Hirsch D., Rudy H.R. High-speed digital data transmission over the Telstar satellite. Proceedings of the IEEE. 1963, April, Volume 51, Issue 4, pp. 609 – 609.
- [31] Antonini M., De Luise A., Ruggieri M., Teotino D. Satellite data collection & forwarding systems. IEEE Aerospace and Electronic Systems Magazine. 2005, September, Volume 20, Issue 9, pp. 25 – 29.
- [32] Young-Wan Kim, Yun-Jeong Song, Nae-Soo Kim, Dong-Chul Park. Performance analysis of channel impairment in high data rate satellite communication service. Proceedings of the IEEE International Microwave and Optoelectronics Conference, 2001. Volume 1, pp. 47-50.
- [33] Sooyoung Kim, Sungmoon Yeo, Kota S. ITU-R Standardization of Digital Performance for Fixed Satellite Services. International Symposium on Information Technology Convergence. 2007, November 23-24, pp. 363 – 367.
- [34] Thomas A. Milligan. Modern Antenna Design. IEEE Press. Wiley Inter Science. 2nd Edition. 2005.
- [35] Simon Haykin. Digital Communications. John Wiley & Sons, 2000.
- [36] Simon Haykin. An introduction to Analog and Digital Communications. Wiley-India, 2007.
- [37] Timothy Pratt, Charles Bostian, Jeremy Allnut. Satellite Communications, Second Edition. Wiley – India. 2007.

- [38] Maral G, Bousquet M. *Satellite Communication Systems – Systems, Techniques and Technology*. John Wiley & Sons. Second Edition. 1993.
- [39] Spilker J.J. *Digital Communications*, Prentice-Hall Inc., Englewood Cliffs, NJ, 1977.
- [40] Dr. Kamilo Feher, *Digital Communications Satellite/Earth Station Engineering*, Prentice-Hall Inc., Englewood Cliffs, NJ, 1981.
- [41] Wilbur L Pritchard, Jenri G Suyderhoud, Robert A. Nelson. *Satellite Communication Systems Engineering*, Pearson Education, 2nd Edition, 2003.
- [42] John A Tague, Lisa M Shimoda., Precision waveform shaping and precompensation for high data rate space communications systems. *International Journal of Satellite Communications and Networking*. 2007, March 22, Volume 12, Issue 2, pp. 157 – 166.
- [43] Lam A.C.C., Elkhazin A., Pasupathy S., Plataniotis K.N. Pulse shaping for differential offset-QPSK. *IEEE Transactions on Communications*, 2006, October, Volume 54, Issue 10, pp. 1731 – 1734.
- [44] Kim J. Bit by bit error rate performance of land mobile satellite system(LMSS) under fading channel using QPSK/MSK. *Military Communications Conference – MILCOM 89*. 1989, October 15-18, Volume3. pp. 715 – 719.
- [45] Tellambura C., Mueller A.J, Bhargava V.K. BER and outage probability for land mobile satellite channel with maximal ratio combining. *Electronics Letters*. 1995, April 13, Volume 31, Issue 8, pp. 606 – 608.
- [46] Daniel Cygan. Analytical evaluation of average bit error rate for the land mobile satellite channel. *International Journal of Satellite Communications and Networking*. 2006, December 19, Volume 7, Issue 2, pp. 99 – 102.
- [47] Cossu M., Lapos, Abbate M., Lupi A., Pattacini U., Venditti P. Non ideal behaviour of TXA equipment: Simulated BER performance. *IEEE International Geoscience and Remote Sensing Symposium-IGARSS 2007*. 2007, July 23-28, pp. 2951 – 2954.
- [48] Geran iotis E., Gerakoulis D. Bit error rate evaluation of a spectrally efficient CDMA scheme for geostationary satellite communications. *Proceedings of .IEEE Symposium on Computers and Communications, ISCC 2000, France*. 2000, pp. 254-258.

- [49] Sasada T., Shirakura, Yajima M.M. A feasibility study of adaptive modulation techniques for small satellite communications. Proceedings of The 4S Symposium: Small Satellites, Systems and Services (ESA SP-571). La Rochelle, France. 2004, September 20 – 24.
- [50] 2nd TDRSS Workshop, June 25-26, 1996., Sponsored by NASA Headquarters' Office of Space Communications and Goddard Space Flight Center's Mission Operations and Data Systems Directorate. GSFC Code 530. homepage at <http://www530.gsfc.nasa.gov/tdrss/tdrsshome.html>
- [51] Bricker P., Luecke J., Herr D. Integrated receiver for NASA tracking and data relay satellite system. IEEE Conference on Military Communications 1990. MILCOM 90, 1990, September 30-October 3, Volume1, pp. 1 – 5.
- [52] Osborne W., Wolcott T. Performance of trellis coded modulation with 8PSK through TDRSS. IEEE Conference on Military Communications 1993. MILCOM 93. 1993, October 11-14, Volume 3, pp. 963 – 967.
- [53] Lecureux Y. Optical sensors and data transmission. IEE Colloquium on Earth Resource Sensing and the Data Relay Satellite, 1990, March 30, pp. 3/1 – 315.
- [54] Cartier N., Oster J., Lesthievant G. High data rate 8PSK transmitter for X-band payload telemetry. European Radar Conference, EURAD 2005. 2005, October 6-7, pp. 93-96.
- [55] Lam A.C.C., Elkhazin A., Pasupathy S., Plataniotis K.N. Pulse shaping for differential offset-QPSK. IEEE Transactions on Communications, 2006, October. Volume 54, Issue 10, pp. 1731-1734.
- [56] Pal S., Sambasiva Rao V., Rajangam R.K. Data Handling Systems of Indian Remote Sensing satellites-IRS 1A & 1B. Journal of Spacecraft Technology. 1993, July, Volume 3, No. 2, pp. 16-24.
- [57] Suryanarayana Rao K. N., Nagraj S. R., Sambasiva Rao V., Nicholas L., Rajangam R.K., Pal S. Data handling System for IRS 1C. Journal of Spacecraft Technology. 1995, July, Volume 5, No. 2, pp.84-94.

- [58] Zhang Zhengguang, Ye Yunshang . (Chinese Acad. of Space Technol., Beijing, China) Design of shaped reflector antenna of low orbit satellites for data transmission. Proceedings of 6th International Symposium on Antennas, Propagation and EM Theory, 2003, October 28- November 1, pp.132- 136.
- [59] Lakshmeesha V.K., Nicholas L., Mahadevan V., Pal S. S-Band shaped beam antenna for Indian Remote Sensing Satellite. IEEE AP Symposium, Vancouver, Canada. 1985, June, pp. 629-632.
- [60] Charles C., Auen. Shaped Beam Antenna for Satellite Direct Readout Communications. IEEE AP Symposium; 1980, pp 101-104.
- [61] Kumar A., Highly shaped beam telemetry antenna for the ERS-1 satellite. Proceedings of IEEE, Montech; 1986: Conference on Antennas and communication. Montreal, Canada. 1986, October, IEEE Cat no. 0156-0.
- [62] Kumar A. Shaped beam antennas for RADARSAT. Proceedings of IEEE AP-MTT-S seventh annual Benjamin Franklin Symposium, Cherry Hill, N.J.1989, March, pp. 54-55.
- [63] Schlobohm B., Arndt F., Kless J., Renner T. Direct PO Design of Dual Offset Reflector Antennas with High Efficiency and for Sub reflector Beam Steering. Conf. Proceedings JINA, Nice, France. 1990, November, pp. 176-179.
- [64] Weerackody V., Gonzalez,L. Performance of Satellite Communications On The Move Systems in the Presence of Antenna Pointing Errors. IEEE Conference on Military Communications-. MILCOM 2006, Washington, DC. Pp. 1-7.
- [65] Rai E., Nishimoto S., Katada T., Watanabe H. Historical overview of phased array antennas for defense application in Japan. IEEE International Symposium on Phased Array Systems and Technology. 1996, October 15-18, pp. 217 – 221.
- [66] Katagi T., Chiba I. Review on recent phased array antenna technologies in Japan. IEEE International Symposium on Antennas and Propagation. 2000, July 16-21, Volume 2, pp. 570 – 573.
- [67] Vendik O.G., Yegorov Y.V. The first phased-array antennas in Russia: 1955-1960, IEEE Transactions on Antennas and Propagation. 2000, August, Volume 42, Issue 4, pp. 46 – 52.

- [68] Broas R.F.J., Sievenpiper D.F., Yablonovitch E. An application of high-impedance ground planes to phased array antennas. *IEEE Transactions on Antennas and Propagation*, 2005, April, Volume 53, Issue 4, pp. 1377 – 1381.
- [69] Kuwahara Y. Phased array antenna with temperature compensating capability. *IEEE International Symposium on Phased Array Systems and Technology*. 1996, October 15-18, pp. 21 – 26.
- [70] Fund D., Cable J., Cecil T. Time delayed directional beam quadrifilar helix phased array antenna. *IEEE International Symposium on Phased Array Systems and Technology*. 2003, October 14-17, pp. 306 – 311.
- [71] Lars Josefsson, Patrik Persson. *Conformal Array Antenna Theory and Design*, IEEE Press series, Wiley-Interscience, New York, 2006.
- [72] Staraj R., Cambiaggio E., Papiernik A. Infinite phased arrays of microstrip antennas with parasitic elements: application to bandwidth enhancement. *IEEE Transactions on Antennas and Propagation*. 1994, May, Volume 42, Issue 5, pp. 742 – 746.
- [73] Karmakar N.C., Bialkowski M.E., Padhi S.K. Microstrip circular phased array design and development using microwave antenna CAD tools. *IEEE Transactions on Antennas and Propagation*. 2002, July, Volume 50, Issue 7, pp. 944 – 953.
- [74] Young-Ho Suh, Kai Chang. A new Millimeter-wave printed dipole phased array antenna using microstrip-fed coplanar stripline tee junctions. *IEEE Transactions on Antennas and Propagation*. 2004, August, Volume 52, Issue 8, pp. 2019 – 2026.
- [75] Whicker L.R. Active phased array technology using coplanar packaging technology. *IEEE Transactions on Antennas and Propagation*. 1995, September, Volume 43, Issue 9, pp. 949 – 952.
- [76] Tahim R.S., Foshee J., Chang K. Multi-band phased array antennas for air-platforms. *IEEE International Symposium on Antennas and Propagation Society*. 2002, June 16-21, Volume 4, pp. 204 – 207.
- [77] Tong D.T.K., Wu M.C. Multiwavelength optically controlled phased-array antennas. *IEEE Transactions on Microwave Theory and Techniques*. 1998, January, Volume 46, Issue 1, pp. 108 – 115.

- [78] Ruey-Shi Chu, Kuan Min Lee, Wang A.T.S. Multiband phased-array antenna with interleaved tapered-elements and waveguide radiators. AP-S. Digest of Antennas and Propagation Society International Symposium.1996, July 21-26, Volume 3, pp.1616–1619.
- [79] Coirault R., Kriedte W. Multibeam generation at L-band - A phased-array approach. ESA Journal. 1980, Volume 4, no. 4, pp. 319-336.
- [80] Farzaneh S., Sebak A.R. A novel amplitude-phase weighting for analog microwave beamforming. IEEE Transactions on Antennas and Propagation. 2006, July, Volume 54, Issue 7, pp. 1997 – 2008.
- [81] Southall H.L., Simmers J.A., O'Donnell T.H. Direction finding in phased arrays with a neural network beamformer IEEE Transactions on Antennas and Propagation 1995, December, Volume 43, Issue 12, pp. 1369 - 1374.
- [82] Denno S., Ohira T. Modified constant modulus algorithm for digital signal processing adaptive antennas with microwave analog beamforming. IEEE Transactions on Antennas and Propagation. 2002, June, Volume 50, Issue 6, pp. 850 – 857.
- [83] Agrawal A.K., Williamson E.L., Ferrante J.G. Design criteria for wideband active phased array antennas. IEEE Symposium on Antennas and Propagation Society International. 1997, July 13-18, Volume 2, pp.714 – 717.
- [84] Yajima M., Hasegawa T. Beam Pointing Error of Wideband Planar Phased Array Antennas with Reduced True-Time-Delay Devices. IEEE International Conference on Communications. 2006, June, Volume 9, pp. 4161 – 4166.
- [85] Hara S., Irie U., Nakaya U., Toda T., Oishi A. Acceleration of beamforming speed for RF MEMS-implemented phased array antenna. IEEE Topical Conference on Wireless Communication Technology. 2003, October 15-17, pp. 400 – 401.
- [86] Morsink B.J., Werkhoven G.H.C. van, Tjihuis A.G. A Coupled Feed-Radiator-Frequency Selective Surface Model for the Next Generation Active Phased Array Systems. *Proceedings 25th ESA Antenna Workshop on Satellite Antenna Technology*; ESTEC, Noordwijk, The Netherlands. 2002, pp. 247-255.
- [87] Agrawal A.K., Holzman E.L. Beamformer architectures for active phased-array radar antennas. IEEE Transactions on Antennas and Propagation. 1999, March, Volume 47, Issue 3, pp. 432 – 442.

- [88] Shelley M.W., Kalatizadeh Y. High power, precision beamforming networks for radar phased arrays. IEE Colloquium on Active and Passive Components for Phased Array Systems, 1992, April 24, pp. 6/1 - 6/5.
- [89] Jespersen N.V., Herczfeld P.R. Optical techniques for reconfiguring microwave phased arrays. IEEE Transactions on Antennas and Propagation. 1990, July, Volume 38, Issue 7, pp. 1054 – 1058.
- [90] Ng W., Walston A.A., Tangonan G.L., Lee J.J., Newberg I.L., Bernstein N. The first demonstration of an optically steered microwave phased array antenna using true-time-delay. Journal of Lightwave Technology. 1991, September, Volume 9, Issue 9, pp.1124 – 1131.
- [91] Daryoush A.S., Saedi R., Samant N., Herczfeld P.R., Belaga M. Fiber optic fed C-band active phased array antennas. IEEE MTT-S International Microwave Symposium Digest. 1992, June 1-5, pp. 437 – 440.
- [92] Liu D., Charette D., Bergeron M., Karwacki H., Adams S., Kustas F., Farley K., Munson R. A 1-18 GHz photonicly-reconfigurable phased-array antenna. IEEE Proceedings of Aerospace Conference. 1998, March 21-28, Volume 3, pp.483 – 490.
- [93] Jespersen N.V., Herczfeld P.R. Optical techniques for reconfiguring microwave phased arrays. IEEE Transactions on Antennas and Propagation. 1990, July, Volume 38, Issue 7, pp. 1054 – 1058.
- [94] Tomasic B., Liu S. Phased Arrays for Ground Based Satellite Payload and Control Applications. USNC/IRSI Rsdio Science Meeting, Orlando, FL. 1999, July.
- [95] Wu T.K. Phased Array Antenna for Tracking and Communication with LEO Satellites, IEEE International Symposium on Phased Array Technology, Boston, MA, 1996, October.
- [96] Jamnejad V., Huang J., Cesarone R.J. A study of Phased Array Antennas for NASA's Deep Space Network. Proceedings of the 2001 Antenna Applications Symposium. 2001, September, Volume 11.
- [97] Schuss J.J., Upton J., Myers B., Sikina T., Rohwer A., Makridakas P., Francois R., Wardle L., Smith R. The IRIDIUM main mission antenna concept. IEEE Transactions on Antennas and Propagation. 1999, March, Volume 47, Issue 3, pp. 416 – 424.

- [98] Bharj S., Mershevskiy A., Oleski P., Tomasic B. Affordable Antenna Array for Multiple Satellite Links. Proceedings of the 2000 Antenna Applications Symposium, Allertan Park, Monticello IL, 2000, September, pp. 401-414.
- [99] Chen M., Riemer D.E., Rasmussen D.N., Wallace J.E., Redd H.J., Ettore R.C., Peterson D.B., Bostwick R.N., Miller G.E. A 20-GHz active receive phased array antenna for Navy surface ship satellite communications applications. IEEE International Symposium on Antennas and Propagation Society. 1999, July11-16, Volume 4, pp. 2310 – 2313.
- [100] Choi J.P., Chan V.W.S. Joint phased array antenna gain patterning and scheduling for satcom transmission. IEEE Military Communications Conference- MILCOM 2005. 2005, October 17-20, Volume 3, pp. 1380 – 1389.
- [101] Warshowsky J., Kulisan C., Vail D. 20 GHz phased array antenna for GEO satellite communications. MILCOM 2000. 21st Century Military Communications Conference Proceedings. 2000, October 22-25, Volume 2, pp. 1187 – 1191.
- [102] Kemerley R.T., Kiss S. Advanced technology for future space-based antennas. IEEE MTT-S International Microwave Symposium Digest., 2000 , June 11-16, Volume 2, pp. 717 - 720.
- [103] Urasaki S., Chiba I., Konishi Y., Yonezawa R., Iso A., Katagi T. Inclined GEO satellite communication system with deployable phased array antennas. IEEE International Symposium on Antennas and Propagation Society.1998, June 21-26,Volume 1, pp.24-29.
- [104] Bocon P., McGree T., Renfro J. Phased array performance characteristics and compliance with SATCOM military standards. IEEE Military Communications Conference. 2005, October 17-20, pp. 1712 – 1718.
- [105] Young Keun Yoon, Joung Myoun Kim. Grating lobe suppression of phased array antenna for mobile satellite communications, IEEE International Symposium on Antennas, Propagation and EM Theory. 2003, October 28-1 November 1, pp.222 – 224.
- [106] Kawaguchi Y., Nakagawa H., Tanaka S., Yamada T. Application of phased-array antenna technology to the 21 GHz broadcasting satellite for rain-attenuation compensation. IEEE International Conference on Communications-ICC 2002. 2002, April 28- May 2, Volume 5, pp. 2962 – 2966.

- [107] Wallis R.E., Sheng Cheng. Phased-array antenna system for the MESSENGER deep space mission. IEEE Proceedings of Aerospace Conference. 2001 March 10-17, Volume 1, pp. 1/41 - 1/49.
- [108] Soon Ik Jeon, Deock Gil Oh. Active phased array antenna for mobile multimedia services via satellite. IEEE Aerospace Conference Proceedings. 2000, March 18-25, Volume 5, pp. 165 – 170.
- [109] Reinhart R.C., Johnson S.K., Acosta R.J., Sands S. Phased array antenna-based system degradation at wide scan angles. IEEE International Symposium on Phased Array Systems and Technology. 2003, October 14-17, pp. 446 – 451.
- [110] Ho T.Q., Hewett C.A., Hunt L.N., Ready T.G. Lattice spacing effect on scan loss for bat-wing phased array antennas. IEEE/ACES International Conference on Wireless Communications and Applied Computational Electromagnetics. 2005, April 3-7, pp. 245 – 248.
- [111] Araki K., Tanaka A., Matsumura E. Wide scanning phased array antenna design in Ka band. IEE Proceedings on Microwaves, Antennas and Propagation. 2003, 10 October 10, Volume 150, Issue 5, pp. 379-384.
- [112] Boris Tomasic, John Turtle, Shiang Liu, Robert Schmied, Sarjit Bharj, Paul Oleski. The Geodesic dome phased array antenna for satellite control and communication-subarray design, development and demonstration. IEEE International Radar Conference. Arlington, Virginia, USA. 2005, May 9-12,
- [113] Sengupta D.L., Smith T.M., Larson R.W.. Radiation Characteristics of a Spherical Array of Circularly Polarized Elements. IEEE Transactipons on Antennas. and Propagation 1968, January, Volume AP-16, No.1, pp. 2-7.
- [114] Schwartzman L., Stangel J. The Dome Antenna. The Microwave Journal. 1975, October, pp.31-34.
- [115] Kinsey R. An Objective Comparison of the Dome Antenna and a Conventional Four-Face Planar Array. Antenna Application Symposium 2000, Allerton, IL, 2000, September.
- [116] Liebman P.M. Dome Radar- A New Phased Array System. Digest of IEEE International Radar Conference, Washington, D.C. 1975, April.

- [117] Schrank H.E. Basic Theoretical Aspects of Spherical Phased Arrays. Conformal Antenna Array. Design Handbook, Naval Air Systems Command, Editor R.C. Hansen, 1981, September, pp. 323-327.
- [118] Tomasic B., Turtle J., Shiang Liu, Schmier R., Bharj S., Oleski P. The geodesic dome phased array antenna for satellite control and communication - subarray design, development and demonstration. IEEE International Symposium on Phased Array Systems and Technology. 2003, October 14-17, pp. 411 – 416.
- [119] Tahim R.S., Foshee J., Chang K. Integrated multifrequency phased array antenna. IEEE International Symposium Antennas and Propagation Society. 2001, July 8-13, Volume 2, pp. 432 – 435.
- [120] Trunk G., Patel D. Optimal Number of Phased Array Faces for Horizon Surveillance. IEEE International Symposium on Phased Array Technology, Boston, MA. 1996, October.
- [121] Rhodes M., Lane A.A. Monolithic five-bit phase shifter for Artemis space application. IEE Colloquium on Active and Passive Components for Phased Array Systems. 1992, April 24, pp. 10/1 - 10/4.
- [122] McDonald G., Willson C. High power ferrite phase shifters for phased array radars. IEE Colloquium on Active and Passive Components for Phased Array Systems. 1992, April 24, pp.2/1 - 2/7.
- [123] Tae-Yeoul Yun, Kai Chang. A low-cost 8 to 26.5 GHz phased array antenna using a piezoelectric transducer controlled phase shifter. IEEE Transactions on Antennas and Propagation. 2001, September, Volume 49, Issue 9, pp. 1290 – 1298.
- [124] Miura A., Fujino Y., Taira S., Obara N., Tanaka M., Ojima T., Sakauchi K. S-Band Active Phased Array Antenna With Analog Phase Shifters Using Double-Balanced Mixers for Mobile SATCOM Vehicles. IEEE Transactions on Antennas and Propagation. 2005, August, Volume 53, Issue 8, Part 1, pp.2533 – 2541.
- [125] Norvell B.R., Hancock R.J., Pugh M.L., Theis S.W., viatkofsky J.K. Micro Electro Mechanical Switch (MEMS) Technology Applied to Electrically Scanned Arrays (ESA). Proc. Of the International Radar Symposium- IRS98, Munich, 1998, pp 867-875.

- [126] Uher J., Arndt F., and Bornemann J. Field Theory Design of Ferrite-Loaded Waveguide Nonreciprocal Phaseshifters with Multisection Ferrite or Dielectric Slab Impedance Transformers. *IEEE Transactions on Microwave Theory and Techniques*. 1987, June, Volume MTT-35, pp. 552-560.
- [127] Arndt F., Bornemann J., Vahldieck R. Design of Multisection Impedance-Matched Dielectric-Slab Filled Waveguide Phase Shifters. *IEEE Transactions on Microwave Theory and Techniques*. 1984, January, Volume MTT-32, pp. 34-39.
- [128] Hector C., Brunt J., Arnold J. T/R module MMIC components for spaceborne SAR. *IEE Colloquium on Active and Passive Components for Phased Array Systems*. 1992, April 24, pp.12/1 - 12/7.
- [129] van den Boogaart F.L.M., G.bij de Vaate J. Production results of a transmit/receive-MMIC chip set for a wide band active phased array radar at X-band. *Conf. Proc. MM92*, Brighton (UK). 1992, pp 138-143.
- [130] Wallis R.E., Bruzzi J.R., Malouf P.M. Testing of the MESSENGER spacecraft phased-array antenna. *IEEE Photonics Technology Letters*. 2005, February, Volume 47, Issue 1, pp. 204 – 209.
- [131] Pozar D.M. The active element pattern. *IEEE Transactions on Antennas and Propagation*. 1994, August, Volume 42, Issue 8, pp.1176 – 1178.
- [132] Chang W.C., Wunsch G.J., Schaubert D.H. Back-to-back measurement for characterization of phased-array antennas. *IEEE Transactions on Antennas and Propagation*. 2000, July, Volume 48, Issue 7, pp.1079 – 1085.
- [133] Kojima N., Shiramatsu K., Chiba I., Ebisui T., Kurihara N. Measurement and evaluation techniques for an airborne active phased array antenna. *IEEE International Symposium on Phased Array Systems and Technology*. 1996., October 15-18, pp. 231 – 236.
- [135] Sorace R. Phased array calibration. *IEEE Transactions on Antennas and Propagation*. 2001, April, Volume 49, Issue 4, pp.517 – 525.
- [136] Agrawal A., Jablon, A. A calibration technique for active phased array antennas. *IEEE International Symposium on Phased Array Systems and Technology*. 2003. October 14-17, pp. 223 – 228.

- [137] Aumann H.M., Fenn A.J., Willwerth F.G. Phased array antenna calibration and pattern prediction using mutual coupling measurements. *IEEE Transactions on Antennas and Propagation*. 1989, July, Volume 37, Issue 7, pp. 844 – 850.
- [138] Aumann H.M., Fenn A.J., Willwerth F.G. Phased array antenna calibration and pattern prediction using mutual coupling measurements. *IEEE Transactions on Antennas and Propagation*. 1989, July, Volume 37, Issue 7, pp.844 – 850.
- [139] Lier E., Cherrette A. An intermodulation suppression technique for transmit active phased array satellite antennas with multiple shaped beams. *IEEE Transactions on Antennas and Propagation*. 2005, May, Volume 53, Issue 5, pp. 1853 – 1858.
- [140] Ngamjanyaporn P., Phongcharoenpanich C., Akkaraekthalin P., Krairiksh M. Signal-to-interference ratio improvement by using a phased array antenna of switched-beam elements. *IEEE Transactions on Antennas and Propagation*. 2005, May, Volume 53, Issue 5, pp. 1819 – 1828.
- [141] Kaho T., Nakagawa T., Araki K., Horikawa K. Carrier power to intermodulation-distortion power-ratio-increasing technique in active phased-array antenna systems. *IEEE Transactions on Microwave Theory and Techniques*. 2002, December, Volume 50, Issue 12, pp. 2987 – 2994.
- [142] Kaho T., Nakagawa T., Araki K. Reduction of intermodulation distortion in active phased array antenna systems using a distortion controller. *IEEE MTT-S International Microwave Symposium Digest*. 2002, June 2-7, Volume 2, pp. 781 – 784.
- [143] Keizer W.P.M.N. PHASIM, a sophisticated phased array antenna software simulator implemented in MATLAB 5.2. *IEEE International Symposium on Antennas and Propagation*. 1999, July 11-16, Volume 4, pp.2508 – 2511.
- [144] Enneking, F. Arndt. Fast Spectral Domain Analysis of Large Finite Microstrip Patch Arrays. *AP-S Int. Antennas and Propagation Symp. Digest*, Orlando. 1999, July, pp. 2092-2095.
- [145] Leatherwood D.A., Corey L.E., Cotton R.B., Mitchell B.S. Time-domain properties of phased array antennas. *IEEE International Conference on Phased Array Systems and Technology*. 2000, May 21-25, pp. 25 – 28.

- [146] Mariottini F., Capolino F., Maci S., Felsen L.B. Asymptotic high-frequency Green's function for a large rectangular planar periodic phased array of dipoles with weakly tapered excitation in two dimensions. *IEEE Transactions on Antennas and Propagation*. 2005, February, Volume 53, Issue 2, pp.608 – 620.
- [147] Arndt F., Catina V., Brandt J. Fast hybrid CAD technique for the optimization of advanced waveguide components and aperture antennas. *Proceedings 22nd Annual Review of Progress in Applied Computational Electromagnetics (ACES)*, Miami, FL. 2006, March, pp. 192 - 197.
- [148] Arndt F., Wolff K. H., Bruenjes J., Heyen R., Siefken-Herrlich F., Bothmer W., Forgber E. Generalized Moment Method Analysis of Planar Reactively Loaded Rectangular Waveguide Arrays. *IEEE Transactions on Antennas Propagation*. 1989, March, Volume AP-37, pp. 329-338.
- [149] Fenn A.J. Evaluation of adaptive phased array antenna, far-field nulling performance in the near-field region. *IEEE Transactions on Antennas and Propagation*. 1990, February, Volume 38, Issue 2, pp. 173 – 185.
- [150] Subbaram H., Abend K. Interference suppression via orthogonal projections: a performance analysis. *IEEE Transactions on Antennas and Propagation*. 1993, September, Volume 41, Issue 9, pp.1187 – 1194.
- [151] McGrath D.T., Pyati V.P. Phased array antenna analysis with the hybrid finite element method. *IEEE Transactions on Antennas and Propagation*. 1994, December, Volume 42, Issue 12, pp. 1625 – 1630.
- [152] Bhattacharyya A.K. A numerical model for multilayered microstrip phased-array antennas. *IEEE Transactions on Antennas and Propagation*. 1996, October, Volume 44, Issue 10, pp. 1386 – 1393.
- [153] Povolotsky F.K., Sydorova T.P. Phase synthesis of antennas for a given radiation pattern in one plane using piecewise linear aperture phase distribution. *IEEE Transactions on Antennas and Propagation*. 1999, September, Volume 47, Issue 9, pp. 1449 – 1453.
- [154] Schippers H., Spalluto G., Vos G. Radiation analysis of conformal phased array antennas on distorted structures. *Twelfth International Conference on Antennas and Propagation*. 2003, March31-April 3, Volume 1, pp.160 – 163.

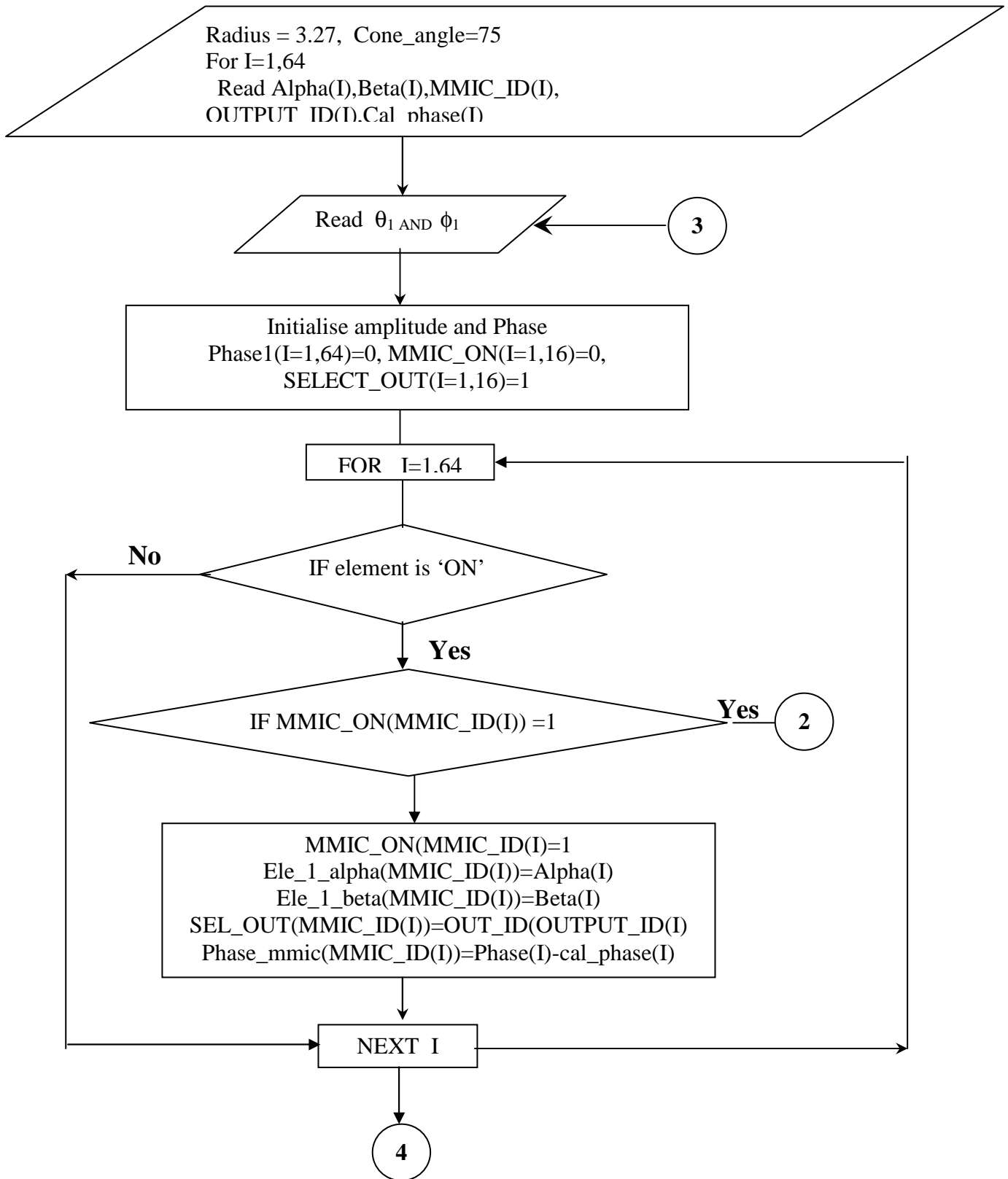
- [155] Turner G.M., Christodoulou C. FDTD analysis of phased array antennas. IEEE Transactions on Antennas and Propagation. 1999, April, Volume 47, Issue 4, pp. 661 – 667.
- [156] Whitehurst J., Holloway J.R. Modelling high power planar beamformers for phased arrays. IEE Colloquium on Active and Passive Components for Phased Array Systems. 1992, April 24, pp. 1-4.
- [157] Radio Regulations, International Telecommunication Union, Geneva.
- [158] Spectrum Requirements and Allocation Survey Report and Recommendations. NASA Crosslink Spectrum Report, pt. 1, version 1.0, 2002, June 5.
- [159] CCSDS Standards
- [160] Sacchi C., Musso M., Gera G., Regazzoni C., De Natale F.G.B., Jebiril A., Ruggieri M. An efficient carrier recovery scheme for high-bit-rate W-band satellite communication systems. IEEE Aerospace Conference, 2005, March 5-12, Volume , pp.1379 – 1390.
- [161] Understanding Satellite Link Budgets.
Source:<http://engr.nmsu.edu/~etti/spring97/communications/nsn/linkbudget.html>.
- [162] Bantin C., Lyons R. The Evaluation of Satellite Link Availability. IEEE Transactions on Communication. 1978, June, Volume26, Issue 6, pp.847-853.
- [163] Karim M. Effective Path Length for Terrestrial Microwave Links Prediction based on Rain Attenuation Measurements in Malaysia. M.Sc Thesis, Universiti Teknologi Malaysia, Malaysia, 2000.
- [164] Sidney Skjei. Using a Fishbone Diagram to Troubleshoot a Satellite Link. The Orbiter-The society of satellite Professionals international, 2005, April/May.
- [165] Dong You Choi. Rain attenuation prediction model by using the 1-hour rain rate without 1-minute rain rate conversion. International Journal of Computer Science and Network Security. 2006, March, Volume 6, No.3A, pp. 131-133.
- [166] Crane.R.K. Prediction of Attenuation by Rain. IEEE Transactions on Communication. 1980, Volume COM-28, No.9, pp.1717-1733.
- [167] Boris Grémont Dr. Simulation of Rainfield Attenuation for Satellite Communication Networks. 1st International Workshop, COST Action 280, 2002, July.

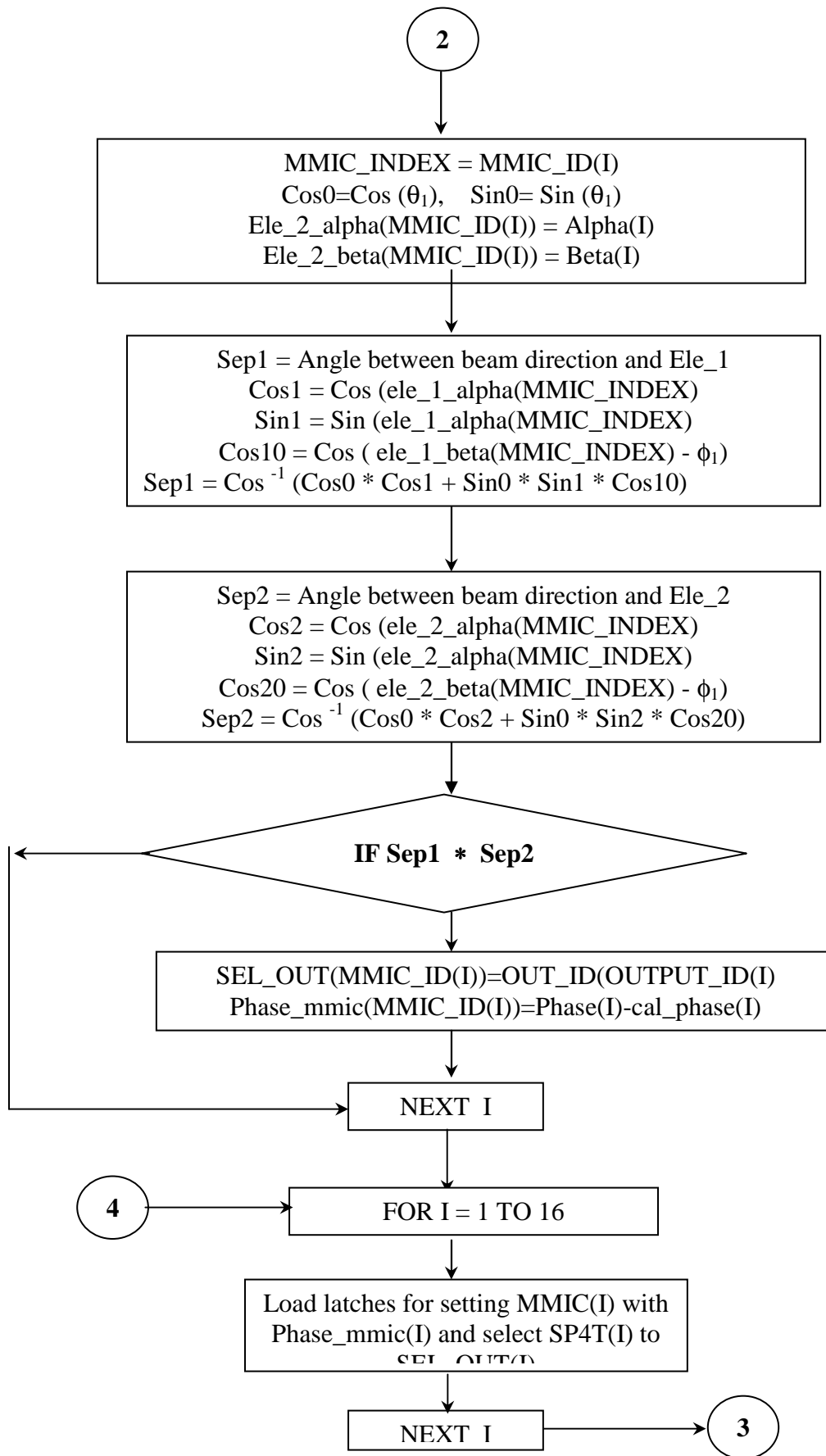
- [168] Panagopoulos A.D., Fikioris G., Kanellopoulos J.D. Rain attenuation power spectrum of slant path. *Electronics Letters*. 2002, September 26, Volume 38, Issue 20, pp.1220 – 1222.
- [169] Matricciani E. A relationship between phase delay and attenuation due to rain. *IEEE Workshop on International Satellite and Space Communications- IWSSC 2008*. Volume , 2008, October 1-3, Issue pp. 35 – 39.
- [170] Mandeep Singh Jit singh, Syed Idris Syed Hassan, Mohd Fodzil Ain. Rain fall attenuation and rain fall rate measurements in Malaysia comparison with prediction models, *American Journal of Applied Sciences*. 2007, January, pp 5-7.
- [171] Panagopoulos A.D., Arapoglou P.D.M., Kanellopoulos J.D., Cottis P.G. Long-term rain attenuation probability and site diversity gain prediction formulas. *IEEE Transactions on Antennas and Propagation*. 2005, July, Volume 53, Issue 7, pp.2307-2313.
- [172] Miller G. E., Rasmussen D. N. Measurement of the G/T of a 20-GHz active receive phased array antenna. *Antennas and Propagation Society International Symposium- 1994: AP-S Digest*. 1994, June 20-24, Volume 1, pp. 258 – 261.
- [173] Ohmaru K., Mikuni Y. Direct G/T Measurement for Satellite Broadcasting Receivers. *IEEE Transactions on Broadcasting*, 1984, June, Volume BC-30, Issue 2, pp 38-43.
- [174] Itoh Kiyohiko, Ogawa Yasutaka, Purwanto Yuliman. A Continuous G/T Measurement Technique for Satellite Broadcasting Receivers. *24th European Microwave Conference*. 1994, October, Volume 2, pp. 1876 – 1881.
- [175] Chen Hu, Yasutaka Ogawa, Kiyohiko Itoh. A study on a continuous measurement of G/T for satellite broadcasting antenna systems. *Electronics and Communications in Japan (Part I: Communications)*, 2001 January 16. Volume 84 Issue 5, pp 40 – 47.
- [176] Jezek K.C., Merry C., Cavalieri D., Grace J, Bedner S., Wilson D., Lampkin D. Comparison between SMMR and SSM/I passive microwave data collected over the Antarctic Ice Sheet. *Byrd Polar Research Center, The Ohio State university, Columbus, OH., BPRC Technical Report Number 91-03, ISSN: 1056-8050*.
- [177] IKONOS satellite. Source: <http://www.satimagingcorp.com/satellite-sensors/ikonos.html>
- [178] Krishnaswamy M. Sensors and Platforms for High Resolution Imaging for Large Scale Mapping Applications – Indian Scenario. *Indian Cartographer*, 2002 DAPI-01. Source: (www.incaindia.org/technicalpapers/02_DAPI01.pdf)

- [179] Naderi F., Freilich M. H., Long D. G. Spaceborne Radar Measurement of Wind Velocity Over the Ocean-An Overview of the NSCAT Scatterometer System. *Proceedings of the IEEE*, 1991, June, Volume 79, No. 6, pp. 850-866.
- [180] Tsai W.Y., Graf J.E., Winn C., Huddleston J.N., Dunbar S., Freilich M.H., Wentz F.J., Long D.G., Jones W.L. Postlaunch Sensor Verification and Calibration of the NASA Scatterometer. *IEEE Transactions on Geoscience and Remote Sensing*. 1999, Volume 37, No. 3, pp. 1517-1542.
- [181] Grantham W.L. The SeaSat-A Satellite Scatterometer. *IEEE Journal of Oceanic Engineering*. 1977, Volume OE-2, pp 200-206.
- [182] Attema E. The Active Microwave Instrument Onboard the ERS-1 Satellite. *Proceedings of the IEEE*. 1991 Volume 79, No.6, pp. 791-799.
- [183] Louis Cuccia C. QPSK System Performance and impairments, *The Handbook of Digital Communications*. Microwave System News. 1979, Volume9, pp. 87-93.
- [184] Rao U.R., Kasturirangan K., Sridhara Murhi K.R., Surendra Pal. *Perspectives in Communications*. World Scientific Publishing, 1987.
- [185] Sambasiva Rao V., D V Ramana D.V., Suvarna L., Bhaskaranarayana A., Pal S. X-band high bit rate QPSK Modulator. *IETE Technical Review*. 1993, July-August, Volume 10, No.4, pp.305-309.
- [186] Pitchaiah B., Sambasiva Rao V., Ramana D.V., Tomy Jon., Mishra R.M., Suvarna L., Parimalavalli V., Bhaskaranarayana A., Pal S. X-band Data Transmitters for Space Remote Sensing Missions. *IETE Technical Review*. 1994, March-June, Volume11, No.2&3, pp. 129-135.
- [187] Pal S., Sambasiva Rao V. TT&C and Data handling Systems for spacecrafts. *Telematics -93*, Bangalore. 1993, July, pp.28-30.
- [188] Sambasiva Rao V., et.al. QPSK Modulator in thick film at X-band. *RF Expo West*, Santa Clara, Calif.1991, February.
- [189] Krishnaswamy M., Kalyanaraman S. Indian Remote Sensing Satellite Cartosat-1: Technical features and data products. *The Geospatial Research Portal*, <http://www.gisdevelopment.net/technology/rs/techrs023.htm>.

- [190] Sambasiva Rao V., Pal S. Techniques for high bit rate data transmission from remote sensing satellites. IEEE-International Symposium on Microwaves (ISM-06), Bangalore, 2006, December 15-17.
- [191] Prateek Bansal, Shafali Tandon, Bindu K.R., Mishra R.M., Picjayya B., Sambasiva Rao V., Pal S. High bit rate Ka-band Data Transmission system for Satellite Application. Indicon 2007 & 16th Annual Symposium of IEEE Bangalore Section, Bangalore. 2007, September 6-8.
- [192] Sambasiva Rao V., Surendra Pal. A Unique Space to Earth Data Transmitting System. International Astronautical Congress – IAC 2007, Hyderabad. 2007, September 24-28.
- [193] Sambasiva Rao V., Surendra Pal. An insight into the factors affecting high bitrate data transmission from satellites to ground stations. BITS Curie Journal. 2008, July, Volume 1, No.2, pp33-40.
- [194] Sambasiva Rao V., Pal S. Study of implications of using a single TWTA for power amplification of two high bit rate data modulated carriers. IEEE-International Symposium on Microwaves (ISM-06), Bangalore, 2006, December 15-17.
- [195] Sambasiva Rao V., Ramana D.V., Surendra Pal. Some Experimentation on X-band Offset QPSK Modulator. IETE Technical Review, 1999, March-April, Volume 16, No.2, : 191-196.
- [196] Sambasiva Rao V., Surendra Pal. Spectral distortion in the high data rate remote sensing data links. High Frequency Electronics, May, 2008, pp 48-55.
- [197] Ramana D.V., Jolie R., V. S. Rao V.S., Pal S. A Satellite Telemetry Transmitting System with Pre-Modulation Filtering, High Frequency Electronics, 2008, November, pp42-47.
- [198] Sambasiva Rao V., Surendra Pal, High bit rate Data Transmitting system for Remote Sensing Satellites, High Frequency Electronics, April 2009, pp 18-26.
- [199] Pal S., Sambasiva Rao V. Spherical Phased Array Links Remote Sensors. Microwaves & RF. 2009, September.
- [200] Sambasiva Rao V., Srinivasan V.V., Surendra Pal. Generation of Dual Beams from Spherical Phased Array Antenna. Electronics letters-2009, April 23, Volume 45. Issue 9, pp. 441-442.

Flow chart for beam steering in spherical array (Cartosat-2A)
 (MMICs shared by 4 elements)





Annexure B

Determination of G/T by Richard Flagg, AH6NM ([rf @ hawaii.rr.com](mailto:rf@hawaii.rr.com))

G/T - A Receiving System Figure of Merit

The sensitivity of a radio telescope is a function of many factors including antenna gain (**G**) and system noise temperature (**T**). We all understand the need for high gain antennas and low noise preamplifiers. But how do we measure just how well the system is performing? A convenient figure of merit is the ratio (**G/T**) - the higher this ratio the better the sensitivity of the system to weak signals. To obtain G/T one could determine G and T separately, but these are difficult measurements. Fortunately it is relatively easy to obtain the ratio (G/T) by a single measurement (and a little arithmetic).

T - The Total System Noise Temperature

Before proceeding with the measurement of G/T let's discuss T in a little more detail. T is the total system noise temperature (in degrees Kelvin) and is equal to the sum of the noise generated in the receiving system (T_r) and the noise delivered from the antenna (T_a) when the antenna is looking at a region of the sky free of strong sources. T_a includes the galactic background temperature as well as additional noise picked up by the antenna sidelobes viewing the earth at ambient temperature.

The receiving system temperature (T_r) is related to the system noise factor (F_n) by:

$$T_r = (F_n - 1) * 290 \text{ (Equation 1)}$$

Where the noise factor (F_n) is simply the noise figure (NF) in dB expressed as a ratio:

$$F_n = (\text{Log}^{-1}) (NF / 10) \text{ (Equation 2)}$$

Determining G/T

The principle behind determination of G/T is to measure the increase in noise power which occurs when the antenna is pointed first at a region of cold sky and then moved to a strong source of known flux density - usually the sun.

This ratio of received power is known as the Y-factor.

$$Y = P_{\text{sun}} / P_{\text{cold sky}} \text{ (Equation 3)}$$

The following equation shows the relationship between G/T, the measured Y-factor, and the value of solar flux (F) at the observing frequency.

$$G/T = (Y - 1) * 8 * \pi * k * L / (F * \text{Lam}^2) \text{ (Equation 4)}$$

where:

- Y = sun noise rise expressed as a ratio (not dB)
- k = Boltzmann's constant $1.38 * 10^{-23}$ joules/deg K
- L = beamsize correction factor
- Lam = wavelength in meters (at the operating frequency fo)
- F = solar flux at fo in watts / meter² / Hz

Beamsize Correction (L)

The beamsize correction factor (L) is dependent upon antenna beamwidth. and approaches unity for small dishes with beamwidths larger than a few degrees. If your dish has a beamwidth larger than 2 or 3 degrees just set L=1 and forget about equation (5).

$$L = 1 + 0.38 (W_s / W_a)^2 \text{ (Equation 5)}$$

where:

- W_s = diameter of the radio sun in degrees at fo
- W_a = antenna 3 dB beamwidth at fo

The diameter of the radio sun (W_s) is frequency dependent. Assume a value of 0.5 degrees for frequencies above 3000 MHz, 0.6 degrees for 1420 MHz, and 0.7 degrees for 400 MHz.

Solar Flux Density (F)

The next term which we need to discuss is (F) - the solar flux density at the test frequency. The USAF Space Command runs a worldwide solar radio monitoring network with stations in Massachusetts, Hawaii, Australia, and Italy. These stations measure solar flux density at 245, 410, 610, 1415, 2695, 4995, 8800, and 15400 MHz. If you are lucky enough to be operating near one of these eight "standard" frequencies then all you have to do is use the reported flux density. However if you are operating - say midway - between two given frequencies then you will need to interpolate between flux densities at the lower and higher frequencies. The best interpolation scheme is to graph the flux density at several frequencies and use a curve fitting routine to determine the flux density at your operating frequency.

The solar flux density obtained from the USAF must be multiplied by 10^{-22} in order to get the units correct for use in equation (4). In other words, if the 1415 MHz solar flux density is 98 $* 10^{-22}$ watts/meter²/Hz, the operator may simply state "the solar flux at 1415 Mhz is 98".

The solar flux at 2800 MHz (10.7 cm) is measured at the Dominion Radio Astronomy Observatory in Canada. This flux should only be used for G/T calculations if you are operating at or near 2,800 MHz.

G/T Sample Calculation

Assume that you have measured a sun noise rise of 9 dB using your 1420 MHz radio telescope. The solar flux density at the test frequency of 1415 MHz is reported to be 98.

First convert the sun noise rise in dB to a power ratio:

$$Y = \text{Log-1}(\text{dB increase}/10) = \text{Log}^{-1}(9/10) = 7.94$$

Determine the other factors:

$$\begin{aligned} f_0 &= 1420 \text{ MHz, so} \\ \text{Lam} &= (300/1420) = 0.211\text{m} \\ \text{and Lam}^2 &= 0.045 \text{ m}^2 \\ \mathbf{F} &= \mathbf{98 * 10^{-22} \text{ w/m}^2/\text{Hz}} \end{aligned}$$

$L = 1$ (since you know that your 3 meter dish has a beamwidth of about 5 degrees)

and finally solving for G/T:

$$\begin{aligned} \mathbf{G/T} &= \mathbf{(Y-1)*8*\pi*k*L / (F*Lam^2)} \\ &= \mathbf{((7.94-1)*8**3.14*1.38*10^{-23}) / (98*10^{-22}*0.045)} \\ \mathbf{G/T} &= \mathbf{5.5} \end{aligned}$$

or expressed in dB:

$$\mathbf{G/T (dB) = 10 \text{ Log}(G/T) = 10\text{Log}(5.5) = 7.4 \text{ dB}}$$

Great - the G/T is 7.4 dB - so what? Should you be walking around with a silly grin - or slinking around looking for a rock to hide under? Well, for one thing this number is a reference point by which to judge the value of any future modifications to the system. To put it in perspective lets do the calculation in reverse and estimate what values of G/T and Y are expected given an antenna size (gain) and preamp noise temperature.

Assume that your 3 meter dish with an efficiency of 50% has a calculated gain of 30 dBi (power ratio of 1000) and that your preamp is advertised to have a noise temperature of 45 degrees K. Further assumptions include 10 deg K due to the galactic background, 25 deg K due to spillover, 30 deg K due to 0.5 dB of attenuation between the feed and the preamp and 5 deg K due to the receiver and cable following the preamp. Therefore the total receiving system temperature is estimated to be:

$$\mathbf{T = 45 + 25 + 30 + 10 + 5 = 115 \text{ deg K.}}$$

The expected value of G/T is therefore $(1000/115) = 8.7 = 9.4 \text{ dB}$

By the way, we can do this calculation by converting temperature into dB referenced to 1 deg K. and leaving the dish gain in dBi. Our temperature expressed in this way is

$$T \text{ dB} = 10 \text{ Log} (115/1) = 20.6$$

And G/T in dB is simply (30dB - 20.6dB) = 9.4 dB

So the expected value of G/T was 9.4 dB but we measured 7.4 dB. Why? A number of factors could be responsible, but the effect has been to either lower the dish gain or raise the system temperature from what was assumed. Its time to make sure the feed is focused and free of bird nests, and that no unexpected losses exist in the receiving system.

One final calculation shows what value of Y is expected given assumptions about antenna gain and system temperature.

Rewriting equation (4) and solving for Y yields:

$$Y = ((G/T)(F*\text{Lam}^2)/(8*\text{pi}*k*L)) + 1 \text{ (Equation 6)}$$

Remember to enter G/T as the ratio - not in dB.

$$Y = 12.1, \text{ or expressed in dB, } Y = 10.8 \text{ dB}$$

If our system was working exactly as expected a sun noise rise of 10.8 dB would have been measured - corresponding to a calculated G/T of 9.4 dB.

Measuring Y

The determination of G/T is completely dependent on an accurate measurement of Y. Perhaps the easiest measurement technique is to use a power meter (or a true RMS voltmeter) connected to the receiver IF . For this measurement to work the receiver must be operating in a linear region. If the receiver saturates when the antenna is pointed to the sun you are going to measure a dissappointing Y factor and spend lots of time trying to fix something that isn't broken. Of course the receiver AGC should be turned off. The Y factor is simply the change in meter reading on and off the sun. The accuracy of this method is dependent on the linearity of both the power meter and the receiver.

A better technique is to use a precision adjustable RF attenuator located between the preamp and the receiver. An RF power meter is connected to the receiver IF. Set the attenuator to 0 dB when the antenna is looking at the cold sky and adjust the receiver gain to get a convenient reference level on the power meter. Point the dish at the sun and crank in attenuation until the power meter once again reads the cold sky reference level. The Y factor is equal to the amount of attenuation needed to return the meter reading to the reference. This technique could also be used by measuring the DC output voltage from the receiver detector if a power meter is not available. Accuracy of the attenuator method depends on calibration of the attenuator - not receiver and power meter linearity.

Whatever technique you use - measure Y several times and take an average. The average of five measurements is probably adequate. Try and use solar flux measurements obtained about the same time your measurements were made for the calculation of G/T.

Where to get the Solar Flux

As mentioned earlier - the USAF operates a worldwide solar flux monitoring network. These data are disseminated thru NOAA's Space Environment Center - Space Weather Operations group in Boulder, Colorado (303 497-3171). The Space Environment Center also distributes the solar flux data for all eight frequencies via the world wide web. Set your browser to:

<gopher://solar.sec.noaa.gov/00/latest/curind>

The 2,800 MHz flux from Canada is available at:

<http://www.drao.nrc.ca/icarus/www/current/current.flx>

The Learmonth, Australia eight frequency data may be found at:

<http://www.ips.oz.au/Main.php?CatID=5&SecID=3&SecName=Learmonth%20Observatory&SubSecID=4&SubSecName=Radio%20Flux&LinkName=Quiet%20Solar>

And finally - for the most recent 45 days of solar flux measurements, see:

http://www.sec.noaa.gov/ftplib/lists/radio/45day_rad.txt

Origin: Publications Department, The SETI League,

Annexure C

Rec. ITU-R P.838-3

1

RECOMMENDATION ITU-R P.838-3

Specific attenuation model for rain for use in prediction methods

(Question ITU-R 201/3)

(1992-1999-2003-2005)

The ITU Radiocommunication Assembly,

considering

a) that there is a need to calculate the attenuation due to rain from a knowledge of rain rates,

recommends

1 that the following procedure be used.

The specific attenuation γ_R (dB/km) is obtained from the rain rate R (mm/h) using the power-law relationship:

$$\gamma_R = kR^\alpha \quad (1)$$

Values for the coefficients k and α are determined as functions of frequency, f (GHz), in the range from 1 to 1 000 GHz, from the following equations, which have been developed from curve-fitting to power-law coefficients derived from scattering calculations:

$$\log_{10} k = \sum_{j=1}^4 a_j \exp \left[- \left(\frac{\log_{10} f - b_j}{c_j} \right)^2 \right] + m_k \log_{10} f + c_k \quad (2)$$

$$\alpha = \sum_{j=1}^5 a_j \exp \left[- \left(\frac{\log_{10} f - b_j}{c_j} \right)^2 \right] + m_\alpha \log_{10} f + c_\alpha \quad (3)$$

where:

f : frequency (GHz)

k : either k_H or k_V

α : either α_H or α_V .

Values for the constants for the coefficient k_H for horizontal polarization are given in Table 1 and for the coefficient k_V for vertical polarization in Table 2. Table 3 gives the values for the constants for the coefficient α_H for horizontal polarization, and Table 4 gives the values for the constants for the coefficient α_V for vertical polarization.

Rec. ITU-R P.838-3

TABLE 1
Coefficients for k_H

j	a_j	b_j	c_j	m_k	c_k
1	-5.33980	-0.10008	1.13098	-0.18961	0.71147
2	-0.35351	1.26970	0.45400		
3	-0.23789	0.86036	0.15354		
4	-0.94158	0.64552	0.16817		

TABLE 2
Coefficients for k_V

j	a_j	b_j	c_j	m_k	c_k
1	-3.80595	0.56934	0.81061	-0.16398	0.63297
2	-3.44965	-0.22911	0.51059		
3	-0.39902	0.73042	0.11899		
4	0.50167	1.07319	0.27195		

TABLE 3
Coefficients for α_H

j	a_j	b_j	c_j	m_α	c_α
1	-0.14318	1.82442	-0.55187	0.67849	-1.95537
2	0.29591	0.77564	0.19822		
3	0.32177	0.63773	0.13164		
4	-5.37610	-0.96230	1.47828		
5	16.1721	-3.29980	3.43990		

TABLE 4
Coefficients for α_V

j	a_j	b_j	c_j	m_α	c_α
1	-0.07771	2.33840	-0.76284	-0.053739	0.83433
2	0.56727	0.95545	0.54039		
3	-0.20238	1.14520	0.26809		
4	-48.2991	0.791669	0.116226		
5	48.5833	0.791459	0.116479		

Rec. ITU-R P.838-3

For linear and circular polarization, and for all path geometries, the coefficients in equation (1) can be calculated from the values given by equations (2) and (3) using the following equations:

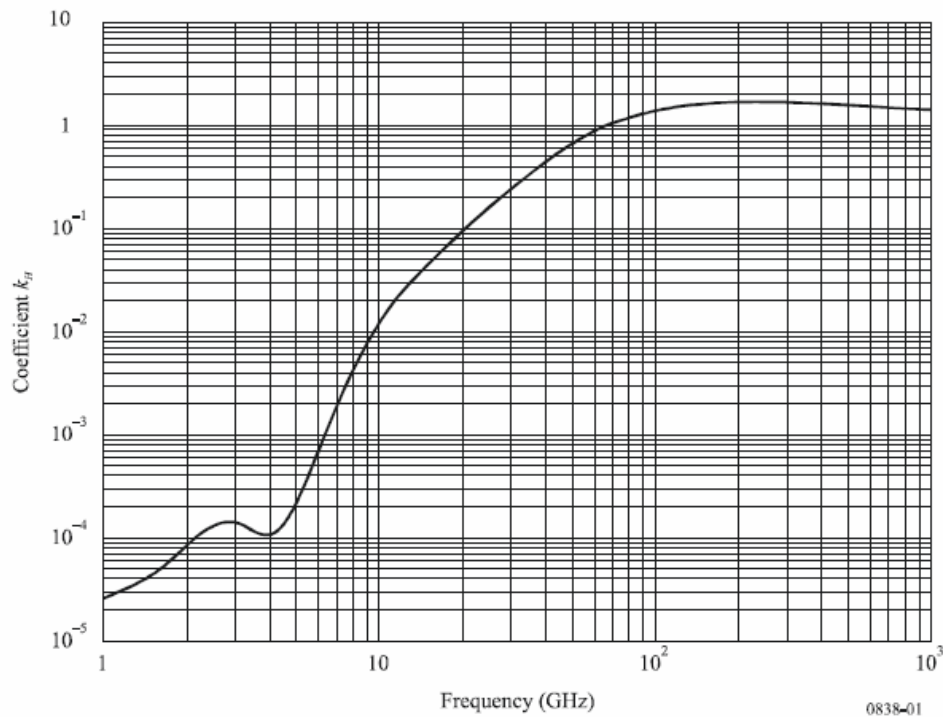
$$k = [k_H + k_V + (k_H - k_V) \cos^2 \theta \cos 2 \tau] / 2 \quad (4)$$

$$\alpha = [k_H \alpha_H + k_V \alpha_V + (k_H \alpha_H - k_V \alpha_V) \cos^2 \theta \cos 2 \tau] / 2k \quad (5)$$

where θ is the path elevation angle and τ is the polarization tilt angle relative to the horizontal ($\tau = 45^\circ$ for circular polarization).

For quick reference, the coefficients k and α are shown graphically in Figs. 1 to 4, and Table 5 lists numerical values for the coefficients at given frequencies.

FIGURE 1
k coefficient for horizontal polarization



Rec. ITU-R P.838-3

FIGURE 2

α coefficient for horizontal polarization

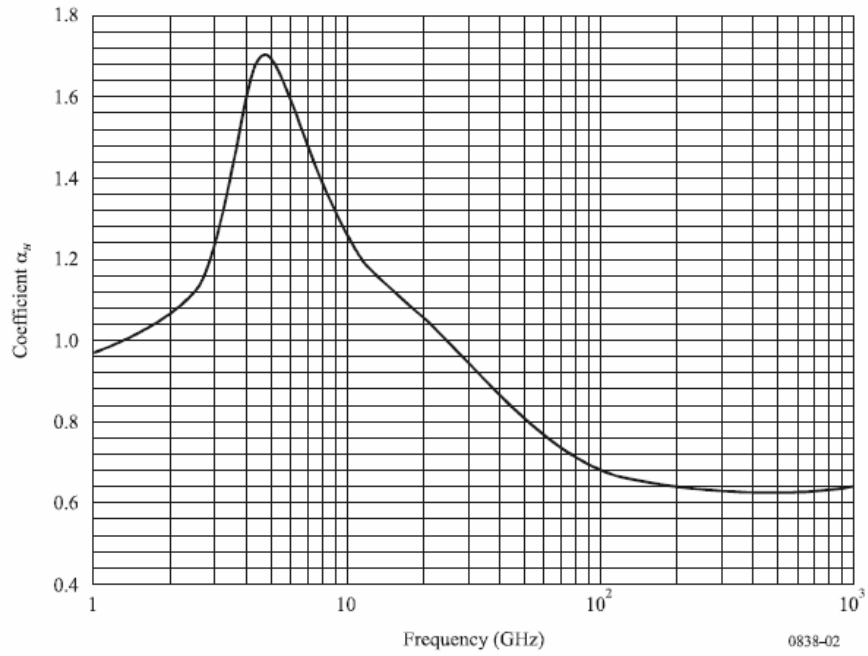


FIGURE 3

k coefficient for vertical polarization

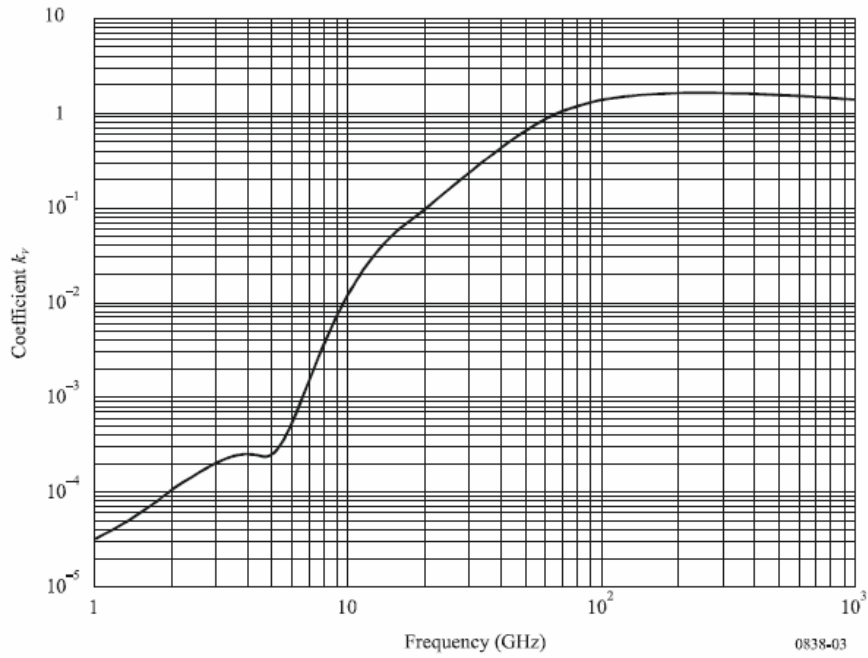


FIGURE 4

α coefficient for vertical polarization

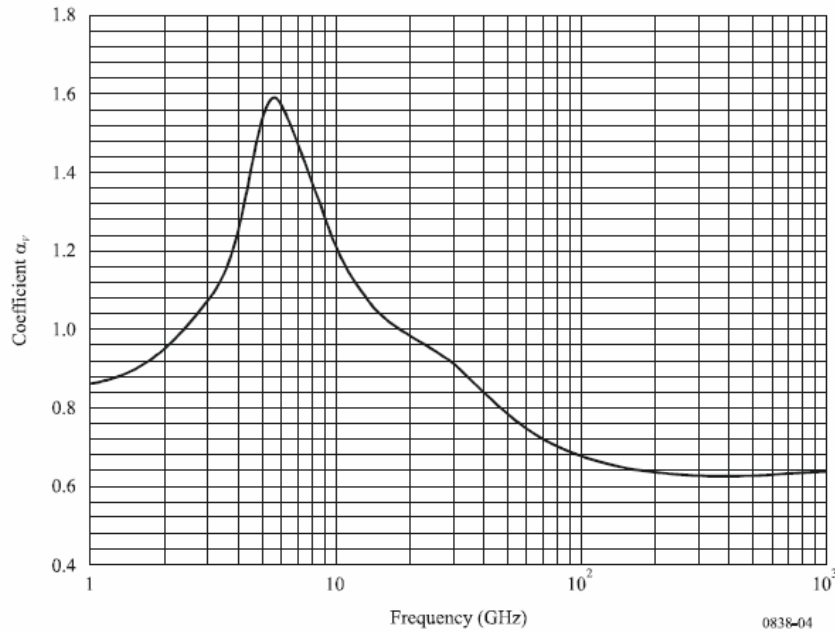


TABLE 5

Frequency-dependent coefficients for estimating specific rain attenuation using equations (4), (5) and (1)

Frequency (GHz)	k_H	α_H	k_V	α_V
1	0.0000259	0.9691	0.0000308	0.8592
1.5	0.0000443	1.0185	0.0000574	0.8957
2	0.0000847	1.0664	0.0000998	0.9490
2.5	0.0001321	1.1209	0.0001464	1.0085
3	0.0001390	1.2322	0.0001942	1.0688
3.5	0.0001155	1.4189	0.0002346	1.1387
4	0.0001071	1.6009	0.0002461	1.2476
4.5	0.0001340	1.6948	0.0002347	1.3987
5	0.0002162	1.6969	0.0002428	1.5317
5.5	0.0003909	1.6499	0.0003115	1.5882
6	0.0007056	1.5900	0.0004878	1.5728
7	0.001915	1.4810	0.001425	1.4745
8	0.004115	1.3905	0.003450	1.3797
9	0.007535	1.3155	0.006691	1.2895
10	0.01217	1.2571	0.01129	1.2156

Rec. ITU-R P.838-3

TABLE 5 (continued)

Frequency (GHz)	k_H	α_H	k_V	α_V
11	0.01772	1.2140	0.01731	1.1617
12	0.02386	1.1825	0.02455	1.1216
13	0.03041	1.1586	0.03266	1.0901
14	0.03738	1.1396	0.04126	1.0646
15	0.04481	1.1233	0.05008	1.0440
16	0.05282	1.1086	0.05899	1.0273
17	0.06146	1.0949	0.06797	1.0137
18	0.07078	1.0818	0.07708	1.0025
19	0.08084	1.0691	0.08642	0.9930
20	0.09164	1.0568	0.09611	0.9847
21	0.1032	1.0447	0.1063	0.9771
22	0.1155	1.0329	0.1170	0.9700
23	0.1286	1.0214	0.1284	0.9630
24	0.1425	1.0101	0.1404	0.9561
25	0.1571	0.9991	0.1533	0.9491
26	0.1724	0.9884	0.1669	0.9421
27	0.1884	0.9780	0.1813	0.9349
28	0.2051	0.9679	0.1964	0.9277
29	0.2224	0.9580	0.2124	0.9203
30	0.2403	0.9485	0.2291	0.9129
31	0.2588	0.9392	0.2465	0.9055
32	0.2778	0.9302	0.2646	0.8981
33	0.2972	0.9214	0.2833	0.8907
34	0.3171	0.9129	0.3026	0.8834
35	0.3374	0.9047	0.3224	0.8761
36	0.3580	0.8967	0.3427	0.8690
37	0.3789	0.8890	0.3633	0.8621
38	0.4001	0.8816	0.3844	0.8552
39	0.4215	0.8743	0.4058	0.8486
40	0.4431	0.8673	0.4274	0.8421
41	0.4647	0.8605	0.4492	0.8357
42	0.4865	0.8539	0.4712	0.8296
43	0.5084	0.8476	0.4932	0.8236
44	0.5302	0.8414	0.5153	0.8179
45	0.5521	0.8355	0.5375	0.8123
46	0.5738	0.8297	0.5596	0.8069
47	0.5956	0.8241	0.5817	0.8017
48	0.6172	0.8187	0.6037	0.7967

TABLE 5 (continued)

Frequency (GHz)	k_H	α_H	k_V	α_V
49	0.6386	0.8134	0.6255	0.7918
50	0.6600	0.8084	0.6472	0.7871
51	0.6811	0.8034	0.6687	0.7826
52	0.7020	0.7987	0.6901	0.7783
53	0.7228	0.7941	0.7112	0.7741
54	0.7433	0.7896	0.7321	0.7700
55	0.7635	0.7853	0.7527	0.7661
56	0.7835	0.7811	0.7730	0.7623
57	0.8032	0.7771	0.7931	0.7587
58	0.8226	0.7731	0.8129	0.7552
59	0.8418	0.7693	0.8324	0.7518
60	0.8606	0.7656	0.8515	0.7486
61	0.8791	0.7621	0.8704	0.7454
62	0.8974	0.7586	0.8889	0.7424
63	0.9153	0.7552	0.9071	0.7395
64	0.9328	0.7520	0.9250	0.7366
65	0.9501	0.7488	0.9425	0.7339
66	0.9670	0.7458	0.9598	0.7313
67	0.9836	0.7428	0.9767	0.7287
68	0.9999	0.7400	0.9932	0.7262
69	1.0159	0.7372	1.0094	0.7238
70	1.0315	0.7345	1.0253	0.7215
71	1.0468	0.7318	1.0409	0.7193
72	1.0618	0.7293	1.0561	0.7171
73	1.0764	0.7268	1.0711	0.7150
74	1.0908	0.7244	1.0857	0.7130
75	1.1048	0.7221	1.1000	0.7110
76	1.1185	0.7199	1.1139	0.7091
77	1.1320	0.7177	1.1276	0.7073
78	1.1451	0.7156	1.1410	0.7055
79	1.1579	0.7135	1.1541	0.7038
80	1.1704	0.7115	1.1668	0.7021
81	1.1827	0.7096	1.1793	0.7004
82	1.1946	0.7077	1.1915	0.6988
83	1.2063	0.7058	1.2034	0.6973
84	1.2177	0.7040	1.2151	0.6958
85	1.2289	0.7023	1.2265	0.6943
86	1.2398	0.7006	1.2376	0.6929

TABLE 5 (*end*)

Frequency (GHz)	k_H	α_H	k_V	α_V
87	1.2504	0.6990	1.2484	0.6915
88	1.2607	0.6974	1.2590	0.6902
89	1.2708	0.6959	1.2694	0.6889
90	1.2807	0.6944	1.2795	0.6876
91	1.2903	0.6929	1.2893	0.6864
92	1.2997	0.6915	1.2989	0.6852
93	1.3089	0.6901	1.3083	0.6840
94	1.3179	0.6888	1.3175	0.6828
95	1.3266	0.6875	1.3265	0.6817
96	1.3351	0.6862	1.3352	0.6806
97	1.3434	0.6850	1.3437	0.6796
98	1.3515	0.6838	1.3520	0.6785
99	1.3594	0.6826	1.3601	0.6775
100	1.3671	0.6815	1.3680	0.6765
120	1.4866	0.6640	1.4911	0.6609
150	1.5823	0.6494	1.5896	0.6466
200	1.6378	0.6382	1.6443	0.6343
300	1.6286	0.6296	1.6286	0.6262
400	1.5860	0.6262	1.5820	0.6256
500	1.5418	0.6253	1.5366	0.6272
600	1.5013	0.6262	1.4967	0.6293
700	1.4654	0.6284	1.4622	0.6315
800	1.4335	0.6315	1.4321	0.6334
900	1.4050	0.6353	1.4056	0.6351
1 000	1.3795	0.6396	1.3822	0.6365

Annexure D

Frequency bands allotted by ITU for satellite communication.

Frequency bands used for Fixed Satellite Service (FSS), Broadcasting Satellite Service (BSS) and Non Geo Synchronous Orbit (NGSO) satellites:

Orbit		Category	Up Link	Down Link	
GEO/GSO	C-BAND (FSS)	Normal C Band	5925-6425 MHz	3700-4200 MHz	
		Lower Ext C Band	6425-6725 MHz	3400-3700 MHz	
		Planned C Band	6725-7025MHz	4500-4800 MHz	
	Ku BAND (FSS and BSS)	Normal Ku band	13.75-14.5 GHz		10.95-11.2 GHz
					11.45-11.7 GHz
					12.2-12.75 GHz
		Planned Ku Band	12.75-3.25 GHz	10.7-10.95 GHz	11.2-11.45 GHz
		Planned BSS Ku Band	14.5-14.8 GHz	11.7-12.2 GHz	
			17.3-8.1 GHz (DTH)	-	
	MSS	S-BAND	2655-2690 MHz	2500-2535 MHz	
	BSS			2550-2630 MHz	
	Emergency Beacon	Meteorology and SAR bands	402.75 MHz	C-band	
	DCP		406-406.1 MHz		
	Meteorology		401-403 MHz		
			-	1670-1710 MHz	

Orbit	Category	Frequency band	Up Link	Down Link
LEO (Near earth Scientific / Remote sensing satellites) Amateur satellite service	TTC	S-band	2025-2110 MHz	2200-2290 MHz
		VHF	148-149 MHz	137-138 MHz
	Data (Remote sensing)	X-band	-	8025-8400 MHz
		Ka band	-	25.5-27 GHz.
	Data (Space research)	X-band	-	8450-8500 MHz
		UHF/VHF	435-438 MHz	144-146 MHz
	Search & Rescue (Cospas Sarsat)	UHF/L band	406-406.1 MHz	1544 to 1544.1 MHz
Deep space	TTC	S-band	2110-2120 MHz	2290-2300 MHz
		S/X-bands	8450-8500 MHz	2025-2110 MHz
			7190-7235 MHz	2200-2290 MHz
			7145-7190 MHz	2290-2300 MHz
		7145-7235 MHz	8400-8500 MHz	
		X/Ka band	7145-7190 MHz	31.8-32.3 GHz
		Ka band	34.2-34.7 GHz	31.8-32.3 GHz
	Data (Space research)	X-band	-	8400-8450 MHz
There are some more frequency bands identified for space to earth application with some conditions laid down by ITU.				

Chapter 11

List of Publications and Presentations

I) Publications in the research period (From 2006 to date):

1. Sambasiva Rao V., Surendra Pal. Spherical Phased Array Links Remote Sensors. **Microwaves & RF**. 2009, September, pp 84-91.
2. Sambasiva Rao V., Srinivasan V.V., Surendra Pal. Generation of Dual Beams from Spherical Phased Array Antenna. **Electronics letters**. 2009, April 23, Vol. 45, Issue 9, pp. 441-442.
3. Sambasiva Rao V., Surendra Pal. High bit rate Transmitting system for Remote Sensing Satellites. **High frequency electronics**. 2009, April, pp.18-26.
4. Sambasiva Rao V., Surendra Pal. An insight into the factors affecting high bitrate data transmission from satellites to ground stations. **BITS Curie Journal**. 2008, July, Vol.1, No.2, pp.33-40.
5. Sambasiva Rao V., Surendra Pal. Spectral Distortion in High Data Rate Remote Sensing Satellite Links. **High Frequency Electronics**. 2008, May, pp.48-55.
6. Sambasiva Rao V., Surendra Pal. A Unique Space to Earth Data Transmitting System. **International Astronautical Congress – IAC 2007**, Hyderabad. 2007, September 24-28.
7. Sambasiva Rao V., Pal S. Study of implications of using a single TWTA for power amplification of two high bit rate data modulated carriers. **IEEE-International Symposium on Microwaves (ISM-06)**, Bangalore. 2006, December 15-17.
8. Sambasiva Rao V., Pal S. Techniques for high bit rate data transmission from remote sensing satellites. **IEEE-International Symposium on Microwaves (ISM-06)**, Bangalore. 2006, December 15-17.
9. Pal S., Rao V S. Satellite Technology Utilization for Rural and Urban India. **IETE Technical Review**. 2007, July-August, Vol. 24, No.4, pp. 277-286.
10. Ramana.D.V., Jolie. R., Rao. V.S., Pal. S. New QPSK Modulator with Pre modulation Filter for Payload Data Transmission in Chndrayaan-1 Mission. **2nd International Conference on RF and Signal Processing Systems (RSPS-2010)**, Guntur, India, 2010, January 02-09, pp135-139.

11. Prateek Bansal, Bindu K. R., Mishra R.M., Pichayya B., Sambasiva Rao V., Pal S. X-Band High Power SSPA for Satellite On-board Applications. **Journal of Spacecraft Technology**. 2009, January, Vol. 19, No.1, pp. 51-59.
12. Shafali Tandon, Mishra R.M., Prateek Bansal, Bindu K.R., Pichayya B., Sambasiva Rao V., Surendra Pal. Advances in SSPA Technology for Space Applications. **IEEE Symposium on Microwaves-ISM 08**, Bangalore. December, 2008.
13. Ramana D.V., Jolie R., Rao V.S., Pal. S. A Satellite Telemetry Transmitting System with Pre-Modulation Filtering. **High Frequency Electronics**. 2008, November, pp. 42-47.
14. Prateek Bansal, Mishra R.M., Bindu K.R., Shafali Tandon, Pichayya B., Sambasiva Rao V., Surendra Pal. Effective Techniques of Data Transmission in Ka-band for space Applications. **International Radar Symposium India 2007 (IRSI 07)**, Bangalore. 2007, December 10-13, pp. 418-421.
15. Prateek Bansal, Shafali Tandon, Bindu K.R., Mishra R.M., Pichayya B., Sambasiva Rao V., Pal S. High bit rate Ka-band Data Transmission system for Satellite Application. **Indicon 2007 & 16th Annual Symposium of IEEE Bangalore Section**, Bangalore. 2007, September 6-8.
16. Mishra R.M., Bindu K.R., Prateek Bansal, Pichayya B., Sambasiva Rao V. X-band High bit rate QPSK Modulator. **IEEE-International Symposium on Microwaves (ISM-06)**, Bangalore. 2006, December 15-17.

II. Presentations in the research period (From 2006 to date):

17. Sambasiva Rao V. Satellite Communication. Lecture at ISRO Satellite Centre, Bangalore. 2007, October 22.
18. Sambasiva Rao V. Advances in Communication Systems. Lecture at Communication Systems Group, ISRO Satellite Centre, Bangalore. 2007, April 28.
19. Sambasiva Rao V. Communication systems for Spacecrafts, Lecture at ISRO Satellite Centre, Bangalore. 2007, March 23.
20. Sambasiva Rao V. Space to earth high bit rate data Transmission - An Indian Scenario. Prof. N S Nagaraja Memorial Lecture at IETE, Bangalore. 2006, June 25.

III. Earlier Publications/Presentations (up to 2005)

21. Lakshmeesha V.K, Srinivasan V.V., Sambasiva Rao V., Reddy P.K., Pal S. A space Borne Hemisphere Active Phased Array antenna at X-band for High Bit Rate QPSK Data Transmission. Progress in electromagnetic Research Symposium (PIERS 2001), Osaka, Japan. 2001.
22. Sambasiva Rao V., Pal S. Microwave Photonics for space applications. Workshop on broadband photonic links, at National Centre for Radio Astrophysics/TIFR, Pune. 2000, August 27-28.
23. Pal S., Lakshmeesha V.K., Mahadevan V., Sambasiva Rao V., Srinivasan V.V. A X band Spherical Array for QPSK data Satellite transmission. International Conference on Communications, Control and Signal Processing in the Next Millenium (CCSP-2000), Bangalore, 2000 July 25-28.
24. Lakshmeesha V.K., Srinivasan V.V., Sambasiva Rao V., Mahadevan V., Pal S. An active, Dual Beam Spherical Phased Array for Data Transmission at X-band from satellite. Radar symposium India-99 (IRSI-99), Bangalore. 1999, December.
25. Sambasiva Rao V., Ramana D.V., Surendra Pal. Some Experimentation on X-band Offset QPSK Modulator. IETE Technical Review, 1999, March-April, Vol.16, No.2,: 191-196.
26. Ramana D.V., Sambasiva Rao V., Pal S. Advanced modulation techniques for data transmission from space. IETE workshop, Hyderabad.1998.
27. Sambasiva Rao V., Mishra R.M., Pal S. X-band Solid State Power Amplifier for IRS P2 Spacecraft. Journal of spacecraft Technology. 1996, January, Vol.6, No.1: 60-71.
28. Sambasiva Rao V., Mishra R.M., Pal S. X-band Solid State Power Amplifier for Space use. Engineering Design, Issue on Microwave and Millimeter wave components, Devices and Systems, 1995, July-September: 27-35.
29. Suryanarayana Rao K.N., Nagraj S R, Sambasiva Rao V, et.al. Data handling System for IRS 1C. Journal of Spacecraft Technology, 1995, July, Vol.5, No. 2: 84-94.
30. Sunil K, Sambasiva Rao V, et.al. Direct Digital Synthesis for S-band TT&C Up link Transmitters. Journal of IETE, 1994, Sept.-December, Vol.40, Nos. 5&6. pp. 223-229.

31. Pitchaiah B., Sambasiva Rao V, et.al. X-band high bit rate data transmitters for Indian Remote Sensing Satellites. IETE Technical Review. 1994, March-June, Vol.11, No.2&3: 129-135.
32. Pal S., Rao V. S., et.al. ISAC Antenna RADCALPLOT. Available with the library of AMTA, USA.
33. Sambasiva Rao V., Ramana D.V., Suvarna L., Bhaskaranarayana A., Pal S.. X-band high bit rate QPSK Modulator. IETE Technical Review. 1993, July-August, Vol. 10, No.4.
34. Pal S., Sambasiva Rao V. TT&C and Data handling Systems for spacecrafts. Telematics - 93, Bangalore. 1993, July:28-30.
35. Pal S., Sambasiva Rao V., Rajangam R.K. Data Handling Systems of Indian Remote Sensing satellites - IRS 1A & 1B. Journal of Spacecraft Technology. 1993, July, Vol. III, No.2: 16-24.
36. Suvarna L., Sambasiva Rao V., et.al. Microprocessor controlled C-band up link transmitter. IETE Technical Review, 1993, January-February, Vol. 10, No.1: 53-56.
37. Ramana D V, Suvarna L, Sambasiva Rao V, et.al. Frequency Multipliers - An overview and a 10.5 GHz frequency multiplier on TFG substrate. IETE Technical Review, 1992, September-October: 356-363.
38. Sambasiva Rao V, et.al. QPSK Modulator in thick film at X-band. RF Expo West, 1991, February. Santa Clara, Calif.
39. Subramanya V, Lakshmeesha V K, Sambasiva Rao V, Pal S. X-band 16 way Radial Power Divider/Combiner for high power SSPA application. RF Expo West, 1991, February. Santa Clara, Calif.
40. Rao V. S., et.al. S-band exciter for up link transmitters. Journal of I E T E. 1991, Vol. 37, No.: 313-315.
41. Sambasiva Rao V., et. Al. X-band Frequency Multiplier in Microstripline Configuration. IETE Technical Review. 1990, July-August, Vol. 7, No.4: 264-267.
42. Pal S., Rao V. S., et.al. Temperature compensation circuits for data transmitters. Proceedings of RF Technology Expo. USA. 1986 : 525-532.

43. Pal S., Saini S.K., Rao V.S., Bhaskaranarayana A. Unequal power splitter hybrid couplers. Proceedings of RF Technology Expo USA. 1986: 447-450.
44. Pal S., Sivaprasad N.V., Sambasiva Rao V. Frequency plan for co-located spacecraft TTC systems. Vth SFCG meeting. 1984, October/November, Orlando, NY.
45. Bhaskaranarayana A, Sambasiva Rao V, et.al. RF Communication systems for spacecrafts. Workshop on Electronics in Space, 1983, Bangalore.
46. Pal S, Reddy P K, Lakshmeesha V K, Mahadevan V, Nicholas L, Sambasiva Rao V. Onboard antenna system for Bhaskara mission. Journal of IETE, 1983, Vol. 29, pp. 154-159.
47. Shamanna K N, Rao V S, Kosta S P. Design of parallel coupled microstrip line band pass filters. International Journal of Electronics. 1978, Vol. 45, N0.1: 89-96.
48. Kosta S P, Pal S, Reddy P K, Lakshmeesha V K, Rao K N S, Shamanna K N, Mahadevan V, Rao V S, Nicholas L. Antenna systems for the Aryabhata mission. Proceedings of Indian Academy of Sciences 1978, September, Vol.C1, No.2: 221-234.
49. Reddy P K, Shamanna K N, Rao V S, Kosta S P. Nomograms for Polarization loss. J I E T E. 1977: 620-621.
50. Shamanna K N, Sambasiva Rao V, Kosta S P. On a multi section helical resonator filter. J I E T E. 1977, Vol. 23, No.1: 22-23.
51. Shamanna K N, Rao V S, Kosta S P. Parallel coupled micro strip line. Electronic design. 1976, May 24: 78-81.

Chapter 12

Biography

12.1 Brief Biography of Venigalla Sambasiva Rao

V. Sambasiva Rao, after graduating in Electronics and Communication Engineering from College of Engineering, Kakinada, (Andhra University) in 1973, joined ISRO Satellite Centre, Bangalore, and has contributed in various capacities, for 34 years. At present, he is Director of Satellite Communication and Navigation Programme at ISRO Head Quarters and takes care of GEOSAT programme of ISRO.

As Group Head at ISRO Satellite Centre, he has lead Communication Systems Group to develop various RF systems and technologies. His indigenous developments replaced many imported RF components/systems for onboard satellite usage. He is principally responsible for the development of high bit rate data transmitters for all IRS satellites and various RF and microwave systems in S, C, X, Ku and Ka bands for IRS and INSAT missions.

He was actively involved in the study & preparation of RF systems/satellite proposals for ISRO missions as well as international missions like INMARSAT/ICO, ITU's RASCOM programme, etc.

He has successfully carried out numerous responsibilities as Project Manager/Deputy Project Director for different satellite projects. He has been Chairman/Member of various committees for technical studies and also for review of RF system/satellite configurations and system designs. He has also been chairing the committees for Test and Evaluation of satellite ground stations of ISRO.

Sambasiva Rao, a Fellow of IETE and a Member of Astronautical Society of India, has received the Distinguished Achievement Award from the Department of Space for launching Aryabhata, NRDC Award 1994 for the development of X-band high bit rate QPSK modulator, IETE-IRSI (83) Award 2006 for the development of high bit rate data transmitters and Team Excellence Award for the development of X-band spherical phased array.

He has published 45 technical papers in national and international journals, and has also given lectures and seminars at diverse forums and training programs.

12.2 Brief Biography of Dr. Surendra Pal (Mentor/Supervisor)

Dr. Surendra Pal

Distinguished Scientist
Associate Director
Program Director, Satellite Navigation
ISRO Satellite Centre, Bangalore-17

Dr. S Pal, an alumnus of Birla Institute of Technology & Science (BITS), Pilani and Indian Institute of Science (IISc), Bangalore, India is presently **Distinguished Scientist & Associate Director and also Program Director, Satellite Navigation Program at ISRO Satellite Centre, Bangalore.**

He joined Indian Space Research Organization (ISRO) in 1971, after a brief tenure at Tata Institute of Fundamental Research. **Dr. Pal pioneered the Microwave & Antenna & RF communication activities at the ISRO Satellite Centre at the inception.** He has been responsible for the development & fabrication of all spacecraft related telecommunication systems for India's all satellites beginning with **Aryabhata** to the present day **IRS & INSAT** series of spacecraft & Chandrayan. Dr. Pal is also responsible for **pioneering satellite based navigation activities in India. He is spear heading the Indian Satellite Based Wide Area Augmentation System – GAGAN (GPS Aided Geo Augmented Navigation System) and Indian Regional Navigation Satellite System (IRNSS) activities for aviation for civilian & restricted users.** Dr Pal and his team successfully took the challenge of designing 32 M diameter antenna system for Indian Deep Space Network for Chandrayaan-I.

He has been consultant to: (I) INMARSAT/ICO (UK) for LEOSAT definitions, responsible for the development of Satellite Hand Held Telephone Antenna System for ICO (UK) (ii) International Telecommunication Union (ITU) for defining Regional African Satellite Communication System and (iii) Nanyang Technological University, Singapore on X-Sat. He was also Chairman of Information Infrastructure Working Group of Ministry of Information Technology. He had also carried out special antenna developments for DRDO-India.

Contd..

He is also on the United Nations panel of experts on Global Navigation Satellite Systems (GNSS) and Chaired/participated in various UN meetings at Vienna, Geneva and at other international venues. Dr. Pal a Distinguished Fellow of IETE, Fellow of Indian National Academy of Engineering, National Academy of Sciences, India, **Fellow IEEE(USA)**, has received more than one and a half dozen national and international awards, including, Performance Excellence Award by ISRO, IEEE Third Millennium Medal, Prof. S N Mitra Memorial Award (INAE), Four National Research and Development Corporation of India invention awards for various developments, inventions and overall contributions towards the growth of communication and space technology in India. Besides these he holds Indian, European & International patents for his various inventions. Recently IEEE has announced its top level awards and him to be the recipient for the prestigious IEEE-2010 Judith Resnik Award .

Dr. Pal has published more than 200 papers in international and national journals of repute , one book on communications & guided number of Ph.D students. He was a Distinguished Visiting Professor of Indian National Academy of Engineering & presently he is on the Distinguished Lecturer Programme of IEEE-USA.

His fields of interest are Microwave Communications, Space Technology, Electromagnetics, Antennas and Satellite Navigation.